

4 SYSTEM-LEVEL SENSITIVITY STUDIES

This chapter describes the sensitivity and uncertainty analysis techniques used in conjunction with results of the TPA Version 4.1 code¹ system-level calculations. In general, a sensitive parameter is defined as one that produces a relatively large change in the output variable for a unit of change in an input parameter. The goal of the sensitivity analyses presented in this report is to determine the parameters to which peak dose for the simulation period shows the most sensitivity. The goal of the uncertainty analyses is to determine the parameters driving uncertainty (i.e., variation) in peak dose output. The analyses were conducted primarily for the basecase; limited analyses were conducted for the igneous activity and faulting disruptive events.

The sensitivity analyses in this report use peak dose as the output variable for each realization because this result is most likely to demonstrate sensitivity relationships among the independent and dependent variables. The performance measure in the Yucca Mountain implementing regulation 10 CFR Part 63 (Code of Federal Regulations, 2002) is stipulated to be the peak of the average dose history within the 10,000-year simulation period. Although there is an important distinction between these two measures of performance, the peak dose for each realization during the simulation period was used. The rationale for doing so is established in Section 4.3.1.

4.1 Sensitivity Analysis Techniques

This section describes the techniques used to determine which input parameters in the TPA Version 4.1 code most influence the results. It is noted that not all the techniques described were applied to all cases.

The output from the TPA Version 4.1 code is given by y , which is a function of random parameters, x_i , deterministic parameters, d_k ; and model assumptions, a_m

$$y_j = f(x_{1_j}, x_{2_j}, \dots, x_{l_j}, d_k, a_m) \quad (4-1)$$

where j represents the j th realization and l is the total number of sampled parameters in the model. It is assumed that the behavior of the system is simulated by appropriately sampling the random parameters and then computing the system output, y , for each realization of the parameters (Figure 4-1). To outline a method for analyzing simulation output, to identify important random parameters, and to develop understanding of their relationship to the output, it is assumed that the decisions about appropriate model assumptions and fixed parameters have been made *a priori*. As a result, the dependence of y on fixed parameters and model assumptions is not considered further and focus is on the dependence of y on the sampled parameters.

¹The specific version of the TPA code used in this chapter is 4.1k.

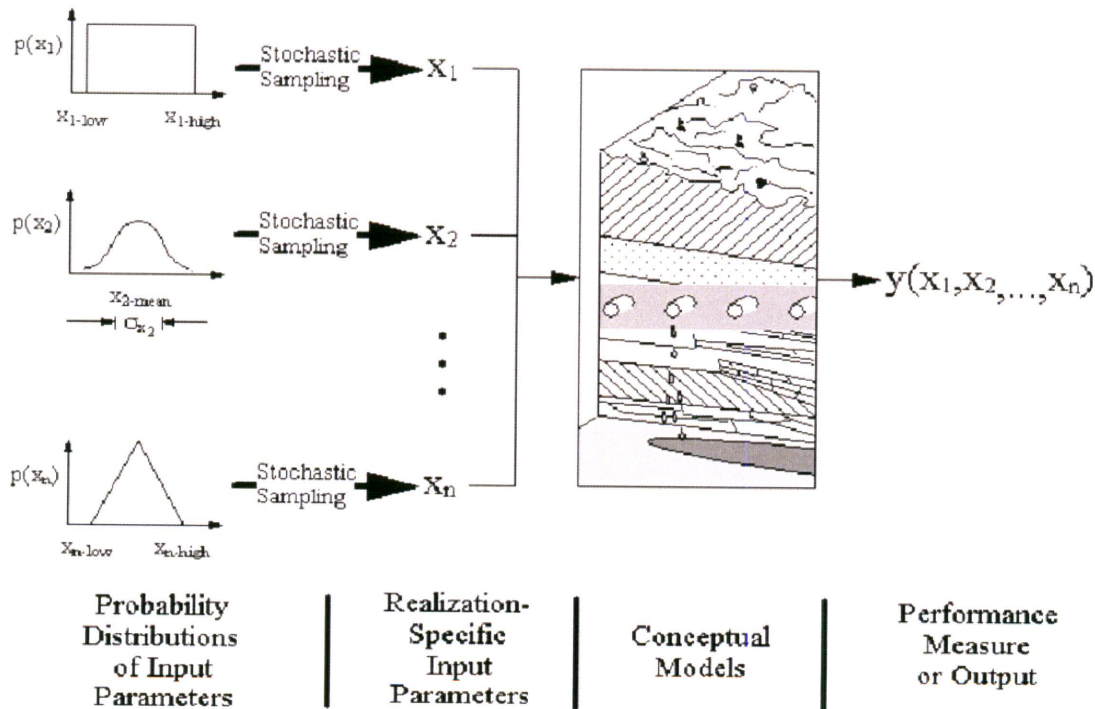


Figure 4-1. A Diagram Illustrating the Use of the Monte Carlo Method in Performance Assessment

4.1.1 Regression Analyses Methods

4.1.1.1 Single Linear Regression on One Variable

Single linear regression (i.e., regression with only the first power of one input variable and an intercept) of the output variable, with respect to each of the input parameters, can give a quantitative measure of the correlation through the coefficient of determination, R^2 . This measure can be misleading, however, in cases where the dependencies are not purely of the first order with respect to the input variable. It is noted in this section and throughout this chapter that linear refers to the functional form of the regression and not the order to which the fitting parameters appear (although the regressions are also linear in the fitting parameters). Even when the output variable is linearly dependent on the input variable being studied, univariate linear regression of Monte Carlo results may fail to show unambiguous correlation because other sampled parameters that affect the output are varying at the same time, and the fitted model is clearly underspecified (i.e., the results depend on more than one variable).

The coefficient of determination, R^2 , is small for most variables in the current analyses and is not necessarily a good indicator of the importance of the variables. A better indication of influence is to determine the probability that the slope of the linear regression line is significantly different from zero. This probability is determined with a t-test as described in succeeding sections.

4.1.1.1.1 Use of the t-Test To Determine Significance of Regression Parameters

The t-test is generally used to determine with a specified confidence level that an estimated parameter value differs from another value. A parameter, x_i , is deemed influential if there is a specified (e.g., 95 percent) confidence that the slope of its regression curve, m_i , is different from zero (Benjamin and Cornell, 1970).

The t-statistic of the slope of a single-variable regression line is defined as

$$t_i = m_i \sqrt{n \frac{S_{i,x}^2}{S^2}} \quad (4-2)$$

where

- t_i — t-statistic for regression coefficient m_i
- m_i — estimated value of regression coefficient i (i.e., slope of the best-fit line for dose versus the independent variable, x_i)
- S — estimated standard deviation of dose
- $S_{i,x}$ — estimated standard deviation of independent variable, x_i
- n — number of samples

For the analyses conducted herein, the number of realizations is large (4,000), which provides essentially an infinite number of degrees of freedom for the t-statistic. The critical value to ensure 95-percent confidence that m_i differs from zero for these conditions is 1.96 (Mason, et al., 1989). Eq. (4-2) is used, therefore, to determine if the absolute value of the t-statistic for each independent variable is greater than 1.96. If not, the hypothesis that the independent variable was significant is rejected.

The t-statistic was used for the single variable regressions and multiple linear regressions as described in Eq. (4-2).

4.1.1.2 Variable Transformations and Their Attributes

The correlation between input and output variables can be enhanced by transforming the variables. In general, variable transformations are used to (i) eliminate dimensionality of the variables, (ii) reduce the role of points at the tails of the distributions, and (iii) properly scale the resulting sensitivities to the variability of the input variables. Although transformations generally increase the goodness of the fit analyses, they distort the meaning of the results. For example, transformations such as rank and logarithmic applied to the dependent variable (dose) frequently give unfair weight to small doses, which do not affect the mean results as much as the higher doses. Because the proposed regulations are based on mean doses, regression results based on transformed variables should be used cautiously.

4.1.1.2.1 Normalization

In normalization, the input variable, x_i , is transformed by dividing it by its mean value (or another baseline value such as the median or 90th percentile):

$$X_i^* = \frac{X_i}{\bar{X}_i} \quad (4-3)$$

Normalized variables are dimensionless and are scalar multiples of their baseline values. Dimensionless variables allow the comparison of sensitivities to other independent variables with different dimensions. Other types of normalization can also be used and will be shown later in this chapter.

Sensitivity measures based on normalized variables describe only the relative change in the dependent variable (peak dose) to changes in the independent variables. Although normalization allows useful measure of sensitivity, it does not consider the ranges of the variability of the independent and dependent variables (see standardization, following).

4.1.1.2.2 Rank Transformation

Rank transformation, a dimensionless transform, replaces the value of a variable by its rank (i.e., the position in a list that has been sorted from largest to smallest values) (Iman and Conover, 1979). Analyses with ranks tend to show a greater sensitivity than results with untransformed variables. If the distribution of doses is skewed toward the low end, which is usually the case, rank transformation can give unfair weights to lower doses.

4.1.1.2.3 Logarithmic Transformation

For situations in which input and output variables range many orders of magnitude, it may be advantageous or even necessary to perform analyses on the logarithm of the variables instead of on the variable values themselves. The log transformation is also valuable for creating regression equations, where the subprocesses of the model multiply each other to form the output variable. For the present situation in which the dose calculation results from radionuclide releases from the waste form, transport through the geosphere, and uptake by humans, the processes are indeed largely multiplicative rather than additive. Log transforms, therefore, tend to give better fits to the Monte Carlo results than untransformed variables, but again at the expense of unfairly weighting the smaller doses. The log transformation may be used in conjunction with normalization.

4.1.1.2.4 Standardization

The independent and dependent variables can be standardized by subtracting the mean and dividing by the standard deviation

$$X_i^* = \frac{X_i - \bar{X}}{\sigma_x} \quad (4-4)$$

Sensitivity measures based on standardized variables (standardized sensitivities) have the advantage of considering the range of the independent variable. Standardized variables can be greater or less than zero, hence, they cannot be used directly in the regression analyses using the log-transformed variables. Instead, the standardized sensitivities can be derived from sensitivities based on logs of the normalized variables:

$$\frac{\partial y^*}{\partial x^*} = \frac{\sigma_{x_i}}{\sigma_y} \left(\frac{\partial y}{\partial x_i} \frac{x_i}{y} \right) \quad (4-5)$$

where y^* and x^* are the standardized dependent and independent variables as defined by Eq. (4-4). The quantity in parentheses is the sensitivity derived from regression analysis with the logs of the normalized variables. Direct linear regression with standardized variables properly weights all doses.

A modified form of the standardized sensitivities approach was also used in the differential analysis described in Section 4.1.2. In this case, only seven points were defined for the parameter space, so the independent variables were standardized by the same standard deviations used in the regression analyses (i.e., the standard deviation based on 4,000 samples generated in the Monte Carlo analyses). Peak dose did not need to be standardized to show the relative sensitivities to the standardized independent variable. Therefore, those sensitivities have units of dose.

4.1.1.3 Stepwise Multiple Linear Regression

Stepwise multiple linear regression (stepwise regression) determines the most influential input parameters according to how much each input parameter reduces the residual sum of squares (Helton, et al., 1991). The form of the regression equation is

$$y = m_1x_1 + m_2x_2 + m_jx_j + m_nx_n + b \quad (4-6)$$

where

y	—	dependent variable
x_i	—	independent variables
m_i	—	regression coefficients
b	—	intercept

The regression coefficients, m_i , are measures of the linear sensitivity of y to input x_i (Draper and Smith, 1981). The variables may be the raw variables, transformed variables, or ranks. The stepwise algorithm calculates the reduction in the residual sum of squares for the independent variables in the order that gives the greatest reduction first. In the implementation of the procedure, a multiple linear regression model is fitted to the data in an iterative fashion. The procedure starts with the variable, x_i , which explains most of the variations in the model output, y . Then it adds additional variables (one at a time) to maximize the improvement in fit of the model according to the R^2 value. In the regression model, R^2 , the coefficient of determination indicates the fraction of variability in the data explained by all the variability in the model. The sequence in which the inputs are selected is a useful measure of their uncertainty importance, as is the increment in R^2 they produce. Iman and Conover (1979) also suggest the use of partial correlation coefficients, which are measures of the contribution of each uncertain

input to the output uncertainty, after removing the effects attributable to other inputs. These coefficients are useful when there are significant correlations between the inputs (Morgan and Henrion, 1990).

The regression coefficients, m_i , are the partial derivatives of the dependent variable with respect to each of the independent variables. The correlation coefficient reflects the fractions of the variability explained by the individual variables (Zimmerman, 1991). The form of the linear regression equation that gave the best fit used the log of the normalized peak dose and the log of the normalized independent variables, x_n :

$$\log\left(\frac{y}{\bar{y}}\right) = b + m_1 \log\frac{x_1}{\bar{x}_1} + m_2 \log\frac{x_2}{\bar{x}_2} + \dots + m_i \log\frac{x_i}{\bar{x}_i} + \dots + m_n \log\frac{x_n}{\bar{x}_n} \quad (4-7)$$

where b is the intercept, m_i is the coefficient of the regression, and the overbars denote the value of the quantities used for normalization (generally the mean value).

When the antilog of both sides of Eq. (4-7) is computed, the resulting equation becomes
After computing the partial derivative of both sides of Eq. (4-8) with respect to the independent variables and rearranging, the equation is reduced to

$$\frac{y}{\bar{y}} = 10^b \left(\frac{x_1}{\bar{x}_1}\right)^{m_1} \left(\frac{x_2}{\bar{x}_2}\right)^{m_2} \dots \left(\frac{x_n}{\bar{x}_n}\right)^{m_n} \quad (4-8)$$

Therefore, the normalized sensitivities are exactly the coefficients of the regression equation using the logs of the normalized peak dose and independent variables. The form of the sensitivities shown by Eq. (4-9) is the same measure calculated by the differential method of Eq. (4-11) in Section 4.1.2.

4.1.1.4 Application of the Kolmogorov-Smirnov and Sign Tests for Determining Important Parameters

The Kolmogorov-Smirnov and Sign tests differ from regression because they are nonparametric; that is, these tests do not require the assumption that the data have prespecified functional forms (e.g., normal).

$$\frac{x_i}{y} \frac{\partial y}{\partial x_i} = m_i \quad (4-9)$$

4.1.1.4.1 The Kolmogorov-Smirnov Test

The Kolmogorov-Smirnov test determines if a set of samples was drawn from a given distribution (Bowen and Bennett, 1988). This test is used to determine if an independent variable is influential by comparing the distribution of a subset of the independent variables, corresponding to the values from the highest 10 percent of the peak dose realizations, to the

theoretical distribution of that variable. If the two distributions are equivalent, peak dose is not sensitive to the variable in question. Conversely, if the distributions are different, the variable in question does have an effect on peak dose. For the present study, there are 4,000 vectors in the entire set, and the subset consists of the 400 vectors corresponding to the top 10 percent of the peak doses. The distribution of the variable in the 4,000-vector set is taken as the theoretical distribution, although it would also be possible to get the theoretical distribution directly from the generating function specified in the Latin Hypercube Sampling routine. The significance of the Kolmogorov-Smirnov test was determined at the 95-percent confidence level.

4.1.1.4.2 The Sign Test

The Sign test is another nonparametric test used to determine if a set of data corresponds to a given theoretical distribution (Bowen and Bennett, 1988). This test is used in a manner similar to the Kolmogorov-Smirnov test. In the Sign test, each observation of the input variable is represented by either a plus sign (+) or a minus sign (-), depending if the variable is greater than or less than the median value estimated by the theoretical distribution. The subset of the input parameter values corresponds to the highest 10 percent of the calculated peak doses. The subset is compared to the theoretical distribution, which, in this case, is assumed represented by the entire set of 4,000 vectors. The significance of the Sign test was determined at the 90-percent confidence level to be consistent with previous total-system performance assessment analyses. The Sign test was combined with the Kolmogorov-Smirnov test so that both tests must pass to conclude the hypothesis that the variable is significant is not rejected.

4.1.2 Differential Analysis Technique

Regression analysis of the Monte Carlo results can only determine the most influential parameters when those parameters also have large enough regression coefficients that they are distinguishable from the confounding effects of the simultaneous sampling of all other independent variables. Differential analysis determines sensitivity unambiguously because it deals with changes in only one independent variable at a time. Differential analysis determines sensitivity of parameters only at local points in parameter space and does not consider the wide range of parameter variations like the Monte Carlo method does. However, by determining local sensitivities at several points using the Monte Carlo sampling framework, the local effects can be partially mitigated.

Differential analysis tests were conducted through multiple deterministic runs in which a single input parameter was changed by a known amount compared to its initial baseline value, while all other input parameters were held at a baseline value. The baseline value for this report is a sampled value for the input parameter. The sensitivity of a performance measure (in this case, peak dose for the simulation period) to a parameter is estimated as the first derivative of the performance measure with respect to that parameter.

$$\frac{\delta y}{\delta x_i} = \frac{y(x_1, x_2, \dots, x_i + \Delta x_i, \dots, x_l)}{\Delta x_i} - \frac{y(x_1, x_2, \dots, x_i, \dots, x_l)}{\Delta x_i} \quad (4-10)$$

Usually Δx_i is relatively small (e.g., 10 percent of the parameter value). These estimates of sensitivity are local (i.e., the value of the derivative may change at different points in the sample space). To partially alleviate this concern, the derivative may be evaluated at several points in the sample space. In the analyses presented herein, the derivative is transformed in one of two ways to allow comparison of sensitivity coefficients between parameters with different units. The first transformation is described by

$$S_i = \frac{\delta y}{\delta x_i} \frac{\bar{x}_i}{\bar{y}} \quad (4-11)$$

where S_i is the dimensionless normalized sensitivity coefficient. These normalized sensitivity coefficients are in the same form as the sensitivities defined by the regression analyses with the log of the normalized variables. Because S_i does not account for the range of the input parameter, a second transformation of the derivative is also performed. In the second transformation, the derivative is multiplied by the standard deviation of the input parameter distribution. This transformation is described by

$$S_\sigma = \frac{\delta y}{\delta x_i} \sigma_{x_i} \quad (4-12)$$

Baseline cases were run with input parameter values set at seven random points within each parameter distribution range selected using the Latin Hypercube Sampling technique. Seven points may not cover the whole space, but this limitation was imposed for expediency.

4.1.3 Morris Method Technique

The Morris Method (Morris, 1991) considers $\partial y / \partial x_i$ as a random variable and uses the mean and standard deviation of the random variable to determine the sensitivity of y to x_i . A large mean value for $\partial y / \partial x_i$ implies that x_i has a large overall influence on y . A large standard deviation value for $\partial y / \partial x_i$ implies that either x_i has significant interactions with other input parameters or its influence on the y is highly nonlinear. Therefore, both the mean and standard deviation of $\partial y / \partial x_i$ are used to rank the influence of input parameters.

In the Morris method, the random variable, $\partial y / \partial x_i$, is evaluated using the current and previous values of y :

²Strictly speaking, $\partial y / \partial x_i$ should be denoted as $\Delta y / \Delta x$ because Δx_i is not necessarily a small value as in the case of differential analysis. Here, the notation is maintained to simplify the comparison with the differential analysis method.

$$\frac{\partial y}{\partial x_i} = \frac{y(x_1 + \Delta x_1, x_2 + \Delta x_2, \dots, x_i + \Delta x_i, \dots, x_l)}{\Delta x_i} - \frac{y(x_1 + \Delta x_1, x_2 + \Delta x_2, \dots, x_i, \dots, x_l)}{\Delta x_i} \quad (4-13)$$

This method is in contrast to the differential analysis method in which $\partial y/\partial x_i$ is evaluated using the current and baseline values of y , as presented in Eq. (4-10).

To compute $\partial y/\partial x_i$, a design matrix was constructed using input variables as shown:

$$\begin{bmatrix} x_1 & x_2 & \dots & x_{i-1} & x_i & x_{i+1} & \dots & x_l \\ \dots & \dots \\ x_1 + \Delta_1 & x_2 + \Delta_2 & \dots & x_{i-1} + \Delta_{i-1} & x_i & x_{i+1} & \dots & x_l \\ x_1 + \Delta_1 & x_2 + \Delta_2 & \dots & x_{i-1} + \Delta_{i-1} & x_i + \Delta_i & x_{i+1} & \dots & x_l \\ x_1 + \Delta_1 & x_2 + \Delta_2 & \dots & x_{i-1} + \Delta_{i-1} & x_i + \Delta_i & x_{i+1} + \Delta_{i+1} & \dots & x_l \\ \dots & \dots \\ x_1 + \Delta_1 & x_2 + \Delta_2 & \dots & x_{i-1} + \Delta_{i-1} & x_i + \Delta_i & x_{i+1} + \Delta_{i+1} & \dots & x_l + \Delta_l \end{bmatrix} \begin{matrix} 1 \\ \\ i \\ i+1 \\ i+2 \\ \\ l \end{matrix}$$

where $\Delta_i = \Delta x_i$. To construct this matrix, the range of each variable is subdivided into p intervals using p equally spaced points. Then x_i values are randomly sampled from these p intervals. It should be noted that each interval represents the left-most value in the original distribution. The increment, Δ , is now represented by $\Delta_i = p/2(p - 1)$.

To implement the Morris Method, the input variables are first normalized using the following transformation so the transformed input parameter, x_i^* , ranges from 0 to 1.

$$x_i^* = \frac{x_i - x_{i \min}}{x_{i \max} - x_{i \min}}, \quad i = 1, 2, \dots, l \quad (4-14)$$

To minimize the localization effect from the selection of the baseline value, seven random points in the jointly distributed sample space were selected using the Latin Hypercube Sampling technique for each random variable, $\partial y/\partial x_i$. The steps necessary to obtain the design matrix, which includes these samples, are presented in Appendix A.

4.1.4 The Fourier Amplitude Sensitivity Test Method

Both the differential analysis and the Morris Method handle one input parameter at a time. For a nonlinear computational model, input parameters are likely to have strong interactions. It would be desirable, therefore, to have a sensitivity analysis method that would investigate the influence of all input parameters at the same time. The Fourier Amplitude Sensitivity Test method (Cukier, et al., 1973) does this by first applying trigonometric transforms to the input parameters:

$$x_i = g_i(\sin \omega_i s), \quad i = 1, 2, \dots, I \quad (4-15)$$

The trigonometric transforms relate each input parameter, x_i , to a unique integer frequency, ω_i . All transforms have a common parameter, s , where $0 \leq s \leq 2\pi$. As s varies from 0 to 2π , all the input parameters vary through their ranges simultaneously at different rates controlled by the integer frequencies assigned to them through Eq. (4-15). Equally spaced values of s between 0 and 2π are chosen to generate values of x_i in Eq. (4-15). Because trigonometric transforms and integer frequencies are used in Eq. (4-15), the output, y , becomes periodic in s , and discrete Fourier analysis can be used to obtain the Fourier coefficients of y with respect to each integer frequency (Appendix B). The sensitivity of y to x_i is measured by the magnitudes of the Fourier coefficients for ω_i , and y is considered sensitive to the input parameters if the Fourier coefficients are relatively large.

The use of integer frequencies causes some errors because of aliasing among Fourier coefficients. The integer frequencies in Eq. (4-15) were chosen to minimize interactions among Fourier coefficients to ensure, as much as possible, that the particular coefficient, A_i (Appendix B), through the particular integer frequency, ω_i , represents only the influence of the corresponding input parameter, x_i . Appendix B explains how the integer frequencies are selected and how the Fourier Amplitude Sensitivity Test method is implemented. Assuming $0 \leq x_i \leq 1$, the trigonometric transformation functions used here were

$$x_i = \frac{1}{2} + \frac{1}{\pi} \arcsin[\sin(\omega_i s + r_i)], \quad i = 1, 2, \dots, I \quad (4-16)$$

where r_i and $i = 1, 2, \dots, I$ are random numbers. If the range of variation of a parameter is different from $[0, 1]$, Eq. (4-16) can be modified easily.

Currently, implementation of the Fourier Amplitude Sensitivity Test method is limited to 50 input parameters. According to Cukier, et al. (1975), as many as 43,606 realizations are needed to perform a satisfactory analysis on 50 input parameters to avoid aliasing among any four Fourier amplitudes.

4.1.5 Parameter Tree Method

The parameter tree method (Appendix C) examines total system output relative sensitivity (i.e., sensitivity of one parameter compared with another) and correlations of output to

subgroups of input parameters. In this technique, the Monte Carlo (or Latin Hypercube Sampling) method is used to examine the possible outcomes of a combination of parameter sets. Bins of realizations are constructed based on their input parameter states (e.g., all sampled input parameters above their median value).

To analyze the outputs, y_j , in Eq. (4-1) to determine the sensitivity and correlations of output, y , to subgroups of the input parameters, x_n , $n = 1, 2, \dots, N$, where $N < I$, a tree structure is developed. The parameter tree partitions input parameter space into bins, each bin forming a branch of the tree based on a partitioning (or branching) criterion. The simplest branching criterion is a classification based on parameter magnitude that treats sampled input values as either a + or a - depending on if the sampled value is greater or less than the branching criterion value.

Figure 4-2 depicts a general parameter tree. To explain Figure 4-2 using a system model, numerous realizations are generated for a given scenario class. Next, the realizations are partitioned into two subsets determined by whether the first influential parameter, x_i , is greater than or less than a specified level. Realizations with high values are all treated as + and low values as -, regardless of their position within the subset.

Let the number of realizations associated with the two branches be N_{1+} and N_{1-} . Next, the output variable is examined for realizations associated with each branch of the tree. The number of realizations with y greater than a criterion (e.g., mean) are counted for both branches. Let these numbers be L_{1+} ($L_{1+} \leq N_{1+}$) and L_{1-} ($L_{1-} \leq N_{1-}$). The difference between L_{1+}/N_{1+} and L_{1-}/N_{1-} is a measure of the sensitivity of y to x_i . The procedure is repeated in each of these two subsets with the next influential parameter to be considered (and so on) until each of the influential parameters is considered. This procedure determines 2^M bins of realizations where M is the number of influential parameters. Note that not every sampled parameter in the system model needs to be considered if a subset of the sampled parameters satisfactorily explains the system behavior of interest. Sensitivity measures similar to those explained for one parameter are developed for a set of parameters (Jarzemba and Sagar, 2000).

4.1.6 Fractional Factorial Method

Factorial methods are used in designing experiments (Box and Hunter, 1961) and more recently, in testing computer codes and models (Schmidt and Launsby, 1991). The basic approach is to sample each of the parameters at two or three fixed values (e.g., for two parameter values, perhaps choosing the 5th and 95th percentile of the distribution to represent low and high values), and then run the model to determine the response. A full-factorial design looks at all possible combinations of sampled input variables; (e.g., for two parameter values, there would have to be 2^N samples, where N is the number of variables). Because the current problem has as many as 330 sampled variables, and each run requires several minutes of computer time, a full-factorial design is infeasible.

Fractional factorial designs require fewer than 2^N runs, but may produce ambiguous results. For example, a so-called level-4 design for 330 variables requires 2,048 runs. Such a level-4 experimental design can yield results for which the main effects of all variables are distinct from each other and two-way interactions of other variables but can be confounded by some three-way or higher interactions of other variables. It is possible, however, to use other information

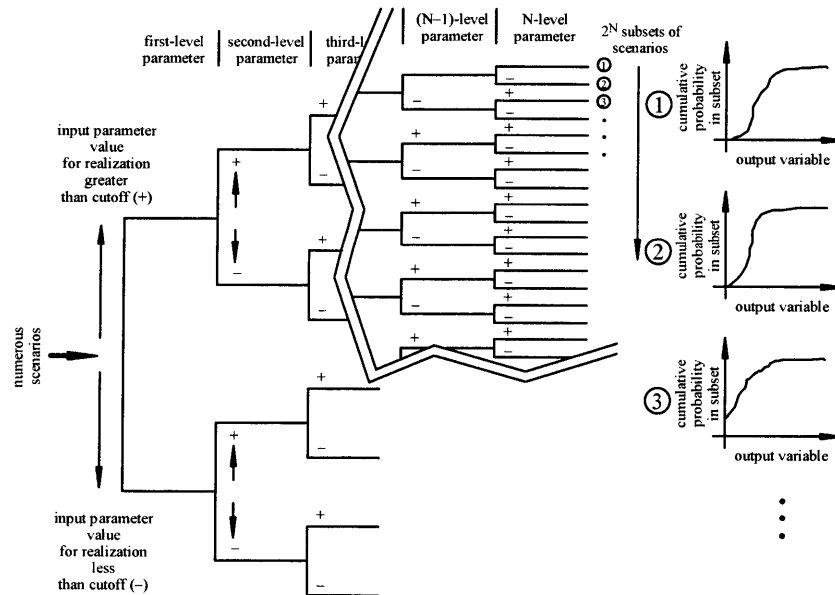


Figure 4-2. General Parameter Tree

generated in the runs to determine, in many cases, if the results of the fractional factorial design are truly measuring main effects or higher-order interactions.

In general, the fractional factorial analysis for this report was conducted in the following steps: (i) develop a fractional factorial design for all variables in the problem considering the largest number of runs that reasonably can be handled; (ii) from the results of the preliminary screening, perform an analysis of variance (ANOVA) to determine those variables that appear significant at a specified significance level; (iii) screen further the list of statistically significant variables on the basis of information other than the ANOVA results; and (iv) repeat the analyses with a refined set of variables and higher-resolution designs until results are acceptably unambiguous.

Results are presented as the F statistical parameter, which is a measure of the probability that the variable, or interaction of several variables, is significant to a specified degree of confidence, with a large F being higher confidence. The full-factorial results are also used to draw detailed tree diagrams that show explicitly the direct effect of the high and low parameters in combination on peak dose.

4.1.7 Cumulative Distribution Function-Based Sensitivity Method

The cumulative distribution function sensitivity method is a fast and accurate method for analysis of results from computationally intensive and numerically complex models with large numbers of variables. The framework of the method is based on a hybrid approach that

combines sampling that explores the parameter space and advanced reliability methods that focus the analysis at the tail of the probability distribution (Wu, 1994; Mohanty and Wu 2001). The details of this method can be found in Appendix D. The method is briefly described next.

The cumulative distribution function of a response function $Y = Y(X)$ can be represented as

$$p = F_Y(y_0) = P(Y < y_0) = \int_{\Omega} \dots \int f_x(x) dx \quad (4-17)$$

where $x = (x_1, x_2, \dots, x_L)$ is a vector of L input parameters, and Ω is the region of X for $Y(X) < y_0$.

From Eq. (4-17), the sensitivity of p with respect to a distribution parameter, θ , can be formulated as

$$\frac{\partial p}{\partial \theta} = \int_{\Omega} \dots \int \frac{\partial f_x}{\partial \theta} dx \quad (4-18)$$

which can be presented by an expectation function

$$\frac{\partial p / p}{\partial \theta / \theta} = \int_{\Omega} \dots \int \frac{\theta \partial f_x}{f_x \partial \theta} \left(\frac{f_x}{p} \right) dx = E \left[\frac{\theta \partial f_x}{f_x \partial \theta} \right]_{\Omega} \quad (4-19)$$

in which (f_x / p) is the sampling density function that corresponds to the sampling region, Ω .

The expected value in Eq. (4-19) is estimated using the samples in Ω . By applying this method for different percentiles, the sensitivities for the entire cumulative distribution function of Y can be estimated.

Based on Eq. (4-19), the two sensitivity measures developed are S_{σ_i} (standard deviation sensitivity) and S_{μ_i} (the mean sensitivity). These sensitivities are defined as

$$S_{\sigma_i} = \frac{\partial p / p}{\partial \sigma_i / \sigma_i} \quad (4-20)$$

$$S_{\mu_i} = \frac{\partial p / p}{\partial \mu_i / \sigma_i} \quad (4-21)$$

where μ_i is the mean and σ_i is the standard deviation of the random variable x_i . In Eqs. (4-20) and (4-21), the standard deviations, σ_i , are used as standardization factors to make the sensitivities dimensionless.

The function within the expectation operator in Eq. (4-19) can be computed by using standard numerical methods to differentiate the density function. The computation of the function, however, becomes difficult when the random variables x_i 's are nonnormal and correlated. The

sensitivity analysis can be simplified if the original random variables are transformed to standard normal variables using

$$u_i = \Phi^{-1}(F_{x_i}(x_i)) \quad (4-22)$$

The transformation results in generating u_i samples for each random variable for the sensitivity analyses. For correlated x_i 's, the variables produced remain correlated, and their sensitivities are correlated as well. The correlation, however, does not affect the identification of the significant variables because the adopted identification procedure was based on testing whether a variable has a zero sensitivity. The hypothesis can be tested without using the correlations.

By applying Eq. (4-22) to define the joint probability distribution function in Eq. (4-19), the sensitivities in Eqs. (4-20) and (4-21) can be simplified to (Wu, 1994).

$$S_{\sigma_i} = E[u_i^2]_{\Omega} - 1 \quad (4-23)$$

$$S_{\mu_i} = E[u_i]_{\Omega} \quad (4-24)$$

These sensitivities can be used to identify important variables. Note that each sampled parameter is treated as a random variable and is represented through x_i . Two new sensitivity measures that are consistent with the peak expected dose regulatory criterion are $\bar{S}_{Y_{\mu}}$ and $\bar{S}_{Y_{\sigma}}$. These two measures are referred to as performance mean-based measures. These measures were originally developed in an internal research and development project at Southwest Research Institute and have been applied in this report to the performance assessment results. These two sensitivity measures can be expressed as

$$\bar{S}_{Y_{\mu}} = \partial\mu_Y / \partial\mu_{x_i} = \frac{1}{k} \sum_{j=1}^k [u_i Y]_j \quad (4-25)$$

and

$$S_{Y_{\sigma}} = \partial\mu_Y / \partial\sigma_{x_i} = \frac{1}{k} \sum_{j=1}^k [(u_i^2 - 1)Y]_j \quad (4-26)$$

To implement the method, the following steps are followed. A value, K , for random sampling is selected. Based on K , confidence limits are constructed for $\bar{S}_{Y_{\sigma}}$, $\bar{S}_{Y_{\mu}}$, or other sensitivity measures for non-participating random variables. Then K realizations of the response variable are computed based on the K sets of random input parameters. The K realizations of sampled values are then sorted and divided into a variety of regions. In each region, each set of an input parameter that corresponds to the realizations of the response variable is identified. For each

input parameter, the identified samples are mapped to standardized normal variables. The standardized normal samples are used to compute sensitivities. The computed sensitivities are compared with the confidence limits to identify the influential random variables. If the calculated sensitivities are outside the acceptance limits (Mohanty and Wu, 2001), the alternative hypotheses are accepted that the sensitivities are greater than zero at the corresponding confidence level. If the calculated point lies well outside the limits, the variable is likely important. In such cases, the magnitudes of the sensitivities may be used to rank the important variables. The number of samples can be adaptively increased to reduce the sampling error and identify the important variables and their ranking with confidence.

4.2 Sensitivity Analysis Results from Monte Carlo Runs

This section presents the sensitivity and uncertainty analyses results generated using methods described in Section 4.1. Statistical results of the 4,000-vector Monte Carlo runs, which are treated separately from the differential analysis, Morris method, and the Fourier amplitude sensitivity test method, will be presented first in this section. A comparison of the results of the different methods will be presented in subsequent sections.

4.2.1 Procedure for Screening Monte Carlo Sensitivity Results

The Monte Carlo simulation results were screened to estimate which variables were likely to be influential and provide an estimate of the sensitivity coefficients.

The first part of the analyses involved preliminary screening. This stage of the analyses used a variety of techniques to determine in gross terms if an independent variable affects dose. All variables that passed any of the screening tests were included in the subsequent analyses. For all analyses, zero values of dose were eliminated from the data sets because they cannot be log transformed. For each simulation period (10,000 or 100,000 years), the following procedures were employed:

- t-statistic test for single linear regression of dose versus each variable
 - Raw variables
 - Rank of variables
- Stepwise linear regression
 - Normalized variables
 - Log of normalized variables
 - Ranks of variables
- Nonparametric tests
 - Kolmogorov-Smirnov test and Sign test combined

4.2.1.1 Sensitivity Results from Monte Carlo Analysis

This section presents the sensitivity results from the statistical analysis of a 4,000-vector Monte Carlo analysis of the basecase for 10,000- and 100,000-year simulation periods. The screening and regression analyses are summarized in Tables 4-1 and 4-2 for the 10,000- and 100,000-year simulation periods. The column headings in Tables 4-1 and 4-2 have the following explanations:

Table 4-1. Ranks of Significant Variables for 10,000 Years from Statistical Tests. Appendix E Provides a Description of the Variables.							
Variable Name	KS + Sign Test	t-Norm	Step Raw	Step Rank	t-Rank	Step Lnorm	Overall Rank
AAMAI@S	5	5	–	4	4	7	7
MAPM@GM	–	–	–	10	–	15	–
FOC-R	10.5	10	9	5	5	6	8
FOCTR	7	9	8	3	3	8	6
TempGrBI	–	–	–	7	8	10	–
DSFailTi	3.5	4	4	1	1	4	1
WPFlowMF	2	8	6	2	2	1	3
SbArWt%	3.5	1	1	9	6	3	2
WP-Def%	6	2	2	8	9	5	5
PSFDM1	1	3	3	6	7	2	4
Mprm_TSw	8	12	–	–	10	–	–
ARDSAVNp	12	–	–	4	–	–	–
DTFFAVIF	10.5	6	5	11	12	9	9
WPRRG@20	9	7	7	12	15	11	10
gen_dwc5	–	13	11	–	–	–	–
genKDsl	–	11	10	–	–	–	–

- **Variable Name**—The abbreviated name of the independent variable appearing potentially sensitive in any of the screening analyses. A complete list of the variable names is in Appendix E.
- **Kolmogorov-Smirnov + Sign Test**—The rank of variables that passed both the Kolmogorov-Smirnov and Sign tests.
- **t-Norm**—The rank of the t-value of a single-variable regression of the normalized variables greater than 1.96 (95-percent confidence level).
- **Step Raw**—The rank of the variables from stepwise regression of the normalized variables.
- **Step Rank**—The rank of the variables from stepwise regression of the ranks of the variables.

Table 4-2. Ranks of Significant Variables for 100,000 Years from Statistical Tests

Variable Name	K-S+Sign Test	t-Norm	Step Raw	Step Rank	t-Rank	Step Lnorm	Overall Rank
AAMAI@S	8.5	4	–	–	4	8	8
MAPM@GM	2.5	–	–	11	18	9	9
AA_1_1	–	3	3	3	3	3	3
WPFlowMF	11	22	9	5	7	4	6
SbArWt%	4	2	2	2	1	1	2
PSFDM1	1	1	1	1	2	2	1
InitRSFP	–	10	7	9	–	15	–
Solbl-Np	15.5	14	8	8	–	10	–
SFWt%S44	–	17	12	13	–	–	–
SFWt%C2	–	25	–	–	16	17	–
MPrm_TSw	–	8	–	–	6	–	–
FPrs_CHz	–	18	–	15	–	–	–
IPPFSTFF	12.5	11	10	11	19	14	–
ARDSAVAm	6	16	–	–	9	–	–
ARDSAVNp	2.5	6	–	–	5	5	4
ARDSAV_U	9.5	15	–	–	10	–	–
ARDSAVPu	5	5	4	–	8	–	7
ARDSAVRa	14	29	–	14	–	–	–
DTFFAVIF	7.5	7	5	6	11	7	5
WPRRG@20	14	9	6	7	17	13	–
PWPRRG20	–	–	–	–	15	12	–
gen_ifi	16.5	12	11	10	13	11	10
genovitC	–	27	–	16	–	19	–

- t-Rank—The rank of the t-value of a single-variable regression of the rank-transformed variables greater than 1.96 (95-percent confidence level).
- Step Lnorm—The rank of the variables from stepwise regression of the log of the normalized variables.
- Overall Rank—The reciprocal ranks of the six sensitivity tests. For each variable, take the reciprocal of each non-zero rank from each of the 6 tests and sum over all 6 tests. The overall rank is the rank of the sum of the reciprocals.

Results for 10,000-Year Simulation Period

For each of the statistical tests, the resulting regression coefficients were sorted; the highest values received the best scores. Parameter sensitivities that ranked below the 95th percentile, either as t-statistic or F-statistic, were eliminated from consideration (rank = ∞). The overall rank for a variable consisted of two parts: (i) the number of times the variable appeared in the six tests with a finite rank (0 to 6) and (ii) the sum of the reciprocal of the rank for the six tests. A variant of the second test replaced the rank with its square, but the results did not change the conclusions. The top 10 variables in order of apparent importance from statistical measures are (i) DSFailTi, (ii) SbArWt%, (iii) WPFlowMF, (iv) PSFDM1, (v) WP-Def%, (vi) FOCTR, (vii) AAMAI@S, (viii) FOC-R, (ix) DTFFAVIF, and (x) WPRRG@20. The description of these variables can be found in Appendix E.

Results for 100,000-Year Simulation Period

Like with the 10,000-year results, the regression results were combined to give a single overall score that included the number of times the variable appeared in the six tests and the sum of the reciprocal of the rank for the six tests. The top 10 variables in order of apparent importance are (i) PSFDM1, (ii) SbArWt%, (iii) AA_1_1, (iv) ARDSAVNp, (v) DTFFAVIF, (vi) WPFlowMF, (vii) ARDSAVPu, (viii) AAMAI@S, (ix) MAPM@GM, and (x) WPRRG@20.

Regression Results for Extrusive Volcanism Parameters

The sensitivity analyses for volcanism parameters were treated separately because, in most cases, extrusive volcanic doses would be much larger than nonvolcanic groundwater doses, and, therefore, the groundwater doses can be neglected. It is important to note that the sensitivity analyses for igneous activity parameters in the report use conditional dose (i.e., does not factor in the volcanism event probability). The influential parameters may be different if the igneous activity event probability is accounted for. With probability weighting, the large ground surface dose with low probability can be comparable to small groundwater dose with high probability. Several groundwater dose parameters may then be more important than the ground surface dose parameters when the igneous activity contribution to the peak expected dose is reduced.

The extrusive volcanism model was run for 1,000 Latin Hypercube Sampling vectors, varying the parameters VC-Dia, WindSpd, VE-Durat, VE-Power, AshMnPLD, ABMLAAsh, and AMLASoil. Because there were only seven variables, only a stepwise regression of the raw variables and single parameter t-test were run for sensitivity, and both gave the same results. The tests showed six significant parameters in the following order: VE-Power, VC-Dia,

WindSpd, VE-Durat, ABMLAAsh, and AshMnPLD. The variable AMLASoil was below the 5-percent significance level for inclusion.

4.3 Analysis of Sensitivity from Nonparametric Methods

4.3.1 Results from Differential Analyses

Differential analyses were performed using the TPA Version 4.1 code with the basecase. A total of 330 input parameter values were perturbed for each series. The input parameters perturbed are the sampled parameters in the TPA code.

Seven random sets (considered adequate for obtaining a stable average) of input parameters were evaluated. Perturbations to the parameters in these random sets were selected so that the parameter values were maintained in their defined ranges. The selection of random values yields calculations similar to one realization of a probabilistic TPA code run. The perturbations (1 percent) are applied to the baseline (i.e., local) parameter value. The percentage is that of the range of the distribution [i.e., (maximum value - minimum value) × 0.01] rather than that of the baseline value.

In the TPA Version 4.1 code, transport through the unsaturated zone stratigraphic units is not considered for units where the groundwater residence time is less than 10 years or 10 percent of the residence time for the entire unsaturated zone below the repository (Mohanty and McCartin, 1998). Differential analyses will result in the peak dose showing no sensitivity to parameters that describe unsaturated zone properties in those stratigraphic units excluded from the transport calculations. For example, when all parameters were set at their mean values, the unsaturated zone portion of NEFTRAN was omitted for a majority of the subareas. Thus, sampled unsaturated zone flow and transport parameters did not show any sensitivity in these calculations. When the transport times in the subunits of the unsaturated zone that control the bulk of the unsaturated zone transport are short, however, it is unlikely that any of the unsaturated zone parameters would have a substantial effect on the peak dose, therefore the aforementioned exclusion of stratigraphic units should not significantly affect results of the differential analyses.

For all sets of the random parameters, the waste packages did not fail from either seismicity or corrosion in the 10,000-year simulated period but did fail from corrosion within the 100,000-year simulated period. The baseline dose values in these cases are solely caused by initially defective waste packages.

The results of the differential analysis are shown for simulation periods of 10,000 and 100,000 years in Tables 4-3 and 4-4 for the basecase. The top 10 parameters are based on the mean of S_{σ} as shown in Eq. (4-12). These sensitivities were calculated using the arithmetic mean of the derivative weighted by the standard deviation of the input parameter. This measure was used to sort the input parameters in descending order because it reflects both the absolute value of peak dose and the uncertainty in the independent variables. This sensitivity measures the response of peak dose to each of the independent variables weighted by their standard deviation. The standard deviations are determined by the parameter range and distribution used in the Monte Carlo analyses. This measure considers the magnitude of the change in peak dose and the uncertainty in the independent variables. For comparison, the normalized

Table 4-3. Top 10 Influential Parameters from Statistical and Nonstatistical Analyses for the 10,000-Year Simulation Period

Rank	Statistics/ Regression	Differential Analysis	Fractional Factorial	Morris Method	Fourier Amplitude Sensitivity Test Method	Parameter Tree Method	Cumulative Distribution Function Sensitivity
1	DSFailTi	WPFlowMF	DSFailTi	AAMAI@S	DSFailTi	PSFDM1	WPFlowMF
2	SbArWt%	PSFDM1	WPFlowMF	MAPM@GM	gen_PUSF	WPFlowMF	PSFDM1
3	WPFlowMF	DSFailTi	FOCTR	DSFailTi	WPRRG@20	SbArWt%	SbArWt%
4	PSFDM1	SbArWt%	SbArWt%	WPFlowMF	gen_ifi	DSFailTi	WP-Def%
5	WP-Def%	genKDsTc	WP-Def%	gen_PUSF	ARDSAVNp	FOCTR	AAMAI@S
6	FOCTR	SFWt%I2	PSFDM1	WPRRG@20	InvMPerm	*Chlorid	DSFailTi
7	AAMAI@S	AAMAI@S	AAMAI@S	ARDSAVNp	MPrm_PPw	Solbl-Np	DTFFAVIF
8	FOC-R	SFWt%I1	WPRRG@20	IPPFSTFF	AAMAI@S	gen_hirP	WPRRG@20
9	DTFFAVIF	SFWt%I10	DTFFAVIF (*)	PSFDM1	SFWt%I2	SSMOV404	ARDSAVNp
10	WPRRG@20	WPRRG@20	InvMPerm (*)	SbArWt%	IPPFSTFF	AAMAI@S	FOCTR

*These parameters are included for reference, but are below the 5-percentile cutoff from analysis of variance probability.

Abbreviation	Description	Abbreviation	Description
AAMAI@S	ArealAverageMeanAnnualInfiltrationAtStart[mm/yr]	PSFDM1	Preexponential_SF Dissolution Model 2
ARDSAVNp	AlluviumMatrixRD_SAV_Np	SbArWt%	SubAreaWetFraction
DSFailTi	DripShieldFailureTime[yr]	SFWt%I1	SFWettedFraction_Initial 1
DTFFAVIF	DistanceToTuffAlluviumInterface[km]	SFWt%I2	SFWettedFraction_Initial 2
FOC-R	FractionOfCondensateRemoved[1/yr]	SFWt%I10	SFWettedFraction_Initial 10
FOCTR	FractionOfCondensateTowardRepository[1/yr]	SFWt%S17	SFWettedFraction_SEISMO1_7
gen_hirP	HomeIrrigationRatePB[in/yr]	Solbl-Np	SolubilityNp[kg/m3]
gen_ifi	InterceptionFraction/Irrigate	SSMOV404	VerticalExtentOfRockFall4_4[m]
gen_PUSF	PlantUptakeScaleFactor	TempGrBI	TemperatureGradientInVicinityOfBoilingIsotherm[K/m]
genKDsTc	KD_Soil_Tc[cm3/g]	WP-Def%	DefectiveFractionOfWPs/cell
InvMPerm	InvertMatrixPermeability[m^2]	WPFlowMF	WastePackageFlowMultiplicationFactor
IPPFSTFF	ImmobilePorosityPenetrationFraction_STFF	WPRRG@20	WellPumpingRateAtReceptorGroup20km[gal/day]
MAPM@GM	MeanAveragePrecipitationMultiplierAtGlacialMaximum	*Chlorid	ChlorideMultFactor
MPrm_PPw	MatrixPermeability_PP2 [m2]		
MPrm_TSw	MatrixPermeability_TSw [m2]		

4-20

Table 4-4. Top 10 Influential Parameters from Statistical and Nonstatistical Analyses for the 100,000-Year Simulation Period

Rank	Statistics/ Regression	Differential Analysis	Fractional Factorial	Morris Method	Fourier Amplitude Sensitivity Test Method	Parameter Tree Method
1	PSFDM1	WPFlowMF	PSFDM1	ARDSAVNp	PSFDM1	PSFDM1
2	SbArWt%	PSFDM1	WPFlowMF	WPRRG@20	gen_ifi	SbArWt%
3	AA_1_1	ARDSAVNp	ARDSAVNp	gen_ifi	InvMPerm	ARDSAVNp
4	ARDSAVNp	SbArWt%	SbArWt%	DTFFAVIF	SFWt%C9	AA_1_1
5	DTFFAVIF	genKDsTc	SFWt%C2	MPrm_PPw	gen_PUSF	WPFlowMF
6	WPFlowMF	WP-Def%	gen_ifi	InvMPerm	WPFlowMF	SSMO-RPR
7	ARDSAVPu	AA_1_1	WPRRG@20	gen_PUSF	ARDSAVNp	ARDSAVAm
8	AAMAI@S	Solbl-Np	AAMAI@S	AAMAI@S	WPRRG@20	SFWt%S29
9	MAPM@GM	DSFailTi	—	genIvitC	SFWt%C1	AAMAI@S
10	WPRRG@20	gen_AUSF	—	InitRSFP	genIvitC	MAPM@GM

4-21

<u>Abbreviation</u>	<u>Description</u>	<u>Abbreviation</u>	<u>Description</u>
AA_1_1	AA_1_1[C/m2/yr]	InvMPerm	InvertMatrixPermeability[m^2]
AAMAI@S	ArealAverageMeanAnnualInfiltrationAtStart[mm/yr]	MPrm_PPw	MatrixPermeability_PP2_[m2]
ARDSAVNp	AlluviumMatrixRD_SAV_Np	PSFDM1	Preexponential_SF Dissolution Model2
DSFailTi	DripShieldFailureTime[yr]	SbArWt%	SubAreaWetFraction
DTFFAVIF	DistanceToTuffAlluviumInterface[km]	SFWt%C1	SFWettedFraction_Corrosion_1
gen_AUSF	AnimalUptakeScaleFactor	SFWt%C9	SFWettedFraction_Corrosion_9
gen_ifi	InterceptionFraction/Irrigate	Solbl-Np	SolubilityNp[kg/m3]
gen_PUSF	PlantUptakeScaleFactor	WP-Def%	DefectiveFractionOfWPs/cell
genKDsTc	KD_Soil_Tc[cm3/g]	WPFlowMF	WastePackageFlowMultiplicationFactor
genIvitC	LeafyVegetableIrrigationTimeCB[mo/yr]	WPRRG@20	WellPumpingRateAtReceptorGroup20km[gal/day]
InitRSFP	InitialRadiusOfSFParticle[m]		
	Note new entries in table ARDSAVPu, SFWt%C2, MAPM@GM		

sensitivity measure, S_i , in Eq. (4-11) is a relative sensitivity where the slope is scaled by the local values of dose and the independent variable. Therefore, S_i does not depend on whether the baseline dose is small or large, but only on the change in dose relative to the change in the independent variable.

4.3.2 Results from the Morris Method

The Morris Method was applied to the TPA Version 4.1 code results from the basecase scenario. A total of 330 input parameters were investigated. A $2,317 \times 330$ matrix was generated and used in sampling input parameters for the 2,317 $[(330 + 1) \times 7]$ realizations, which produced 7 samples for each $\partial y / \partial x_i$. These samples were used to calculate the mean and standard deviation for each $\partial y / \partial x_i$. Seven samples were chosen to be consistent with the differential analysis method.

Figures 4-3 and 4-4 show graphs for the values of mean (abscissa) and standard deviation (ordinate) of $\partial y / \partial x_i$ values for the 10,000- and 100,000-year simulated periods. As described earlier, the greater the distance $\partial y / \partial x_i$ for parameter x_i is from zero, the more influential parameter x_i is. A point with large values of both mean and standard deviation suggests that the corresponding input parameter has a strong nonlinear effect itself and also strong interactive effects with other parameters on the output.

The top 10 most influential input parameters identified by the Morris Method are listed in Table 4-3 for the 10,000-year simulation period and in Table 4-4 for the 100,000-year simulation period, where each parameter was normalized according to Eq. (4-14). For the 10,000-year simulation period, the top 10 parameters are (i) AAMAI@S, (ii) MAPM@GM, (iii) DSFailTi, (iv) WPFlowMF, (v) gen_PUSF, (vi) WPRRG@20, (vii) ARDSAVNp, (viii) IPPFSTFF, (ix) PSFDM1, and (x) SbArWt%. The majority of these parameters are flow parameters that control the volume of water contacting spent nuclear fuel and the time at which the contact begins. The remaining parameters are related to calculations regarding the spent nuclear fuel dissolution rate, transport properties in alluvium, dilution of radionuclide concentrations, and plant uptake in the biosphere.

For the 100,000-year simulated period, 3 of the parameters are related to biosphere calculations, and 2 are flow rate parameters that also were ranked for the 10,000-year simulated period. The parameter WPRRG@20 {well pumping rate for farming receptor group located at or beyond 20 km [12.4 mi] from Yucca Mountain} appears in both 10,000- and 100,000-year simulated periods, as well as some parameters related to transport properties in alluvium and spent nuclear fuel dissolution. The sensitivity of dose to the well pumping rate may no longer be relevant because this value is fixed at $10,140 \text{ m}^3/\text{day}$ [$3,000 \text{ acre-ft/yr}$] in the final regulation.

The most influential parameters from the Morris Method analysis for the igneous activity disruptive event scenario in the 10,000-year simulated period are shown in Table 4-5. The top ten influential parameters identified by the Morris method are (i) ABMLAAsh, (ii) WindSpd, (iii) VC-Dia, (iv) VE-Power, (v) VE-Durat, (vi) VEROI-Tn, (vii) AshMnPLD, (viii) VEi/e-R#, (ix) SFWt%V0, and (x) PSFDM1. The results contrast with the regression-method-based results presented in Section 4.2.1.1 because the latter section used only the peak dose from direct releases resulting from extrusive igneous activity. The top six parameters identified by this

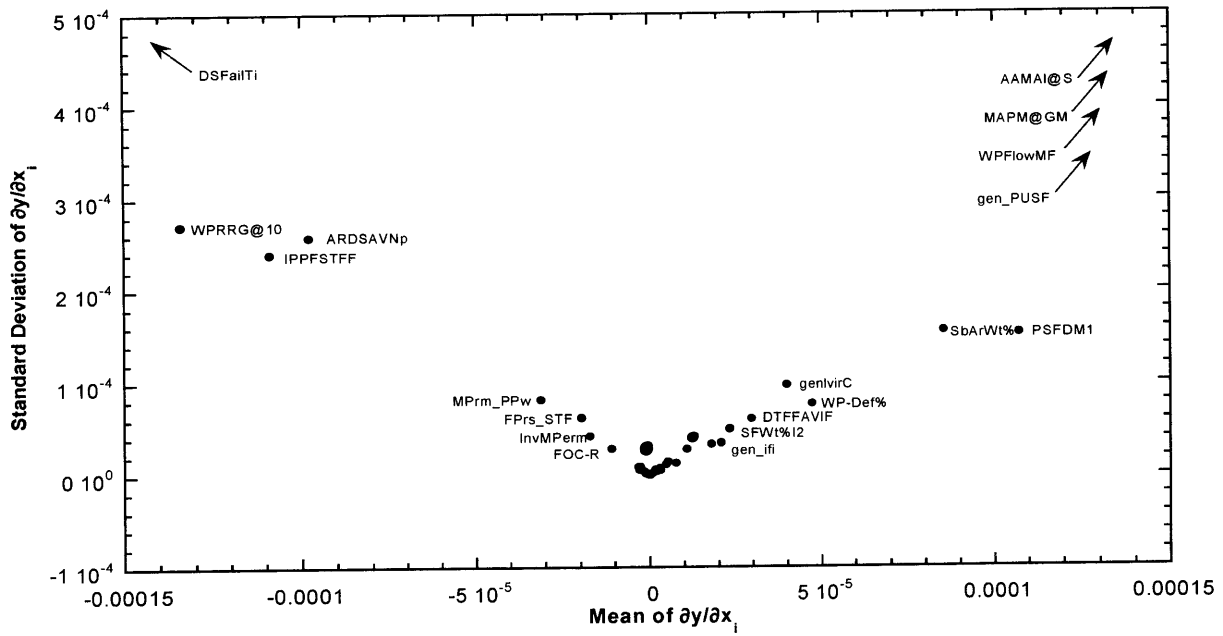


Figure 4-3. Results from the Morris Method from the Basecase for the 10,000-Year Simulation Period. Arrows Indicate the Associated Points Are Outside the Graph.

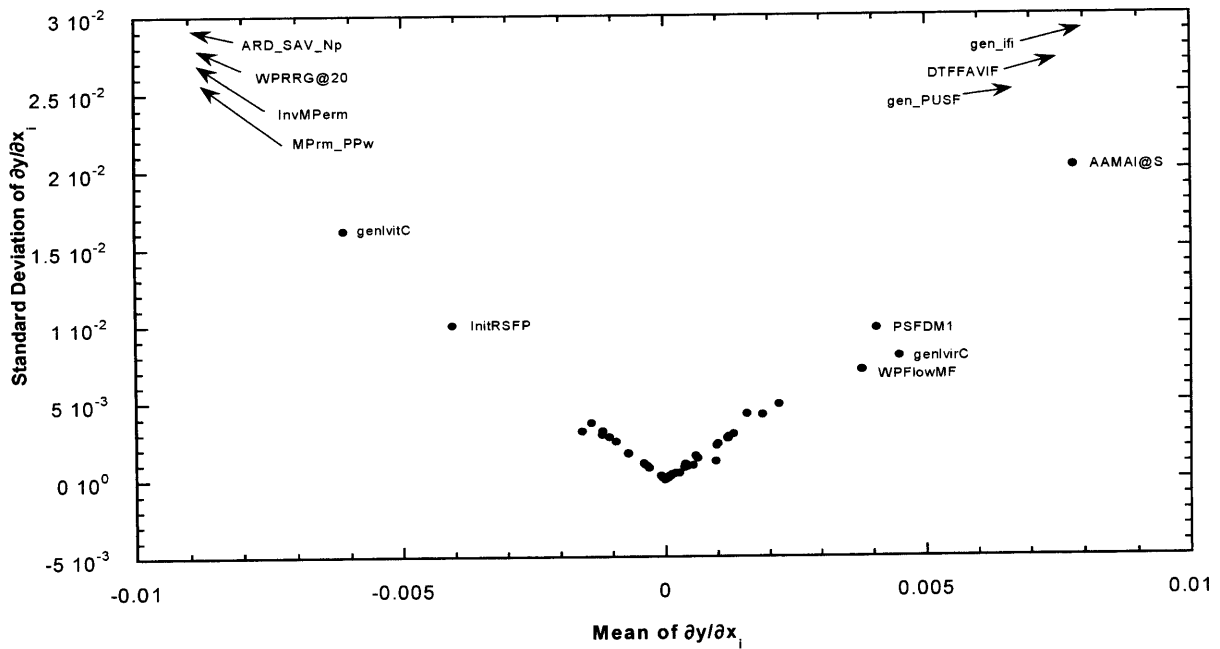


Figure 4-4. Results from the Morris Method from the Basecase for the 100,000-Year Simulation Period. Arrows Indicate the Associated Points Are Outside the Graph.

Table 4-5. Top 20 Influential Parameters Identified by the Morris Method in the Igneous Activity Case Contributing to Both Groundwater and Ground Surface Releases

Rank	Parameter Identification	Parameter Abbreviation	Parameter Description
1	329	ABMLAAsh	Mass of Soil in the Air above a Fresh Volcanic Ash blanket
2	325	WindSpd	Wind speed
3	322	VC-Dia	Conduit diameter
4	327	VE-Power	Volcanic Event Power
5	326	VE-Durat	Volcanic Event Duration
6	317	VEROI-Tn	Time Of Next Volcanic Event
7	328	AshMnPLD	Relative Size of Ash and Spent Nuclear Fuel Particulates from a Volcanic Event
8	318	VEi/e-R#	Random Number to Determine Volcanic Event Type
9	80	SFWt%V0	Spent Nuclear Fuel Wet Fraction for Volcanic Events
10	63	PSFDM1	Preexponential Factor for Spent Nuclear Fuel Dissolution Rate from ($\text{mgm}^{-2}\text{d}^{-1}$)
11	64	InitRSFP	Initial radius of spent nuclear fuel particle—affects spent nuclear fuel alteration rate and transport out of a failed waste package in EBSREL
12	239	WPRRG@20	Well pumping rate for residential receptor group located less than 20 km [12.4 mi] from Yucca Mountain
13	61	SbArWt%	Subarea Wet Fraction
14	223	IPPFSTFF	Effective fraction of saturated rock matrix accessible to matrix diffusion; during the time scale for transport from source to receptor, used to calculate effective immobile porosity and matrix diffusion mass-transfer rate coefficient in NEFTRAN
15	4	FOC-R	Fraction of water condensate removed in each reflux3 time step

Table 4-5. Top 20 Influential Parameters Identified by the Morris Method in the Igneous Activity Case Contributing to Both Groundwater and Ground Surface Releases (continued)

Rank	Parameter Identification	Parameter Abbreviation	Parameter Description
16	1	AAMAI@S	Mean areal average infiltration into the subsurface at the start of a TPA Version 4.1 code run
17	244	gen_ifi	Irrigation interception fraction
18	12	DSFailTi	Time of failure of the dripshield
19	235	FPrs_STF	Fracture of saturated tuff porosity
20	203	MPrm_CHv	Calico Hills–nonwelded vitric matrix permeability

method are identical to the top six identified by the statistical method in Section 4.2.1.1, though the ranking is different. As mentioned earlier, these six parameters pertain to dose from ground surface release caused by extrusive igneous events. The Morris Method also identified SFWt%V0 and PSFDM1 among the top 10 parameters, which are relevant to dose from groundwater release from intrusive igneous activity. Table 4-5 also shows that most parameters among the top 10 parameters from the basecase also appear as important among the top 20 parameters in the conditional igneous activity dose calculation. It is important to note that the sensitivity analyses for igneous activity parameters used conditional dose (i.e., did not factor in the volcanism probability). The influential parameters may be different if the igneous activity event probability is accounted for, that is, several groundwater parameters become more important (see explanation in Section 4.2.1.1).

For comparison purposes, sensitivities were computed using two performance measures: (i) the contribution of each realization to the overall peak risk (the overall peak risk will occur at a single point in time, and each realization will contribute to this single overall peak) and (ii) the peak dose from each realization. The relative sensitivity for the top 20 influential parameters identified using these 2 performance measures is presented in Figures 4-5 and 4-6. The relative sensitivity on the y-axis shows the relative influence the parameter has on the output variability. Although many similarities are identified in the results comparing both methods, the few differences provide useful insights. Four variables (SFWt%I10, SFWt%I5, SFWt%I3, and SFWF1 in Figure 4-6) do not appear in the sensitivity analysis of dose corresponding to the peak expected dose shown in Figure 4-5. Four parameters (genlvirc, Morm-PPw, DTFFAVIF, and Fprs-STF in Figure 4-5) identified by the first method do not appear in the list identified by the second method. The rankings from the two methods were also somewhat different. For example, parameter DSFailTi in Figure 4-5, which appears as the 3rd most important parameter in the 1st method, is ranked 20th using the second method (Figure 4-6). No change in rank was observed only for AAMAI@S and MAPM@GM, the top two parameters in both methods.

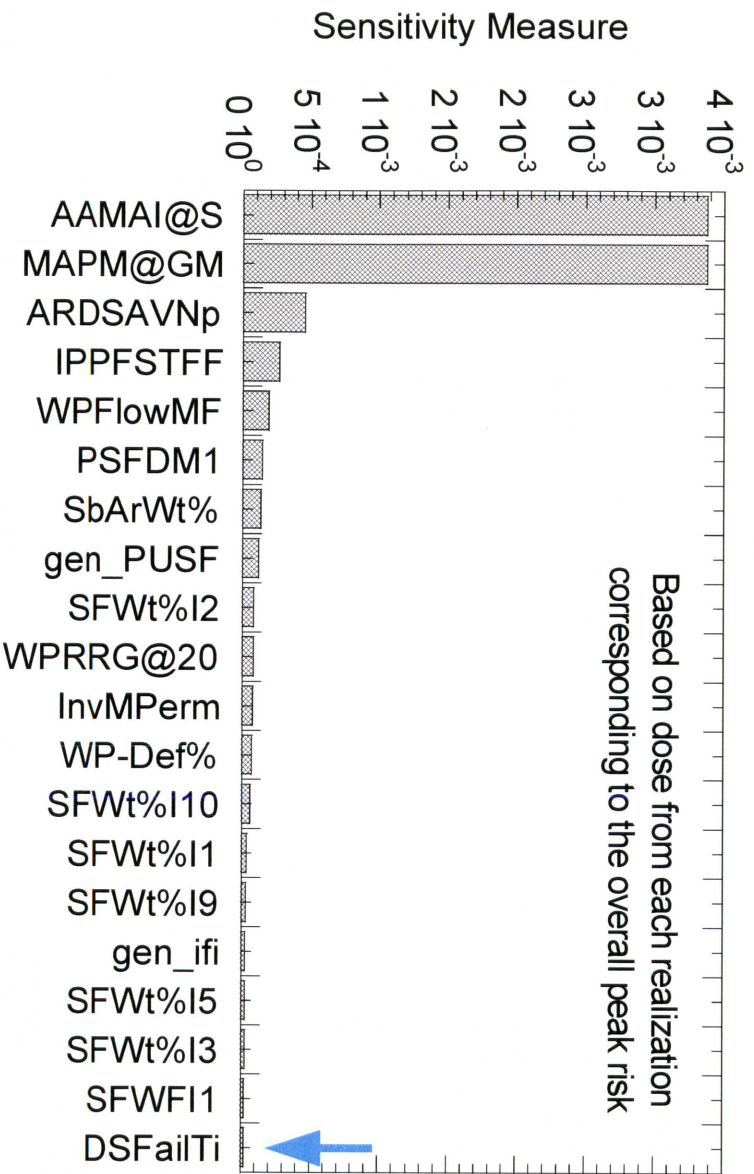


Figure 4-5. Influential Parameters Identified Using the Dose from Each Realization Corresponding to the Time the Peak Expected Dose Occurs

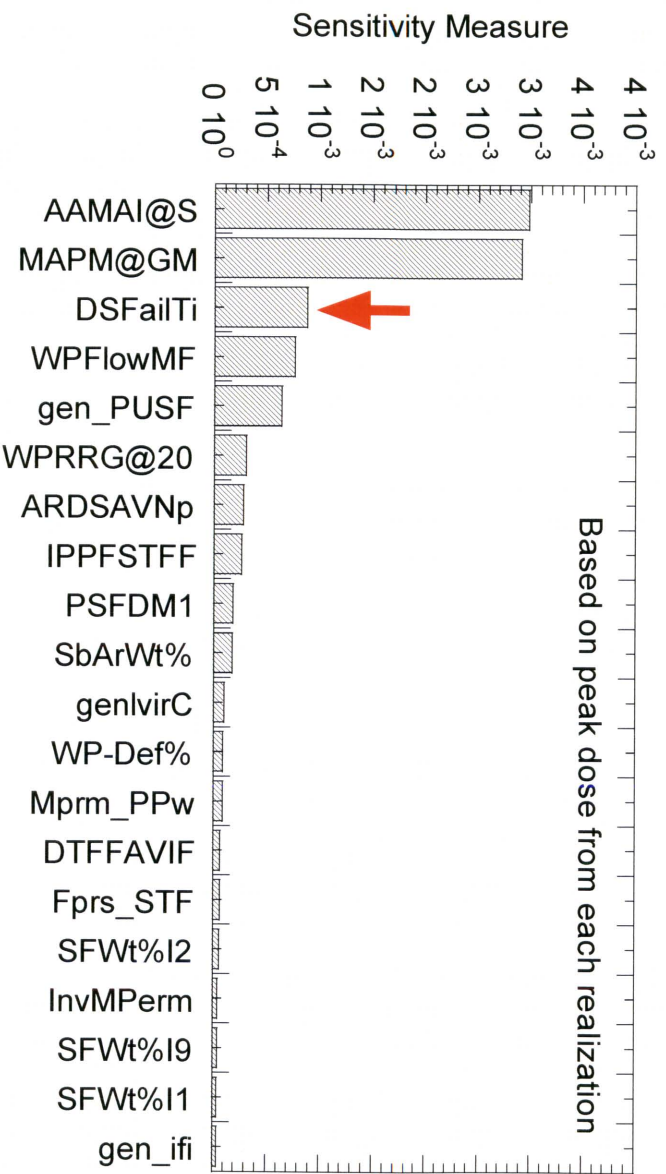


Figure 4-6. Influential Parameters Identified Using the Peak Dose from Each Realization

In Figure 4-5 and 4-6, the variable DSFailTi ranks high in importance for peak of the realizations and low in importance for time of the peak expected dose. When using the criterion for peak of the expected dose, variables like DSFailTi that determine mainly the time of the peak dose for a realization will show less sensitivity than variables that determine mainly the amplitude of the peak. This is because the peak of the expected dose curve is sensitive to the timing of the peaks from the individual realizations that make up the mean (i.e., a parameter that causes the peaks to be dispersed in time leads to non-alignment that when averaged over the realizations, leads to a lower peak of the expected dose curve).

4.3.3 Results from the Fourier Amplitude Sensitivity Test Method

In this report, the Fourier amplitude sensitivity test method is applied to the 20 parameters identified by the Morris Method presented in Table 4-6 for the two simulation periods. For the 20 parameters, only 4,174 realizations are needed to avoid aliasing among any 4 Fourier amplitudes (Appendix B). To account for the range of an input parameter, each Fourier amplitude was multiplied by the standard deviation of the corresponding input parameter as defined by Eq. (4-12). Ranking for the top 10 parameters using the Fourier amplitude sensitivity test method is listed in Tables 4-3 and 4-4 for the 10,000- and 100,000-year simulation periods.

It should be noted that the analysis presented here is limited by the initial selection of 20 parameters from the Morris Method analysis. Thus, some influential parameters may be identified by other nonstatistical methods but not by the Fourier amplitude sensitivity test method.

4.3.4 Results from the Parameter Tree Method

Figure 4-7 shows the parameter tree based on median values as the branching criterion. A set of 4,000 realizations of the TPA Version 4.1 code was used, and 330 input parameters were sampled for the basecase. In Figure 4-7, column A is the number of realizations of peak dose above the overall median value (i.e., of the 4,000 realizations) in that bin. For example, row 3 in column A shows that 127 of 4,000 realizations have 4 of the important parameters with values above the median, and 1, DSFailTi is below the median. Of these 127 realizations, 123 have peak doses above the median value for all 4,000 realizations $\{3.63 \times 10^{-9}$ Sv/yr $[3.63 \times 10^{-7}$ rem/yr]. Column B shows that for these 127 realizations, the mean value of peak dose is $\{5.57 \times 10^{-6}$ Sv/yr $[5.57 \times 10^{-4}$ rem/yr], and column C shows these 127 realizations accounted for 33.4 percent of the population mean of peak doses. This analysis reinforces the notion that these are indeed influential parameters because slightly less than 3.2 percent of the realizations account for more than 33 percent of the mean from all realizations.

Column D shows an importance factor, R , which is determined as the ratio of the contribution to the overall mean from realizations in that bin to the average contribution of the same number of realizations to the overall mean, that is,

$$R = \frac{\text{fractional contribution to the overall mean dose (Column C)}}{\left(\frac{\text{number of realizations in bin}}{\text{total number of realizations}} \right)} \quad (4-27)$$

$$= \frac{\text{mean peak dose in bin (Column B)}}{\text{mean peak dose over all realizations}}$$

Table 4-6. Morris Results Derived from Peak Dose and Dose Corresponding to Peak Expected Dose for 10,000- and 100,000-Year Simulation Periods

Rank	10,000 Years		100,000 Years	
	Based on Peak Dose	Based on Dose Corresponding to Peak Expected Dose	Based on Peak Dose	Based on Dose Corresponding to Peak Expected Dose
1	AAMAI@S (*)	AAMAI@S	ARDSAVNp (*)	DTFFAVIF
2	MAPM@GM	MAPM@GM	WPRRG@20	WPRRG@20
3	DSFailTi	ARDSAVNp	gen_ifi	gen_ifi
4	WPFlowMF	IPPFSTFF	DTFFAVIF	ARDSAVNp
5	gen_PUSF	WPFlowMF	MPrm_PPw	IPPFSTFF
6	WPRRG@20	PSFDM1	InvMPerm	InvMPerm
7	ARDSAVNp (*)	SbArWt%	gen_PUSF	MPrm_PPw
8	IPPFSTFF	gen_PUSF	AAMAI@S (*)	AAMAI@S
9	PSFDM1	SFWt%l2	genIvirC	genIvirC
10	SbArWt% (*)	WPRRG@20	InitRSFP	APrs_SAV
11	genIvirC	InvMPerm	PSFDM1	MKDCHvNp
12	WP-Def%	WP-Def%	genIvirC	PSFDM1
13	MPrm_PPw	SFWt%l10	WPFlowMF	InitRSFP
14	DTFFAVIF	SFWt%l1	SFWt%C2	genIvirC
15	FPrs_STF	SFWt%l9	SFWt%C1	FPrs_STF
16	SFWt%l2	gen_ifi	MAPM@GM	SFWt%C2
17	InvMPerm	SFWt%l5	DSFailTi	SFWt%C1
18	SFWt%l9	SFWt%l3	AA_1_1	SFWt%C9
19	SFWt%l1	SFWF11	APrs_SAV	SFWt%C6
20	gen_ifi	DSFailTi	SFWt%C9	SFWFC1
<i>Abbreviation</i>	<i>Description</i>		<i>Abbreviation</i>	<i>Description</i>
AA_1_1	AA_1_1[C/m2/yr]		InvMPerm	InvertMatrixPermeability[m^2]
AAMAI@S	ArealAverageMeanAnnualInfiltration AtStart[mm/yr]		MPrm_PPw	MatrixPermeability_PP2_[m2]
ARDSAVNp	AlluviumMatrixRD_SAV_Np		PSFDM1	Preexponential_SFDissolutionModel2
DSFailTi	DripShieldFailureTime[yr]		SbArWt%	SubAreaWetFraction
DTFFAVIF	DistanceToTuffAlluviumInterface[km]		SFWt%C1	SFWettedFraction_Corrosion_1
gen_AUSF	AnimalUptakeScaleFactor		SFWt%C9	SFWettedFraction_Corrosion_9
gen_ifi	InterceptionFraction/Irrigate		Solbl-Np	SolubilityNp[kg/m3]
gen_PUSF	PlantUptakeScaleFactor		WP-Def%	DefectiveFractionOfWPs/cell
genKDsTc	KD_Soil_Tc[cm3/g]		WPFlowMF	WastePackageFlowMultiplicationFactor
genIvirC	LeafyVegetableIrrigationTimeCB[mo/yr]		WPRRG@20	WellPumpingRateAtReceptorGroup20km [12.4 mi]
InitRSFP	InitialRadiusOfSFParticle[m]			

*Correlated parameters

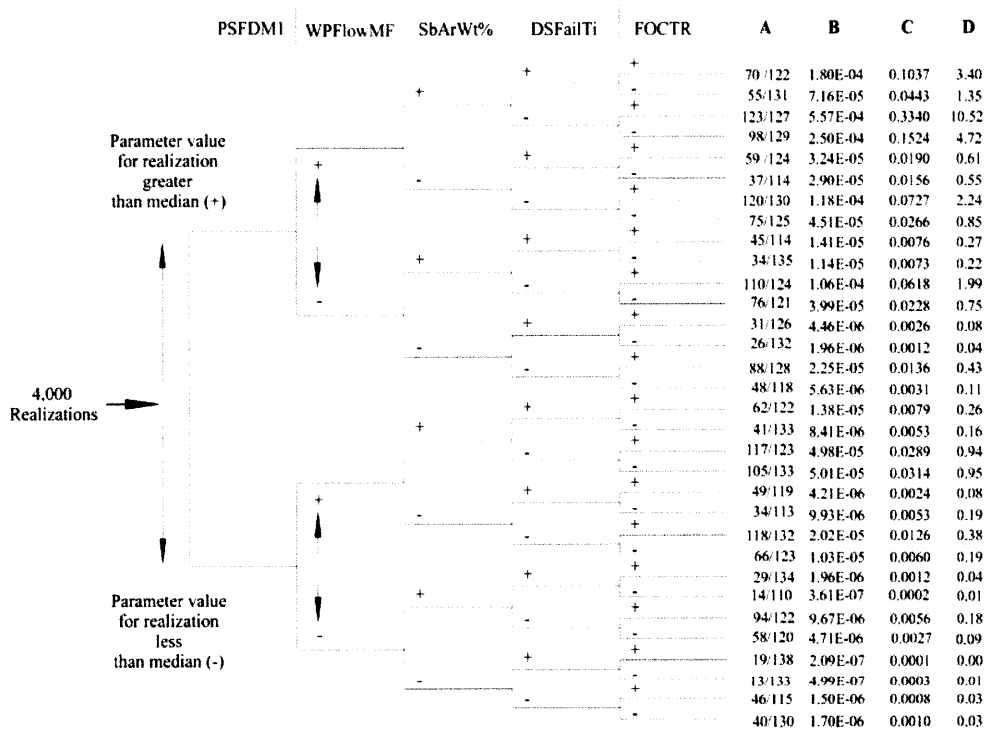


Figure 4-7. Median-Based Parameter Tree Describing the Technique for Examining System Sensitivity to Groups of Parameters

Data in columns A–D serve as figures of merit for characterizing the group of realizations in a bin. Two other interesting observations can be made about Figure 4-7. First, the realizations where none or one of the input parameters is a -, account for 51.6 percent of the mean from all realizations (includes 740 of 4,000 realizations). Second, only 6 of 32 bins have importance factors above unity, indicating the output variable distribution is skewed (the 6 bins include 763 of 4,000 realizations). Symbols x_1 to x_5 for this column correspond to the five influential parameters shown in Figure 4-7.

Using the parameter tree based on median values as the branching criterion, the influential parameters are obtained for 10,000 and 100,000 years. Parameters identified as influential in the 10,000-year simulation period are PSFDM1, WPFLOWMF, SbArWt%, DSFailTi, FOCTR, *Chlorid, Solbl-Np, gen_hirP, SSMOV404, and AAMAI@S. Parameters identified as influential in the 100,000-year simulation period are PSFDM1, SbArWt%, ARDSAVNp, AA_1_1, WPFLOWMF, SSMO-RPR, ARDSAVAm, SFWt%S29, AAMAI@S, and MAPM@GM. Several parameters, such as SSMOV404 and SSMO-RPR, should be considered spurious because no waste package failures from seismic activity take place in 10,000 years. It should be noted the variables that can be captured by this method are limited by the number of realizations because each new branch of the tree cuts the number of samples by approximately half. Therefore, as the depth of the tree increases, the precision of the method decreases. In this regard it appears that more confidence can be attributed to the first 5 than the last 5 of these 10 influential parameters.

4.3.5 Results from the Fractional Factorial Design Method

The initial screening with the fractional factorial method used a level-4 design for 330 input variables and 2,048 runs. There were two values for each of the input parameter models chosen as the 5th and 95th percentiles of the parameter distributions. The TPA Version 4.1 code was run for this experimental design to calculate the peak doses for the 10,000- and 100,000-year simulation periods. Results from the set of 2,048 were analyzed by ANOVA, using a 95 percent confidence level.

4.3.5.1 Results for the 10,000-Year Simulation Period

The ANOVA yielded a set of 100 potentially important variables for the 10,000-year simulation period. The results for the 10,000-year simulation period were refined to a list of 37 variables by observations from other information generated by the code; for example, it was possible to eliminate all variables related to seismic failure of the waste packages by observing from other code outputs that there were no seismic failures in any of the runs.

Using the reduced set of 37 variables from the initial screening, another level-4 factorial design, which requires 2,048 runs was set up. With only 37 variables, it was possible to observe 2- and 3-way interactions that are combinations of the main effects and to make inferences about the 4th and higher-order interactions of those variables that might be explored by additional factorial designs. Several possible variables that showed significant main effects were eliminated by examining their aliases and judging that they were likely 3-way or higher-order effects. This intermediate list consisted of eight variables: AAMAI@S, FOCTR, DSFailTi, WPFlowMF, SbarWt%, WP-Def%, PSFDM1, and WPRRG@20. From this list of 8 variables, a full-factorial design of 256 runs was constructed. ANOVA performed on the results led to the conclusion that all eight variables were significant and that there were significant interactions, up to six-way. Table 4-7 shows the main and largest multiway interactions among the variables. The column labeled fstat is the F statistic, which is a measure of the strength of the effect. Figure 4-8 also shows the full-factorial results as a regression tree. This figure demonstrates clearly the relationships among the independent variables and the order of the variables in importance to the peak doses for 10,000 years.

4.3.5.2 Results of the 100,000-Year Factorial Design Experiments

The same level-4 design used for the 10,000-year results was used for 100,000 years. For the 100,000-year results, the initial ANOVA indicated that there are as many as 29 variables of the 330 that could be important. This list was further reduced to 17 variables based on information other than direct sensitivity from the ANOVA (e.g., all variables dealing with rockfall, volcanism, and seismicity were eliminated from the list because additional output from the code indicated there were no waste package failures from these mechanisms). Results showing sensitivity to these variables were caused by confounding of main effects with three-way and higher parameter interactions, which are known to be present in the level-4 fractional factorial design. The 17 variables are AAMAI@S, MAPM@GM, MATI@GM, AA_1_1, WPFlowMF, SbarWt%, WP-Def%, PSFDM1, SFWt%C1, SFWt%C2, SFWt%C3, ARDSAVAm, ARDSAVNp, ARDSAV_U, ARDSAVPu, PWPRRG20, and gen_ifi.

The next fractional factorial design for 100,000 years was of level-5 resolution, requiring 2,048 vectors. From the level-5 design, the number of possible factor interactions is

Table 4-7. Main Effects and Strongest 2-Way Through 6-Way Interactions for the 10,000-Year Full Factorial Design. (Appendix E Provides Full Description of Parameters.)

FOCTR	DSFailTi	WPFlowMF	SbArWt%	WP-Def%	PSFDM1	WPRRG@20	Fstat
x							36
	x						36
		x					36
			x				29
				x			31
					x		29
						x	7
x	x						36
x		x					36
x			x				29
x				x			30
x					x		31
	x	x					36
	x		x				29
	x			x			30
	x				x		31
		x	x				29
		x		x			30
		x			x		31
			x	x			24
			x		x		26
				x	x		26
x	x	x					36
x	x		x				31
x	x			x			31
x		x	x				29
x		x		x			30
x		x			x		31

Table 4-7. Main Effects and Strongest 2-Way Through 6-Way Interactions for the 10,000-Year Full Factorial Design. (Appendix E Provides Full Description of Parameters) (continued.)

FOCTR	DSFailTi	WPFlowMF	SbArWt%	WP-Def%	PSFDM1	WPRRG@20	Fstat
x			x	x			24
x			x		x		26
x				x	x		26
	x	x	x				29
	x	x		x			30
	x	x			x		31
	x		x	x			26
	x		x		x		26
	x			x	x		26
			x	x	x		24
			x	x		x	26
		x		x	x		26
			x	x	x		21
x	x	x	x				29
x	x	x		x			30
x	x	x			x		31
x	x		x	x			24
x	x		x		x		26
x	x			x	x		26
x		x	x	x			24
x		x	x		x		26
x		x		x	x		26
x			x	x	x		21
	x	x	x	x			24
	x	x	x		x		26
	x	x		x	x		26
	x		x	x	x		21
		x	x	x	x		21
x	x	x	x	x			24

Table 4-7. Main Effects and Strongest 2-Way Through 6-Way Interactions for the 10,000-Year Full Factorial Design. (Appendix E Provides Full Description of Parameters) (continued.)

FOCTR	DSFailTi	WPFlowMF	SbArWt%	WP-Def%	PSFDM1	WPRRG@20	Fstat
x	x	x	x		x		26
x	x	x		x	x		26
x	x		x	x	x		21
x		x	x	x	x		21
	x	x	x	x	x		21
x	x	x	x	x	x		21

Low parameter value ←————→ High parameter value

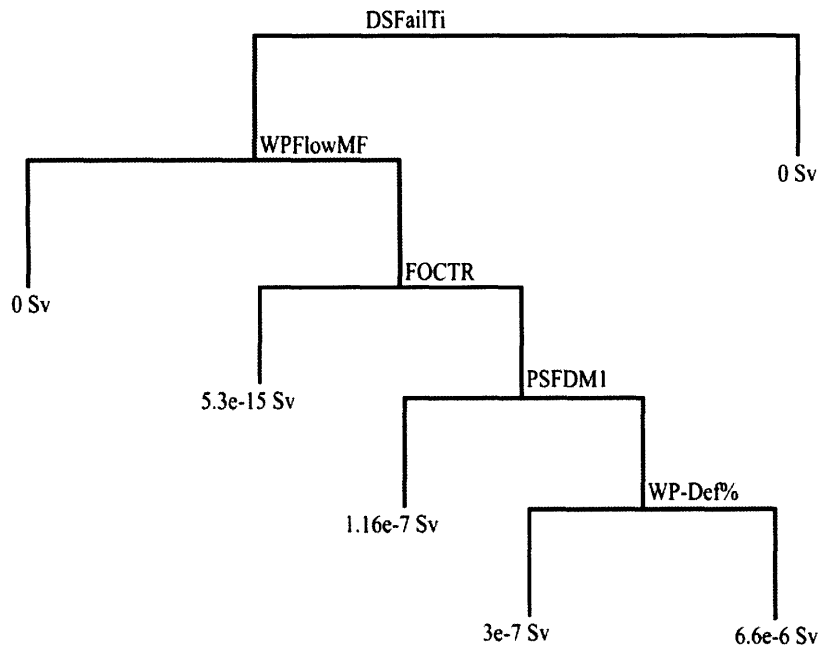


Figure 4-8. Factorial Design Results for 10,000-Year Simulation Period

manageable; therefore, it was possible to judge whether a main effect associated with a particular variable was actually an alias caused by a multiple-way effect of other variables. While investigating the possible main effects and their aliases, 10 variables, which are most likely to be important were screened from the ANOVA result.

The final full-factorial design for 100,000 years looks at the 1,024 possible combinations of the 10 screened variables. Results of the full-factorial design show that 8 of the variables are likely to be important. The 8 variables are AAMAI@S, WPFlowMF, SbArWt%, PSFDM1, SFWt%C2, ARDSAVNp, PWPRRG20, and gen_ifi. In addition, the ANOVA on these 8 variables shows there are many important interactions up to 6-way. Table 4-8 shows the 8 significant variables and the strongest 2-way to 6-way combinations that could be important for the 100,000-year simulation period. The columns of the table show the variable in the interaction. Like the 10,000-year results, there are many other smaller, but credible, interactions not listed. Figure 4-9 also shows the full-factorial results as a regression tree. This figure demonstrates clearly the relationships among the independent variables and the order of the variables in importance to the peak doses for 100,000 years.

The fractional factorial design method is a useful addition to the other sensitivity methods. It formally addresses the problem encountered in other sensitivity methods of confounding (mistaking true sensitivities with spurious results that may be caused by interactions of other variables). The factorial method allows the formal demonstration of the interaction among variables that can only be inferred by some of the other methods (e.g., the parameter tree method can show combinations of variables that lead to high doses, but only to a limited extent). The full-factorial results of the reduced set of variables from screening provides valuable information about the combination of extreme values of input variables (i.e., 5th- and 95th-percentile values) that could lead to the poorest repository performance. The tree diagrams that can be drawn from the full-factorial results on the reduced set of variables are explicit and show the exact relationship between the values of the variables and performance. Factorial design methods, however, are difficult to implement and, with the available tools, require a significant expenditure of staff and computer resources. The successive screening of variables is particularly demanding of staff time as is setting up the TPA Version 4.1 code to accept input from the factorial designs produced externally to the code. Another potential disadvantage of the factorial design is the reliance in this application to only two levels of sampling. This limitation presents the possibility of for misidentification of variables for which the greatest sensitivities or most adverse results occur in the middle of the ranges rather than at the extremes. This limitation could be mitigated by including a midrange sample so there are three levels rather than two, but this would further increase the computational effort.

4.3.6 Results from the Cumulative Distribution Function-Sensitivity Method

Cumulative distribution function sensitivities have been evaluated at 9 performance (i.e., peak dose) cumulative distribution function values, ranging from 10th to 90th percentiles, with a 10 percent increment. Figure 4-10 shows S_{μ} sensitivity results for the top 10 influential parameters. The figure also shows the 90-percent test-of-hypothesis confidence limits. As noted earlier, the parameters not influential are close to the zero sensitivity line and within the 90 percent confidence limits. The farther the curve is outside the test-of-hypothesis acceptance limits, the more sensitive the performance cumulative distribution function is to the corresponding input parameter. The influential parameters can be ranked based on this

Table 4-8. Main Effects and Strongest 2-Way Through 6-Way Interactions for the 100,000-Year Full-Factorial Design. (Appendix E Provides Full Description of Parameters.)

AAMAI@S	WPFlowMF	SbArWt%	PSFDM1	SFWt%C2	ARDSAVNp	PWPRRG20	gen_ifi	F-Stat
x								37
	x							57783
		x						55989
			x					63135
				x				7812
					x			57703
						x		48
							x	5174
	x	x						47954
	x		x					54907
	x				x			53561
		x	x					52398
		x			x			47887
			x		x			57578
	x	x	x					45568
	x	x			x			44445
	x		x		x			53629
		x	x		x			47783
	x	x	x	x				6314
	x	x	x		x			44501
	x	x	x				x	3499
	x	x		x	x			6158
	x	x		x			x	432
	x	x			x		x	3434
	x		x	x	x			7407
	x		x	x			x	496
	x		x		x		x	4140
	x			x	x		x	479
		x	x	x	x			6047

Table 4-8. Main Effects and Strongest 2-Way Through 6-Way Interactions for the 100,000-Year Full-Factorial Design. (Appendix E Provides Full Description of Parameters) (continued)								
AAMAI@S	WPFlowMF	SbArWt%	PSFDM1	SFWt%C2	ARDSAVNp	PWPRRG20	gen_ifi	F-Stat
		X	X	X			X	411
		X	X		X		X	3719
		X		X	X		X	396
			X	X	X		X	473
	X	X	X	X	X			6154
	X	X	X	X			X	415
	X	X	X		X		X	3447
	X	X		X	X		X	400
	X		X	X	X		X	480
	X	X	X	X	X		X	401

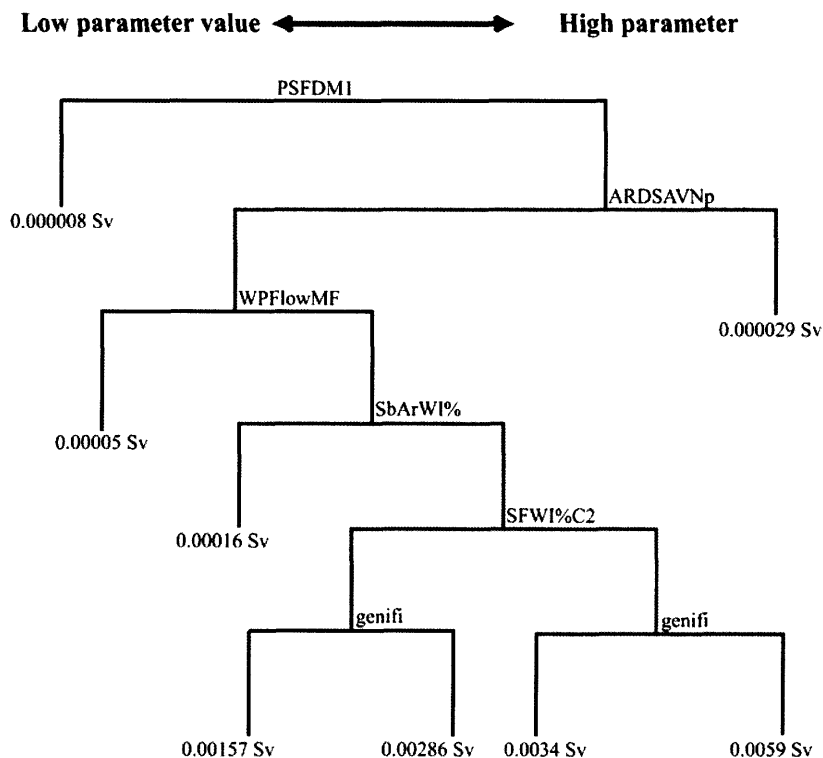


Figure 4-9. Factorial Design Results for the 100,000-Year Simulation Period

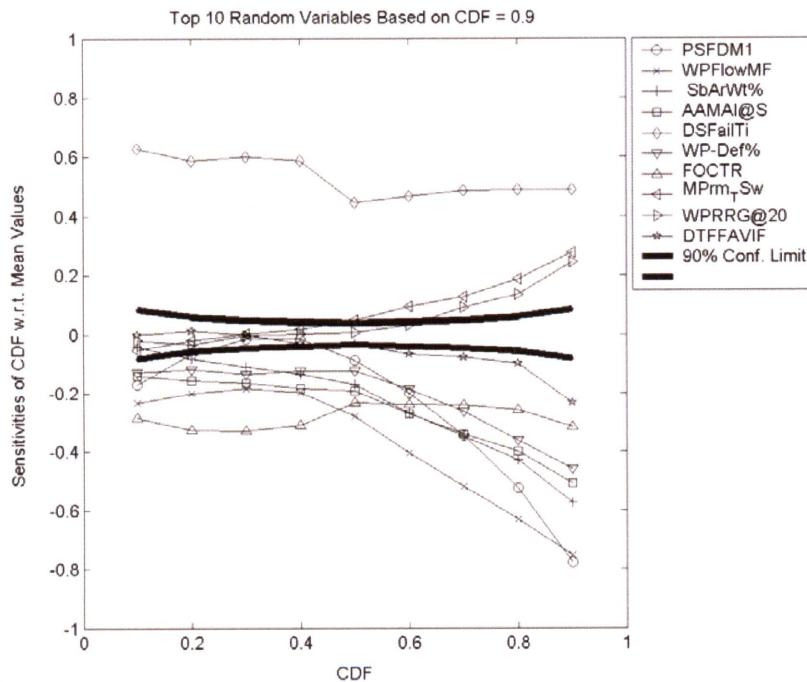


Figure 4-10. Sensitivity of Performance Cumulative Distribution Function to Input Variable Mean for Top 10 Variables Having Highest Average

departure from the zero line, which could be different for a given random variable at different cumulative distribution function levels.

Table 4-9 and Figures 4-10 through 4-12 present influential parameters identified by the S_{μ} sensitivity at cumulative distribution function = 0.9, the S_{μ} sensitivity at average cumulative distribution function, and the $S_{y_{\mu}}$ sensitivity. These sensitivities have been calculated using a 4,000-vector TPA Version 4.1 code run. At the 90 percent confidence level, more than 10 parameters are identified as influential, but only the top 10 are shown in Table 4-9. Figures 4-10 and 4-11 show that the ranking varies for different cumulative distribution function levels. This ranking implies that the functional relationship between the performance and the input variables is not linear (i.e., the sensitivity varies for the range of performance). For example, in Figure 4-11, the variable DSFailTi parameter (drip shield failure time) has a higher sensitivity at cumulative distribution function = 0.1 than at cumulative distribution function = 0.9. In contrast, PSFDM1 (preexponential term for the spent nuclear fuel-dissolution Model 2) has the highest sensitivity at cumulative distribution function = 0.9, low sensitivity at cumulative distribution function = 0.1, and no acceptable sensitivity (i.e., <90-percent confidence) between the cumulative distribution function values of 0.25 and 0.45. Figure 4-12 shows results for $S_{y_{\mu}}$ sensitivity at the 90 percent confidence level. The top 10 influential parameters from $S_{y_{\mu}}$ sensitivity are presented in Table 4-3 for the 10,000-year simulation period. These parameters from $\bar{S}_{y_{\mu}}$ sensitivity are (i) WPFlowMF, (ii) PSFDM1, (iii) SbArWt%, (iv) WP-Def%, (v) AAMAI@S, (vi) DSFailTi, (vii) DTFFAVIF, (viii) WPRRG@20, (ix) ARDSAVNp, and (x) FOCTR. These 10 parameters were ultimately selected to represent the cumulative distribution function sensitivity analysis method for comparison against other methods, primarily

Table 4-9. Top 10 Parameters from the Cumulative Distribution Function, Sensitivity Method with 1,000 Samples Using Various Sensitivity Measures (Appendix E Provides a Full Description of the Parameters)

S_{μ} Sensitivity (At Cumulative Distribution Function = 0.9)		S_{μ} Sensitivity (Average over Cumulative Distribution Function)		$\bar{S}_{Y_{\mu}}$ Sensitivity	
Variable Identification Number	Variable Abbreviation	Variable Identification Number	Variable Abbreviation	Variable Identification Number	Variable Abbreviation
63	PSFDM1	12	DSFailTi	60	WPFlowMF
60	WPFlowMF	60	WPFlowMF	63	PSFDM1
61	SbArWt%	5	FOCTR	61	SbArWt%
1	AAMAI@S	1	AAMAI@S	62	WP-Def%
12	DSFailTi	63	PSFDM1	1	AAMAI@S
62	WP-Def%	61	SbArWt%	12	DSFailTi
521	FOCTR	62	WP-Def%	237	DTFFAVIF
202	MPrm_TSw	4	FOC-R	239	WPRRG@20
239	WPRRG@20	6	TempGrBI	225	ARDSAVNp
237	DTFFAVIF	202	MPrm_TSw	5	FOCTR

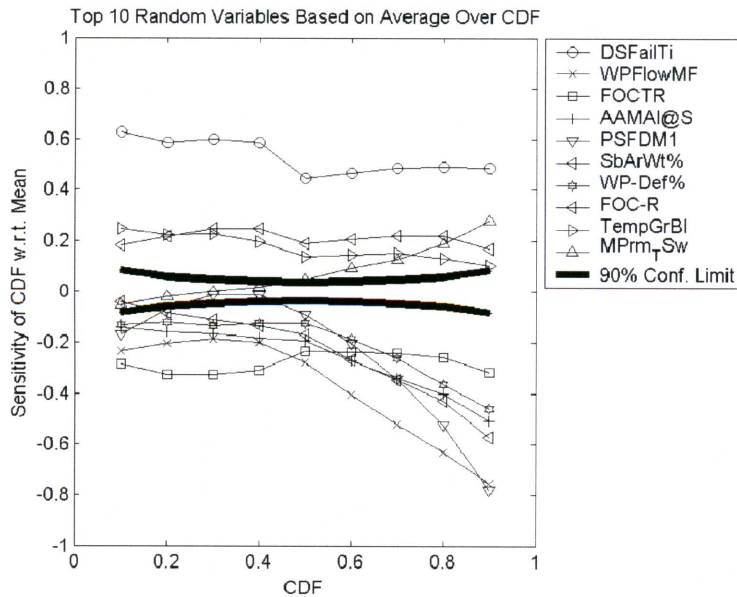


Figure 4-11. Sensitivity of Performance Cumulative Distribution Function to Input Variable Standard Deviation for Top 10 Variables Having Highest Average; Sensitivity Calculated for Average over Cumulative Distribution Function

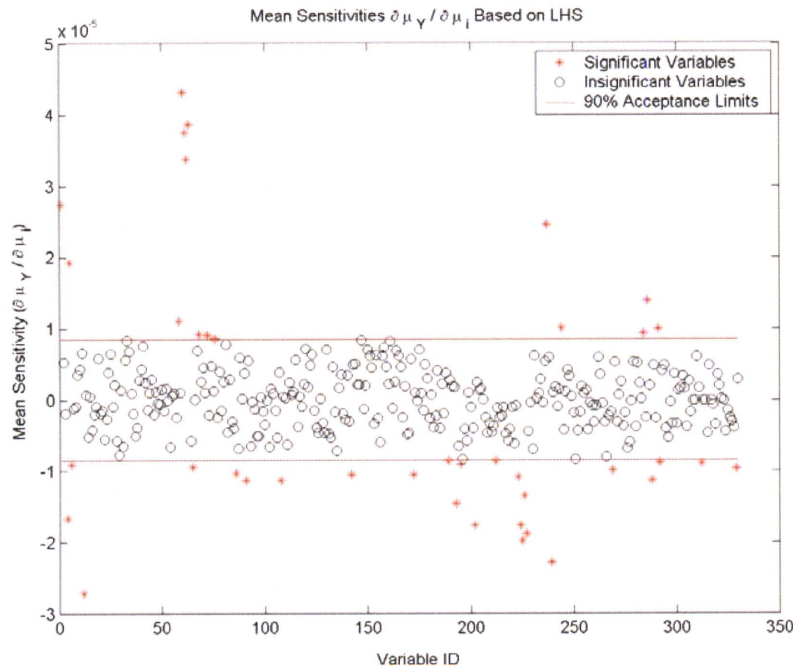


Figure 4-12. Important Variables Identified by the $S_{Y_{\mu}} (\partial \mu_Y / \partial \mu_i)$ Sensitivity. The Top 10 Parameters Identified with Asterisks (Farthest from the Confidence Limit) Are Shown in Last Column of Table 4-9

because the $\bar{S}_{Y_{\mu}}$ sensitivity represented the sensitivity consistent with the peak expected dose regulatory basis. These parameters are similar to those identified by the S_{μ} sensitivity averaged-over-cumulative distribution function and S_{μ} sensitivity at cumulative distribution function = 0.9, with a few exceptions. Parameter TempGrBI is identified as important by the S_{μ} averaged-over-cumulative distribution function sensitivity but does not show up with the $\bar{S}_{Y_{\mu}}$ sensitivity or the S_{μ} at-cumulative distribution function = 0.9 sensitivity. Parameter MPrm_TSw appears in the S_{μ} at-average-cumulative distribution function sensitivity and the S_{μ} at-cumulative distribution function = 0.9 sensitivity but does not appear with the $\bar{S}_{Y_{\mu}}$ sensitivity.

The ranking based on S_{σ} was different from that based on S_{μ} . The influential parameters identified by the $\bar{S}_{Y_{\sigma}}$ sensitivity were also substantially different from those identified by the $\bar{S}_{Y_{\mu}}$ sensitivity when analyzing the results from the TPA Version 4.1 code. Therefore, the results are not discussed in this report. An investigation of the implication of the S_{σ} and $\bar{S}_{Y_{\sigma}}$ sensitivity results is currently under way. When these two measures were applied to the previous version of the TPA code, the difference between the two sets of influential variables was small.

Table 4-9. Top 10 Parameters from the Cumulative Distribution Function, Sensitivity Method with 1,000 Samples Using Various Sensitivity Measures (Appendix E Provides a Full Description of the Parameters)

S_{μ} Sensitivity (At Cumulative Distribution Function = 0.9)		S_{μ} Sensitivity (Average over Cumulative Distribution Function)		$\bar{S}_{Y_{\mu}}$ Sensitivity	
Variable Identification Number	Variable Abbreviation	Variable Identification Number	Variable Abbreviation	Variable Identification Number	Variable Abbreviation
63	PSFDM1	12	DSFailTi	60	WPFlowMF
60	WPFlowMF	60	WPFlowMF	63	PSFDM1
61	SbArWt%	5	FOCTR	61	SbArWt%
1	AAMAI@S	1	AAMAI@S	62	WP-Def%
12	DSFailTi	63	PSFDM1	1	AAMAI@S
62	WP-Def%	61	SbArWt%	12	DSFailTi
521	FOCTR	62	WP-Def%	237	DTFFAVIF
202	MPrm_TSw	4	FOC-R	239	WPRRG@20
239	WPRRG@20	6	TempGrBl	225	ARDSAVNp
237	DTFFAVIF	202	MPrm_TSw	5	FOCTR

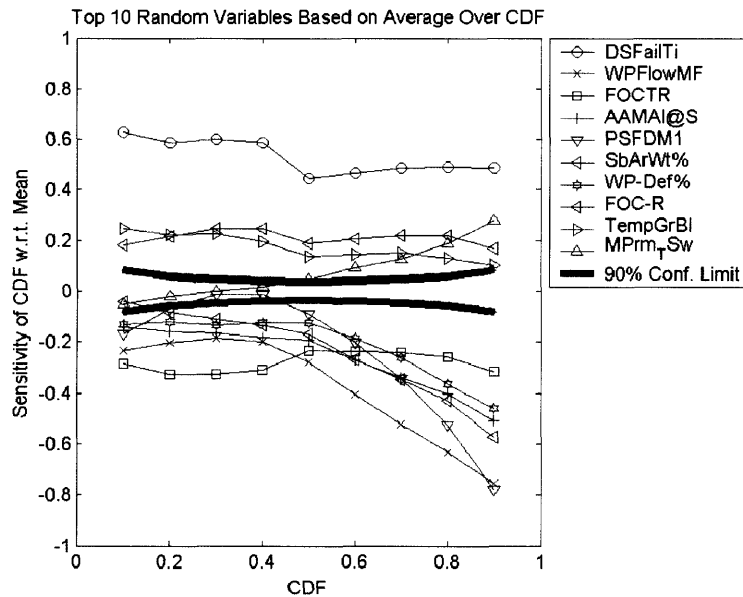


Figure 4-11. Sensitivity of Performance Cumulative Distribution Function to Input Variable Standard Deviation for Top 10 Variables Having Highest Average; Sensitivity Calculated for Average over Cumulative Distribution Function

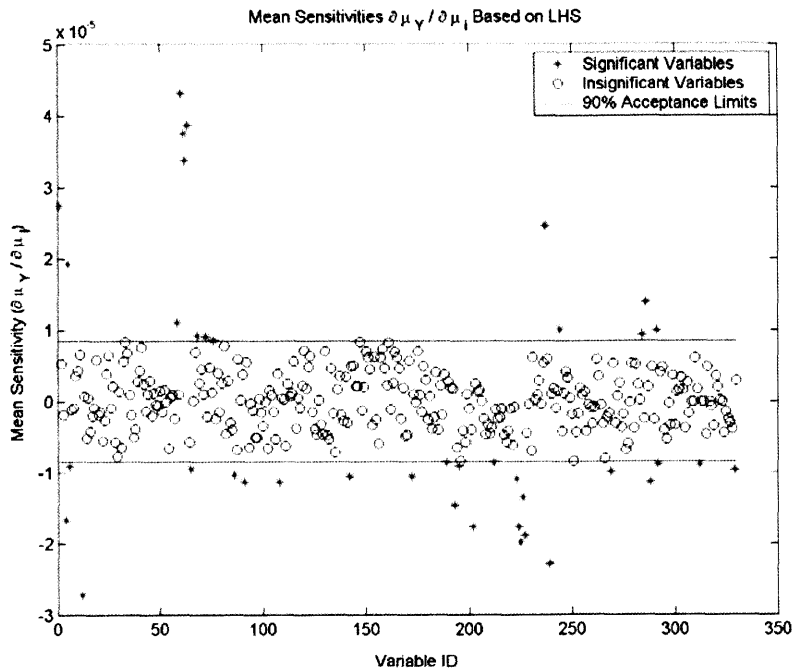


Figure 4-12. Important Variables Identified by the $S_{Y_\mu} (\partial\mu_y / \partial\mu_i)$ Sensitivity. The Top 10 Parameters Identified with Asterisks (Farthest from the Confidence Limit) Are Shown in Last Column of Table 4-9

because the \bar{S}_{Y_μ} sensitivity represented the sensitivity consistent with the peak expected dose regulatory basis. These parameters are similar to those identified by the S_μ sensitivity averaged- over-cumulative distribution function and S_μ sensitivity at cumulative distribution function = 0.9, with a few exceptions. Parameter TempGrBI is identified as important by the S_μ averaged-over-cumulative distribution function sensitivity but does not show up with the \bar{S}_{Y_μ} sensitivity or the S_μ at-cumulative distribution function = 0.9 sensitivity. Parameter MPm_TSw appears in the S_μ at-average-cumulative distribution function sensitivity and the S_μ at-cumulative distribution function = 0.9 sensitivity but does not appear with the \bar{S}_{Y_μ} sensitivity.

The ranking based on S_σ was different from that based on S_μ . The influential parameters identified by the S_{Y_σ} sensitivity were also substantially different from those identified by the \bar{S}_{Y_μ} sensitivity when analyzing the results from the TPA Version 4.1 code. Therefore, the results are not discussed in this report. An investigation of the implication of the S_σ and \bar{S}_{Y_σ} sensitivity results is currently under way. When these two measures were applied to the previous version of the TPA code, the difference between the two sets of influential variables was small.

The peak dose values showed, on an average, 1 potential outlier per 1,000 realizations. Conducting sensitivity analyses using the cumulative distribution function sensitivity method with and without the outliers had a profound effect on the response statistics, the sensitivities, and the rankings. One particular example is the 265th realization in the 1,000-vector run. In this run, the peak dose was nearly 238 times larger than the average peak dose. Further analysis revealed that in the 265th realization there were several influential variables with large parameter values that led to a very large peak dose value. Consequently, one must use as many realizations as feasible to compute the sensitivities no matter what method is used. Fortunately, the top five random variables in the $S_{y,\mu}$ sensitivity remain on the top even though they are in a different order when more realizations are systematically considered.

4.4 Influential Parameters Based on Parametric Sensitivity

In the previous section, seven different sensitivity analyses methods were used to determine the most influential parameters. Several of these methods scale parameters so the sensitivity results reflect the variability of the inputs. Several methods do not standardize but scale parameters because their results are based on ranking the input variables using a set of predetermined criteria. The seven methods have different approaches for determining sensitivity. For example, regression with log-transformed variables places greater emphasis on smaller doses than regression with untransformed variables. The cumulative distribution function sensitivity method uses three different types of sensitivity measures, though the mean-mean sensitivity is used because it is consistent with the peak expected dose regulatory criterion. It is not clear that any one method was superior to another for this determination of sensitivity (or influence), and consequently, no method can be fully relied on to provide a unique ranking of parameters. Therefore, the final list of parameters was selected on the basis of frequency of occurrence among various methods.

The selected parameters are presented in Table 4-10 for 10,000 years. The scores in these tables specify the number of methods that select a particular parameter among the top 10. For example, a score of 7/7 for the "areal average mean annual infiltration at start" parameter, AAMAI@S, implies the parameter ranks among the top 10 in all 7 methods. Also note that, among the seven methods, there is one statistical/regression method that relies on the combined results of Monte Carlo input-output response using linear and stepwise linear regressions of raw, rank, normalized, or log of normalized variables for parameter screening. Two other methods (parameter tree and cumulative distribution function sensitivity) are also based on Monte Carlo results. The other four methods are nonstatistical (differential analysis, fractional factorial design method, Morris Method, and Fourier amplitude sensitivity test method), for which the sampled parameters were determined specifically for the method. It should be noted that the Fourier amplitude sensitivity test method selects only the most influential parameters of the top 20 listed in the peak dose column for the 10,000-year case of Table 4-6. The parameters that do not make the final list include those selected as influential by only one or two of the seven methods.

4.5 Verification of Sensitivity Analysis Results

Because most of the sensitivity analysis methods neither guarantee that the parameters are influential nor establish a degree of influence, it is important to verify if the group of parameters identified by various methods is truly influential. Because the system response is most affected

No.	Parameter Abbreviation	Parameter Name	Score
1	AAMAI@S	Areal average mean annual infiltration at start	7/7
2	DSFailTi	Drip shield failure time	7/7
3	PSFDM1	Preexponential term for spent nuclear fuel-dissolution Model 2	6/7
4	SbArWt%	Subarea wet fraction	6/7
5	WPFlowMF	Waste package flow multiplication factor	6/7
6	WPRRG@20	Well pumping rate at 20-km [12.4-mi] receptor group	6/7
7	FOCTR	Fraction of condensate toward repository	4/7
8	ARDSAVNp	Alluvium R_a for Np-237	3/7
9	DTFFAVIF	Distance to Tuff-alluvium interface	3/7
10	WP-Def%	Waste package initially defective fraction	3/7

by the most influential parameters identified with the sensitivity analysis, it is intuitive that the variance of the system response will be significantly reduced if the input variances of the influential parameters are reduced.

In the following sections, the variance reduction is shown for the entire complementary cumulative distribution functions when all influential parameters are treated as a group. When the influential variables were studied individually, however, only the overall reduction in variance was computed. Variance reductions were computed using 350 Latin Hypercube Sampling realizations for each case. The performance value used in the variance reduction calculations was the realization peak dose.

For convenience, the variance reduction for the group of influential parameters is shown as a change in the shape of a complementary cumulative distribution function. A cumulative distribution function was constructed from N performance values. Each value of y was assumed to have a probability of occurrence of $1/N$. If, by holding the influential parameters at their mean values, there is a decrease in the spread of N values of y , it can be concluded that the parameters are indeed influential. If the ranking produced by the majority rule is correct, the transition between the highest and lowest probability of exceedance values is expected to be sharp.

4.5.1 Verification of the Basecase Influential Parameters as a Group

Figure 4-13 shows complementary cumulative distribution functions of peak doses for 3 cases: (i) basecase—all 330 input parameters were allowed to be sampled within their ranges of variation, (ii) top 10 influential parameters were held fixed at their mean values while the remaining 320 input parameters are allowed to be sampled within their ranges of variation, and (iii) all but the top 10 influential input parameters were frozen at their mean values. For each case, results were plotted for the 10,000-year simulation period. Each curve represents the output from 350 runs using Latin Hypercube Sampling.

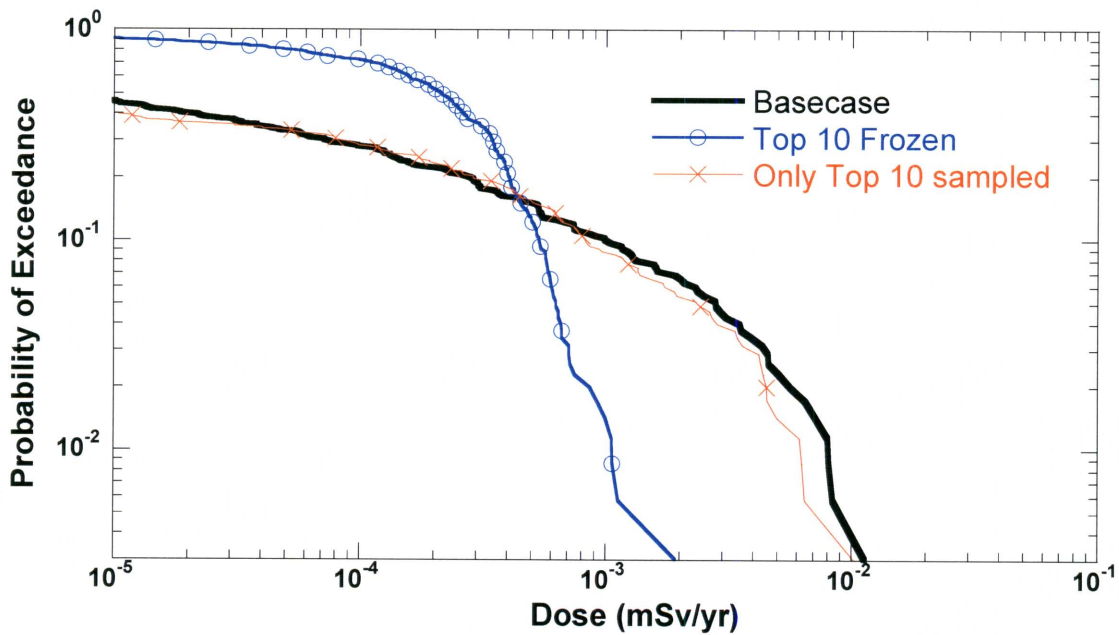


Figure 4-13. Conditional Complementary Cumulative Distribution Function of Peak Total Effective Dose Equivalents for the 10,000-Year Simulation Period from the Basecase, Conditioned by Holding 0 (Basecase) and 10 Most Influential Parameters Fixed at Their Mean Values and Fixing All but 10 Most Influential Variables

Case 1 in Figure 4-13 is the complementary cumulative distribution function of peak doses from the basecase run. Case 2 resulted in a sharp drop in variance of the peak doses. The standard deviation dropped from $\{1.32 \times 10^{-3} \text{ to } 1.9 \times 10^{-4} \text{ mSv/yr} [1.32 \times 10^{-1} \text{ to } 1.90 \times 10^{-2} \text{ mrem/yr}]\}$, which is nearly a 2 orders of magnitude decrease. A large drop like that is expected if the influential parameters are truly important. Moreover, Case 3 results are similar to the Case 1 results. This similarity is expected if the influential parameters are truly important, because fixing the less influential parameters is expected to make little difference. The slight difference between Case 1 and Case 2 indicates there may be more than 10 parameters that could be influential. Based on Figure 4-13, it appears the scoring method ranked the top parameters correctly.

4.5.2 Verification of the Igneous Activity Case Influential Parameters as a Group

Figure 4-14 shows complementary cumulative distribution functions of peak doses for 3 cases: (i) igneous activity conditional dose case—all 330 input parameters were allowed to be sampled within their ranges of variation, (ii) top 9 influential parameters were held fixed at their mean values while the remaining 321 input parameters were allowed to be sampled within their ranges of variation, and (iii) top 9 influential parameters were allowed to be sampled within their

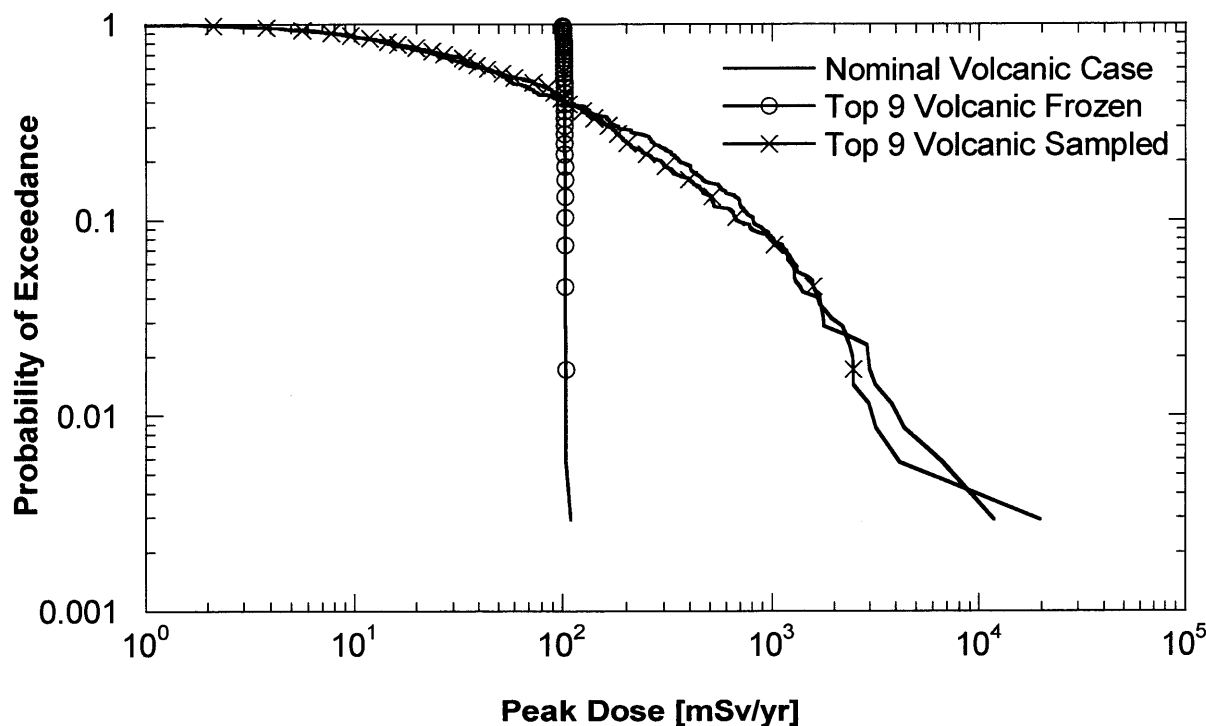


Figure 4-14. Conditional Complementary Cumulative Distribution Function of Peak Total Effective Dose Equivalents for the 10,000-Year Simulation Period from the Igneous Activity Case (Not Probability Weighted) Conditioned by Holding 0 and 10 Most Influential Parameters Fixed at Their Mean Values and Fixing All but 10 Most Influential Variables

ranges of variation while the remaining 321 influential input parameters were frozen at their mean values. Only 9 parameters were selected because parameter 10 had already been considered in the basecase. For each case, results were plotted for a 10,000-year simulation period. The outputs were conditioned by holding the parameters fixed at their mean values and sampling the remaining 321 input parameters within their ranges of variation. Each curve represents the output from 350 runs using Latin Hypercube Sampling. Case 1 is the complementary cumulative distribution function of peak doses from the nominal case run. Case 2 resulted in a sharp drop in variance of the peak doses. The standard deviation dropped six orders of magnitude from $\{8.98 \times 10^2 \text{ to } 9.42 \times 10^{-1} \text{ mSv/yr } [8.98 \times 10^4 \text{ to } 9.42 \times 10^{-1} \text{ mrem/yr}]\}$. This drop was expected if the influential parameters were truly important. Moreover, the Case 3 results in Figure 4-5 are close to the Case 1 results. This correlation was expected if the influential parameters are truly important, because fixing the less influential parameters is expected to make little difference to the nominal case complementary cumulative distribution function. The slight difference between Case 1 and Case 2 indicates there may be more than nine parameters that could be influential. Based on Figure 4-14, it appears the scoring method ranked the top parameters correctly.

4.5.3 Verification of Individual Basecase Influential Parameters

For the analysis of variance reduction for individual influential parameters, each influential parameter was held fixed at its mean value while the remaining input parameters were sampled. The results of this analysis are presented in Table 4-11.

One finding from this analysis is that freezing an influential parameter at its mean value does not always lead to a corresponding reduction in output variance for the peak doses from each realization (see last three columns of Table 4-11). For example, freezing drip shield failure time at a fixed value increases response (i.e., output) variability. This result implies that the scaled variability (i.e., coefficient of variation) displayed in the complementary cumulative distribution function for Case 2 (see Figure 4-13) would have been reduced further by fixing some of the top 10 influential parameters at their mean values.

It is also important to note that some top influential parameters influence the mean, others influence the variance, and some affect both mean and variance. The process-level analyst must be aware of this aspect and set the goal before embarking on the process of acquiring new data for uncertainty reduction. The effect of the parameter distributional assumption on dose should also be considered.

Reduction of uncertainties in parameters PSFDM1, DSFailTi, WPFlowMF, and WP-Def% influenced the output uncertainty most (i.e., >5 percent). Reduction of uncertainties in parameters DSFailTi, PSFDM1, WPFlowMF, SArWt%, ARDSAVNp, WP-Def%, and DTFFAVIF influenced the output mean most (i.e., >5 percent). All but DSFailTi decreased the mean. For parameters DSFailTi, PSFDM1, WPFlowMF, and WP-Def%, both mean and standard deviations of the output changed (i.e., >5 percent) when the uncertainty in the parameters was suppressed. Reduction of uncertainties in 14 out of 20 parameters reduced scaled variability in dose whereas the remaining 6 increased scaled variability.

4.5.4 Verification of Individual Igneous Activity Influential Parameters

For the variance reduction analysis of individual influential parameters in the igneous activity case, each influential parameter was held fixed at its mean value while the remaining input parameters were sampled. A conditional dose calculation was then performed corresponding to each influential parameter by holding each parameter fixed at the mean value and performing a 350-realization Monte Carlo run. Changes to the mean, variance standard deviation, and coefficient of variation of the peak dose values are presented in Table 4-12.

The largest output uncertainty reduction occurred for parameters VEROI-Tn and VE-Power (~30 percent), followed by WindSpd and VE-Durat (~15 percent). The largest increase to scaled variability resulted from fixing parameter ABMLAAsh its mean value. The ABMLAAsh parameter increased the scaled variability by approximately 34 percent. Table 4-12 shows that parameters VEi/e-R# and SFWt%V0 affected neither the output scaled variability nor the output mean. The lack of variability reduction for VEi/e-R# (Random Number to determine volcanic event type) can be attributed to the fact that in the model, the sampled event is nonvolcanic if this parameter value exceeds 0.999. Because all sampled values in the basecase are less than 0.999 and because for the variance reduction calculation this parameter is set at 0.5, in both cases the volcanic event occurred. Therefore, no difference was observed in the basecase or the variance reduction case.

Table 4-11. Variance Reduction for Most Influential Parameters in the Basecase					
Abbreviation	Description of Influential Parameters	Mean of Peak Doses (mrem/yr)	Variance of Peak Doses (mrem/yr) ²	Standard Deviation of Peak Doses (mrem/yr)	Coefficient of Variation (Unitless)
Basecase	—	4.2×10^{-5}	1.8×10^{-8}	0.00013	3.124
AAMAI@S	Areal average mean annual infiltration at start	4.2×10^{-5}	1.9×10^{-8}	0.00014	3.261
MAPM@GM	Mean average precipitation multiplier at glacial maximum	4.3×10^{-5}	1.9×10^{-8}	0.00014	3.188
DSFailTi	Drip shield failure time	7.2×10^{-5}	4×10^{-8}	0.0002	2.783
WPFlowMF	Waste package flow multiplication factor	3.6×10^{-5}	1.1×10^{-8}	0.0001	2.864
gen_PUSF	Plant uptake scale factor	4.2×10^{-5}	1.7×10^{-8}	0.00013	3.123
WPRRG@20	Well pumping rate at receptor group 20 km [12.4 mi]	4.1×10^{-5}	1.6×10^{-8}	0.00013	3.093
ARDSAVNp	Retardation factor for Np in saturated zone alluvium matrix	4×10^{-5}	1.6×10^{-8}	0.00013	3.207
IPPFSTFF	Immobile porosity penetration fraction for STFF	4.4×10^{-5}	1.9×10^{-8}	0.00014	3.160
PSFDM1	Preexponential term for spent nuclear fuel-dissolution Model 2	2.6×10^{-5}	4.8×10^{-9}	6.9×10^{-5}	2.684
SbArWt%	Subarea wet fraction	3.9×10^{-5}	1.3×10^{-8}	0.00012	2.993
genIvirC	Leafy vegetable irrigation rate at compliance boundary	4.2×10^{-5}	1.7×10^{-8}	0.00013	3.116
WP-Def%	Defective fraction of waste packages per subarea	4.0×10^{-5}	1.4×10^{-8}	0.00012	2.967
MPrm_PPw	Matrix permeability for PPw	4.24×10^{-5}	1.76×10^{-8}	1.32×10^{-4}	3.124
DTFFAVIF	Distance to tuff-alluvium interface	4×10^{-5}	1.7×10^{-8}	0.00013	3.284
FPrs_STF	Fracture porosity in STFF	4.25×10^{-5}	1.68×10^{-8}	1.30×10^{-4}	3.056
SFWt%I2	Spent nuclear fuel wetted fraction for initially defective failure in subarea 2	4.3×10^{-5}	1.8×10^{-8}	0.00013	3.094
InvMPerm	Invert matrix permeability	4.2×10^{-5}	1.8×10^{-8}	0.00013	3.122
SFWt%I9	Spent nuclear fuel wetted fraction for initially defective failure in subarea 9	4.3×10^{-5}	1.9×10^{-8}	0.00014	3.164
SFWt%I1	Spent nuclear fuel wetted fraction for initially defective failure in subarea 1	4.3×10^{-5}	1.8×10^{-8}	0.00013	3.081
gen_ifi	Irrigation interception fraction	3.95×10^{-5}	1.62×10^{-8}	1.27×10^{-4}	3.230

Table 4-12. Variance Reduction for Most Influential Parameters in the Igneous Activity Case Identified by the Morris Method; Analysis Results Are Presented Using Conditional Dose (i.e., No Probability Weighting)						
No.	Abbreviation	Description of Influential Parameters	Mean of Peak Doses (mrem/yr)	Variance of Peak Doses (mrem/yr)²	Standard Deviation of Peak Doses (mrem/yr)	Coefficient of Variation (Unitless)
N/A	Igneous Activity Case	Basecase with igneous activity	32.45	8,056.48	89.76	2.766
1	ABMLAAsh	Airborne mass load above fresh ash blanket	28.93	11,412.68	106.83	3.693
2	WinSpd	Wind speed	43.55	8,922.01	94.46	2.169
3	VC-Dia	Diameter of volcanic cone	29.12	4,607.78	67.88	2.331
4	VE-Power	Volcanic event power	20.25	1,338.06	36.58	1.806
5	VE-Durat	Volcanic event duration	28.73	4,234.55	65.07	2.265
6	VEROI-Tn	Time of next volcanic event in region of interest	19.56	1,119.61	33.46	1.711
7	AshMnPLD	Ash man particle log diameter	32.33	7,990.29	89.39	2.765
8	Ve/e-R#	Random number to determine if extrusive or intrusive volcanic event	32.45	8,056.48	89.76	2.766
9	SFWt%V0	Spent nuclear fuel wetted fraction for intrusive igneous activity	32.45	8,056.48	89.76	2.766

4.6 Alternative Conceptual Models and Scenario Cases Studied at the System Level

Alternative conceptual models are either explicitly specified in the TPA Version 4.1 code or are created by assigning a set of predetermined values to input parameters to mimic an alternative conceptualization. Analyses include full ranges of parameter variations for all parameters (i.e., similar to the nominal case). This process is a departure from the analyses using the previous versions of the TPA code in which parameters were set at their respective mean values. The results reflect model runs that compare the basecase with alternative conceptual models. First, the basecase was evaluated with a 350-vector run. Alternative conceptual model tests were conducted with 350-vector runs, and the results were compared with the basecase. The alternative conceptual models were selected to evaluate (i) the effect on repository performance of several repository design features currently being considered by U.S. Department of Energy, (ii) the effect on repository performance of plausible alternate thermo-hydrologic conditions in the repository near field, and (iii) bounding engineered or natural system behaviors.

For each alternative conceptual model, only the noted changes, as described in Section 2.7.2 to the total-system performance assessment input file, were made, with all other input parameters set to the values used in the basecase. Results are presented as the percentage change of peak expected dose with respect to the basecase peak expected dose.

Figure 4-15 shows the results for the 10,000-year simulation period, while Figure 4-16 is for the 100,000-year results.

Various observations can be made based on the results shown in this section.

- The largest mean doses resulted from the NoRet assumption for both the 10,000- and 100,000-year simulation periods, demonstrating the importance of retardation of plutonium, americium, and thorium in the alluvium.
- The No Sol Limit Flowthru alternative conceptual model (i.e., no solubility limit + flow-through spent nuclear fuel wetting mode) led to a 353 percent increase in dose compared to the basecase during the 10,000-year simulation period. In the 100,000-year simulation period, this alternative conceptual model led to an 75-percent increase in dose compared to the basecase. This increase suggests that the solubility limit controls the release from the spent nuclear fuel.
- The No Sol Limit (Bathtub) conceptual model (i.e., no solubility limit + bathtub spent nuclear fuel wetting mode) had less effect on the peak expected dose than the No Sol Limit (Flowthru) alternative conceptual model. The peak expected dose changed by 141 percent for 10,000 years and by 67 percent for 100,000 years.
- The Flwthru-1 alternative conceptual model (i.e., flow-through spent nuclear fuel wetting mode + spent nuclear fuel-dissolution Model 1) increased the peak expected dose by 240 percent in the 10,000 simulation period and by 50 percent in the 100,000-year simulation period.

- Fast dissolution in the case of Model 1 (i.e., spent nuclear fuel-dissolution Model 1) and Grain 1 (i.e., particle size model) alternative conceptual models led to an increase in the peak expected dose for the 10,000-year simulation period, but the increase is not proportional to the increased rate of dissolution. In some cases, the high rate of dissolution does not contribute to an overall increase of dose for the 100,000-year simulation period. This increase probably indicated that the high dissolution rate of the fuel led to near-total depletion of the spent nuclear fuel.
- Alternatives based on natural analog data (Natan) and assumptions about the behavior of radionuclides in secondary uranium minerals (Schoepite) led to much smaller peak doses.
- Protection of the fuel by cladding (Clad-M1) led to a large reduction in peak doses.
- Removing matrix diffusion increases the peak expected dose by 50 percent for the 10,000-year simulation period and by 10 percent for the 100,000-year simulation period.

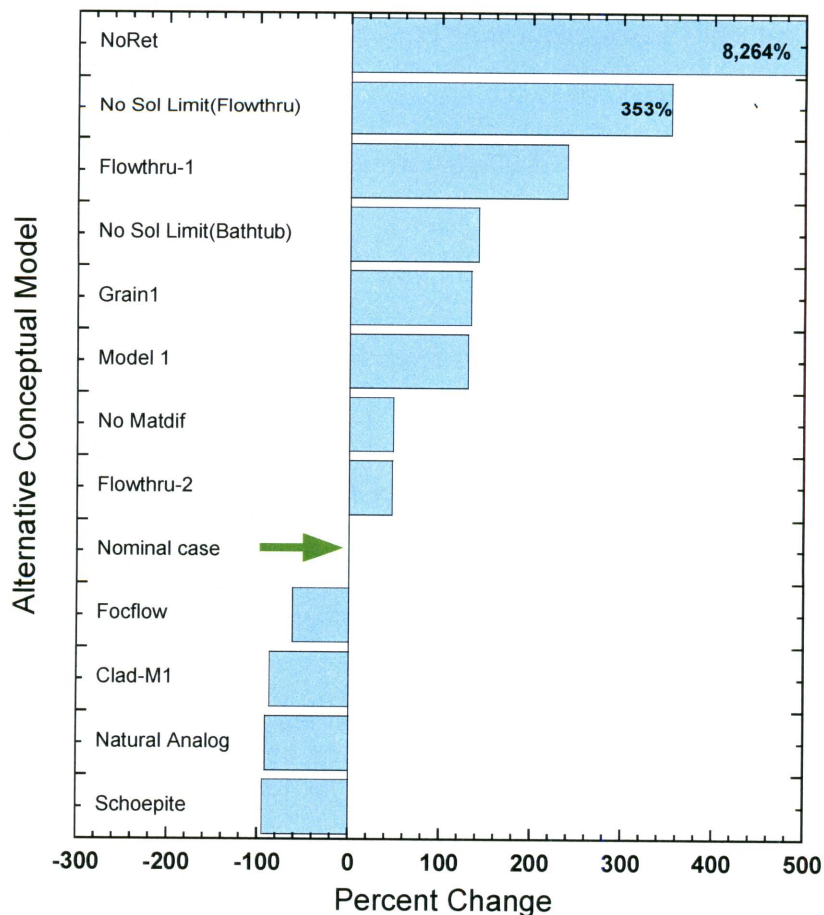


Figure 4-15. Bar Chart Showing the Effects of Alternative Conceptual Models at 10,000 Years

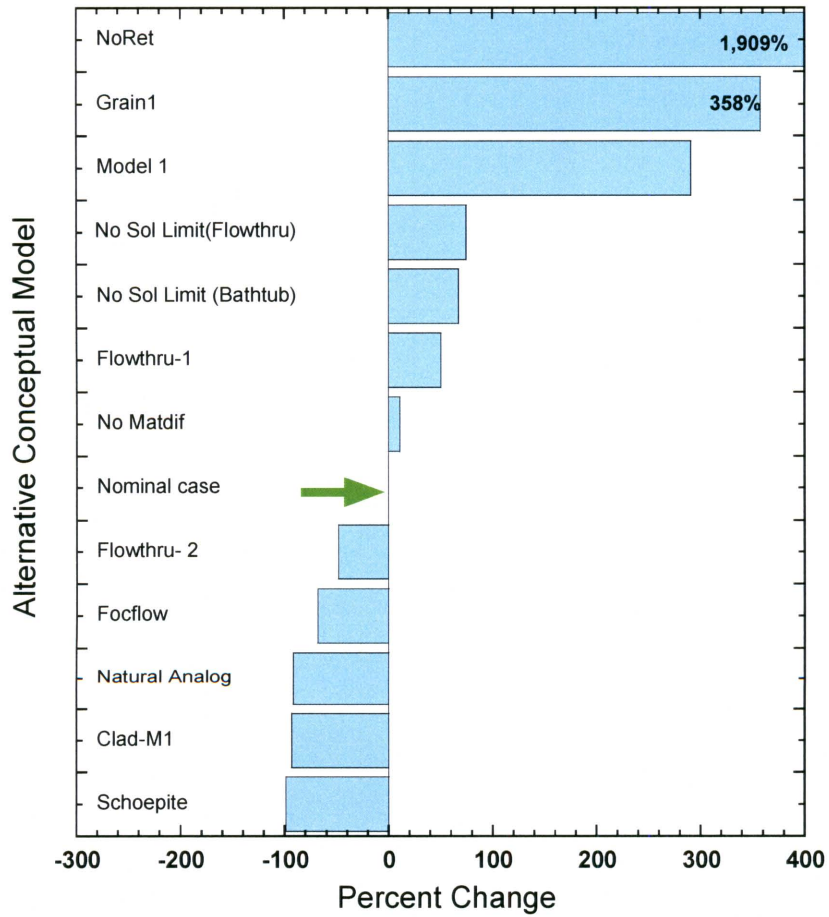


Figure 4-16. Bar Chart Showing the Effects of Alternative Conceptual Models at 100,000 Years.

5 DISTRIBUTIONAL SENSITIVITY ANALYSIS

5.1 Background

The quality of performance assessment results depends in part on the process used for determining the probability distribution function for each sampled input parameter. The effect of distributional uncertainty is studied by conducting sensitivity or relative impact analyses of the uncertainty in the distribution functions on the peak expected dose as well as the shape of the peak dose cumulative distribution function. Because of the large number of sampled parameters in the TPA Version 4.1 code, only a small set of parameter distributions was evaluated. For the analyses presented in this report, only the shape of the distribution function is varied, the parameter range remains unchanged. In the following sections, the analysis method is presented, the results from the implementation of the method are presented, and some recommendations are made for future studies.

5.2 Analysis Method

The general approach for distributional sensitivity involves determination of the relative change to the performance measure for a prespecified perturbation to the distribution function. The direct (i.e., brute force) method involves performing several Monte Carlo runs corresponding to each change to the distribution function (i.e., the basecase and the sensitivity cases). Only one parameter is changed at a time. Each Monte Carlo run set corresponds to and is identical to the basecase run except that one input parameter has a distribution function different from the basecase. The relative change to the performance measure is expressed as (i) the difference between the old (i.e., the basecase) and the new (i.e., sensitivity case) peak expected dose and (ii) an effective distance between the old and new output distributions. Several notable methods have been proposed in the past by Beckman and McKay (1987) for fast computation focusing on improvement to the computational efficiency by eliminating the need to perform any Monte Carlo runs additional to a standard basecase run. One of these methods is based on the weighing method (Kahn and Marshall, 1953), and another method is the rejection method (Kennedy and Gentle, 1980). These methods, however, appear to have some limitations that could lead to approximations in the analysis if used outside the recommended limits. The efficiency of each method has been shown to decrease rapidly as large differences occur between the old and the new probability density functions. For this report, the direct (i.e., brute force) method was used because of these limitations.

The two measures used for estimating the sensitivity of performance on the distributional change to a parameter were (i) change in the peak expected dose and (ii) change to the peak dose cumulative distribution function. For the first measure, the expected dose was computed as a function of time from the Monte Carlo run set; the peak expected dose was then computed from the expected dose curve. The second measure was useful especially for cases where the peak expected dose remains the same as the basecase dose. Where the variance of peak dose is different, however, one could use complementary cumulative distribution functions instead of cumulative distribution functions—this will only add extra computational steps without any change in the results.

The change in output distribution in the second distributional sensitivity measure can be measured simply by measuring the area between two cumulative distribution functions, one for

the basecase and one for the sensitivity case. Chun, et al. (2000) used metric distance to represent this shaded region based on a Minkowski norm. Other measures can be found in Iman and Hora (1990); Khatib-Rahbar, et al. (1989); Park and Ahn (1994); and Chun, et al. (2000). The metric distance, D , is defined as

$$D = \left[\sum_{x \in X} |F_1(x) - F_2(x)|^w \right]^{\frac{1}{w}}, w > 1 \quad (5-1)$$

where

- $F_1(x)$ — the basecase output cumulative distribution function
- $F_2(x)$ — the sensitivity case output cumulative distribution function
- w — an exponent

When $w = 2$, D represents the Euclidian metric distance between the two cumulative distribution functions.

$$D = \left[\int_0^1 |F_1(x) - F_2(x)|^2 dx \right]^{\frac{1}{2}} \quad (5-2)$$

The two cumulative distribution functions are normalized with the mean of the original cumulative distribution function. The parameter x represents the quantile. Then as noted earlier, the sensitivity case output cumulative distribution function refers to the case where the input distribution of only one of the parameters is changed by a prespecified value. Normalization with the mean value of the basecase makes the metric distance dimensionless.

Metric distance reflects the degree of impact an input parameter makes on the output distribution when the input distance is changed. A large value of the metric distance represents a large impact of the change in the input distribution on the output distribution.

For Monte Carlo or Latin Hypercube Sampling results, the metric distance can be expressed as

$$D = \left[\frac{1}{N} \sum_{n=1}^N [F_1^i(x) - F_2^i(x)]^2 \right]^{\frac{1}{2}} / \frac{1}{N} \sum_{n=1}^N F_2(x)_n \quad (5-3)$$

where i is the parameter of interest, N is the total number of realizations, n is the current realization, $F_1^i(x)_{n/N}$ is the $(n/N)^{\text{th}}$ quantile of the basecase ($0 < n < N$) and $F_2^i(x)_{n/N}$ is the $(n/N)^{\text{th}}$ quantile for the sensitivity case. Equation (5-3) shows the method used to compute the metric distance in this report.

5.3 Implementation Procedure

For the distributional sensitivity analysis, first the sensitivity cases are designed and then the TPA code is run for the sensitivity cases.

The sensitivity case can be created in several ways:

- Change the variance of the distribution function. This changes the range of the data.
- Shift the mean of the distribution without changing the data range (i.e., fixed variance)
- Change the mean of the distribution while keeping the end points fixed (the variance and other moments may change)

In this report, Case 3 (the third bullet) has been used. The changes have been accomplished by

- Changing the mean by 10 percent of the range while keeping the minimum and maximum values fixed (see Figure 5-1). (Note: The shifted distribution function will not be symmetrical because the maximum and minimum values are forced to remain fixed.)
- Changing the distribution function from one type to another while keeping the minimum and maximum values fixed (see Figure 5-2).

A 10 percent shift to the mean changes the entire distribution function. As a convention in this report, the 10 percent shift in the mean is always positive. For example, if the original distribution function is normal, the new distribution function, after a 10 percent shift to the mean, is no longer a normal distribution. Therefore, another distribution function must be used to represent the new distribution function with a new mean value but fixed endpoints. Beta distributions have been chosen to represent the new distribution function because the four parameters that define a beta distribution provide sufficient flexibility to represent a large suite of distribution functions. The log-beta distribution function is used if the original distribution is a log distribution (e.g., log-uniform or lognormal). The beta distribution is used primarily to represent shifts to normal, uniform, and exponential distribution functions. Several distribution functions in the TPA Version 4.1 code representing the basecase data set do not need beta or log beta representation of the new distribution function. For example, in a triangular distribution, a 10-percent shift to the mean can easily be accomplished by appropriately shifting the distribution apex.

The sensitivity cases in which the entire distribution function is changed are obtained by changing the original uniform to normal, log-uniform to log beta, and lognormal to log beta. The sensitivity case for the parameters with log distributions can be created by switching from log-uniform to lognormal or vice versa; however, such switching shifts the mean of the distribution, even if the means are identical in the log scale. Therefore, log-beta distributions with appropriate shape parameters are used so the sensitivity case has the same mean value as the basecase. This process is illustrated in Figure 5-3. All changes to symmetric distributions preserve the mean value, thus no special treatment is necessary. Note that the change from uniform to normal decreases the frequency of values near the high and low limits, and from normal to uniform increases the frequency of the values near the high and low limits

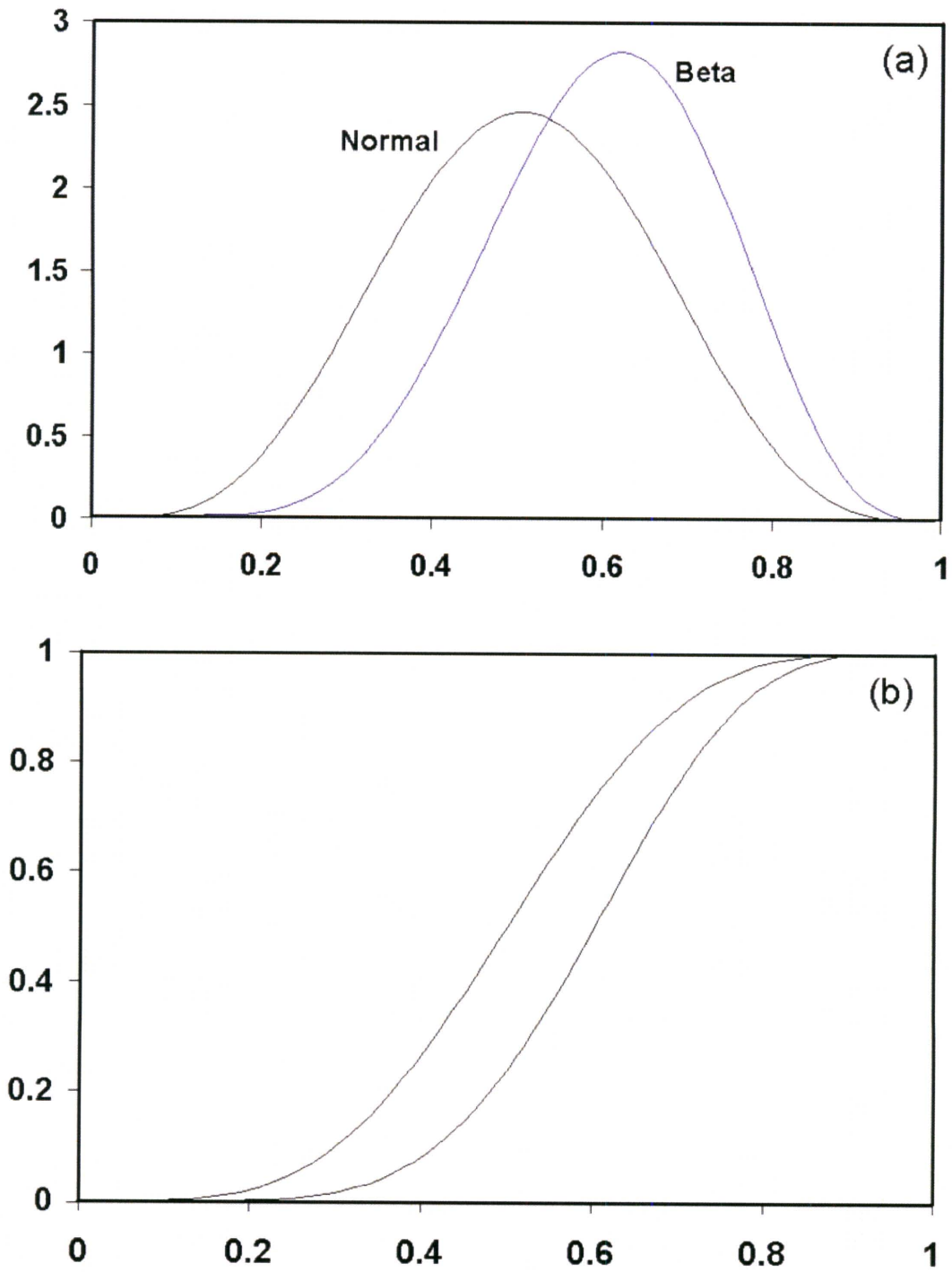


Figure 5-1. Example of (a) Changing the Probability Density Function for an Input Parameter by Shifting the Mean Value of a Normal Distribution Without Changing the End Points and (b) the Corresponding Changes to the Cumulative Distribution Functions. The New Distribution Is Approximated by a Beta Distribution.

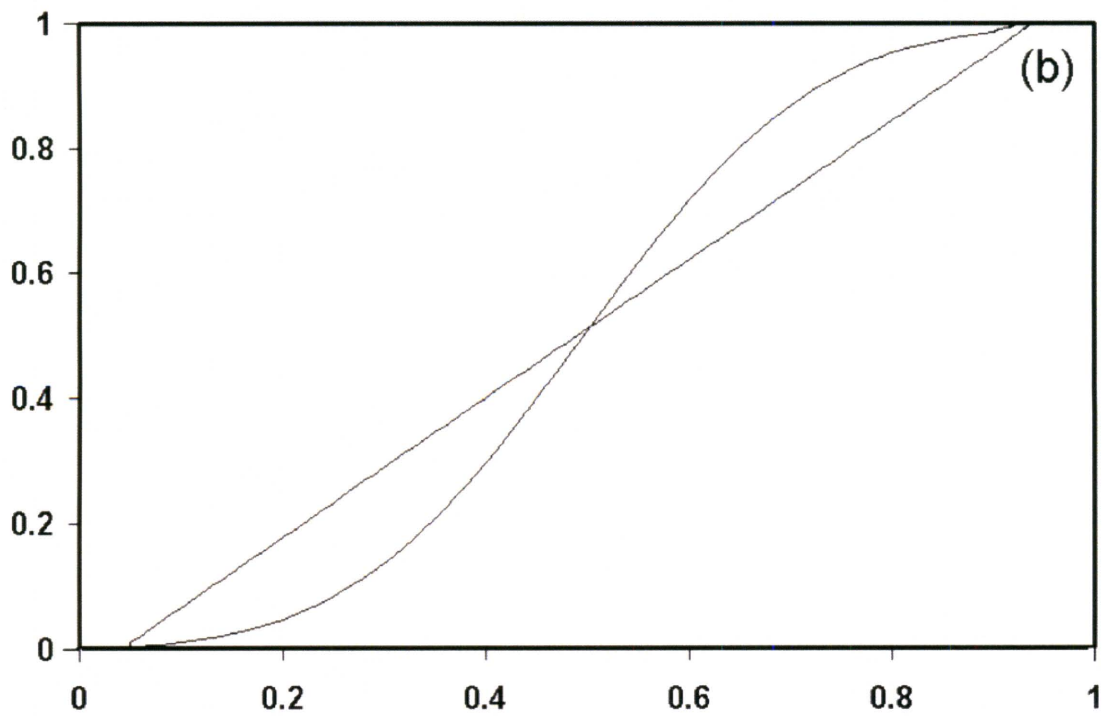
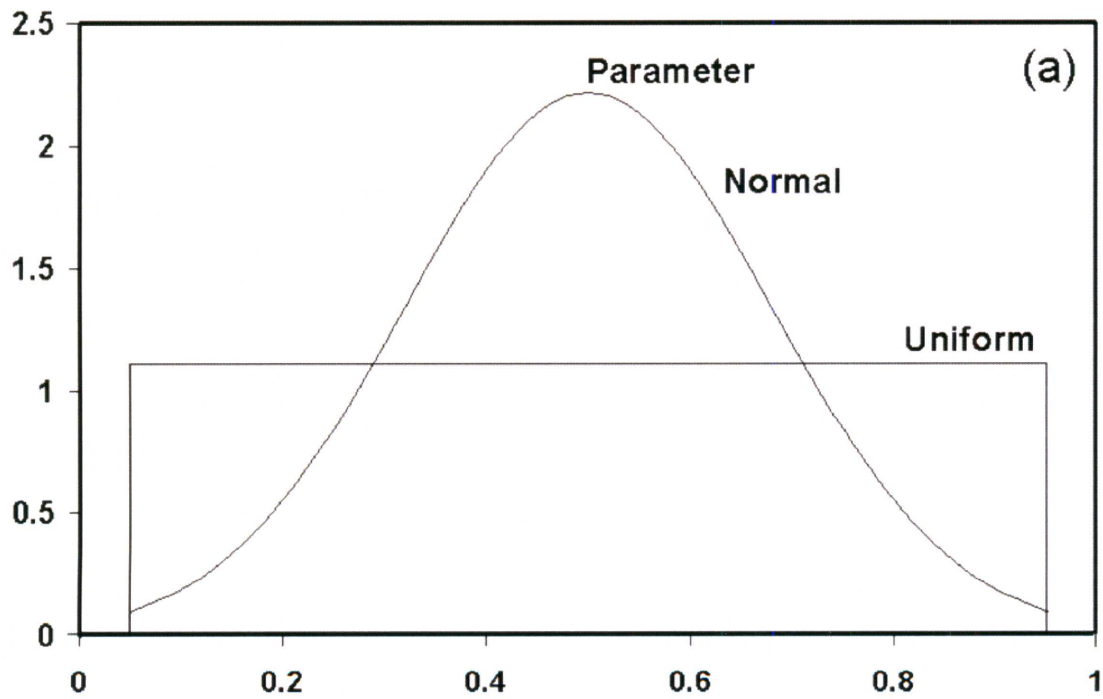


Figure 5-2. Example of (a) Changing the Probability Density Function by Changing the Distribution Type from Uniform to Normal and (b) the Corresponding Changes to the Cumulative Distribution Functions

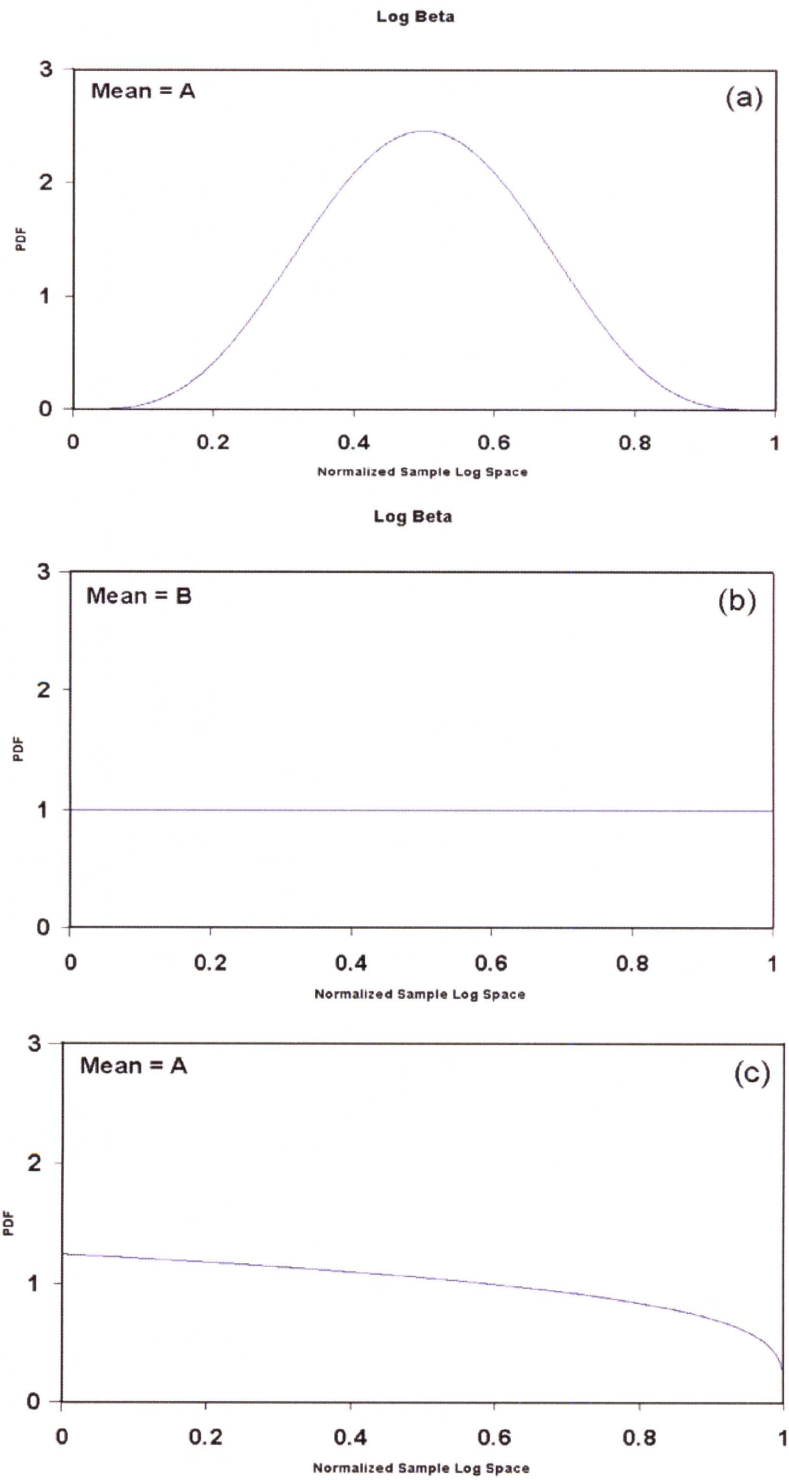


Figure 5-3. (a) Logbeta Representation of Lognormal with Mean A, (b) Logbeta Representation of Loguniform with Mean B, (c) Logbeta (b) with Shape Parameters adjusted to Obtain Mean A

while keeping the mean value unchanged. The shape parameters in the log-beta distribution provide numerous possibilities for the shape of the distribution function while the mean is invariant. Therefore, while switching from lognormal to log-beta, the shape parameters are selected so that the log-beta distribution is as close as possible to the log-uniform distribution. Similarly, while switching from log-uniform to log-beta, the shape parameters for the log-beta distribution are selected so the shape of the log beta distribution is as close as possible to the lognormal distribution. Figure 5-2 shows the minimum and maximum for the sensitivity case (i.e., the uniform distribution) are identical to the basecase (i.e., the normal distribution).

The sensitivity case was obtained by a 330-vector run after changing the distribution function for one parameter. To implement this method, the distribution function for only one parameter was changed for a given sensitivity case. The peak expected dose for the sensitivity case was computed using the same procedure used in computing peak expected dose from the basecase.

Because Latin Hypercube Sampling is used, the sampling sequence changes for other parameters when the distribution function is changed for the parameter of interest. Therefore, the original distribution is represented by a beta-equivalent approximation to obtain a modified basecase so that when the mean of the original distribution is shifted by 10 percent, there is no difference in the sampled values for the parameters other than the one that is changed. In effect, two Monte Carlo run sets were needed to perform consistent comparisons between the basecase and the sensitivity case.

Distributional sensitivity analysis was performed for the top 10 most influential parameters identified by the parametric sensitivity analysis methods described in Chapter 4. For the top 10 parameters, ideally, 3,630 realizations (i.e., $330 \times 10 + 330$ for the basecase) would be needed for constructing cumulative distribution functions and obtaining peak expected dose. Because of the need to obtain a modified basecase corresponding to each parameter, however, 6,600 realizations (i.e., 330×10 for the sensitivity case + 330×10 for the basecase) were needed to estimate the metric distance and the differences in the peak expected dose values.

5.4 Results

In this section, results are presented for the 10 percent shift to the mean of the input parameter distribution functions for the top 10 influential parameters. Then, the results for the change in the distribution type are presented. For both cases, results are presented for the 10,000-year simulation period.

Changes to the distribution function for the parameter set (i.e., 10-percent change to the mean for the top 10 parameters previously identified by the parametric sensitivity analysis methods) are shown in Table 5-1. The top 10 parameters used in the distributional sensitivity studies are the top 10 influential parameters based on the 10,000-year simulation period. In this table, column three shows the basecase distribution, column four shows the beta distribution equivalent of the basecase distribution, and column five shows the 10 percent shift to the means in the sensitivity case beta distribution. As mentioned before, this shift is 10 percent of the range of the distribution function.

Table 5-1. Modified Distribution Functions for the Top 10 Influential Parameters for Creating Sensitivity Cases

Parameter		Basecase Distribution	Revised Basecase Distribution	Sensitivity Case Distribution
Abbreviation	Description			
WPFlowMF	Waste Package Flow Multiplication Factor	lognormal 3.15×10^2 , 1.05×10^3	log beta 3.15×10^2 , 1.05×10^3 , 5.0,5.0	log beta 3.15×10^2 , 1.05×10^3 , 8.2, 3.0
PSFDM1	Preexponential term for the spent nuclear fuel-dissolution Model 2	log-uniform 1.2×10^3 , 1.2×10^6	log beta 1.2×10^3 , 1.2×10^6 , 1.0,1.0	log beta 1.2×10^3 , 1.2×10^6 , 1.97,1.0
SbArWt%	Subarea wet fraction	uniform 0.0, 1.0	beta 0.0,1.0, 1.0,1.0	beta 0.0,1.0, 1.5,1.0
AAMAI@S	Areal average mean annual infiltration at start, [mm/yr]	uniform 4.0,13.0	beta 4.0,13.0, 1.0,1.0	beta 4.0,13.0, 1.5,1.0D
DSFailTi	Drip shield failure time [yr]	lognormal 2700.0, 20400.0	log beta 2700.0, 20400.0, 5.0, 5.0	log beta 2700.0, 20400.0, 7.8, 5.0
WPRRG@20	Well pumping rate at the 20-km [12.4 mi] receptor Group location [gal/day]	uniform 4.5×10^6 , 1.3×10^7	beta 4.5×10^6 , 1.3×10^7 , 1.0, 1.0	beta 4.5×10^6 , 1.3×10^7 , 1.5, 1.0
WP-Def%	Fraction of total waste packages in a subarea that fails at time $t = 0$	uniform 1.0×10^4 , 1.0×10^2	beta 1.0×10^4 , 1.0×10^2 , 1.0, 1.0	beta 1.0×10^4 , 1.0×10^2 , 1.5, 1.0
DTFFAVIF	Distance traveled in tuff [km]	uniform 10.0, 19.9	beta 10.0, 19.9, 1.0, 1.0	beta 10.0, 19.9, 1.5, 1.0
FOCTR	Fraction of water condensate moving toward repository	uniform 0.05, 1.0	beta 0.05, 1.0, 1.0, 1.0	beta 0.05, 1.0, 1.5, 1.0
ARDSAVNp	Matrix retardation for neptunium in the saturated zone of the Amargosa Valley alluvium	lognormal 1.0, 3.9×10^3	log beta 1.0, 3.9×10^3 , 5.0, 5.0	log beta 1.0, 3.9×10^3 , 8.2, 3.5

Table 5-2 shows that a 10-percent shift to the mean of the input distribution function toward high values resulted in a definite shift of the peak dose cumulative distribution function for each input parameter. The sensitivity case cumulative distribution functions shifted in such a way that, in all cases, the metric distance and peak expected dose changed. The minus sign for the peak expected dose implies there is an inverse relationship between the input and output parameters. This shift in the cumulative distribution function to higher values appears to be intuitively correct because a positive shift of the mean in the input distribution corresponds to sampling smaller values less frequently and sampling larger values more frequently. If the output value is directly proportional to the input value, the sensitivity case peak expected dose cumulative distribution function also shifts toward higher values and vice versa. The more pronounced the separation between the basecase and the sensitivity case cumulative distribution functions, the larger the magnitude of the metric distance. Because the whole cumulative distribution function shifted in the increasing direction without significant overlap, the metric distance is expected to correlate well with the magnitude of the change in the peak expected dose. Table 5-2 shows good correlation between metric distance and the relative change to the peak expected dose indicating, for the top 10 influential parameters, a shift in the mean of the input distribution directly resulted in a correspondingly large shift in the mean and variance of the dose values.

Table 5-2 shows that in 10,000 years, the WPFlowMF parameter is most sensitive to the change in the distribution function. For this parameter, the peak expected dose changed nearly 150 percent, with a metric distance of 4.78. Recall that a metric distance of zero means no effect of the distributional change to the input on the output. Another parameter that showed a large change to the peak expected dose (i.e., 57.2 percent) is PSFDM1. Parameters with a moderate metric distance and change in peak expected dose are DSFailTi, WP-Def%, DTFFAVIF, and SbArWt%. Anomalous results have been observed only for ARDSAVNp. Although ARDSAVNp showed a change in peak expected dose comparable to WPRRG@20, its metric distance was much smaller compared to the latter. Such a difference in metric distance, with almost identical changes in peak expected dose, reveals that WPRRG@20 equally affected the realization peak doses as well as the peak expected dose, and ARDSAVNp affected the realization peak doses much less than the peak expected dose.

The next set of analyses involved changing the distribution type. Table 5-3 shows the basecase and the sensitivity case distributions with the associated parameters defining these distribution functions. Table 5-4 shows metric distance and the percentage changes to the peak expected dose for the 10,000-year simulation period corresponding to the sensitivity cases presented in Table 5-3. The percentage change in peak expected dose did not appear to correlate well with the metric distance for the parameters with lower metric distances, (i.e., less than 1.0). Three of six parameters (DTFFAVIF, SbArWt%, and WP-Def%) that have linear (i.e., nonlogarithmic) distribution functions showed a reasonably high metric distance (~0.7). Only one (DTFFAVIF) of the three showed greater than a 10 percent change to the peak expected dose. FOCTR showed a higher (i.e., ~10 percent) change in peak expected dose, while its corresponding metric distance was lowest among all parameters. This combination implies that the FOCTR parameter affected the peak expected dose but had minimal impact on peak dose. Only two parameters (ARDSAVNp and WPFlowMF) had metric distances greater than 1.0 and appear to have good correlation to the percentage change to the peak expected dose.

Table 5-2. Metric Distances for the 10,000-Year Simulation Period for the Top 10 Influential Parameters with 10 Subareas and 330 Realizations Where the Mean of the Distribution Is Shifted by 10 Percent of the Range				
Top 10 Parameters			Metric Distance (mrem/yr)	Change in Peak Expected Dose (percent)
Abbreviation	Description	Distribution Type		
WPFlowMF	Waste package flow multiplication factor	Lognormal	4.78×10^0	149.88
PSFDM1	Preexponential term for the spent nuclear fuel dissolution Model 2	Log-uniform	1.40×10^0	57.20
SbArWt%	Subarea wet fraction	Uniform	4.98×10^{-1}	24.93
AAMAI@S	Areal average mean annual-infiltration at start [mm/yr]	Uniform	2.09×10^{-1}	5.28
DSFailTi	Drip shield failure time [yr]	Lognormal	9.98×10^{-1}	-24.83
WPRRG@20	Well pumping rate at the 20-km [12.4-mi] receptor group location [gal/day]	Uniform	3.24×10^{-1}	-8.62
WP-Def%	Fraction of total waste packages in a subarea that fails at $t = 0$	Uniform	5.30×10^{-1}	22.06
DTFFAVIF	Distance traveled in tuff [km]	Uniform	5.16×10^{-1}	19.89
FOCTR	Fraction of water condensate moving toward the repository	Uniform	2.15×10^{-1}	4.41
ARDSAVNp	Matrix retardation for neptunium in the saturated zone of the Amargosa Valley alluvium	Lognormal	8.88×10^{-2}	-8.35

In the case of the uniform-to-normal change, the metric distance will change, but it is possible that the peak expected dose did not change because the mean of the distribution was preserved. The frequency values on both sides of the mean near the limits decrease symmetrically. The same is true for the normal to uniform case except that the frequency of values on both sides of the mean near the limits increased symmetrically. If the relationship between the input parameter and the peak expected dose is linear, the metric distance can be large even if the peak expected dose does not change; such is the case for AAMAI@S. If a change in the peak expected dose does occur, it is an indication the relationship between the dose and the parameter being studied is nonlinear.

Table 5-4 also shows that changing the distribution from lognormal to log-uniform and vice versa resulted in larger changes in the peak expected dose and overall larger metric distances. The percentage change in peak expected dose for the logarithmic distributions (4 of 10 parameters) ranged between 12.41 and 94.98 percent; whereas, for the parameters

Table 5-3. Changes to Distribution Type (One Parameter at a Time) to Create the Sensitivity Case in Which the Entire Distribution Function Is Changed; Metric Distances for the 10,000-Year Simulation Periods Using 10 Subareas and 330 Realizations Where the Distribution Type Is Changed Only One Parameter at a Time

Top 10 Parameters			
Abbreviation	Description	Basecase	Sensitivity Case
WPFlowMF	Waste package flow multiplication factor	log beta 3.15 × 10 ² , 1.05 × 10 ³ , 5.0, 5.0	log beta 3.15 × 10 ² , 1.05 × 10 ³ , 1.0, 2.096
PSFDM1	Preexponential term for the spent nuclear fuel-dissolution Model 2	log beta 1.2 × 10 ³ , 1.2 × 10 ⁶ , 1.0, 1.0	log beta 1.2 × 10 ³ , 1.2 × 10 ⁶ , 4.0, 2.35
SbArWt%	Subarea wet fraction	uniform 0.0, 1.0	normal 0.0, 1.0
AAMAI@S	Areal average mean annual-infiltration at start [mm/yr]	uniform 4.0, 13.0	normal 4.0, 13.0
DSFailTi	Drip shield failure time [yr]	log beta 2700.0, 20400.0, 5.0, 5.0	log beta 2700.0, 20400.0, 1.0, 1.247
WPRRG@20	Well pumping rate at the 20-km [12.4 mi] receptor group location [gal/day]	uniform 4.5 × 10 ⁶ , 1.3 × 10 ⁷	normal 4.5 × 10 ⁶ , 1.3 × 10 ⁷
WP-Def%	Fraction of total waste packages in a subarea that fails at time t = 0	uniform 1.0 × 10 ⁴ , 1.0 × 10 ²	normal 1.0 × 10 ⁴ , 1.0 × 10 ²
DFFAVIF	Distance traveled in tuff [km]	uniform 10.0, 19.9	normal 10.0, 19.9
FOCTR	Fraction of water condensate moving toward repository	uniform 0.05, 1.0	normal 0.05, 1.0
ARDSAVNp	Matrix retardation for neptunium in the saturated zone of the Amargosa Valley alluvium	log beta 1.0, 3.9 × 10 ³ , 5.0, 5.0	log beta 1.0, 3.9 × 10 ³ , 1.0, 1.91

with linear (i.e., nonlogarithmic) distributions (6 of 10), the range is 0.86 to 16.89 percent. Note that 3 of 4 parameters with logarithmic distributions showed the 3 largest metric distances and changes in peak expected dose when the mean of the distributions is shifted by 10 percent. This analysis, however, revealed that the appropriate selection of distribution functions, especially for the parameters with logarithmic distribution is important. A wrong selection of a lognormal distribution instead of a loguniform distribution may have a greater impact than the wrong selection of a uniform distribution for a normal distribution.

Table 5-4. Metric Distances for the 10,000-Year Simulation Period for the Top 10 Influential Parameters with 10 Subareas and 330 Realizations Where Distribution Type Is Changed

Top 10 Parameters				
Abbreviation	Description	Distribution Type	Metric Distance (mrem/yr)	Changes in Peak Expected Dose (Percent)
WPFlowMF	Waste package flow multiplication factor	Log beta to log beta(See Table 5-3)	1.24×10^0	-44.10
PSFDM1	Spent nuclear fuel dissolution (Preexponential term)	Log beta to log beta (See Table 6-5)	6.94×10^{-1}	42.09
SbArWt%	Subarea wet fraction	Uniform to normal	7.01×10^{-1}	-6.13
AAMAI@S	Areal average mean annual-infiltration at start [mm/yr]	Uniform to normal	2.50×10^{-1}	-0.86
DSFailTi	Drip shield failure time [yr]	Log beta to log beta (See Table 5-3)	6.22×10^{-1}	-12.41
WPRRG@20	Well pumping rate at the 20-km [12.4-mi] receptor group location [gal/day]	Uniform to normal	3.77×10^{-1}	-3.56
WP-Def%	Fraction of total waste packages in a subarea that fails at time $t = 0$	Uniform to normal	6.08×10^{-1}	-3.31
DTFFAVIF	Distance traveled in tuff [km]	Uniform to normal	7.81×10^{-1}	-16.89
FOCTR	Fraction of water condensate moving toward repository	Uniform to normal	2.13×10^{-1}	9.25
ARDSAVNp	Neptunium retardation in alluvium	Log beta to log beta (See Table 5-3)	2.30×10^0	94.98

In summary, distributional sensitivity analyses showed that improper choice of distribution function for certain variables can affect significantly the dose responses. Distributional sensitivity also reveals important information about the input-output relationship. For some parameters, the output was affected at all cumulative distribution function levels. For some other parameters, the output was affected at all cumulative distribution function levels except at the mean values. The two dose measures showed high distributional sensitivity, especially when the mean values were changed for the most influential parameters identified by the parametric sensitivity analysis methods. The two parameters are (i) the flow multiplication factor that determines the quantity of water entering the waste package (a 10 percent change to the parameter mean resulted in a 150 percent change in the dose) and (ii) the preexponential term for the spent nuclear fuel model used in the basecase (a 10 percent change to the parameter mean resulted in a 57 percent change in the dose). Any log distribution for a parameter should be developed correctly because the dose responses appear more sensitive to log distributions,

especially for those parameters that are influential (compared to linear distributions). The analysis also revealed that, for some parameters (e.g., FOCTR), the output may not be affected significantly at any cumulative distribution function level although the peak expected dose can be affected substantially. This combination revealed that the FOCTR parameter could influence the dose curve throughout (especially where the peak expected dose occurred) except where the peak occurred.

The distribution of sensitivity analysis presented in this report was limited because the analysis focused only on the top 10 parameters identified by the parametric sensitivity analysis method and the range of the distribution function constrained to the range used in the basecase. The analyses should be extended to all 330 input parameters for a complete analysis of distribution sensitivity. Analyses could be extended to (i) change the variance of the input parameter distribution function and (ii) change the mean of the distribution while keeping the variance fixed. The significance of the metric measure should be analyzed further to identify what additional information (other than the variance) can be derived, especially when there is no difference in the peak expected dose between the basecase and the sensitivity case.

6 REPOSITORY COMPONENT SENSITIVITY ANALYSIS

6.1 Background

This chapter focuses on repository component sensitivity analysis in which the change in repository performance in response to a specified level of degradation in the functionality of the repository component is assessed. The repository system can be categorized into components in many ways. In this report, the components or subsystems are defined as physical entities of the repository. Because physical entities are easy to visualize, insights into repository performance can be readily gained. Although the repository has been divided into physical components to facilitate visualization of system performance, the repository system performance is still best described as the interaction of the physical features and processes that represent the natural and engineered systems with driving forces in the repository environment.

Repository component sensitivity analysis is different from standard sensitivity analysis in several ways. Generally, sensitivity analysis is used in the context of studying the effect of parameters, conceptual models, and scenario definitions on the system model response. Parametric, model, and scenario sensitivity analyses, however, do not readily get at the structural role of repository components. Also, if a component is modeled conservatively, parametric or conceptual model sensitivity analyses will fail to identify the true influence of the component or the overall system performance. An example is the role of the invert as a repository component. If the flow in the invert is conservatively assumed to be high, fracture flow would dominate, and, thus, the model parameters for transport processes in the invert would not be sensitive. Consequently, it can be concluded the invert is not important. Besides, the model predicts the waste package will last beyond the simulation period; parametric sensitivity analysis also will not identify the waste package as important because the waste package does not fail during that period. Sensitivity analysis, however, does not provide an understanding of the level of performance attributable to the waste package because in the system-level model, great effort is made to include as many process couplings as possible, which leads to masking the importance of one repository component or process by another. Sensitivity analysis is limited only to the model or submodels used in the system-level model. System-level modeling makes two inherent assumptions: all scenarios have been evaluated and the abstraction model appropriately accounts for all important scenarios, together with the couplings among processes in the presence of all features and events. Some residual uncertainty always remains in spite of the best effort, the scenario analysis and the model representation may have errors. In such a case, repository component sensitivity analysis provides an added degree of confidence by answering the following question: How will the system perform under assumed errors in modeling repository components?

Repository component analysis in this report was conducted by comparing the repository-system performance loss (or improvement) for a repository component case (i.e., the sensitivity case) with the basecase performance. A sensitivity case involves suppression or elimination of a repository component functions or functions of a combination of components from the performance assessment calculation. After the repository component functions are suppressed, the performance assessment calculations are performed as usual. The suppression of a repository component function is accomplished by (i) selection of an appropriate alternative conceptual model (that already exists in the system-level performance assessment model) and (ii) appropriate modifications to model parameters.

The suppression of a repository component only implies that the component no longer performs its intended function. It does not mean the component is physically removed because the removal would completely alter the conceptual framework. In this sense, the estimated repository component sensitivity is dependent on the modeling approaches, assumptions, variability, and uncertainty in the system model for the repository components that are not suppressed.

The performance metric used for repository component sensitivity analyses is the ratio between peak expected doses in the sensitivity case and in the basecase. The sensitivity cases are run for 10,000 years with the critical group located 20 km [12.4 mi] from the proposed repository footprint. The sensitivity cases represent either treatment of one repository component or a group of repository components. Because this approach requires one or more large sets of Monte Carlo calculations for each repository component or group of repository components tested, computational requirements are large. It should be noted that completely suppressing the functions of a repository component is clearly not realistic and therefore any dose results from such an analyses must not be compared to the regulatory standard. However, this device of suppressing repository component functions provides another powerful tool for understanding system behaviors under conditions not envisioned to exist in the completed case.

The repository component sensitivity analysis described is not intended to provide either guidance to U.S. Department of Energy or describe a preferred approach for demonstrating the capabilities of barriers. These analyses were performed to further the staff efforts to understand the TPA Version 4.1 code and to explore ways to improve understanding the repository system.

6.2 Description of Repository Components

For the purposes of this report, the repository system was divided into the following components: (i) drip shield, (ii) waste package, (iii) spent nuclear fuel, and (iv) invert. For the natural barrier, only the unsaturated zone and saturated zone as repository components will be studied.

In the following subsections, the functionality of the repository components selected for the repository component sensitivity analysis and the approach taken to suppress a repository component are briefly described. Discussions are provided as applicable whenever modification to one repository component will require changes to another repository component.

6.2.1 Drip Shield

By design, the drip shield, which is made of titanium, is expected to prevent aggressive chemicals in the flowing water during the early stage of repository closure from contacting the waste package. An intact drip shield is expected to prevent water from the drift wall from contacting waste packages, although the presence of the drip shield may lead to condensation of water underneath it. Corrosive chemicals (e.g., the deliquescence effect) could lead to early waste package failure because of corrosion and could readily dissolve already exposed spent nuclear fuel. The drip shield is also expected to prevent the waste package from damage by rockfall resulting from seismic events. Rockfall could lead to direct mechanical failure of the waste package, augment stress corrosion cracking, or create permanent deformation on the waste package where water could accumulate for an early start of corrosion after drip-shield failure.

The drip shield itself can undergo localized corrosion, uniform corrosion, or both. Effects, such as displacement of drip shields or development of a stress state in the materials that can lead to stress corrosion cracking, are not included in the model. The degradation of the drip shield is specified by a failure-time distribution that already accounts for any potential exposure to a stressful environment or degradation process.

The drip shield failure time in the basecase ranges between 2,700 and 20,400 years and is described by a lognormal distribution with a mean failure time of 7,241 years. For repository component sensitivity analysis, the suppression of the drip shield as a repository component is achieved by forcing the drip shield to fail immediately after closure of the repository.

Consequently, the waste package is now exposed to the chemical environment that the drip shield was exposed to in the most likely scenario. Because the drip shield in the basecase is assumed completely suppressed at the time of failure, it does not limit the dripping water from entering a failed waste package.

6.2.2 Waste Package

By design, the waste package prevents water and dissolved chemicals from contacting the spent nuclear fuel. The waste package comprises an outer overpack of Alloy 22 to provide corrosion resistance and an inner overpack of stainless steel to provide mechanical strength. Mechanical disruption of the waste package includes residual stress and seismically induced rockfall that could hit the waste package and the drip shield, or, if the drip shield is not present, the rock could hit the waste package directly. Effects, such as mechanically deformed drip shields impinging on the waste package and development of a stress state in the materials that can lead to stress corrosion cracking, are not currently included in the performance assessment model.

The thermo-hydro-chemical environment dictates the nature of the waste package failure, which could be either small-diameter pits if localized corrosion is dominant or large patches if uniform corrosion is dominant. In the absence of igneous activity and faulting disruptive events, three failure modes occur: seismic rockfall, initial defects, and corrosion. These failure modes may create bathtubs after waste package failure. Basecase calculations show most waste packages fail from uniform corrosion. Therefore, large patches instead of pits are expected on the waste package.

For repository component sensitivity analysis, suppression of the waste package as a repository component is achieved by forcing the two waste package overpacks to fail at the time of repository postclosure. Therefore, all waste packages, including the packages that fail immediately after closure of the repository, are available for potential release. In the basecase, these remaining 8,828 (8,877 - 49) waste packages fail on average, at year 59,637. In the basecase, when the waste package fails naturally as a function of corrosion, it forms a bathtub. For the waste package repository component suppression case, however, the waste package is assumed to be completely removed. Consequently, the water contact mode is changed from bathtub to flow-through, and, instead of only a fraction of spent nuclear fuel being wet, all spent nuclear fuel is wet. Because the waste package layers are assumed to be completely removed, no flow diversion will occur. Therefore, all water impinging on a waste package in a basecase now contacts the spent nuclear fuel.

6.2.3 Waste Form

The spent nuclear fuel in the waste package consists of UO_2 pellets inside zircaloy clad fuel rods, hence, water must penetrate the fuel clad before contacting the spent nuclear fuel. In the basecase scenario, fuel clads are assumed not present; therefore, water will contact spent nuclear fuel as soon as it enters the waste package. Spent nuclear fuel must dissolve in the contacting water for release to take place. Water may contact the spent nuclear fuel pellets at their surface and the walls of the interconnected pores. In the release model, it is assumed the radionuclides will be released congruently with the dissolution of the UO_2 matrix that forms the spent nuclear fuel pellet.

The basecase spent nuclear fuel-dissolution model is a function of temperature and assumes that Ca^{2+} and Si^{2+} are present in the water. With this dissolution model, spent nuclear fuel takes more than 10,000 years for complete dissolution. For the repository component sensitivity analysis, suppression of the waste form as a repository component is achieved by forcing all spent nuclear fuel in the waste package to dissolve instantaneously at the first contact with water. Because the radionuclides are released from the spent nuclear fuel congruently, the associated radionuclides are available for instantaneous release from the waste package. Because the release is solubility controlled for some nuclides, however, those nuclides are not expected to be released any faster than the basecase if the flow rates are identical for the two cases. As in the basecase, only the spent nuclear fuel immersed in the bathtub will contribute to release.

6.2.4 Invert

Releases from the waste package will travel through the invert before entering the drift floor. Water running off or passing through the waste package would fall onto the invert. The current design shows the waste package on a v-shaped pallette held together by stainless steel supports over a porous invert made of carbon steel with a sand or gravel ballast. The invert material is expected to sorb several radionuclide species, thereby providing an additional repository component to impede their release into the geosphere. Flow through the invert or mass transfer can be both advective and diffusive. Sorption of radionuclides from the flowing water may offer a significant reduction in releases. In the model, if the water flow rate exceeds the hydraulic conductivity of the invert material, the invert model becomes a passthrough with no radionuclide holdup or retardation. In the current design, with a porous medium invert, this bypass is unlikely. The model does not account for colloidal transport and the possibility that radionuclides in the water might be captured along the liquid-water pathway by precipitation or sorption on material inside the waste package.

For repository component sensitivity analysis studies, the functions of the 0.75-m [2.5-ft] thick invert as a repository component is suppressed by specifying the invert thickness as zero at the time of repository closure; thus, there is no delay in fluid flow, and there is no retardation of the radionuclides.

6.2.5 Unsaturated Zone

The repository is located in the unsaturated zone, roughly halfway between the ground surface and the water table. The unsaturated zone is a repository component because it has the potential to substantially reduce flow of water and delay the transport of radionuclides to the

water table. The portion of the unsaturated zone above the repository is a repository component relevant only to flow of water, whereas the unsaturated zone below the repository is relevant as a repository component to both flow of water and transport of radionuclides. In this report, the unsaturated zone above and below the repository level are jointly referred to as the unsaturated zone. Hydrology of the unsaturated zone is represented as flow in both porous and fractured media, considering fracture versus matrix flow, groundwater velocity, moisture content, stratigraphic thickness, and fracture and matrix porosity and permeability. Time-varying, deep percolation is derived from the time-varying climate and shallow infiltration. Deep percolation is perturbed at the near field by decay heat at the repository level, resulting in alterations to the amount, arrival time, and chemical composition of the fluid to which the waste packages and waste forms may be exposed. Movement of water toward or away from the waste package is expected to take place by potential large-scale (external to the drift) focusing or diversion, film flow at the surface of the drift, capillary diversion in the fractures near the drift, and diversion of flow caused by the presence of corrosion products in corroded waste packages.

Radionuclide transport in the unsaturated zone between the repository horizon and the water table is primarily a function of groundwater travel time, sorption, matrix diffusion, and longitudinal dispersion. Retardation of radionuclides in fractures caused by sorption is expected to be small and, therefore, is not represented in the basecase. Although the mathematical model can handle matrix diffusion in the unsaturated zone, it is expected to be minor on the basis of off-line modeling studies. Therefore, it is conservatively assumed not to occur for the basecase.

Suppression of the unsaturated zone repository component requires consideration of its characteristics as a flow repository component (above and below the repository) and its characteristics as a transport repository component below the repository. In the total system performance assessment model, water is assumed to percolate directly through fractures to the repository near field after shallow infiltration in the surficial soil, which, to some degree, tempers the temporal variation of the infiltration. Suppression of the unsaturated zone as a flow repository component above the repository requires modifications to only the infiltration in the surficial soil, thermo-hydrological refluxing, and near-field flow convergence or divergence. The shallow infiltration rate is replaced with precipitation to reflect suppression of the unsaturated zone above the repository. To suppress the near-field flow diversion, parameters representing the thermal dryout zone thickness, the fraction of condensate removed from the reflux zone, the fraction of condensate moving toward the repository, and the fraction of condensate removed by other processes are adjusted in such a way that water from the deep percolation can reach the waste package without the delay or loss caused by the reflux. To suppress flow diversion, the flow multiplication factors (F_{ow} , together with its multiplier that reflects uncertainty) are adjusted so that all deep percolation will reach the waste packages, and waste packages in the repository are exposed to deep percolation.

Suppression of the unsaturated zone as an impediment to flow and transport below the repository requires modifications to the thicknesses of the stratigraphic units. Consequently, the effective distance between the repository and the saturated zone becomes zero. When only the unsaturated zone repository component is suppressed, the waste packages still form bathtubs for radionuclide release, though the filling time will be different compared with the basecase.

6.2.6 Saturated Zone

The alluvium unit layer of the saturated zone is expected to substantially delay transport of radionuclides. A two-dimensional horizontal flow model is used to construct the steady-state velocity fields represented through a series of three, one-dimensional flow tubes from the water table (at locations directly below the repository) to the receptor location. The model for radionuclide transport in the saturated zone considers longitudinal dispersion, retardation, and matrix diffusion. Lateral dispersion and sorption of radionuclides on fracture surfaces are not included.

Repository component analysis of the saturated zone repository component requires suppression of those characteristics that delay the transport of radionuclides, such as modifications to length of the flow path in the fractured tuff aquifer and length of the flow path in alluvium between the repository footprint and the receptor located at 20 km [12.4 mi] from the repository. In the basecase the projected radionuclide transport path length from the repository footprint to the tuff-alluvium contact (via the fractured tuff aquifer) ranges between 10 and 20 km [6.2 and 12.4 mi], has a uniform distribution, and has a mean distance of 15 km [9.3 mi], which results in an average alluvium length of 5 km [3.1 mi]. By specifying the alluvium length essentially 0 km [0 mi], the beneficial sorption capacity and high kinematic porosity of the saturated alluvium were excluded from the calculation. By adjusting the alluvium length, the tuff aquifer was extended to the 20-km [12.4-mi] compliance point so the reasonably maximally exposed individual at 20 km [12.4 mi] can be used. The flow in the fractured tuff aquifer is predominantly in fractures and is assumed to be fast. The nominal fracture porosity, which is log-uniformly distributed ranging between 1×10^{-3} and 1×10^{-2} , was changed to a constant value of 1×10^{-4} , and the fracture-to-matrix diffusion coefficient was changed from 1×10^{-3} to 0.0 so the traveltime in the artificially established 20-km [12.4-mi] fractured tuff was small (~12 to 15 years). Other parameters, such as (i) longitudinal dispersivity (sampled as a fraction of the transport path length), (ii) effective flow porosities, (iii) matrix (immobile) porosity, and (iv) fraction of the immobile porosity penetrated for the saturated tuff have little if any effect under the neutralized conditions, and did not need to be changed from the values used in the basecase.

6.3 Effects of Disruptive Events on Repository Components

Three disruptive events were included in the performance assessment model: seismicity, faulting, and volcanism. Although the primary effect of seismicity and faulting in the system performance calculation was to cause additional waste package failures, the effect of an igneous activity disruptive event was broader. An intrusive igneous activity event results in failure of waste packages, whereas an extrusive igneous activity event creates a new source term because of waste-form entrainment to the atmosphere and a new biosphere pathway resulting from airborne transport of radionuclides and redistribution of radionuclides in soil. Repository component sensitivities also may be influenced by these external events.

Because seismicity, faulting, and intrusive igneous activity are modeled primarily to disrupt waste packages, the waste package repository component sensitivity analysis already provides needed information. Repository component sensitivity analysis for extrusive igneous activity requires somewhat complicated calculations involving convolution of as many as 12 sets of Monte Carlo calculations completed for various time periods. In the current model, the 12 sets are computed at fixed volcanic event times: 100; 500; 1,000; 2,000; 3,000; 4,000; 5,000; 6,000;

7,000; 8,000; 9,000; and 10,000 years for a given repository component suppression case. In this report, simulations have been conducted for a 10,000-year simulation period, with the volcanic event time at 10,000 years omitted from each set. All volcanism runs were made with both ground surface and groundwater dose contributions. Normal igneous activity calculations assumed groundwater dose can be neglected because the dose consequence (not risk) for igneous activity far exceeds the groundwater dose, and the calculations are configured to consider only ground surface contributions.

6.4 Results

This section presents results from repository component sensitivity analyses using either individual repository components or a combination of repository components. For 6 repository components there can be 64 (i.e., 2^6) possible unique combinations. In this report, a selected list of combinations was used with the assumption that other combinations either (i) do not have significant sensitivity or (ii) do not help identify the influential repository components. Because the identification of influential repository components is based on relative change and because results from 100 realizations are comparable to results from 350 Latin Hypercube samples, performing the limited calculations of a single set of 100 realizations for each configuration of suppressed barriers is consistent with the goals for conducting this analysis. Results for the basecase {i.e., a peak expected annual dose of 2.0×10^{-4} Sv/yr [0.02 mrem/year] within 10,000 years} are based on a single set of 350 realizations—the best estimate for peak expected dose may be higher or lower (see Appendix H for a related discussion on the stability of the results for limited realizations), similarly, the results presented for each suppressed configuration may be higher or lower than the best estimate. Consequently, if the ratio of the peak expected dose for the suppressed configuration to the peak expected dose of the basecase is close to one, suppressing the barrier or barriers may have no effect or a slight effect on the calculated dose.

6.4.1 One-Off Repository Component Sensitivity Analysis

The one-off repository component results are presented in Figure 6-1.

Drip Shield

Suppression of the drip shield resulted in a 34-percent increase in the dose level compared with the basecase. Suppression of the drip shield can potentially hasten the corrosion process and permit early contact of infiltrating water with the spent nuclear fuel. Suppression of the drip shield did not result in early failure of the waste package from corrosion but did permit water to contact spent nuclear fuel at early times. On average, the drip shield delays water contacting spent nuclear fuel in the initially defective waste packages for 7,830 years.

Waste Package

The suppression of the waste package repository component resulted in a 68,200 percent increase in dose with respect to the basecase. In the basecase, only the initially defective waste packages contributed to dose. In the waste package repository component sensitivity case, all waste packages dripped on are available for release at the beginning of the simulation. The average waste package failure time in the basecase is 59,637 years.

DS		DS	DS	DS	DS	DS
WP	WP		WP	WP	WP	WP
WF	WF	WF		WF	WF	WF
Invert	Invert	Invert	Invert		Invert	Invert
UZ	UZ	UZ	UZ	UZ		UZ
SZ	SZ	SZ	SZ	SZ	SZ	
0	34	68,233	61	6	1,979	883

Figure 6-1. Single Repository Component Suppression (One-Off Sensitivity Analysis). Each Row Represents a Monte Carlo Analysis with a Repository Component Suppressed. The First column represents the Basecase with Sx Repository Components. The Gray Color Indicates the Corresponding Repository Component Has Been Suppressed. The Value at the Bottom of Each Column is the Relative Change To the Peak Expected Dose in Percent.

Waste Form

The suppression of the waste form as a repository component increased the dose by 60 percent. The dissolution time was set at 50 years for numerical efficiency in this case. The suppression of the waste form repository component decreased the time in which the spent nuclear fuel completely dissolved in water from more than 100,000 years (for 60 percent of the cases) to 50 years. It could be assumed that this would result in a many fold increase in the dose, but this is not the case. The less than two-fold increase in dose implies that even if

spent nuclear fuel dissolved quickly, the solubility limit of the radionuclides constrained their removal from the waste package.

Invert

The suppression of the invert as a repository component increased dose by 6 percent. This small change can be attributed to a short {0.75-m [2.5-ft]} transport path. Depending on the infiltration rate, flow through the invert is either predominantly matrix flow or predominantly fracture flow. Because the flow in the invert in the basecase was predominantly fracture flow (contrary to the original hypothesis) and because of the assumption that the radionuclides were not retarded in fractures, it comes as no surprise that the dose was insensitive to invert suppression.

Unsaturated Zone

For the purposes of this analysis, the upper unsaturated zone (above the repository) and the lower unsaturated zone (below the repository) are considered as a single repository component called the unsaturated zone. The suppression of the unsaturated zone as a repository component resulted in a 2,000 percent increase in peak expected dose. Travel times were relatively fast through the lower unsaturated zone, and none of the radionuclides were retarded in the fractures. In subareas where the Calico Hills vitric layer was thin or absent, soluble, unretarded species such as Tc-99 and I-129, were minimally influenced by transport through the lower unsaturated zone matrix. The lower unsaturated zone matrix may retard some species, such as uranium and thorium, but because of the predominant fracture flow in most of the subareas, these nuclides did not travel much faster in the repository component sensitivity case. Therefore, radionuclide transport in the lower unsaturated zone does not influence repository component sensitivity. Consequently, the sensitivity of dose to this repository component can be attributed to the ability of the upper unsaturated zone to limit the amount of water reaching the waste packages. This both increases the transport of radionuclides from the waste packages, and reduces the filling time of those waste packages. On an average, approximately 6 percent of precipitation at the surface of Yucca Mountain infiltrates. The remaining 94 percent is either diverted at the surface or lost by evapotranspiration. With the unsaturated zone suppressed, 100 percent of the water moves toward the waste package. Moreover, the absence of fractures does not focus flow into limited repository areas; hence, all waste packages are dripped on. Therefore, the repository performance shows significant sensitivity to the upper unsaturated zone.

Saturated Zone

The suppression of the saturated zone as a repository component resulted in a 900 percent increase in peak expected dose. The increase in dose resulted from the reduction in the length of alluvium, through which the radionuclides may be transported, and a variation in the flow fields. Tc-99, I-129, and Cl-36 are expected to be primary dose contributors in the basecase and are unretarded in porous alluvium, hence, variations in the flow fields (porosity, permeability, and such) have only a small effect on Tc-99 and I-129 arrival times in 10,000 years. For Np-237, which is moderately retarded in alluvium, however, the impact is more significant when the saturated zone repository component is suppressed. For the 10,000-year simulation period, 85.4 percent of the dose is composed of Np-237, and the

unretarded species (Tc-99, I-129, and Cl-36) compose 14.5 percent of the dose. The remainder of the radionuclides never reach the critical group in the 10,000-year simulation period.

6.4.2 One-On Repository Component Sensitivity Analysis

One-on repository component sensitivity analysis was conducted by first suppressing all repository components and then adding only one repository component. The relative change in dose from the one-repository component case and the case with all repository components suppressed was the sensitivity measure for the one-on repository component sensitivity analysis. The one-on repository component results are presented in Figure 6-2.

One-on sensitivity analysis showed that repository components influenced performance in the following order: waste package, unsaturated zone, saturated zone, waste form, drip shield, and invert. Calculations also clearly showed that only three repository components were most influential: waste package (>99.9-percent decrease in dose), unsaturated zone (96 percent decrease in dose), and saturated zone (94 percent decrease in dose). One-on repository component sensitivity analysis also showed that the invert barely made any contribution to performance. This information is important because with the knowledge of poor performance of the invert, it can be determined if excessive conservativeness could be responsible for this result. Drip shield and waste form repository components showed only moderate sensitivity. Although the analysis presented in Chapter 4 indicated that the drip shield failure time uncertainty significantly influenced repository performance uncertainty, the calculation did not provide insight into the level of performance. One-on sensitivity analysis showed the peak expected dose decreased by 63 percent, a value that can be compared against performance of other individual repository components such as 99.9 percent for the waste package repository component. The absolute performance of the drip shield was not obvious in the one-off analysis because, even if the drip shield performance was suppressed, the waste package prevented water from contacting the spent nuclear fuel.

6.4.3 Cumulative One-On Repository Component Sensitivity Analysis

To illustrate the effects of repository component suppression more clearly, all repository components were suppressed sequentially and cumulatively. By proceeding in a sequence that represents the vertical spatial positions of the repository components from bottom to top, performance of the newly added repository component was not masked by the previously added repository components. The cumulative one-on repository component results are presented in Figure 6-3. The left-most column in Figure 6-3 reflects a case in which all repository components are suppressed. When the saturated zone repository component was added, the peak expected dose decreased by nearly 94 percent. When the unsaturated zone repository component was added cumulatively to the saturated zone repository component, the peak expected dose decreased by nearly 99.2 percent.

Gradual addition of invert and waste form repository components only marginally changed the peak expected dose, whereas addition of the waste package repository component reduced the dose by 99.99 percent. Finally, adding the drip shield repository component reduced the peak expected dose by 99.999 percent.

	DS					
		WP				
			WF			
				Invert		
					UZ	
						SZ
0	-63.4	-99.9	-72.2	-0.2	-95.5	-94.4

Figure 6-2. Single-Repository Component Added to a System in Which All Repository Components Have Been Suppressed (One-On Sensitivity Analysis). The Left-Most Column Represents the Case with All Repository Components Suppressed. The Gray Box Indicates the Corresponding Repository Component Has Been Suppressed. The Values at the Bottom Represent Relative Change to the Peak Expected Dose in Percent.

The row 2 (i.e., the bottom row) values in Figure 6-3 shows the relative change in dose compared with the case to its immediate left. This change can be used to rank the repository components in their ability to decrease the dose. Again, it can be seen that the saturated and unsaturated zones and the waste package are the major contributors to dose reduction.

6.4.4 Repository Component Combination Sensitivity Analysis

In addition to the suppression of one repository component at a time (i.e., one-off analysis) as discussed previously, repository component sensitivity analysis was also performed with suppression of two or more repository components at a time, referred to in this report as the repository component combination sensitivity analysis. The repository component combinations (i) drip shield + waste package, (ii) invert + unsaturated zone + saturated zone, and (iii) drip shield + waste package + waste form + invert, are presented in Figure 6-4 as the relative change to the peak expected dose compared with the basecase. Analyses with combinations of repository components may reveal the cases where the performance of one component masks the performance of another component. For example, the presence of the drip shield may mask the determination of the waste package repository component sensitivity. Instead of

						DS
					WP	WP
				WF	WF	WF
			Invert	Invert	Invert	Invert
		UZ	UZ	UZ	UZ	UZ
	SZ	SZ	SZ	SZ	SZ	SZ
0	-94.5	-99.3	-99.6	-99.8	-99.9	-99.9
0.0	-94.5	-85.8	-51.9	-54.0	-99.9	-25.5

Figure 6-3. Addition of Repository Components to a Completely Suppressed System. Each Column Represents a Monte Carlo Analysis with One Repository Component Added To the Suppressed System at a Time. The Left-Most Column Represents the System with all Six Barrier Components. The Black Color Indicates That the Corresponding Repository Component Has Been Suppressed. The Right Most Column Represents the Basecase in Which All Barrier Components Are Present. The Bottom Row of Values Represents the Change in Peak Expected Dose Relative to the Case to its Immediate Left. The Values in the Next Higher Row Represent Change to the Peak Expected Dose from 100 Realizations Relative to the Left-Most Column.

using an exhaustive set of combinations for repository component combination sensitivity analysis, selected combinations were used.

The drip shield and waste package combination represents the main elements of the engineered barrier subsystem. A common characteristic is the ability to divert the in-drift flow of water. Analysis of this case showed an increase of 179,000 percent (see the column 4, Figure 6-4) when these 2 repository components are suppressed. As expected, this increase exceeded the sum or the product of the relative change to dose associated with the waste package and the drip shield repository components individually as evident from the one-off analysis. Suppression of the waste package and drip shield repository components greatly magnified the dose despite the minor increase in dose when only the drip shield was suppressed. This increase is intuitively correct because when only the drip shield is suppressed, releases take place from the initially defective waste packages only. Likewise, when the waste package repository component was suppressed, the drip shield prevented water from entering these waste packages for an average of 7,800 years; thus, release takes place for an average of 2,200 years. When both barriers are suppressed, however, all waste packages (breached) are exposed to water from year zero. Thus, the analysis revealed the sensitivity of repository performance to the waste package repository component without the masking effect of the drip shield.

A similar analysis can be performed with the remaining cases in Figure 6-4, however, it is not presented here. While performing barrier combination sensitivity analyses, it is important to note that when one repository component is suppressed, the suppression could influence how the repository components it is combined with are treated. For example, when the waste form repository component is suppressed in the single-repository component sensitivity analysis, the bathtub water contact mode is applied. In this model, not all spent nuclear fuel in the waste package is wet, and water diversion takes place on top of the waste package. When the waste package repository component is simultaneously suppressed with the waste form, however, a bathtub cannot form, and flow diversion cannot occur because the waste package is suppressed. Consequently, all spent nuclear fuel in a waste package will be contacted by water.

In summary, the repository component sensitivity analyses (i.e., one-off, one-on, cumulative one-on, and selected combination sets) provide useful information about the sensitivity of the repository performance to the repository subsystems. The influential repository components in order of influence are (i) waste package, (ii) unsaturated zone, (iii) saturated zone, (iv) waste form, and (v) drip shield. By analyzing the repository component sensitivity results in conjunction with the system-level results, it can be inferred that the waste package and the unsaturated and saturated zones substantially delay release. The repository component sensitivity results also showed the drip shield and waste form provide system resiliency. Because many scenarios presented in this analysis represent extreme and often physically unrealistic cases, caution should be exercised when interpreting the calculated dose.

DS	DS			DS
WP	WP			WP
WF	WF		WF	WF
Invert	Invert		Invert	
UZ		UZ	UZ	
SZ		SZ	SZ	
0	59,900	808,233	179,067	59,900

Figure 6-4. Combination Repository Component Suppression Sensitivity Analysis. Each Row Represents a Monte Carlo Analysis with a Combination of Repository Component Suppressed. The First Column Represents the Basecase With Six Repository Components. The Gray Color indicates the Corresponding Repository Component Has Been Suppressed. The Value at the Bottom of Each Column Is the Relative Change to the Peak Expected Dose in Percent.

7 SYNTHESIS OF RESULTS AND RISK INSIGHTS

This chapter synthesizes information from the analyses presented in Chapters 3, 4, 5, 6, and Appendixes F and G. Chapter 3 presented trends in repository system and subsystem responses to models and data, including the effects of input uncertainty and variability on the output uncertainty. Chapters 4–6 presented parametric, distributional, and subsystem (or repository component) sensitivity analyses and their results, as well as results from alternative conceptual models. Appendixes F and G present risk calculations for stylized human intrusion and in-package criticality. This chapter (7) focuses on identifying the important parameters, alternative models, and subsystems that significantly influence performance.

The following sections discuss the system-level overall performance results including the basecase, disruptive event cases, stylized human intrusion, and in-package criticality. Barrier capability, as derived from the analysis of total system behavior calculations (Chapter 3), is presented next, followed by sensitivity analysis results from various methods (parametric, distributional, alternative conceptual model, and repository component). Parametric sensitivity analysis results from Chapter 4 are aggregated to extract the final list of the top 10 influential parameters from the basecase and the igneous activity case. These results are then verified by runs that demonstrate that most uncertainty in the dose is a result of uncertainty in the chosen parameters. Finally, the influential parameters, alternative conceptual models, and repository components are linked with integrated subissues to identify the parameters significant to performance for higher doses and maximum sensitivity to changes in parameters and conceptual models.

Although the radionuclide C-14 was included in the calculations of release, transport and dose, it will not be included in the synthesis of results. Currently, the TPA 4.1 code considers that C-14 would be in equilibrium between the water and gas phases, and would mostly partition into the gas stream, thereby being released primarily to the atmosphere (Codell and Murphy, 1992). Under 10 CFR Part 60, the staff considered that the atmospheric releases of C-14 were more important for a geologic repository than the liquid releases because of the consideration in that rule of population dose, and therefore the TPA code considered all released to be to the gas phase. The regulations in 10 CFR Part 63, consider the dose to an individual rather than a population, places far less emphasis on doses from gaseous C-14. Conservatively, all releases of C-14 could have been included in the liquid phase, but the TPA 4.1 code does not have this provision. The staff does not believe that the omission of C-14 from the results will alter any conclusions.

Insights gained from the risk analyses produced by the TPA Version 4.1 code must be tempered by the following considerations:

- There are many assumptions, uncertainties, conservatisms, and other limitations in the analyses.
- The results of the TPA Version 4.1 code are only pertinent to those conceptual models embodied in it (e.g., there is no diffusion from the waste packages and no cladding degradation, so no pertinent results on these phenomena can come directly from the analyses).

- The TPA Version 4.1 code was not developed as a tool to demonstrate compliance of the Yucca Mountain repository with 10 CFR Part 63 regulations; this is not the U.S. Nuclear Regulatory Commission's (NRC) responsibility. Instead, the TPA code is a tool for use by NRC to better understand the functioning of the repository, and to allow independent review of the U.S. Department of Energy (DOE) performance assessment.

7.1 Overall Performance Analyses

7.1.1 Basecase

The results from the Monte Carlo sampling with 350 realizations using the basecase data set with a total of 950 parameters (330 sampled) show a peak risk value of 2.1×10^{-7} Sv/yr [0.021 mrem/yr] occurring at approximately 10,000 years. The peak dose from the mean value data set is 3.5×10^{-7} Sv/yr [0.035 mrem/yr]. Although the doses from these two cases are similar, they cannot be interpreted in the same way. For example, in the case of the 10,000-year simulation period, the major contributors to dose in the mean value data set case are I-129 and Tc-99. For multiple realizations, Np-237 is also a major contributor because Monte Carlo analysis allows the code to investigate regions of parameter space where Np-237 reaches the users in 10,000 years. Such an insight is not likely from a single, representative data set like the mean. Monte Carlo results show the doses at the time of peak expected dose in 10,000 years range from 0 to 6.95×10^{-6} Sv/yr [0.695 mrem/yr] {standard deviation = 7.1×10^{-7} Sv/yr [0.071 mrem/yr]} with 33 percent of realizations resulting in zero dose.

7.1.2 Disruptive Events

Igneous activity increases the peak risk from 2.1×10^{-7} Sv/yr [0.021 mrem/yr] for the basecase to 3.49×10^{-6} Sv/yr [0.349 mrem/yr], a 16 fold increase. Moreover, igneous activity shifts the time of occurrence of peak risk from ~10,000 for the basecase to 245 years. Probability-weighted faulting events do not influence the peak risk significantly. Seismic disruptive events did not contribute to peak risk in the Monte Carlo runs with 350 or 4,000 vectors for the 10,000-year simulation period.

7.1.3 Human-Intrusion Scenario Analysis

A stylized, very conservative and nonmechanistic analysis of the human-intrusion scenario calculations (see Appendix F) show a peak dose of approximately 10^{-6} Sv/yr [0.1 mrem/yr] in the 10,000-year simulation period. This peak dose is approximately one order of magnitude higher than the peak expected risk for the basecase but is still much smaller than that the 0.15 mSv/yr [15 mrem/yr] in the regulation. The results reflect limited spent nuclear fuel inventory available for additional release in this scenario. Only 1 waste package of 8,877, or less than 0.012 percent of the spent nuclear fuel, is made available for release by the stylized human-intrusion scenario. The conservative choice of the grain-size model for the human-intrusion analysis instead of the particle-size model for the basecase increases the surface area by a factor of approximately 150 for the TPA Version 4.1 code mean value data set. Because only 1 waste package is breached by human intrusion, compared with approximately 45 waste packages breached by initial defects, the net increase in available surface area is approximately a factor of three greater for human intrusion. As estimated in the TPA Version 4.0 code user's guide (Mohanty, et al., 2002), selection of fuel-dissolution Model 1 alone results in approximately a 100-times faster dissolution rate than Model 2 used in the basecase. This

faster dissolution rate, along with the higher flow rate of water into the waste package for the human-intrusion scenario, and the high solubility of Cl-36, Tc-99, I-129, and Np-237 contribute significantly to the higher expected annual doses for the human-intrusion scenario.

7.1.4 In-Package Criticality Analysis

Both steady-state and transient criticality show an increase in the conditional peak expected dose following a criticality event (see Appendix G). The staff made no attempt to estimate the probability of criticality, although it is expected to be small. DOE used a probability of 0.001 to 0.005 criticality events in 10,000 years for its total system performance assessment analyses (DOE, 1998b).

The steady-state case assumes the energy produced by the nuclear chain reaction is balanced exactly by the heat lost through thermal conduction in the rock and evaporation of water from the waste package. Several likely conservatisms are in this analysis: (i) criticality is assumed in all 32 initially defective waste packages starting at 5,000 years; (ii) all critical waste packages were under drips, and (iii) release continued to occur during the criticality, despite heat release from the spent nuclear fuel. Criticality in the prematurely failed waste packages results in a conditional peak expected dose higher than the basecase dose by approximately a factor of three.

In-package transient criticality calculations assume the contents of a waste package containing spent nuclear fuel undergo a fast transition to criticality, followed by an energetic steam explosion that destroys the container and disperses the spent nuclear fuel as fine, easily dissolved particles. The analysis used a highly conservative release rate model that led to a relatively fast release of the entire content of the waste package. The conditional peak expected dose for this event exceeds that of the basecase in the 10,000-year simulation period by an order of magnitude but nonetheless is considerably smaller than the 0.15 mSv/yr [15 mrem/yr] standard in 10 CFR Part 63. Transient criticality gives rise to a relatively large peak in conditional dose shortly after the event is assumed to occur and quickly drops below the basecase peak expected dose. The staff considers the risk from this event to be small because the conditional dose is below the standard, and probability of the event is expected to be low. Therefore, the staff does not plan to refine this analysis further.

7.2 Barrier Capability Analysis

The barrier capabilities presented in this section are derived from the system-level and intermediate-level performance assessment results presented in Chapter 3. The barriers are defined as materials or structures that prevent or substantially delay movement of water or radionuclides. The intent is to emphasize how well the barriers prevent or delay release of most radionuclides rather than to focus on the peak expected dose. Results presented below reflect the conceptual models in the TPA Version 4.1 code and the input parameters used.

7.2.1 Length of Time Waste Packages Remain Intact

The repository is specified to have 8,877 waste packages; 1 to 88 (an average of 44) of which are specified to have undergone initially defective failure (i.e., failure year 0). Aside from these initially defective waste packages, the other waste packages are subject to corrosion or mechanical failure because of seismicity, faulting, and igneous activity. No corrosion

failure is observed within 10,000 years. The waste packages remain intact from corrosion for 37,900–100,000 years (and longer), with an average life of 68,000 years. Waste packages do not fail from seismicity during the 10,000-year simulation period. On an average, 33 waste packages fail from faulting events and 47 waste packages fail from igneous activity events [4 from extrusive (range: 1–9) and 43 from intrusive (range: 6–88)]. These 47 waste packages could fail as early as 100 years, however, the event probabilities are low. Accounting for failures from the basecase and all disruptive event scenarios, on average, 124 waste packages could fail within 10,000 years. In other words, 8,753 (i.e., 8,877 – 44 – 33 – 47) waste packages that account for 98.6 percent of the total wastes, would remain intact for 10,000 years.

7.2.2 Length of Time the Drip Shield Remains Intact

The drip shield is specified to remain intact for 2,700–20,400 years (lognormally distributed), with an average lifetime of 7,422 years. Depending on the type and location of failure, a partially failed drip shield could prevent water from entering the breached waste packages. The TPA Version 4.1 code, however, assumes that once the drip shield fails, it is no longer a barrier to flow.

The drip shield could lose its integrity more quickly because failure from rockfall has not been considered in the model. Failure of the drip shield in the first few thousand years, however, would be mitigated by thermal effects, which would reduce or eliminate dripping. The drip shield may minimize localized corrosion by preventing aggressive chemicals from contacting the waste package at high temperature. As modeled in the TPA Version 4.1 code, however, the corrosion models assume that aggressive chemistry would be present regardless of the effects of the drip shield, so the drip shield is given no credit for this protection. Drip shield behavior, therefore, appears simply as a barrier to flow, redundant with the waste package and thermal effects, through the engineered barrier subsystem.

7.2.3 Amount of Meteoric Water Percolating into the Repository Horizon

For the models and parameters chosen, the cumulative amount of meteoric water percolating to the repository horizon in 10,000 years is $5.323 \times 10^8 \text{ m}^3$ [$1.88 \times 10^{10} \text{ ft}^3$], which gives rise to an average rate of $53,230 \text{ m}^3/\text{yr}$ [$1.88 \times 10^6 \text{ ft}^3/\text{yr}$]. This amount contrasts with the cumulative precipitation averaged for all realizations [$8.771 \times 10^9 \text{ m}^3$ [$3.1 \times 10^{11} \text{ ft}^3$]], which gives rise to an average of $8.77 \times 10^5 \text{ m}^3/\text{yr}$ [$3.1 \times 10^7 \text{ ft}^3/\text{yr}$] and amounts to approximately 6 percent of the precipitation at the surface of Yucca Mountain. The remaining 94 percent is either diverted at the surface by runoff or lost because of evapotranspiration. The model assumes the infiltration outside the column representing the repository block is not diverted laterally toward the repository.

7.2.4 Packages That Experience Dripping

Waste packages that experience dripping are assumed to vary from 0 to 100 percent with a uniform distribution and an average of 50 percent. This assumption implies that, on average, 4,439 waste packages would experience dripping after the drip shield fails. Dripping is not expected on all waste packages because flow is contained primarily in channels through fractures, and not all fractures are flowing. The location of drips in tunnels could change with

time because of changes in fracture dimensions caused by chemical, mechanical, or thermal effects, but this potential change is not modeled in the TPA Version 4.1 code.

7.2.5 Amount of Water that Contacts Waste

On average, $1.765 \times 10^6 \text{ m}^3$ [$6.23 \times 10^7 \text{ ft}^3$] of water falls on to the dripshield (and eventually on to the waste package) in 10,000 years for the models and parameters assumed. This total amounts to an average rate of $176.5 \text{ m}^3/\text{yr}$ [$6.23 \times 10^3 \text{ ft}^3$] of water, which is 0.02 percent of the precipitation and 0.332 percent of the 10,000-year average infiltrations. Dripping water will contact waste packages only after the drip shield fails. Some water would be diverted around the drift by capillarity in the rock. Another portion would flow along the drift wall. The remainder of the water would drip into the drift, with some of that falling onto the drip shield and subsequently onto the waste package after drip shield failure. Of the part that falls directly onto the waste package, only a fraction would enter through openings that were either directly under the drip or in the path of the runoff. Approximately 300 m^3 [$10,600 \text{ ft}^3$] of water enter into failed waste packages during the 10,000 year simulation period after the drip shields fail {i.e., 6.71 m^3 [237 ft^3] per waste package}, which is 0.0037 percent of the infiltration and 0.002 percent of the precipitation.

7.2.6 Release Rates of Particular Radionuclides Based on Solubility Limits and Water Flow

The release of all but 7 of 19 radionuclides is controlled by the radionuclide solubility limits, for the models and parameters assumed. Radionuclides that experience a solubility-limited release are U-238, U-234, Pu-239, Pu-240, Nb-94, Am-241, Am-243, Np-237, Th-230, Cm-246, Cm-245, and Ra-226. The release is solubility limited greater than 90 percent of the time for U-238, U-234, Pu-239, Pu-240, and Nb-94. The release is solubility limited more than 50 percent of the time for Am-241, Am-243, and Np-237 and the release is solubility limited less than 50 percent of the time for Th-230, Cm-246, Cm-245 and Ra-226. The radionuclides that do not undergo solubility-limited release are Pb-210, Cs-135, I-129, Tc-99, Ni-59, Se-79, and Cl-36. The radionuclides that experience solubility-limited release are determined by the solubility limits, time-dependent flowrate, radionuclide half life and the radionuclide inventory. Note that because of the time-varying flow rate, all of the nuclides having a solubility-limited release also switch between solubility-limited and dissolution-limited release from the waste package (see the 3rd and 5th columns in Table 7-1). Although barrier capability analysis does not show the magnitude of decrease in the release rate because of the solubility limits, the analysis indicates that release of the majority of the radionuclides are limited at the specified solubility values. The degree to which solubility limits restrict release of radionuclides from the engineered barrier system can be found under the summary of alternative conceptual model results presented later in this chapter.

Table 7-1. Time that Radionuclide Releases Are Controlled by the Solubility Limit and the Frequency of the Release Mode Switching from Solubility Limited to Dissolution Limited in 10,000 Years (All Isotopes of Radioelement Have the Same Solubility Limit)

Radionuclide	Average Length of Time Release Is Solubility Limited	Time Span (Out of 10,000 Years) That the Nuclide Is Solubility Limit Controlled (%)	Rank by Average Length of Time Release Is Solubility Limited	Average Number of Cycles Release Switches from Solubility Limited to Dissolution Limited	Ranking by the Average Number of Cycles Release Switches from Solubility Limited to Dissolution-Limited
U-238	1,224	12.2	1	0.001	9
U-234	1,224	12.2	1	0.001	9
Pu-239	1,223.7	12.2	3	0.001	9
Pu-240	1,223.7	12.2	3	0.001	9
Nb-94	1,194.2	11.9	5	0.018	8
Am-241	1,065.5	10.7	6	0.073	6
Am-243	1,065.5	10.7	6	0.073	6
Np-237	764.85	7.6	8	0.149	1
Th-230	513.05	5.1	9	0.142	4
Cm-246	285.75	2.9	10	0.143	2
Cm-245	285.75	2.9	10	0.143	2
Ra-226	236.35	2.4	12	0.08	5
Pb-210	0	0	13	0	13
Cs-135	0	0	13	0	13
I-129	0	0	13	0	13
Tc-99	0	0	13	0	13
Ni-59	0	0	13	0	13
Se-79	0	0	13	0	13
Cl-36	0	0	13	0	13

7.2.7 Delay in Release of Particular Radionuclides in the Engineered Barrier Subsystem

The percentage of the initial inventory of radionuclides specified for groundwater release that leaves the engineered barrier subsystem in 10,000 years is shown in Table 7-2 for the models and parameters chosen. Note that the releases of Pb-210 and Ra-226 exceed 100 percent of the initial inventory, caused by ingrowth of these radionuclides along the transport pathway from U-234 transport. Ingrowth from U-234 transport also causes the relatively high release of Th-230 for 7 percent of the initial inventory. The next greatest level of release is 0.02 percent of the initial inventory for seven radionuclides: I-129, Tc-99, Cl-36, Se-79, Np-237, Ni-59, and Cs-135, several of which ultimately reach the pumping well. For the three radionuclides that

Table 7-2. Percentage of Individual Radionuclides Released in 10,000 Years with Respect to Initial Inventory at Engineered Barrier Subsystem, Unsaturated Zone, and Saturated Zone Outlets

Groundwater Radionuclide	Initial Inventory (Ci)	Cumulative Release (Percentage of Initial Inventory)		
		Engineered Barrier Subsystem	Unsaturated Zone	Saturated Zone
I-129	3×10^3	2×10^{-2}	2×10^{-2}	2×10^{-2}
Tc-99	1×10^6	2×10^{-2}	2×10^{-2}	2×10^{-2}
Cl-36	8×10^2	2×10^{-2}	2×10^{-2}	2×10^{-2}
Se-79	2×10^3	2×10^{-2}	1×10^{-2}	4×10^{-4}
Np-237	3×10^4	1×10^{-2}	5×10^{-3}	3×10^{-5}
Ni-59	2×10^5	2×10^{-2}	1×10^{-2}	4×10^{-6}
Pb-210	4×10^{-3}	6×10^4	3×10^4	2×10^{-7}
Ra-226	3×10^{-2}	4×10^3	2×10^3	1×10^{-7}
Th-230	1×10^1	7×10^0	3×10^0	5×10^{-8}
U-234	8×10^4	7×10^{-6}	3×10^{-6}	7×10^{-9}
U-238	2×10^4	6×10^{-6}	3×10^{-6}	6×10^{-9}
Cm-246	5×10^3	5×10^{-3}	5×10^{-3}	0×10^0
Cm-245	3×10^4	8×10^{-3}	8×10^{-3}	0×10^0
Am-241	2×10^8	7×10^{-8}	4×10^{-8}	0×10^0
Am-243	2×10^6	4×10^{-4}	2×10^{-4}	0×10^0
Pu-239	3×10^7	1×10^{-5}	5×10^{-6}	0×10^0
Pu-240	4×10^7	6×10^{-6}	3×10^{-6}	0×10^0
Cs-135	4×10^4	2×10^{-2}	1×10^{-2}	0×10^0
Nb-94	6×10^4	1×10^{-4}	1×10^{-4}	0×10^0

contribute greatest to dose, approximately 0.02 percent of the inventory is released from the engineered barrier subsystem.

Delay in release is the result of several factors. First, most of the radionuclides are released from spent nuclear fuel congruently, which implies the delay in spent nuclear fuel dissolution delays release of the radionuclides. With the fastest dissolution rate model, the time for spent nuclear fuel dissolution is less than 1,300 years. Second, the bathtub formed in the failed waste package for several failure modes must fill before radionuclides can leave the waste package. Third, the invert may delay release of the radionuclides. Fourth, the radionuclides are restricted to leave the waste package at a rate less than or equal to the solubility limit times the flow rate. The analysis presented in Chapter 3 does not reveal the extent to which the invert delays radionuclide transport. Information, however, can be extracted from the repository component sensitivity analysis results presented in Chapter 6.

Nineteen radionuclides in the TPA Version 4.1 code have been considered for groundwater releases. The minimum breakthrough from the engineered barrier subsystem time for all 19 radionuclides is 2,730 years. The average breakthrough time for all these radionuclides ranges between 16,225 and 19,614 years. The minimum, average, and maximum arrival times at the end of each barrier for all 19 radionuclides are presented in Table 7-3.

7.2.8 Delay in Transport of Particular Radionuclides in the Unsaturated Zone

For the models and parameters chosen, the average groundwater traveltime in the unsaturated zone (averaged for time and realization) varies spatially among subareas between ~12 years (in Subarea 10) to 769 years (in Subarea 7), with a repository average of 209 years. These traveltimes may be artificially low because of assumptions made in the abstraction of transport in the unsaturated zone, particularly the deliberate bypassing of thin layers for computational efficiency. The shortest groundwater traveltime in any realization is 10 years (in Subarea 10), and the longest in any realization is 3,437 years (occurs in Subarea 7). The largest factor in the arrival time appears to be the presence of the Calico Hills vitric layer because of its high porosity and lack of fracture flow.

The minimum arrival time at the end of the unsaturated zone is 2,933 years for the radionuclides, which include Am-241, Cl-36, Cm-245, Cm-246, I-129, Nb-94, Np-237, Pb-210, Ra-226, Tc-99, Th-230, U-234, and U-238. The average arrival times for the same radionuclides vary between 16,271 and 31,525 years. The arrival time for the remaining six radionuclides (Am-243, Cs-135, Ni-59, Pu-239, Pu-240, and Se-79) is at least 3,635 years. The average arrival time for these radionuclides varies between 22,087 and 66,497 years.

The percentage of initial inventory of the radionuclides specified for groundwater release that leaves the unsaturated zone in 10,000 years is shown in Table 7-2. Pb-210 and Ra-226 leaving the unsaturated zone are 30,000 and 2,000 percent of the initial inventory, caused by ingrowth from U-234 transport. Aside from these two radionuclides, the largest amount of radionuclides leaving the unsaturated zone is Th-230, which is 3 percent of the initial inventory, also largely because of U-234 transport and ingrowth. The next level of release 0.01–0.02 percent of the initial inventory, includes I-129, Tc-99, Cl-36, Se-79, Ni-59, and Cs-135, several of these ultimately reach the pumping well. For the three radionuclides that contribute most to dose, only 0.02 percent of the inventory is released from the engineered barrier subsystem and the unsaturated zone. The difference in the cumulative 10,000-year release for unretarded radionuclides between the engineered barrier subsystem and the unsaturated zone can be seen only in the third or fourth decimal place, which is not shown in Table 7-2. This difference is consistent with the short arrival in subareas of the unsaturated zone that do not contain the Calico Hills vitric unit.

Although relatively unretarded radionuclides like Tc-99, I-129, Cl-36, Se-79 and Ni-59 are not delayed greatly by the unsaturated zone, it would be a mistake to say that the unsaturated zone is not an effective barrier. For the 10 computed subareas, 6 include the Calico Hills vitric unit, and account for about half of the waste packages. For subareas where the Calico Hills vitric unit is present, there would be substantial delays for both unretarded and retarded radionuclides. Virtually no retarded radionuclides would escape those subareas in the regulatory period of 10,000 years.

The minimum, average, and maximum arrival times for all 19 radionuclides are presented in Table 7-3.

Table 7-3. Time of First Arrival of the Radionuclides at the Outlet of Engineered Barrier Subsystem, Unsaturated Zone, and Saturated Zone. Shown Are the Minimum, Average (Averaged over All Subareas and Realizations), and Maximum Breakthrough Times.									
Radionuclide	Minimum Time Engineered Barrier Subsystem	Average Time Engineered Barrier Subsystem	Maximum Time Engineered Barrier Subsystem	Minimum Time Unsaturated Zone	Average Time Unsaturated Zone	Maximum Time Unsaturated Zone	Minimum Time Saturated Zone	Average Time Saturated Zone	Maximum Time Saturated Zone
Am-241	2,730	18,786	100,000	2,933	18,992	100,000	28,000	99,644	100,000
Am-243	2,730	17,388	100,000	3,635	66,496	100,000	100,000	100,000	100,000
Cl-36	2,730	16,225	100,000	2,933	16,271	100,000	3,076	16,379	100,000
Cm-245	2,730	18,525	100,000	2,933	18,577	100,000	17,200	98,697	100,000
Cm-246	2,730	18,525	100,000	2,933	18,607	100,000	26,200	99,832	100,000
Cs-135	2,730	16,268	100,000	3,635	38,466	100,000	8,490	82,744	100,000
I-129	2,730	16,225	100,000	2,933	16,271	100,000	3,076	16,379	100,000
Nb-94	2,730	16,460	100,000	2,933	16,503	100,000	7,376	45,385	100,000
Ni-59	2,730	16,243	100,000	3,635	36,628	100,000	4,291	46,693	100,000
Np-237	2,730	16,692	100,000	2,933	17,434	100,000	4,191	33,755	100,000
Pb-210	2,730	19,614	100,000	2,933	31,525	100,000	5,696	51,651	100,000
Pu-239	2,730	17,388	100,000	3,635	66,489	100,000	6,560	76,424	100,000
Pu-240	2,730	17,388	100,000	3,635	66,496	100,000	6,875	82,263	100,000
Ra-226	2,730	16,460	100,000	2,933	28,539	100,000	5,564	47,930	100,000
Se-79	2,730	16,225	100,000	3,635	22,087	100,000	4,191	32,367	100,000
Tc-99	2,730	16,225	100,000	2,933	16,271	100,000	3,076	16,379	100,000
Th-230	2,730	17,388	100,000	2,933	29,517	100,000	5,308	46,992	100,000
U-234	2,730	16,460	100,000	2,933	27,985	100,000	5,308	45,553	100,000
U-238	2,730	16,460	100,000	2,933	16,980	100,000	4,945	33,909	100,000

7.2.9 Delay in Transport of Particular Radionuclides in the Saturated Zone

The average groundwater traveltime in the saturated zone varies among subareas between 578 years (in Subareas 2 and 4) and 821 years (in Subarea 9) with a repository average of ~644 years. These averages are taken at a scale that reflects the interface area between an unsaturated zone subarea and a saturated zone streamtube. The shortest groundwater traveltime through the saturated zone for a single realization is 57 years (in Subarea 7). The longest groundwater traveltime through the saturated zone for a single realization is 1,790 years (in Subarea 9).

The combined unsaturated and saturated zones average traveltimes in the 10,000-year simulation period vary spatially between 598 and 1,395 years, with a repository average value of 926 years. Therefore, the radionuclides will be delayed an average of at least 926 years in the natural system.

The minimum arrival time at the end of the saturated zone for Am-241, Am-243, Cm-245, and Cm-246 is greater than 10,000 years (see Table 7-3). Three of the remaining 15 radionuclides (i.e., Tc-99, I-129, and Cl-36) travel at the groundwater velocity. Therefore, the earliest time these three radionuclides can reach the production well is 3,076 years. The earliest arrival time for the remainder of the radionuclides (i.e., Cs-135, Nb-94, Ni-59, Np-237, Pb-210, Pu-239, Pu-240, Ra-226, Se-79, Th-230, U-234, and U-238) ranges between 4,191 (for Np-237 and Se-79) and 8,490 years (for Cs-135). Average arrival times for all the radionuclides is greater than 10,000 years.

One hundred percent of the inventory of 9 of 19 radionuclides is delayed from reaching the pumping well in 10,000 years. Five of the remaining 11 radionuclides (i.e., Pb-210, Ra-226, Th-230, U-234, and U-238) experience only small releases from the saturated zone and a small fraction of the initial inventory of these radionuclides (see Table 7-2) enters the well. Note that in spite of substantial ingrowth of Pb-210 and Ra-226, only a small amount reaches the user's well because of retardation in the saturated zone. Also note that a small fraction of the initial inventory of Se-79, Np-237, and Ni-59 enters the wellbore because most of the mass is retarded in the saturated zone. The 3 primary radionuclides contributing to dose in the 10,000-year simulation period are Tc-99, I-129, and Cl-36. These radionuclides are unretarded. Therefore, all radionuclides leaving the waste packages travel at the velocity of water and reach the wellbore in the 10,000-year simulation period. Approximately 99.98 percent of the initial inventory of these unretarded radionuclides do not reach the pumping well.

7.3 Synthesis of Sensitivity Analysis Results

7.3.1 Influential Parameters from Parametric Sensitivity

Parametric sensitivity analyses have been used to identify influential parameters in the basecase and in the igneous activity case. The influential parameters are the ones for which a unit change in the value leads to a large variation in performance (i.e., dose). In the absence of a suitable sensitivity analysis method that appropriately accounts for event probability, sensitivity analysis is performed using conditional dose for igneous activity.

For the 10,000-year simulation period, the parameters found most influential for the basecase (the basecase is defined as the undisturbed scenario and the effects of rockfall caused by seismicity), are

- Areal average mean annual infiltration at start (AAMAI@S)
- Drip shield failure time (DSFailTi)
- Preexponential term for spent nuclear fuel-dissolution Model 2 (PSFDM1)
- Subarea wet fraction (SbArWt%)
- Waste package flow multiplication factor (WPFlowMF)
- Well pumping rate at 20-km [12.4-mi] receptor group (WPRRG@20)
- Alluvium R_d for Np-237 (ARDSAVNp)
- Distance to tuff-alluvium interface (DTFFAVIF)
- Fraction of condensate toward repository (FOCTR)
- Waste package initially defective fraction (WP-Def%)

The definition of these parameters is given in Appendix A.

For the 10,000-year simulation period, the parameters found most influential for the igneous activity (based on conditional dose, which is not probability weighted), are

- Airborne mass load above the fresh ash blanket (ABMLAAsh)
- Wind speed (WindSpd)
- Diameter of volcanic conduit (VC-Dia)
- Volcanic event power (VE-Power)
- Volcanic event duration (VE-Durat)
- Time of next volcanic event in the region of interest (VEROI-Tn)
- Ash mean particle diameter (AshMnPLD)
- Random number to determine if the event is extrusive or intrusive (VEi/e-R#)
- Spent nuclear fuel wetted fraction for intrusive igneous activity (SFWt%V0)
- Preexponential term for spent nuclear fuel-dissolution Model 2 (PSFDM1)

7.3.2 Influential Parameters Based on Distributional Sensitivity

Distributional sensitivity analyses are performed for 2 sets of parameters, the first consisting of the top 10 influential parameters identified by the parametric sensitivity analysis methods described in Chapter 4 and the second, the last 5 of the 20 most influential parameters. The distributional sensitivities were determined by changing distribution functions by shifting the mean of the distribution by 10 percent of the data range toward higher values (Figure 5-2) and by completely changing the type of distribution function (Figure 5-3).

Several parameters show high distributional sensitivity, especially when the mean values are changed for the two most influential parameters identified by the parametric sensitivity analysis methods. For example, a 10-percent change to the WPFlowMF parameter results in a 150 percent change in the dose. The parameters that show the greatest sensitivity to distributional changes (data range not changed) are

- Waste package flow multiplication factor (WPFlowMF)
- Drip shield failure time (DSFailTi)
- Alluvium R_d for Np-237 (ARDSAVNp)

- Areal average mean annual infiltration at start (AAMAI@S)
- Preexponential term for spent nuclear fuel-dissolution Model 2 (PSFDM1)
- Distance to tuff-alluvium interface (DTFFAVIF)
- Subarea wet fraction (SbArWt%)
- Waste package initially defective fraction (WP-Def%)

7.3.3 Influential Alternative Conceptual Models

For the 10,000-year simulation period, several alternative conceptual models, and combinations thereof, were found most influential for the basecase. The 12 models encompass 3 processes: (i) spent nuclear fuel dissolution (rate and particle size), (ii) spent nuclear fuel wetting type (bathtub versus flow-through), and (iii) radionuclide transport. Details of the analyses can be found in Chapters 2, 3, and 4. Several alternative conceptual models or their combinations increased and others decreased dose. The alternative conceptual models are shown in order of their influence. The values in the parentheses show qualitatively the relative change in peak expected dose compared to the basecase. The minus (-) sign indicates that the dose decreased compared to the basecase. Consequently, from the risk standpoint, the models that increase dose need to be evaluated carefully. The influential alternative conceptual models in order of their influence are

- No retardation of americium, thorium, and plutonium in saturated zone (+++++)
- Flow-through spent nuclear fuel water contact mode with spent nuclear fuel dissolution Model 1 (+++)
- Grain particle-size model with spent nuclear fuel-dissolution Model 1 (+++)
- Spent nuclear fuel dissolution Model 1 (+++)
- Flow-through spent nuclear fuel water contact mode with spent nuclear fuel-dissolution Model 2 (++)
- Cladding credit with spent nuclear fuel-dissolution Model 1 (- -)
- Schoepite spent nuclear fuel-dissolution model (- -)
- Natural analog spent nuclear fuel-dissolution model (- -)
- Focused flow (- -)

7.3.4 Influential Subsystems Based on Repository Component Sensitivity

Dose shows most sensitivity to the waste package and little sensitivity to the invert barrier component. The group of natural repository components (i.e., unsaturated zone and saturated zone together) shows approximately the same level of sensitivity as the waste package repository component. Drip shield and waste form engineered repository components show comparable level of influence on dose (waste form slightly more influential). Between the two natural repository components, the unsaturated zone is slightly more influential than the saturated zone. The main influence of the unsaturated zone is in preventing water from coming into contact with the waste. The main influence of the saturated zone is retarding radionuclide transport. The influential repository components in order of their influence are (i) waste package, (ii) unsaturated zone, (iii) saturated zone, (iv) waste form, and (v) drip shield. By analyzing the repository component sensitivity results in conjunction with the system-level results, it can be inferred that the waste package and the unsaturated and saturated zones substantially delay release. The barrier sensitivity results, however, show that the drip shield and waste form provide system resiliency. Additionally, the drip shield would also serve to protect the waste package from falling rocks and preventing aggressive precipitates from

dripping onto its surface. These phenomena, however, are not modeled in the TPA Version 4.1 code; rock fall does not affect waste package failure time, and aggressive chemicals are already assumed to come into contact with the waste package nonmechanistically.

7.4 Linking Influential Parameters, Models, and Repository Components to Integrated Subissues

The influential parameters, alternative conceptual models, and repository components identified previously are linked to the U.S. Nuclear Regulatory Commission (NRC) integrated subissues (NRC, 2002). The linking of the influential variables, parameters, alternative conceptual models, and repository components is presented in Table 7-4.

7.4.1 Key Integrated Subissues for 10,000-Year Simulation Period

The influential integrated subissues identified in Table 7-4, listed in order of approximate importance, based on the models and parameters assumed in the TPA Version 4.1 code analyses are

- Volcanic disruption of waste packages (DIRECT1)
- Airborne transport of radionuclides (DIRECT2)
- Radionuclide transport in the saturated zone (SZ2)
- Degradation of engineered barriers (ENG1)
- Flow paths in the unsaturated zone (UZ2)
- Quantity and chemistry of water contacting waste packages and waste forms (ENG3)
- Radionuclide release rates and solubility limits (ENG4)
- Climate and infiltration (UZ1)
- Mechanical disruption of engineered barriers (ENG2)

Because many such assumptions and processes (sometimes overlapping) influence the performance assessment results and the process of identifying influential parameters, models, and repository components, it is critical that the key technical issues consider all information in determining whether and where additional refinements will increase confidence.

Based on the system-level results and the parametric, distributional, alternative conceptual model, and repository component sensitivity analysis results, the following specific points can be made for the integrated subissues for the 10,000-year simulation period.

7.4.1.1 Integrated Subissue—Volcanic Disruption of Waste Packages (DIRECT1)

Igneous activity makes the largest contribution to risk in the 10,000-year simulation period. The risk from the igneous activity is more than one order of magnitude higher than the risk in the absence of igneous activities. The diameter of the volcanic conduit that determines the number of waste packages available for airborne transport of radionuclides and the duration and power of the volcanic event that determine the height of the eruption column have significant influence on repository performance. The time of the next volcanic event in the region of interest, which determines the time of the volcanic event in the 10,000-year simulation period, also has significant influence on repository performance.

Table 7-4. A Crosswalk Between the Integrated Subissues, Alternative Conceptual Models, and the Influential Parameters (10,000 Years)			
Integrated Subissues	Influence of Alternative Conceptual Models	Influential Parameters	Influence of Repository Components
Degradation of engineered barriers (ENG1)	Not evaluated	<ul style="list-style-type: none"> Initially defective fraction of waste packages Drip shield failure time 	Waste package (+++++) drip shield (+)
Mechanical disruption of engineered barriers (ENG2)	Not evaluated		Waste package (+++++)
Quantity and chemistry of water contacting waste packages and waste forms (ENG3)	Clad-M1 (-) Focflow (-)	<ul style="list-style-type: none"> Waste package flow multiplication factor Fraction of condensate toward repository 	Unsaturated zone (+++)
Radionuclide release rates and solubility limits (ENG4)	Grain1 (+) NoSolLim-FT (++++) NoSolLim-BT (++) Model1 (++) Flwthru-1 (++) Flwthru-2 (+) Natan (-) Schoepite (-)	<ul style="list-style-type: none"> Spent nuclear fuel-dissolution preexponential term in Model 2 (PSFDM1) 	Waste form (+) Invert (o)
Climate and infiltration (UZ1)	Not evaluated	<ul style="list-style-type: none"> Areal average mean annual infiltration at start 	Unsaturated zone (+++)
Flow paths in the unsaturated zone (UZ2)	Focflow (-)	<ul style="list-style-type: none"> Subarea wet fraction 	Unsaturated zone (+++)
Radionuclide transport in the unsaturated zone (UZ3)	Not evaluated	—	—
Flow rates in the saturated zone (SZ1)	Not evaluated	—	—
Radionuclide transport in the saturated zone (SZ2)	NoRet (+++++) Matdif (o)	<ul style="list-style-type: none"> Alluvium matrix R_d for Np-237 Distance to tuff-alluvium interface 	Saturated zone (+++)
Volcanic disruption of waste packages (DIRECT1)	Evaluated as a special case	<ul style="list-style-type: none"> Volcanic event power* Diameter of volcanic conduit* Volcanic event duration* 	—

Table 7-4. A Crosswalk Between the Integrated Subissues, Alternative Conceptual Models, and the Influential Parameters (10,000 Years) (continued)			
Integrated Subissues	Influence of Alternative Conceptual Models	Influential Parameters	Influence of Repository Components
Airborne transport of radionuclides (DIRECT2)	Evaluated as a special case	<ul style="list-style-type: none"> • Airborne mass load above fresh ash blanket* • Ash mean particle log diameter* • Wind Speed* 	—
Representative volume (DOSE1)	Not evaluated	<ul style="list-style-type: none"> • Well pumping rate at receptor group at 20 km [12.4 mi] 	No repository component analysis permitted because it is fixed by regulation
Redistribution of radionuclides in soil (DOSE2)	Not evaluated	—	—
Biosphere characteristics (DOSE3)	Not evaluated	—	—
*Sensitive parameters obtained directly from disruptive event scenario calculations without any consideration of event probability			

The alternative conceptual model, which accounts for mechanistic consideration of waste package response to rapid influx of basaltic magma, increases the risk by one order of magnitude compared to the original model that uses the volcanic conduit diameter model to determine waste package failure for airborne transport. The increase in risk is directly related to an increase in the number of waste packages available for airborne transport of radionuclides.

7.4.1.2 Integrated Subissue—Airborne Transport of Radionuclides (DIRECT2)

Airborne entrainment of waste in the volcanic ash and the effect on the receptor group of the subsequent deposition of ash on ground surface play important roles in the determination of peak risk.

7.4.1.3 Integrated Subissues—Radionuclide Transport in the Saturated Zone (SZ2)

The dose shows strong sensitivity to the parameters defining the volume of alluvium in the saturated zone (defined in the model through the alluvium length) through which radionuclide must travel before reaching the pumping well. The dose is primarily contributed by the non-sorbing radionuclides. Np-237 sorption plays an important role in the performance of the repository system. Np-237 is the only radionuclide with a nonzero sorption characteristic that still contributes to dose within 10,000 years. Other radionuclides and their associated retardation coefficients do not turn out to be important in the sensitivity analyses because little or none of them reach the pumping well. This fact points to the importance of the geologic barrier to isolating most of the radionuclides released from the repository. Uncertainty in the retardation of Np-237 significantly influences the uncertainty in repository performance. The barrier component sensitivity analysis suggests that alluvium length plays an important role in substantially delaying the release of all sorbing radionuclides and also delaying traveltime of nonsorbing radionuclides. Because of this delay, radionuclides that are sorbed make either little or no contribution to dose in 10,000 years. The alternative conceptual model for no retardation of colloid-forming radionuclides shows that the dose can be highly sensitive to colloidal transport of colloid-forming radionuclides, if those conditions can exist. Matrix diffusion in fractured media does not have as pronounced an effect on the system performance compared to sorption in porous media. However, the model results do not show sensitivities to strongly retarded radionuclides because little or none of them arrive at the pumping well, so it is possible that matrix diffusion might be more significant for those radionuclides.

7.4.1.4 Integrated Subissues—Degradation of Engineered Barriers (ENG1) and Mechanical Disruption of Engineered Barriers (ENG2)

Factors causing waste packages to fail early by mechanisms other than corrosion are important to the 10,000-year simulation period because of the otherwise long waste package lifetime. Corrosion-resistant material significantly increases the life of the container, thus pushing the onset of release from most of the waste packages to beyond 10,000 years. Total system performance is sensitive to the percent of initial defective waste packages. Consistent with the analyses in Chapter 3, repository performance is not sensitive to seismic rockfall or instantaneous fault displacement on new or under-appreciated faults. Barrier component sensitivity analysis suggests that if the waste packages fail early from corrosion or mechanical failure, groundwater dose would increase substantially.

Uncertainty in drip shield failure time moderately influences the uncertainty in repository performance. The drip shield delays water contacting spent nuclear fuel for thousands of years for the initial defective waste packages, during which time the repository temperature falls substantially, thus slowing spent nuclear fuel dissolution. The drip shield has a greater impact on peak dose than on peak expected dose. As a barrier component, the drip shield has less impact compared with other barrier components because (i) the drip shield is a redundant barrier, (ii) the drip shield failure assumptions are conservative, or (iii) when the drip shield is intact, the spent nuclear fuel release would not have been significant because of reduced flow rates from thermal effects on flow in the repository near field. It is important to note that decreasing uncertainty in drip shield failure time increases uncertainty in repository performance. The probable cause for this observation is that a narrow drip shield failure time distribution increases the peak of the expected dose, thereby influencing the uncertainty caused by other parameter variations.

7.4.1.5 Integrated Subissue—Flow Paths in the Unsaturated Zone (UZ2)

Repository performance is sensitive to the unsaturated zone barrier primarily because (i) it limits the amount of water that can reach the waste packages and waste form; evapotranspiration and capillary diversion are the main features of the unsaturated zone expected to divert water; and (ii) for those subareas where the Calico Hills vitric unit is present, retardation of sorbing radionuclides is substantial (see Section 7.2.8)

7.4.1.6 Integrated Subissue—Quantity and Chemistry of Water Contacting Waste Packages and Waste Forms (ENG3)

The amount of dripping water entering the waste package is important to system performance and depends strongly on the number of fractures intersecting the drift, capillary diversion around the drift wall, and the geometry of the defect (e.g., cracks on the waste package and drip shield). Note that increased focusing of flow into fewer waste packages leads to a smaller dose than the case where more waste packages get the same volume of water but at a lesser rate.

The amount of condensate that moves toward the drift is a function of the net infiltration. Because the thermal period lasts for several thousand years, thermally modified flow plays an important role in repository performance.

The alternative conceptual model that assumes partial cladding protection produces a much lower peak expected dose than the basecase, which illustrates the need to improve modeling capability and focus reviews in this area if the DOE decides to take credit for cladding.

7.4.1.7 Integrated Subissue—Radionuclide Release Rates and Solubility Limits (ENG4)

Uncertainty in the spent nuclear fuel dissolution rate has a significant effect on uncertainty in total system performance in the basecase as well as the igneous activity case. The alternative conceptual model studies show that the choice of the flow-through model for spent nuclear fuel wetting, when coupled with a spent nuclear fuel-dissolution model (Model 1), significantly increases risk and uncertainty. The bathtub model takes several hundreds to thousands of years to fill, thereby delaying releases. The natural analog dissolution (Model 3) and schoepite

dissolution (Model 4) alternative conceptual models for spent nuclear fuel dissolution both decrease dose.

Model 2 was the default dissolution rate model for these analyses. However, the sampled preexponential term for the Model 2 rate equation was taken from a lognormal distribution with a wide range. This one term alone caused major problems in statistical convergence, since its value varied so broadly (see Figure 7-1) and the sensitivity of dose to the parameter was strong. The large range destabilizes the system-level results by requiring a very large number of Latin Hypercube Sampling samples for convergence. Further studies are needed to decrease the broad uncertainty currently used in the basecase spent fuel dissolution model, or supporting a different model for spent fuel dissolution.

Parameters representing (i) the fraction of the spent nuclear fuel wet and (ii) the spent nuclear fuel dissolution rate associated with the groundwater release from the intrusive igneous activity influence repository performance. Parametric and distributional sensitivity analyses reveal that both the range and distribution function type of the preexponential term (PSFDM1) controlling the dissolution rate of spent nuclear fuel influence repository performance uncertainty.

In the absence of solubility limits, the peak expected dose increased by 42 percent compared to the basecase. This small change occurred because most of the primary dose contributors in the basecase (Tc-99, I-129, and Cl-36) are not solubility limited. Np-237 is the only major contributor to the basecase peak expected dose for which release is controlled by the solubility limit throughout the 10,000-year simulation period. Because the release is delayed by sorption in the saturated zone, however, the significance of its solubility is mitigated. Also note that in the basecase, all active failure modes (i.e., the modes under which waste packages failed) are specified to form bathtubs. Changing water contact mode for these failed waste packages from bathtub to flow-through resulted in a 544 percent increase in the peak expected dose.

Radionuclides available for instantaneous release (specified through gap fraction) make only a moderate contribution to the peak expected dose. Neglecting the radionuclides specified through the gap fraction decreases dose by only 3.5 percent.

7.4.1.8 Integrated Subissue—Climate and Infiltration (UZ1)

The amount of water entering the waste package depends strongly on infiltration at the surface. Higher infiltration leads to greater release from the engineered barrier subsystem because the bathtub fills faster, and in the case of solubility limited releases, the rate depends directly on the outflow. Higher infiltration also leads to an increased likelihood of fracture flow and faster transport in the unsaturated zone.

7.4.1.9 Discussion

The prominence of the top 8 of 14 integrated subissues resulted from the sensitivity analyses presented. Although parametric, distributional, alternative conceptual model, and barrier component sensitivity analyses complement one another in determining what drives system performance, these techniques also focus on different aspects of the system. For example, the uncertainty in dose is significantly driven by the uncertainty in the preexponential term for spent nuclear fuel dissolution (PSFDM1) because of which the radionuclide release rates and solubility limits (ENG4) integrated subissue appears important. In addition, sensitivity of dose to

seven different alternative conceptual models and two barrier components is evaluated for this integrated subissue. Because the sensitivities to the alternative conceptual models and the barrier components are not significant (see Table 7-4), the importance of the radionuclide release rates and solubility limits (ENG4) integrated subissue is primarily supported by the significant sensitivity of dose to the PSFDM1 parameter. In contrast, the degradation of engineered barriers (ENG1) integrated subissue has been identified as important primarily because of the sensitivity of dose to the waste package barrier components. Although, Table 7-4 shows initial defective fraction of waste packages as an influential parameter, the decision that ENG1 is important is primarily based on the significant sensitivity of dose to waste package barrier component. Another example is the radionuclide transport in the saturated zone (SZ2) integrated subissue. This integrated subissue is identified as important because the dose shows strong sensitivity to the related parameters, the alternative conceptual models, and the barrier component. Distinctly different information can be derived from these three sensitivity types, however. The sensitivity analysis suggests that the alluvium length is influential. The barrier component analysis suggests the same, but it also provides assurance that the importance of alluvium length would not have been missed if a constant value was specified. Sensitivity analysis and the uncertainty analysis methods used in this report cannot identify a parameter as important unless the parameter is specified as a random variable. The alternative conceptual model sensitivity provides yet another relevant piece of information. The dose showing high sensitivity to the no-retardation model indicates that mechanisms like colloid transport of radionuclides may be important, providing that colloids are present in sufficient quantity in the groundwater and filtration is small.

Finally, the influential parameters, alternative conceptual models, and barrier components identified in Table 7-4 must be viewed in the proper context of the assumptions made in the TPA Version 4.1 code and the assumptions made to facilitate sensitivity analyses. The following are some key points to consider when examining these tabulated results:

- All analysis results are based on the models and reference input values used in the TPA Version 4.1 code. The TPA Version 4.0 code user's guide (Mohanty, et al., 2002) presents the key assumptions for the conceptual models. Chapter 3 of this report lists the reference input values.
- Unlike the DOE total system performance assessment analyses; the TPA Version 4.1 code does not consider diffusion through stress corrosion cracks by dissolved radionuclides or colloids. All transport is by advective flow.
- No credit is given to the drip shield as a partial flow barrier after its failure. The current assumption is that the drip shield loses 100 percent of its functionality as a flow barrier once the first failure takes place.
- Fracture-only flow occurs in the unsaturated zone if the flux exceeds the saturated hydraulic conductivity of the rock matrix of a stratigraphic unit. When fracture flow occurs, no credit is attributed to retardation in fractures or matrix diffusion in the unsaturated zone. Retardation in the fractures or diffusion into the matrix would increase traveltime and reduce the 10,000-year peak expected dose. Note that if the traveltime in a stratigraphic unit is less than 10 years, flow and transport in that unit is considered instantaneous. In the majority of the fracture-flow cases, the groundwater traveltime through a single unit is less than 10 years.

- The receptor group is located 20 km [12.4 mi] from the repository and uses groundwater that could become contaminated for drinking and farming. Calculations in this report predate the final publication of the regulation in which the receptor group is specified at 18 km [11.2 mi].
- Well pumping rate is a sampled parameter ranging between $1.7 \times 10^4 \text{ m}^3/\text{day}$ [$4.5 \times 10^6 \text{ gal/day}$] and $4.92 \times 10^4 \text{ m}^3/\text{day}$ [$1.3 \times 10^7 \text{ gal/day}$] at the 20-km [12.4-mi] receptor location. Calculations in this report predate the final publication of the regulation in which a fixed pumping rate of $10,140 \text{ m}^3/\text{day}$ [$2.68 \times 10^6 \text{ gal/day}$ or [3,000 acre ft/yr}] is specified.
- All waste packages that did not fail by other mechanisms in a subarea are assumed to fail from corrosion when the representative waste package fails. Numerous waste packages are available for corrosion failure, which does not imply that all failed waste packages contribute to radionuclide release. A more gradual failure time distribution would have the effect of spreading the release through time, thereby diminishing the peaks. In the current model, none of the waste packages undergo corrosion failure in the 10,000-year simulation period.

8 SUMMARY AND CONCLUSIONS

This report describes a series of computations with the TPA Version 4.1 code with the objective of gaining risk insights with respect to the performance of the proposed repository at Yucca Mountain. Use of this model by the U.S. Nuclear Regulatory Commission (NRC) staff and Center for Nuclear Waste Regulatory Analyses (CNWRA) has allowed them to focus on the most important parts of the analysis of postclosure repository performance.

8.1 System-Level Results

8.1.1 Deterministic Results

The staff made numerous runs with the TPA Version 4.1 code to gain insight into the basic functionality of the models. The first set of runs was deterministic, using the mean value data set (i.e., a single run with all input variables represented as constants, chosen to be the mean value of each of the sampled parameter ranges). Restricting the code to mean value input data allowed the code to be analyzed in detail and check many intermediate data streams from one module that are fed into the next. Results from the mean value data set were also compared to Monte Carlo results but were not expected to be totally representative of the full-range Monte Carlo analyses, however. Results were produced for two simulation periods: 10,000 years, corresponding to the period of regulatory concern; and 100,000 years, looking at long-term processes where many or most of the waste packages would be expected to fail by corrosion.

The mean value data set produced a peak dose of 3.5×10^{-4} mSv/yr [0.035 mrem/yr] occurring at 10,000 years. The dose resulted from the initially defective waste packages only because there were no corrosion failures until after 10,000 years. Peak dose for the 10,000-year simulation period was dominated by the unretarded radionuclides I-129, Tc-99, and Cl-36. For the 100,000-year simulation period, the peak dose of 3.8×10^{-2} mSv/yr [3.8 mrem/yr] occurred at 72,000 years and was dominated by Np-237, which has a large inventory, large dose factor, but greater retardation than those radionuclides important at 10,000 years.

8.1.2 Monte Carlo Results

Most of the calculations with TPA Version 4.1 code were Monte Carlo, for which the values of as many as 330 parameters were sampled randomly from input distributions using the Latin Hypercube Sampling method. The remaining 620 model parameters were specified constant. Some of the sampled parameters were specified partially correlated to other sampled variables. Typically, a set consisted of 350 runs or vectors. The Monte Carlo results were produced for 10,000- and 100,000-year simulation periods. The main purpose of the Monte Carlo calculations was to demonstrate the performance of the repository under as realistic conditions as possible, including the full range of uncertainty in parameters. Monte Carlo results were also used in many of the sensitivity analyses and to look at the ranges of the intermediate outputs. The peak expected dose from the Monte Carlo cases was 2.1×10^{-4} mSv/yr [0.021 mrem/yr] for the 10,000-year simulation period and 9.9×10^{-2} mSv/yr [9.9 mrem/yr] for the 100,000-year simulation period.

8.2 Alternative Conceptual Models

Numerous alternative conceptual models were evaluated. This study considered alternative conceptual models for fuel dissolution, fuel wetting, and transport through the geosphere. These are not the preferred models but in some cases represent possible alternatives that could be supported by available information. In other cases (e.g., no retardation, no solubility limits) the alternative conceptual models represent conservative, bounding analyses that are not necessarily supported by factual information. Conceptual models may be activated in the code by changing the equations describing the model abstraction (e.g., Models 1–4 for the spent nuclear fuel-dissolution model) or changing parameter values (e.g., changing retardation coefficients to simulate no retardation). The range of the expected doses from the alternative conceptual models evaluated in this study spanned four orders of magnitude. The alternative conceptual models with the greatest deviation from the basecase data set peak dose are the no-retardation case, which is two orders of magnitude greater than the basecase peak dose, and the schoepite and Clad-M1 cases, which are two orders of magnitude less than the basecase expected dose.

Choice of the spent nuclear fuel-dissolution models produced a wide variation in expected dose. Model 1, which is based on fuel-dissolution experiments where carbonate ions are present, gives the highest release rate and, therefore, the highest dose, which is approximately three to seven times the basecase results. Model 2, which is the default case used for most other runs in this report, assumes the water in contact with the waste has significant levels of silicate and calcium ions similar to J-13 Well water and has a release rate one to two orders of magnitude less than Model 1. Model 3 is a user-defined rate and, for the purposes of comparison to the other alternative conceptual models, assumes release rates typical of the Peña Blanca natural analog data (Murphy and Codell, 1999). Release rates for this case were significantly smaller than those for Models 1 and 2. Model 4 assumes that the release of all important radionuclide species from the fuel is controlled by dissolution of the secondary uranium mineral schoepite (Murphy and Codell, 1999). Model 4 has the smallest release rates and doses. Assuming the fuel has a surface area equivalent to the size of uranium grains (microns to tens of microns) leads to doses 2 to 12 times higher than the default model, which assumes the fuel surface area is based on larger fuel particles.

Choice of the fuel wetting assumptions has a significant effect on the calculated peak expected dose. The default fuel wetting model is the bathtub, for which water must first fill the waste package and then overflow to release radionuclides. The flow-through model assumes that water flowing into the waste package is released immediately. Assuming there is a focusing effect for infiltrating water so that fewer waste packages get proportionally more infiltrating water allows faster filling of the bathtub and greater release of solubility limited radionuclides. This higher dose is for times less than approximately 5,000 years, but lower doses result in the basecase model beyond 5,000 years. Credit for the protection of the fuel by cladding leads to peak doses that are approximately proportional to the degree of protection.

This report studied three alternative conceptual models for assumptions about transport in the engineered barrier subsystem, unsaturated zone, and saturated zone. Assuming no retardation of the elements plutonium, americium, and thorium in the unsaturated and saturated zones led to doses approximately one to three orders of magnitude greater than for the basecase dose throughout 100,000 years. These elements are normally highly retarded and, assuming they are easily transported in the geosphere, is a conservative bounding analysis that could only

be contemplated if mechanisms such as colloidal transport or fracture flow transport were highly effective.

Solubility limits of the radionuclides appear to play an important role in slowing radionuclide release rates for many radionuclides and therefore delaying dose to the receptor group. Twelve out of 19 radionuclides show solubility limited release over a portion of the 10,000-year simulation period.

Assuming no matrix diffusion (i.e., no diffusion of radionuclides from fractures into rocks) appears to be an important factor in determining the peak dose. The peak expected dose for the no matrix diffusion case is 50 percent higher than the basecase peak expected dose for the 10,000-year simulation period.

8.3 Disruptive Events

Waste package failure caused by rockfall is considered part of the basecase scenario. For the presented definition of the basecase, there were no waste package failures (other than juvenile failures) calculated. Faulting contributes an increase up to a factor of two in peak dose until waste packages start to fail from general corrosion after about 50,000 years. Faulting does not increase risk for the 10,000-year simulation period because of its low probability of occurrence (5×10^{-6} per year).

Igneous activity causes the largest increase in dose conditionally from both groundwater and airborne pathways, but the risk is still small when the probability of the volcanic event is factored into the calculations. The probability-weighted dose from igneous activity is approximately 0.0035 mSv/yr [0.35 mrem/yr], which is greater than the basecase groundwater dose of 0.00021 mSv/yr [0.021 mrem/yr], but still small compared to the regulatory criterion of 0.15 mSv/yr [15 mrem/yr].

Human intrusion is handled as a stylized, bounding case and is not part of the risk calculations from other disruptive scenarios. Human intrusion is based on the drilling of a borehole through a waste package and subsequent releases of waste to the groundwater. The borehole acts as a fast groundwater pathway from the Earth's surface to the water table. Modeling of this scenario gave a conditional dose of 0.001 mSv/yr [0.1 mrem/yr], which is small compared to the regulatory standard of 0.15 mSv/yr [15 mrem/yr].

8.4 Sensitivity Analyses

8.4.1 Parametric Sensitivity

The sensitivity analyses used a variety of statistical, regression, nonparametric, and nonstatistical techniques, building on previous reports on total-system performance assessment results. Most of the statistical analyses relied on a 4,000-vector Monte Carlo set calculated for the uncertainty analysis in the basecase scenario. Sensitivities for igneous activity scenario relied on multiple smaller (350) Monte Carlo run sets. All nonstatistical sensitivity analysis techniques required sets of runs calculated for input variables specified by the method. Sensitivity analyses were used to identify sensitive parameters for which a small input change can have a large effect on estimated repository performance. Data were also scaled or

standardized to take into account the relative change in a variable to allow more accurate ranking of sensitivities.

The regression analyses used both raw and transformed variables, including logarithmic and rank transformations. Although the transformed variables generally led to better coefficients of regression, they also distorted the meaning of the results by giving too much weight to small doses. In addition, this study added a new reliability-based method known as the Cumulative Distribution Function-Based Sensitivity Method (Appendix D).

All the nonstatistical methods used in previous total-system performance assessment sensitivity studies (Morris method, FAST, and differential analysis) were also employed in this study. In addition, this study added the fractional factorial design method.

Rankings for sensitivity took a consensus approach that determined the most sensitive variables according to the relative rank of that variable in each of the separate sensitivity analyses. The ranking of the variables for the 10,000-year simulation period is shown in Table 4-10.

Validation in that the choice of the sensitive parameters by the various methods was correct and was achieved by calculating and comparing Monte Carlo runs with all 330 parameters in the basecase sampled against new Monte Carlo runs for which only the reduced set of sensitive variables were either included or eliminated. Results show that keeping only the most sensitive variables gives results similar to the basecase results. Removing the most sensitive variables from sampling reduces the uncertainty in the results. Both observations demonstrate that the correct variables have been identified as being most sensitive.

8.4.2 Distributional Sensitivity

Another new technique in this study was distributional sensitivity. It was not used directly to rank sensitive variables but to determine the effect of estimation of parameter distributions for important variables on the performance results. In this technique, the input distributions were changed either by shifting the mean of a distribution by 10 percent or changing the shape of the distribution while keeping the minimum and maximum fixed. This study used the 10 most influential variables identified in the sensitivity analyses. In summary, the distributional analyses showed that improper choice of distribution functions can significantly affect the dose response. Two parameters that appear especially important in this regard are the flow multiplication factor that determines the quantity of water entering the waste packages and the preexponential term for the spent nuclear fuel-dissolution model.

8.5 Repository Component Sensitivity Analyses

Repository component sensitivity analyses look at the whole barrier at once, either performing or not performing. In the Monte Carlo uncertainty analysis used, the performance of barriers other than the waste package often could not be seen (e.g., there were never any corrosion failures of the waste packages within 10,000 years). Repository component sensitivity analysis, which assumes failure of specific barriers, allows the exploration of barrier performance by reducing the overlapping capabilities of multiple barriers. The six repository components of the engineered and natural barriers are drip shield, waste package, spent nuclear fuel, invert, unsaturated zone, and saturated zone.

Barrier failure or suppression was simulated by changing input parameters to degrade the performance severely (e.g., setting the alluvium distance to zero). There was no attempt to define a probability associated with the suppressed barrier, and the technique was never used to calculate risk.

The repository component sensitivity analyses considered several possibilities: (i) one-off component suppression, for which the performance was calculated with a single barrier suppressed; (ii) one-on analysis, for which only a single barrier was active at a time; and (iii) multiple barrier suppression.

From the one-off analysis, the largest decrease in performance came from suppression of the waste package, followed by unsaturated zone, saturated zone, waste form, drip shield, and invert. The relatively large impact of the unsaturated zone resulted from its role above the repository in diverting of water away from the waste package and fuel, thereby reducing the mobilization and transport of radionuclides. One-on analysis ranks the contribution to repository performance in the same order as the one-off analysis, but in some respects, the contribution to performance of a single barrier is clearer. For example, the one-on analysis shows that the unsaturated zone alone would reduce the peak dose by more than 95 percent of the value with none of the barriers effective.

Suppression of multiple repository components shows some interesting interactions. For example, when both the drip shield and waste package components are off, the increase exceeds the sum of either component individually, revealing the sensitivity to the drip shield that is otherwise masked in the one-off analysis. In this case, the drip shield and waste package can be seen to be redundant (i.e., the function of the drip shield in shedding water could be assumed by the waste package if the former failed).

8.6 Barrier Capacity Analysis

Multiple barriers can be evaluated by emphasizing barrier capacity to substantially delay movement of water or radionuclides. These analyses show that for the basecase conceptual models (i) the majority of waste packages remains intact for greater than 10,000 years, (ii) the drip shield delays the onset of dripping from the drift wall reaching the waste packages for a large fraction of 10,000 years, (iii) more than 90 percent of meteoric water will be diverted by the unsaturated zone above the engineered barrier, (iv) the properties of the unsaturated zone in conjunction with the drifts will act to divert water from many of the waste packages, (v) the properties of the waste form itself will cause radionuclides to be released slowly once other barriers have failed; and (vi) the unsaturated and saturated zones below the repository will retard and retain many of the radionuclides released from the engineered barrier subsystem for greater than 10,000 years.

8.7 Criticality

A conservative consequence analysis showed that the conditional occurrence of a steady-state or transient criticality would increase doses by an order of magnitude above the basecase dose, but is still well below the regulatory dose limit of 0.15 mSv/yr [15 mrem/yr]. In addition, the probability of conditions leading to this event is believed to be low, so the risk significance of in-package criticality is not expected to be great.

8.8 Importance of Radionuclides

For the basecase, most of the peak expected dose came from the isotopes Np-237, I-129, and Tc-99. The biggest factor in the dominance of these radionuclides is their low retardations, long half-lives, abundance, and dose conversion factors. The vast majority of retarded radionuclides (i.e., plutonium, americium) never arrive at the downgradient pumping well. Therefore, none of the parameters associated with these radionuclides surface as being sensitive in traditional sensitivity analyses. Techniques such as repository component analysis are useful in these cases because they show the effects of the arbitrary elimination of a repository component such as retardation. For the 10,000-year simulation period, the isotope Np-237 was retarded enough in the geosphere that it barely began to arrive at the downgradient well by 10,000 years. Np-237 became overwhelmingly important for the 100,000-year simulation period for which retardation in the geosphere was less of an issue, however.

8.9 Synthesis of Results to Determine Importance of Key Integrated Subissues for 10,000-Year Simulation Period

The important key integrated subissues, as determined by the analyses presented in this report, are

- Volcanic disruption of waste packages (DIRECT1)
- Airborne transport of radionuclides (DIRECT2)
- Degradation of the engineered barriers (ENG1)
- Flow paths in the unsaturated zone (UZ2)
- Quantity and chemistry of water contacting waste packages and waste forms (ENG3)
- Radionuclide release rates and solubility limits (ENG4)
- Mechanical disruption of engineered barriers (ENG2)
- Climate and infiltration (UZ1)
- Radionuclide transport in the saturated zone (SZ2)

This identification of key integrated subissues should be treated with considerable caution, bearing in mind that the TPA Version 4.1 code can only determine the effect of a phenomenon correctly if the physical processes have been included and properly abstracted into the code. The list of important key integrated subissues may change as models embedded in the TPA Version 4.1 code and their associated parameter ranges become better understood.

8.10 Further Study

A TPA Version 5.0 code is planned for 2003. This version will have a variety of improvements to model abstractions. Changes will reflect improvement in our understanding of the conceptual models of the site and their effect on estimated risk.

New models that may be added are

- Drift Collapse—This model will potentially affect seepage, drip shield failure, and flow diversion.

- **Vitrified Waste Form**—This model will calculate the dissolution of the glass waste form and release of radionuclides to the engineered barrier subsystem.
- **Weld Corrosion**—This model will estimate the extent of corrosion in the end cap welds. Estimates of the extent of these failures will potentially be used subsequently in a diffusive transport model.
- **Diffusive Release from Waste Packages**—The current model does not account for the possible release of radionuclides through small cracks in the waste packages. This revision will consider diffusion through thin films and small stress corrosion cracks in end lid welds, for conditions that would allow a diffusive path to the invert.
- **Colloid Source Term**—This model will estimate the rate of release of radionuclides as real and pseudocolloids.
- **Cladding Failure Model**—The current model has a crude accounting for cladding protection, but not a mechanistic model that would predict the corrosion of cladding or unzipping because of fuel degradation. This revision will include time-dependent failure rates for cladding.
- **Microbially Induced Corrosion**—This model will estimate the enhanced corrosion caused by microbially induced corrosion.
- **Plume Capture**—This model will calculate the portion of the plume that would be captured by the reasonably maximally exposed individual, whether at the 18-km [11.2-mi] location or closer.

Modifications to existing models and data are

- Update climate and infiltration data.
- Add runoff effect to the infiltration model.
- Modify shallow infiltration estimate to account for vegetation.
- Add a factor to account for infiltration variance.
- Include a model that accounts for general corrosion, fluoride attack, and mechanical failure of the drip shield—TPA Version 4.1 code treats drip shield failure as simply a sampled parameter.
- Add variability of pH in waste package corrosion model.
- Represent K_d s and retardation factors as functions of the geochemistry.
- Include uncertainty in the Calico Hills nonwelded vitric layer thickness.
- Account for multiple fracture flow and matrix flow episodes.

- Allow variable dispersivity for transport in the unsaturated zone.
- Include uncertainty in the saturated zone streamtube dimensions.
- Allow changes in streamtube flux after climate change.
- Improve mass loading and occupancy factors for igneous activity.
- Modify igneous activity source term to better account for physical processes of mixing fuel and magma.
- Add a short-term ash redistribution model to consider remobilization of ash by overland flow of water.
- Add effects of rockfall on drip shield.

In addition to the technical changes to the TPA Version 4.1 code to address improved model abstractions, data and models will be adjusted where necessary to accommodate changes to the current U.S. Department of Energy (DOE) repository design and thermal loading strategy.

8.11 Conclusions

The TPA Version 4.1 code has been used successfully in a structured way to provide risk insights through investigating the performance of the proposed Yucca Mountain repository and the sensitivity of this performance to repository subsystems and parameters on which they rely. The calculated risk is small within the 10,000-year simulation period, determined with the staff best estimate of models and parameters, and is well below the regulatory limit of 0.15 mSv/yr [15 mrem/yr] to the reasonably maximally exposed individual. Extrusive volcanism was the scenario that produced the maximum calculated risk, 3.5×10^{-3} mSv/yr [0.35 mrem/yr] to the reasonably maximally exposed individual, which is still well below the regulatory limit. Experimentation with a wide range of alternative conceptual models for waste form dissolution, waste package lifetime, and radionuclide transport never led to calculated risks that were close to exceeding the standard.

The staff used a variety of statistical and nonstatistical methods to determine the sensitivity of dose to variations in the input parameters. Three new methods applied to the TPA Version 4.1 code proved useful in determining parametric sensitivities. Fractional factorial design provides a means of unambiguously determining the interactions among variables. Distributional sensitivity illustrates the effect of parameter estimation errors on risk. The cumulative distribution function-based method shows sensitivities in different dose ranges, particularly the high-dose responses. As in previous total-system performance assessment studies, staff relied on a consensus approach for all the parametric sensitivity methods to determine the parameters that appeared most frequently and with the highest rank among all the methods. Using this procedure, a list of the 10 most influential parameters was developed for the regulatory period of 10,000 years. This list consisted of parameters that deal with flow of water to the waste, failure of barriers to flow, retardation along transport pathways of slightly retarded Np-237, fuel-dissolution rates, and dilution at the point of use. There were no parameters in this list that dealt with waste package corrosion because the models predicted that none of the waste packages failed by this mechanism within 10,000 years. A similar list was developed for the

100,000 year simulation period, which is not required by the regulations but serves the purpose of broadening understanding of failure modes for the repository. Parameters dealing with waste package corrosion appeared on this list, together with the retardation factor for Pu-239.

Repository component sensitivity analysis evaluated how repository components behaved in the repository system. Suppression of the performance of the repository components, singly and in combinations, provided useful informational about the sensitivity of the performance to the repository components (i.e., subsystems) although the staff never attached probabilities to these suppressions, and such results had no direct bearing on the overall risk. Repository component analysis pointed out interesting features of the repository such as (i) the redundancy of the drip shield and waste package to shed dripping water, (ii) the capabilities of the unsaturated and saturated zones independent of the waste package, and (iii) the relative unimportance of the invert as a barrier. Important components were also identified based only on their capabilities rather than their direct bearing on dose or risk. In identifying these components, the staff demonstrated that for the conceptual models included in the TPA Version 4.1 code, the drip shield, waste package, waste form, unsaturated zone, and saturated zone all contributed to waste isolation.

The staff evaluated two stylized scenarios for human intrusion and in-package nuclear criticality. Both analyses were conditional, with no assignment of probability although these probabilities are believed to be small. Both produced maximum conditional dose values well below the 0.15 mSv/yr [15 mrem/yr] dose limit specified by the regulations.

This report was prepared to document work performed by the CNWRA for the NRC under Contract No. NRC-02-02-012. The activities reported here were performed on behalf of the NRC Office of Nuclear Material Safety and Safeguards, Division of Waste Management. The report is an independent product of the CNWRA and does not necessarily reflect the views or regulatory position of the NRC.

9 REFERENCES

Bechtel SAIC Company, LLC. "FY01 Supplemental Science and Performance Analyses." Vol. 1: Scientific Bases and Analyses. TDR-MGR-MD-000007. Rev 00 ICN 01. Las Vegas, Nevada: Bechtel SAIC Company, LLC. 2001.

Beckman, R.J. and M.D. McKay. "Monte Carlo Estimation Under Different Distributions Using the Same Simulation." *Technometrics*. Vol. 29, No. 2. pp. 153–160. 1987.

Bell, M.J. "U.S. Nuclear Regulatory Commission Comments on the U.S. Department of Energy Total System Performance Assessment." Letter (July 6) to S.J. Brocoum, DOE. Washington, DC: NRC. 1998.

Benjamin, J.R. and C.A. Cornell. *Probability, Statistics, and Decision for Civil Engineers*. New York City, New York: McGraw-Hill. 1970.

Bowen, W.M. and C.A. Bennett, eds. NUREG/CR-4604, "Statistical Methods for Nuclear Material Management." Washington, DC: NRC. December 1988.

Box, G.E.P. and J.S. Hunter. "The 2^{k-p} Fractional Factorial Designs Part 1, 1961." *Technometrics*. Vol. 42, No 1. pp. 28–47. 2000. (This is a reprint of *Technometrics*. Vol. 3. pp. 311–351. 1961.)

Chun, M.H., H.S.J. Han, and N.I. Tak. "An Uncertainty Importance Measure Using a Distance Metric for the Change in a Cumulative Distribution Function." *Reliability Engineering and System Safety*. Vol. 70. pp. 313–321. 2000.

Code of Federal Regulations. "Disposal of High-Level Radioactive Wastes in a Proposed Geological Repository at Yucca Mountain, Nevada." Title 10–Energy, Chapter 1–NRC, Part 63. Washington, DC: U.S. Government Printing Office. 2002.

———. "Public Health and Environmental Radiation Protection Standards for Yucca Mountain, Nevada." Title 40–Protection of Environment, Chapter 1–EPA, Part 197. Washington, DC: U.S. Government Printing Office. 2001.

———. "Disposal of High-Level Radioactive Wastes in Geological Repositories." Title 10–Energy, Chapter 1–NRC, Part 60. Washington, DC: U.S. Government Printing Office. 1991.

Codell, R.B, N. Eisenberg, D. Fehringer, W. Ford, T. Margulies, T. McCartin, J. Park, and J. Randall. NUREG-1327, "Initial Demonstration of the NRC's Capability to Conduct a Performance Assessment for a High-Level Waste Repository." Washington, DC: NRC. 1992.

Cook, R.D. and S. Weisberg. "An Introduction to Regression Graphics." New York City, New York: John Wiley and Sons, Inc. 1994.

CRWMS M&O. "Total System Performance Assessment for the Site Recommendation." TDR-WIS-PA-000001. Rev. 00 ICN 01. Las Vegas, Nevada: CRWMS M&O. 2001.

- . “Total System Performance Assessment for the Site Recommendation.” TDR-WIS-PA-000001. Rev. 00 ICN 01. Las Vegas, Nevada: CRWMS M&O. 2000a.
- . “Total System Performance Assessment (TSPA) Model for Site Recommendation.” MDL-WIS-PA-000002. Rev. 00. Las Vegas, Nevada: CRWMS M&O. 2000b.
- . “License Application Design Selection Report.” B00000000-01717-4600-00123. Rev. 01. Las Vegas, Nevada: CRWMS M&O. 1999.
- . “Total System Performance Assessment—Viability Assessment (TSPA-VA) Analyses Technical basis Document.” B00000000-01717-4301-00002. Las Vegas, Nevada: TRW Environmental Safety Systems, Inc. 1998.
- Cukier, R.I., H.B. Levine, and K.E. Schuler. “Nonlinear Standard Sensitivity Analysis of Multiparameter Model Systems.” *Journal of Computational Physics*. Vol. 26. pp. 1–42. 1978.
- Cukier, R.I., J.H. Schaibly, and K.E. Schuler. “Study of the Sensitivity of Coupled Reaction Systems to Uncertainties in Rate Coefficients. III: Analysis of the Approximation.” *Journal of Chemical Physics*. Vol. 63, No. 3. pp. 1,140–1,149. 1975.
- Cukier, R.I., C.M. Fortuin, K.E. Schuler, A.G. Petschek, and J.H. Schaibly. “Study of the Sensitivity of Coupled Reaction Systems to Uncertainties in Rate Coefficients. I: Theory.” *Journal of Chemical Physics*. Vol. 59, No. 8. pp. 3,873–3,878. 1973.
- Dalrymple, G.J. “The Use of Expert Opinion in Specifying Input Distributions for Use in Probabilistic Risk Analysis of Radioactive Waste Disposal.” *Waste Management*. Vol. 79, No. 12. pp. 912–922. 1989.
- DOE. “Yucca Mountain Science and Engineering Report: Technical Information Supporting Site Recommendation Consideration.” DOE/RW-0539. Washington, DC: Office of Civilian Radioactive Waste Management. 2001.
- . “Disposal Criticality Analysis Methodology Topical Report.” YMP/TR-004Q. Rev. 0. Las Vegas, Nevada: Office of Civilian Radioactive Waste Management. 1998a.
- . “Viability Assessment of a Repository at Yucca Mountain. Vol. 3: Total System Performance Assessment.” DOE/RW-0508/V3. Washington, DC: Office of Civilian Radioactive Waste Management. 1998b.
- Draper, N.R. and H. Smith, Jr. “Applied Regression Analysis.” 2nd Edition. New York City, New York: John Wiley and Sons, Inc. 1981.
- EPA. “Environmental Radiation Protection Standards for Management and Disposal of Spent Nuclear Fuel, High-Level, and Transuranic Radioactive Wastes.” Washington, DC: U.S. Government Printing Office. 2001.
- Esh, D., R. Codell, and T. McCartin. “Repository Importance Analyses.” Proceedings of the Ninth International Conference on High-Level Radioactive Waste Management, Las Vegas, Nevada, April 29–May 3, 2001. La Grange Park, Illinois: American Nuclear Society. 2001.

- Eslinger, P.W. and B. Sagar. "Use of Bayesian Analysis for Incorporating Subjective Information." Proceedings of the Conference on Geostatistical Sensitivity and Uncertainty Methods for Ground-Water Flow and Radionuclide Transport Modeling, San Francisco, California, September 15–17, 1987. Columbus, Ohio: Battelle Press. pp. 613–627. 1989.
- Helton, J.C., J.W. Garner, R.D. McCurley, and D.K. Rudeen. "Sensitivity Analysis Techniques and Results for Performance Assessment at the Waste Isolation Pilot Plant." SAND90–7103. Albuquerque, New Mexico: Sandia National Laboratories. 1991.
- Iman, R.L. and W.J. Conover. "The Use of the Rank Transform in Regression." *Techtonometrics*. Vol. 21. pp. 499–509. 1979.
- Iman, R.L. and S.C. Hora. "A Robust Measure of Uncertainty Importance for Use in Fault Tree System Analysis." *Risk Analysis*. Vol. 10, No. 3. pp. 401–406. 1990
- Iman, R.L., J. Davenport, and D. Ziegler. "Latin Hypercube Sampling (Program User's Guide)." SAND–1473. Albuquerque, New Mexico: Sandia National Laboratories. 1980.
- Jarzemba M.S. and B. Sagar. "A Parameter Tree Approach to Estimating System Sensitivities to Parameter Sets." *Reliability Engineering and System Safety*. Vol. 67. pp. 89–102. 2000.
- Jarzemba, M.S., P.A. LaPlante, and K.J. Poor. "ASHPLUME Code Version 1.0 Model Description and User's Guide." CNWRA 97-004. San Antonio, Texas: CNWRA. 1997.
- Khatib-Rahbar, M., E. Cassoli, M. Lee, H. Nourbakhsh, R. Davis, and E. Schmidt. "A Probabilistic Approach to Quantifying Uncertainties in the Progression of Severe Accidents." *Nuclear Science Engineering*. Vol. 102. pp. 219–259. 1989.
- Kahn, H. and A.W. Marshall. "Methods of Reducing Sample Size in Monte Carlo Computations." *Journal of the Operations Research Society of America*. Vol. 1. pp. 263–271. 1953.
- Kennedy, W.J. and J.E. Gentle. "Statistical Computing." New York City, New York: Marcel Dekker. 1980.
- Leigh, C.D., B.M. Thompson, J.E. Campbell, D.E. Longsine, R.A. Kennedy, and B.A. Napier. "User's Guide for GENII-S: A Code for Statistical and Deterministic Simulation of Radiation Doses to Humans from Radionuclides in the Environment." SAND91–0561. Albuquerque, New Mexico: Sandia National Laboratories. 1993.
- Lichtner, P.C., M.S. Seth, and S. Painter. "MULTIFLO User's Manual MULTIFLO Version 1.2—Two-Phase Nonisothermal Coupled Thermal-Hydrologic-Chemical Flow Simulator." Rev. 2. Change 1. San Antonio, Texas: CNWRA. 2000.
- Lichtner, P.C. and M.S. Seth. "User's Manual for MULTIFLO: Part II—MULTIFLO 1.0 and GEM 1.0, Multicomponent-Multiphase Reactive Transport Model." CNWRA 96-010. San Antonio, Texas: CNWRA. 1996.

Lu, Y. and S. Mohanty. "Sensitivity Analysis of a Complex, Proposed Geologic Waste Disposal System Using the Fourier Amplitude Sensitivity Test Method." *Reliability Engineering and System Safety*. Vol. 72, No. 3. pp. 275–291. 2001.

Mason, R.L., R.F. Gunst, and J.L. Hess. *Statistical Design & Analysis of Experiments with Applications to Engineering and Science*. New York City, New York: John Wiley and Sons, Inc. 1989.

Merkhofer, M.W. and A.K. Runchal. "Probability Encoding. Quantifying Uncertainty Over Hydrologic Parameters for Basalt." Proceedings of the Conference on Geostatistical Sensitivity and Uncertainty Methods for Ground-Water Flow and Radionuclide Transport Modeling, San Francisco, California, September 15–17, 1987. Columbus, Ohio: Battelle Press. 1989.

Mohanty, S., T.J. McCartin, and D.W. Esh. "Total-system Performance Assessment (TPA) Version 4.0 Code: Module Descriptions and User's Guide." San Antonio, Texas: CNWRA. 2002.

Mohanty, S. and Y-T. (Justin) Wu. "CDF Sensitivity Analysis Technique for Ranking Influential Parameters in the Performance Assessment of the Proposed High-Level Waste Repository at Yucca Mountain, Nevada, USA." *Reliability Engineering and System Safety*. Vol. 73, No. 2. pp. 167–176. 2001.

Mohanty, S., R. Codell, R.W. Rice, J. Weldy, Y. Lu, R.M. Byrne, T.J. McCartin, M.S. Jarzempa, and G.W. Wittmeyer. "System-Level Repository Sensitivity Analyses Using TPA Version 3.2 Code." CNWRA 99-002. San Antonio, Texas: CNWRA. 1999.

Mohanty, S. and T.J. McCartin. "Total-system Performance Assessment (TPA) Version 3.2 Code: Module Description and User's Guide." San Antonio, Texas: CNWRA. 1998.

Morgan, M.G. and M. Henrion. *Uncertainty: A Guide to Dealing with Uncertainty in Quantitative Risk and Policy Analysis*. New York City, New York: Cambridge University Press. 1990.

Morris, M.D. "Factorial Sampling Plans for Preliminary Computational Experiments." *Technometrics*. Vol. 33, No. 2. pp. 161–174. 1991.

Murphy, W.M. and R.C. Codell. "Alternate Source Term Models for Yucca Mountain Performance Assessment Based on Natural Analog Data and Secondary Mineral Solubility." Scientific Basis for Nuclear Waste Management XXII. D.J. Wronkiewicz and J.H. Lee, eds. Materials Research Society Symposium Proceedings. Boston, Massachusetts: Materials Research Society. Vol. 556. p. 551–558. 1999.

Napier, B.A., R.A. Peloquin, D.L. Strenge, and J.V. Ramsdell. "GENII: The Hanford Environmental Radiation Dosimetry Software System. Vols. 1, 2, and 3: Conceptual Representation, User's Manual, and Code Maintenance Manual." PNL-6584. Richland, Washington: Pacific Northwest National Laboratory. 1988.

NRC. NUREG-1804, "Yucca Mountain Review Plan: Draft Report for Comment." Washington, DC: NRC. March 2002.

———. NUREG–1538, “Preliminary Performance-Based analyses Relevant to Dose-Based Performance Measures for a Proposed Geologic Repository at Yucca Mountain.” Washington, DC: NRC. October 2001.

———. NUREG–1668, “NRC Sensitivity and Uncertainty Analyses for a Proposed HLW Repository at Yucca Mountain, Nevada Using TPA 3.1. Volume II: Results and Conclusions.” Washington, DC: NRC. March 1999a.

———. “Disposal of High-Level Radioactive Wastes in a Proposed Geological Repository at Yucca Mountain, Nevada: Proposed Rule.” *Federal Register*. Vol. 64, No. 34. pp. 8640–8679. 1999b.

———. “Issue Resolution Status Report Key Technical Issues: Total-system Performance Assessment and Integration.” Rev. 1.0. Washington, DC: NRC. 1998.

Nuclear Waste Policy Act of 1982. Pub. L. 97–425. 96 Stat. 2201. (1982)

Olague, N.E., D.E. Longsine, J.E. Campbell, and C.D. Leigh. NUREG/CR–5618, “User’s Manual for the NEFTRAN II Computer Code.” Washington, DC: NRC. February 1991.

Park, C.K. and K.I. Ahn. “A New Approach for Measuring Uncertainty Importance and Distributional Sensitivity in Probabilistic Safety Assessment.” *Reliability Engineering and System Safety*. Vol. 46. pp. 253–261. 1994.

Schmidt, S.R. and R.G. Launsby. “Understanding Industrial Designed Experiments.” Colorado Springs, Colorado: Air Force Academy Press. 1991.

Seitz, R.R., A.S. Rood, G.A. Harris, S.J. Maheras, and M. Kotechi. “Sample Application of Sensitivity/Uncertainty Analysis Techniques to a Groundwater Transport Problem.” DOE/LLW–108. Idaho Falls, Idaho: Idaho National Engineering Laboratory. 1991.

Sen, A. and M. Srivastava. *Regression Analysis Theory, Methods, and Applications*. New York City, New York: Springer-Verlag, Inc. 1990.

Stephens, M.E., B.W. Goodwin, and T.H. Andres. “Deriving Parameter Probability Density Functions.” *Reliability Engineering and System Safety*. Vol. 42, Nos. 2–3. pp. 271–292. 1993.

Stothoff, S.A. “Infiltration Abstraction for Shallow Soil Over Fractured Bedrock in a Semi-Arid Climate.” San Antonio, Texas: CNWRA. 1999.

Stothoff, S.A., H.M. Castellaw, and A.C. Bagtzoglou. “Simulating the Spatial Distribution of Infiltration at Yucca Mountain, Nevada.” San Antonio, Texas: CNWRA. 1997.

Strahler, A.N. *Physical Geography*. New York City, New York: John Wiley and Sons, Inc. 1969.

Suzuki, T. “A Theoretical Model for Dispersion of Tephra.” *Arc Volcanism: Physics and Tectonics*. Tokyo, Japan: Terra Scientific Publishing. pp. 95–113. 1983.

Tschoepe, E., III, F. Lyle, Jr., D.M. Dancer, C.G. Interrante, and P.K. Nair. "Field Engineering Experience with Structural Materials." San Antonio, Texas: CNWRA. 1994.

U.S. Congress. "Nuclear Waste Policy Act of 1982." 42 U.S.C. 10101. Washington, DC: U.S. Congress. 1982.

Wescott, R.G., M.P. Lee, N.A. Eisenberg, T.J. McCartin, and R.G. Baca, eds. NUREG-1464, "NRC Iterative Performance Assessment Phase 2." Washington, DC: NRC. October 1995.

Wu, Y-T. "Computational Methods for Efficient Structural Reliability and Reliability Sensitivity Analysis." *AIAA Journal*. Vol. 32, No. 8. pp. 1,717-1,723. 1994.

Zimmerman, D.A. NUREG/CR-5395, "A Review of Techniques for Propagating Data and Parameter Uncertainties in High-Level Waste Performance Assessment Models." Washington, DC: NRC. 1991.

APPENDIX A

DESIGN MATRIX FOR THE MORRIS METHOD

This appendix explains the steps necessary to obtain the design matrix for the parameter values used by the TPA Version 4.1 code for implementing the Morris Method. Let x_i , $i = 1, 2, \dots, l$, be the elements of x , where x is the input parameter vector with l elements. Assuming

$0 \leq x_i \leq 1$, the interval $[0, 1]$ is now divided into p discrete levels. A randomly chosen base vector, x^* , is then obtained by assigning each element of x randomly from a set of discrete values: $\{0, 1/(p-1), 2/(p-1), \dots, 1-\Delta\}$, where $\Delta = p/2(p-1)$. To obtain the matrix, first, a $(l+1)$ -by- l sampling matrix, B , with elements of 0 and 1 is selected

$$B = \begin{bmatrix} 0 & 0 & 0 & \dots & 0 \\ 1 & 0 & 0 & \dots & 0 \\ 1 & 1 & 0 & \dots & 0 \\ \dots & \dots & \dots & \dots & \dots \\ 1 & 1 & 1 & \dots & 1 \end{bmatrix} \quad (\text{A-1})$$

Matrix B has an important property, namely, that any row differs from its immediate neighboring rows only in one column. For instance, the second row differs from the first row only in the first column and the third row in the second column. A matrix obtained by multiplying B with Δ can be used to produce l values of $\partial y / \partial x_i$, based on $(l+1)$ runs. The elements of the matrix are not randomly selected.

To randomize the matrix ΔB , the following operations are performed:

$$B^* = J_{(l+1),l} x^* + (\Delta / 2) \left[(B - J_{(l+1),l}) D^* + J_{(l+1),l} \right] \quad (\text{A-2})$$

where D^* is an l -dimensional diagonal matrix in which each diagonal element is either +1 or -1 with equal probability. The operations defined in Eq. (A-2) randomize the matrix ΔB . The matrix B^* is called the design matrix

Because the input variables are considered random, so is the output $y(x)$. If a distribution of r samples is required for each $\partial y / \partial x_i$, the previous process defined in Eq. (A-2) can be repeated r times to produce an $r(l+1)$ -by- l design matrix X :

$$J_{(l+1),l} = \begin{bmatrix} 1 & 1 & 1 & \dots & 1 \\ 1 & 1 & 1 & \dots & 1 \\ 1 & 1 & 1 & \dots & 1 \\ \dots & \dots & \dots & \dots & \dots \end{bmatrix}_{(l+1),l} \quad (\text{A-3})$$

Each row of X will next be used as input to the TPA code to calculate $y(x)$, and the matrix X will be used to produce rl number of $\partial y / \partial x_i$, which, in turn, will produce l distributions for the input variables, each with r samples

$$X_{r(l+1),l} = \begin{bmatrix} B_1^* \\ B_2^* \\ \dots \\ B_r^* \end{bmatrix} \quad (\text{A-4})$$

Information on Appendix B, C, and D contains copies of three journal articles from the Reliability Engineering and System Safety journal that are copyright information and are therefore not included in this file.

APPENDIX B

APPENDIX C

APPENDIX D

APPENDIX E

**DESCRIPTION OF ABBREVIATIONS USED FOR TPA VERSION 4.1 CODE SAMPLED
INPUT PARAMETERS**

Parameter Identification	Short Name	Full Name	Description
10	AA_1_1	AA_1_1[C/m ² /yr]	A corrosion rate (passive current density) for the waste package outer overpack in EBSFAIL
1	AAMAI@S	ArealAverageMeanAnnualInfiltrationAtStart[mm/yr]	Mean areal average infiltration into the subsurface at the start of a TPA Version 4.1 code run
329	ABMLAAsh	AirborneMassLoadAboveFreshAshBlanket[g/m ³]	Mass of soil in the air above a fresh volcanic ash blanket
330	AMLASoil	AirborneMassLoadAboveSoil[g/m ³]	Mass of soil in air above Amargosa Valley soil
236	APrs_SAV	AlluviumMatrixPorosity_SAV	Amargosa Valley alluvium saturated zone matrix porosity
241	AqThick5	AquiferThickness5km[m]	Thickness of the aquifer at a location 5 km [3.1 mi] south of Yucca Mountain
226	ARDSAV_U	AlluviumMatrixRD_SAV_U	Matrix retardation for uranium in the saturated zone of the Amargosa Valley alluvium
224	ARDSAVAm	AlluviumMatrixRD_SAV_Am	Matrix retardation for americium in the saturated zone of the Amargosa Valley alluvium
231	ARDSAVCs	AlluviumMatrixRD_SAV_Cs	Matrix retardation for cesium in the saturated zone of the Amargosa Valley alluvium
234	ARDSAVNb	AlluviumMatrixRD_SAV_Nb	Matrix retardation for niobium in the saturated zone of the Amargosa Valley alluvium
232	ARDSAVNi	AlluviumMatrixRD_SAV_Ni	Matrix retardation for nickel in the saturated zone of the Amargosa Valley alluvium

**DESCRIPTION OF ABBREVIATIONS USED FOR TPA VERSION 4.1 CODE SAMPLED INPUT
PARAMETERS (continued)**

Parameter Identification	Short Name	Full Name	Description
225	ARDSAVNp	AlluviumMatrixRD_SAV_Np	Matrix retardation for neptunium in the saturated zone of the Amargosa Valley alluvium
230	ARDSAVPb	AlluviumMatrixRD_SAV_Pb	Matrix retardation for lead in the saturated zone of the Amargosa Valley alluvium
227	ARDSAVPu	AlluviumMatrixRD_SAV_Pu	Matrix retardation for plutonium in the saturated zone of the Amargosa Valley alluvium
229	ARDSAVRa	AlluviumMatrixRD_SAV_Ra	Matrix retardation for radium in the saturated zone of the Amargosa Valley alluvium
233	ARDSAVSe	AlluviumMatrixRD_SAV_Se	Matrix retardation for selenium in the saturated zone of the Amargosa Valley alluvium
228	ARDSAVTh	AlluviumMatrixRD_SAV_Th	Matrix retardation for thorium in the saturated zone of the Amargosa Valley alluvium
328	AshMnPLD	AshMeanParticleLogDiameter[d_in_cm]	Relative size of ash/SF particulates from a volcanic event
11	*Chlorid	ChlorideMultFactor	Factor by which chloride concentration in matrix is multiplied to compensate for dripping and drying that would lead to salt accumulation
8	CritRHAC	CriticalRelativeHumidityAqueousCorrosion	Critical relative humidity above which aqueous corrosion may initiate
12	DSFailTi	DripShieldFailureTime[yr]	Time of failure of the dripshield (year)

**DESCRIPTION OF ABBREVIATIONS USED FOR TPA VERSION 4.1 CODE SAMPLED INPUT
PARAMETERS (continued)**

Parameter Identification	Short Name	Full Name	Description
237	DFFAVIF	DistanceToTuffAlluviumInterface[km]	Distance traveled in Tuff
308	FEROI-Tn	TimeOfNextFaultingEventInRegionOfInterest[yr]	Time of the next faulting event in the repository area (years from present)
310	FEROI-X	XlocationOfFaultingEventInRegionOfInterest[m]	X location of the center of the faulting event within the repository area
311	FEROI-Y	YlocationOfFaultingEventInRegionOfInterest[m]	Y location of the center of the faulting event within the repository area
312	FO-Rn#Sd	RntoDetermineFaultOrientation	Random number selected to determine the orientation of the fault within the repository area
4	FOC-R	FractionOfCondensateRemoved[1/yr]	Fraction of water condensate removed in each reflux3 time step
5	FOCTR	FractionOfCondensateTowardRepository[1/yr]	Fraction of water condensate moving towards the repository
214	FPrm_BFw	FracturePermeability_BFw_[m ²]	Bullfrog-welded fracture permeability (UZ)
210	FPrm_CHv	FracturePermeability_CHnv[m ²]	Calico Hills-nonwelded vitric fracture permeability (UZ)
211	FPrm_CHz	FracturePermeability_CHnz[m ²]	Calico Hills-nonwelded zeolitic fracture permeability (UZ)
212	FPrm_PPw	FracturePermeability_PPw_[m ²]	Prow Pass-welded fracture permeability (UZ)
209	FPrm_TSw	FracturePermeability_TSw_[m ²]	Topopah Spring-welded fracture permeability (UZ)
213	FPrm_UCF	FracturePermeability_UCF_[m ²]	Upper Crater Flat fracture permeability (UZ)

**DESCRIPTION OF ABBREVIATIONS USED FOR TPA VERSION 4.1 CODE SAMPLED INPUT
PARAMETERS (continued)**

Parameter Identification	Short Name	Full Name	Description
215	FPm_UFZ	FracturePermeability_UFZ_[m ²]	Unsaturated Fracture Zone fracture permeability (UZ).
221	FPrs_BFw	FracturePorosity_BFw_	Bullfrog-welded fracture porosity (UZ)
217	FPrs_CHv	FracturePorosity_CHv	Calico Hills-nonwelded vitric fracture porosity (UZ)
218	FPrs_CHz	FracturePorosity_CHz	Calico Hills-nonwelded zeolitic fracture porosity (UZ)
219	FPrs_PPw	FracturePorosity_PPw_	Prow Pass-welded fracture porosity (UZ)
235	FPrs_STF	FracturePorosity_STFF	Fracture porosity of saturated tuff (SZ)
216	FPrs_TSw	FracturePorosity_TSw_	Topopah Spring-welded fracture porosity (UZ)
220	FPrs_UCF	FracturePorosity_UCF_	Upper Crater Flat fracture porosity (UZ)
222	FPrs_UFZ	FracturePorosity_UFZ_	Unsaturated Fracture Zone fracture porosity (UZ)
297	genKDsAm	KD_Soil_Am[cm ³ /g]	Soil K _d for americium (cm ³ /g)
306	genKDsC	KD_Soil_C[cm ³ /g]	Soil K _d for carbon (cm ³ /g)
294	genKDsCm	KD_Soil_Cm[cm ³ /g]	Soil K _d for cerium (cm ³ /g)
302	genKDsCs	KD_Soil_Cs[cm ³ /g]	Soil K _d for cesium (cm ³ /g)
303	genKDsI	KD_Soil_I[cm ³ /g]	Soil K _d for iodine (cm ³ /g)
305	genKDsNi	KD_Soil_Ni[cm ³ /g]	Soil K _d for nickel (cm ³ /g)
298	genKDsNp	KD_Soil_Np[cm ³ /g]	Soil K _d for neptunium (cm ³ /g)

E-4

**DESCRIPTION OF ABBREVIATIONS USED FOR TPA VERSION 4.1 CODE SAMPLED INPUT
PARAMETERS (continued)**

Parameter Identification	Short Name	Full Name	Description
301	genKDsPb	KD_Soil_Pb[cm ³ /g]	Soil K _d for lead (cm ³ /g)
295	genKDsPu	KD_Soil_Pu[cm ³ /g]	Soil K _d for plutonium (cm ³ /g)
300	genKDsRa	KD_Soil_Ra[cm ³ /g]	Soil K _d for radium (cm ³ /g)
307	genKDsSe	KD_Soil_Se[cm ³ /g]	Soil K _d for selenium (cm ³ /g)
304	genKDsTc	KD_Soil_Tc[cm ³ /g]	Soil K _d for technetium (cm ³ /g)
299	genKDsTh	KD_Soil_Th[cm ³ /g]	Soil K _d for thorium (cm ³ /g)
296	genKDsU	KD_Soil_U[cm ³ /g]	Soil K _d for uranium (cm ³ /g)
293	gen_AUSF	AnimalUptakeScaleFactor	Animal uptake scaling factor used to scale animal transfer factors in <i>gftrans.dat</i>
292	gen_PUSF	PlantUptakeScaleFactor	Plant uptake scaling factor used to scale plant transfer factors in <i>gftrans.dat</i>
275	gen_bfdf	BeefFreshForageDietFraction	Beef cattle fresh forage diet fraction
277	gen_bfgt	BeefFreshForageGrowTime[day]	Beef cattle fresh forage growing time (day)
287	gen_dwc1	DrinkingWaterConsumptionRate1[L/yr]	Drinking water consumption rate for infant (liters per year)
288	gen_dwc2	DrinkingWaterConsumptionRate2[L/yr]	Drinking water consumption rate for toddler (liters per year)
289	gen_dwc3	DrinkingWaterConsumptionRate3[L/yr]	Drinking water consumption rate for preteen (liters per year)

**DESCRIPTION OF ABBREVIATIONS USED FOR TPA VERSION 4.1 CODE SAMPLED INPUT
PARAMETERS (continued)**

Parameter Identification	Short Name	Full Name	Description
290	gen_dwc4	DrinkingWaterConsumptionRate4[L/yr]	Drinking water consumption rate for teen (liters per year)
291	gen_dwc5	DrinkingWaterConsumptionRate5[L/yr]	Drinking water consumption rate for adult:ICRP72 (liters per year)
261	gen_firC	FruitIrrigationRateCB[in/yr]	Fruit irrigation rate for current biosphere (liters per year)
247	gen_firP	FruitIrrigationRatePB[in/yr]	Fruit irrigation rate for pluvial biosphere (liters per year)
268	gen_fitC	FruitIrrigationTimeCB[mo/yr]	Fruit irrigation time for current biosphere (months per year)
254	gen_fitP	FruitIrrigationTimePB[mo/yr]	Fruit irrigation time for pluvial biosphere (months per year)
262	gen_girC	GrainIrrigationRateCB[in/yr]	Grain irrigation rate for current biosphere (liters per year)
248	gen_girP	GrainIrrigationRatePB[in/yr]	Grain irrigation rate for pluvial biosphere (liters per year)
269	gen_gitC	GrainIrrigationTimeCB[mo/yr]	Grain irrigation time for current biosphere (months per year)
255	gen_gitP	GrainIrrigationTimePB[mo/yr]	Grain irrigation time for pluvial biosphere (months per year)
274	gen_hfgt	HenFeedGrowTime[day]	Egg-laying hen feed growing time (day)
263	gen_hirC	HomeIrrigationRateCB[in/yr]	Residential irrigation rate for current biosphere (liters per year)

**DESCRIPTION OF ABBREVIATIONS USED FOR TPA VERSION 4.1 CODE SAMPLED INPUT
PARAMETERS (continued)**

Parameter Identification	Short Name	Full Name	Description
249	gen_hirP	HomeIrrigationRatePB[in/yr]	Residential irrigation rate for pluvial biosphere (liters per year)
270	gen_hitC	HomeIrrigationTimeCB[mo/yr]	Residential irrigation time for current biosphere (months per year)
256	gen_hitP	HomeIrrigationTimePB[mo/yr]	Residential irrigation time for pluvial biosphere (months per year)
244	gen_ifi	InterceptionFraction/Irrigate	Irrigation interception fraction
245	gen_lirP	LeafyVegetableIrrigationRatePB[in/yr]	Leafy vegetable irrigation rate for pluvial biosphere (inches per year)
276	gen_mfdf	MilkFreshForageDietFraction	Dairy cattle fresh forage diet fraction
278	gen_mfgt	MilkFreshForageGrowTime[day]	Dairy cattle fresh forage growing time (day)
246	gen_oirP	OtherVegetableIrrigationRatePB[in/yr]	Other vegetable irrigation rate for pluvial biosphere (liters per year)
273	gen_pfgt	PoultryFeedGrowTime[day]	Poultry feed growing time (day)
283	genbfirC	BeefFreshForageIrrigationRateCB[in/yr]	Beef cattle fresh forage irrigation rate for current biosphere (inches per year)
279	genbfirP	BeefFreshForageIrrigationRatePB[in/yr]	Beef cattle fresh forage irrigation rate for pluvial biosphere (liters per year)
285	genbfitC	BeefFreshForageIrrigationTimeCB[mo/yr]	Beef cattle fresh forage irrigation time for current biosphere (months per year)

**DESCRIPTION OF ABBREVIATIONS USED FOR TPA VERSION 4.1 CODE SAMPLED INPUT
PARAMETERS (continued)**

Parameter Identification	Short Name	Full Name	Description
281	genbfitP	BeefFreshForageIrrigationTimePB[mo/yr]	Beef cattle fresh forage irrigation time for pluvial biosphere (months per year)
265	genhfirC	HenFeedIrrigationRateCB[in/yr]	Egg-laying hen feed irrigation rate for current biosphere (liters per year)
251	genhfirP	HenFeedIrrigationRatePB[in/yr]	Egg-laying hen feed irrigation rate for pluvial biosphere (liters per year)
272	genhfitC	HenFeedIrrigationTimeCB[mo/yr]	Egg-laying hen feed irrigation time for current biosphere (months per year)
258	genhfitP	HenFeedIrrigationTimePB[mo/yr]	Egg-laying hen feed irrigation time for pluvial biosphere (months per year)
259	genlvirC	LeafyVegetableIrrigationRateCB[in/yr]	Leafy vegetable irrigation rate for current biosphere (liters per year)
266	genlvitC	LeafyVegetableIrrigationTimeCB[mo/yr]	Leafy vegetable irrigation time for current biosphere (months per year)
252	genlvitP	LeafyVegetableIrrigationTimePB[mo/yr]	Leafy vegetable irrigation time for pluvial biosphere (months per year)
284	genmfirC	MilkFreshForageIrrigationRateCB[in/yr]	Dairy cattle fresh forage irrigation rate for current biosphere (liters per year)
280	genmfirP	MilkFreshForageIrrigationRatePB[in/yr]	Milk fresh forage irrigation rate for pluvial biosphere (liters per year)

**DESCRIPTION OF ABBREVIATIONS USED FOR TPA VERSION 4.1 CODE SAMPLED INPUT
PARAMETERS (continued)**

Parameter Identification	Short Name	Full Name	Description
286	genmfitC	MilkFreshForageIrrigationTimeCB[mo/yr]	Dairy cattle fresh forage irrigation time for current biosphere (months per year)
282	genmfitP	MilkFreshForageIrrigationTimePB[mo/yr]	Dairy cattle fresh forage irrigation time for pluvial biosphere (months per year)
260	genovirC	OtherVegetableIrrigationRateCB[in/yr]	Other vegetable irrigation rate for current biosphere (liters per year)
267	genovitC	OtherVegetableIrrigationTimeCB[mo/yr]	Other vegetable irrigation time for current biosphere (months per year)
253	genovitP	OtherVegetableIrrigationTimePB[mo/yr]	Other vegetable irrigation time for pluvial biosphere (months per year)
264	genpfirC	PoultryFeedIrrigationRateCB[in/yr]	Poultry feed irrigation rate for current biosphere (liters per year)
250	genpfirP	PoultryFeedIrrigationRatePB[in/yr]	Poultry feed irrigation rate for pluvial biosphere (liters per year)
271	genpfitC	PoultryFeedIrrigationTimeCB[mo/yr]	Poultry feed irrigation time for current biosphere (months per year)
257	genpfitP	PoultryFeedIrrigationTimePB[mo/yr]	Poultry feed irrigation time for pluvial biosphere (months per year)
9	H2O-FThk	ThicknessOfWaterFilm[m]	Thickness of water film on waste package surface

**DESCRIPTION OF ABBREVIATIONS USED FOR TPA VERSION 4.1 CODE SAMPLED INPUT
PARAMETERS (continued)**

Parameter Identification	Short Name	Full Name	Description
223	IPPFSTFF	ImmobilePorosityPenetrationFraction_STFF	Effective fraction of saturated rock matrix accessible to matrix diffusion; during the time scale for transport from source to receptor, used to calculate effective immobile porosity and matrix diffusion mass-transfer rate coefficient in NEFTRAN
64	InitRSFP	InitialRadiusOfSFPparticle[m]	Initial radius of spent nuclear fuel particle—affects spent nuclear fuel alteration rate and transport out of a failed waste package in EBSREL
131	InvMPerm	InvertMatrixPermeability[m ²]	Matrix permeability of the invert
2	MAPM@GM	MeanAveragePrecipitationMultiplierAtGlacialMaximum	Mean annual precipitation increase at glacial maximum—affects infiltration from the land surface in UZFLOW
3	MATI@GM	MeanAverageTemperatureIncreaseAtGlacialMaximum[°C]	Magnitude of mean annual temperature change at glacial maximum—affects infiltration from the land surface in UZFLOW
151	MKD_BFwU	MatrixKD_BFw_U[m ³ /kg]	Bullfrog-welded matrix K _d for uranium
147	MKD_CHvU	MatrixKD_CHvU[m ³ /kg]	Calico Hills-nonwelded vitric matrix K _d for uranium
148	MKD_CHzU	MatrixKD_CHzU[m ³ /kg]	Calico Hills-nonwelded zeolitic matrix K _d for uranium
149	MKD_PPwU	MatrixKD_PPw_U[m ³ /kg]	Prow Pass-welded matrix K _d for uranium
146	MKD_TSwU	MatrixKD_TSw_U[m ³ /kg]	Topopah Spring-welded matrix K _d for uranium
150	MKD_UCFU	MatrixKD_UCF_U[m ³ /kg]	Upper Crater Flat matrix K _d for uranium

E-10

**DESCRIPTION OF ABBREVIATIONS USED FOR TPA VERSION 4.1 CODE SAMPLED INPUT
PARAMETERS (continued)**

Parameter Identification	Short Name	Full Name	Description
137	MKDBFwAm	MatrixKD_BFw_Am[m3/kg]	Bullfrog-welded matrix K_d for americium
186	MKDBFwCs	MatrixKD_BFw_Cs[m3/kg]	Bullfrog-welded matrix K_d for cesium
193	MKDBFwNi	MatrixKD_BFw_Ni[m3/kg]	Bullfrog-welded matrix K_d for nickel
144	MKDBFwNp	MatrixKD_BFw_Np[m3/kg]	Bullfrog-welded matrix K_d for neptunium
179	MKDBFwPb	MatrixKD_BFw_Pb[m3/kg]	Bullfrog-welded matrix K_d for lead
158	MKDBFwPu	MatrixKD_BFw_Pu[m3/kg]	Bullfrog-welded matrix K_d for plutonium
172	MKDBFwRa	MatrixKD_BFw_Ra[m3/kg]	Bullfrog-welded matrix K_d for radium
200	MKDBFwSe	MatrixKD_BFw_Se[m3/kg]	Bullfrog-welded matrix K_d for selenium
165	MKDBFwTh	MatrixKD_BFw_Th[m3/kg]	Bullfrog-welded matrix K_d for thorium
133	MKDCHvAm	MatrixKD_CHnvAm[m3/kg]	Calico Hills-nonwelded vitric matrix K_d for americium
182	MKDCHvCs	MatrixKD_CHnvCs[m3/kg]	Calico Hills-nonwelded vitric matrix K_d for cesium
189	MKDCHvNi	MatrixKD_CHnvNi[m3/kg]	Calico Hills-nonwelded vitric matrix K_d for nickel
140	MKDCHvNp	MatrixKD_CHnvNp[m3/kg]	Calico Hills-nonwelded vitric matrix K_d for neptunium
175	MKDCHvPb	MatrixKD_CHnvPb[m3/kg]	Calico Hills-nonwelded vitric matrix K_d for lead
154	MKDCHvPu	MatrixKD_CHnvPu[m3/kg]	Calico Hills-nonwelded vitric matrix K_d for plutonium
168	MKDCHvRa	MatrixKD_CHnvRa[m3/kg]	Calico Hills-nonwelded vitric matrix K_d for radium
196	MKDCHvSe	MatrixKD_CHnvSe[m3/kg]	Calico Hills-nonwelded vitric matrix K_d for selenium

**DESCRIPTION OF ABBREVIATIONS USED FOR TPA VERSION 4.1 CODE SAMPLED INPUT
PARAMETERS (continued)**

Parameter Identification	Short Name	Full Name	Description
161	MKDCHvTh	MatrixKD_CHnvTh[m3/kg]	Calico Hills-nonwelded vitric matrix K_d for thorium
134	MKDCHzAm	MatrixKD_CHnzAm[m3/kg]	Calico Hills-nonwelded zeolitic matrix K_d for americium
183	MKDCHzCs	MatrixKD_CHnzCs[m3/kg]	Calico Hills-nonwelded zeolitic matrix K_d for cesium
190	MKDCHzNi	MatrixKD_CHnzNi[m3/kg]	Calico Hills-nonwelded zeolitic matrix K_d for nickel
141	MKDCHzNp	MatrixKD_CHnzNp[m3/kg]	Calico Hills-nonwelded zeolitic matrix K_d for neptunium
176	MKDCHzPb	MatrixKD_CHnzPb[m3/kg]	Calico Hills-nonwelded zeolitic matrix K_d for lead
155	MKDCHzPu	MatrixKD_CHnzPu[m3/kg]	Calico Hills-nonwelded zeolitic matrix K_d for plutonium
169	MKDCHzRa	MatrixKD_CHnzRa[m3/kg]	Calico Hills-nonwelded zeolitic matrix K_d for radium
197	MKDCHzSe	MatrixKD_CHnzSe[m3/kg]	Calico Hills-nonwelded zeolitic matrix K_d for selenium
162	MKDCHzTh	MatrixKD_CHnzTh[m3/kg]	Calico Hills-nonwelded zeolitic matrix K_d for thorium
135	MKDPPwAm	MatrixKD_PPw_Am[m3/kg]	Prow Pass-welded matrix K_d for americium
184	MKDPPwCs	MatrixKD_PPw_Cs[m3/kg]	Prow Pass-welded matrix K_d for cesium
191	MKDPPwNi	MatrixKD_PPw_Ni[m3/kg]	Prow Pass-welded matrix K_d for nickel
142	MKDPPwNp	MatrixKD_PPw_Np[m3/kg]	Prow Pass-welded matrix K_d for neptunium
177	MKDPPwPb	MatrixKD_PPw_Pb[m3/kg]	Prow Pass-welded matrix K_d for lead
156	MKDPPwPu	MatrixKD_PPw_Pu[m3/kg]	Prow Pass-welded matrix K_d for plutonium
170	MKDPPwRa	MatrixKD_PPw_Ra[m3/kg]	Prow Pass-welded matrix K_d for radium

**DESCRIPTION OF ABBREVIATIONS USED FOR TPA VERSION 4.1 CODE SAMPLED INPUT
PARAMETERS (continued)**

Parameter Identification	Short Name	Full Name	Description
198	MKDPPwSe	MatrixKD_PPw_Se[m3/kg]	Prow Pass-welded matrix K_d for selenium
163	MKDPPwTh	MatrixKD_PPw_Th[m3/kg]	Prow Pass-welded matrix K_d for thorium
132	MKDTSwAm	MatrixKD_TSw_Am[m3/kg]	Topopah Spring-welded matrix K_d for americium
181	MKDTSwCs	MatrixKD_TSw_Cs[m3/kg]	Topopah Spring-welded matrix K_d for cesium
188	MKDTSwNi	MatrixKD_TSw_Ni[m3/kg]	Topopah Spring-welded matrix K_d for nickel
139	MKDTSwNp	MatrixKD_TSw_Np[m3/kg]	Topopah Spring-welded matrix K_d for neptunium
174	MKDTSwPb	MatrixKD_TSw_Pb[m3/kg]	Topopah Spring-welded matrix K_d for lead
153	MKDTSwPu	MatrixKD_TSw_Pu[m3/kg]	Topopah Spring-welded matrix K_d for plutonium
167	MKDTSwRa	MatrixKD_TSw_Ra[m3/kg]	Topopah Spring-welded matrix K_d for radium
195	MKDTSwSe	MatrixKD_TSw_Se[m3/kg]	Topopah Spring-welded matrix K_d for selenium
160	MKDTSwTh	MatrixKD_TSw_Th[m3/kg]	Topopah Spring-welded matrix K_d for thorium
136	MKDUCFam	MatrixKD_UCF_Am[m3/kg]	Upper Crater Flat matrix K_d for americium
185	MKDUCFCs	MatrixKD_UCF_Cs[m3/kg]	Upper Crater Flat matrix K_d for cesium
192	MKDUCFNi	MatrixKD_UCF_Ni[m3/kg]	Upper Crater Flat matrix K_d for nickel
143	MKDUCFNp	MatrixKD_UCF_Np[m3/kg]	Upper Crater Flat matrix K_d for neptunium
178	MKDUCFPb	MatrixKD_UCF_Pb[m3/kg]	Upper Crater Flat matrix K_d for lead
157	MKDUCFPu	MatrixKD_UCF_Pu[m3/kg]	Upper Crater Flat matrix K_d for plutonium

**DESCRIPTION OF ABBREVIATIONS USED FOR TPA VERSION 4.1 CODE SAMPLED INPUT
PARAMETERS (continued)**

Parameter Identification	Short Name	Full Name	Description
171	MKDUCFRa	MatrixKD_UCF_Ra[m3/kg]	Upper Crater Flat matrix K_d for radium
199	MKDUCFSe	MatrixKD_UCF_Se[m3/kg]	Upper Crater Flat matrix K_d for selenium
164	MKDUCFTh	MatrixKD_UCF_Th[m3/kg]	Upper Crater Flat matrix K_d for thorium
152	MKDUFZ_U	MatrixKD_UFZ_U[m3/kg]	Unsaturated Fracture Zone matrix K_d for uranium
138	MKDUFZAm	MatrixKD_UFZ_Am[m3/kg]	Unsaturated Fracture Zone matrix K_d for americium
187	MKDUFZCs	MatrixKD_UFZ_Cs[m3/kg]	Unsaturated Fracture Zone matrix K_d for cesium
194	MKDUFZNi	MatrixKD_UFZ_Ni[m3/kg]	Unsaturated Fracture Zone matrix K_d for nickel
145	MKDUFZNp	MatrixKD_UFZ_Np[m3/kg]	Unsaturated Fracture Zone matrix K_d for neptunium
180	MKDUFZPb	MatrixKD_UFZ_Pb[m3/kg]	Unsaturated Fracture Zone matrix K_d for lead
159	MKDUFZPu	MatrixKD_UFZ_Pu[m3/kg]	Unsaturated Fracture Zone matrix K_d for plutonium
173	MKDUFZRa	MatrixKD_UFZ_Ra[m3/kg]	Unsaturated Fracture Zone matrix K_d for radium
201	MKDUFZSe	MatrixKD_UFZ_Se[m3/kg]	Unsaturated Fracture Zone matrix K_d for selenium
166	MKDUFZTh	MatrixKD_UFZ_Th[m3/kg]	Unsaturated Fracture Zone matrix K_d for thorium
207	Mprm_BFw	MatrixPermeability_BFw_[m2]	Bullfrog-welded matrix permeability
203	MPrm_CHv	MatrixPermeability_CHnv[m2]	Calico Hills-nonwelded vitric matrix permeability
204	MPrm_CHz	MatrixPermeability_CHnz[m2]	Calico Hills-nonwelded zeolitic matrix permeability
205	MPrm_PPw	MatrixPermeability_PPw_[m2]	Prow Pass-welded matrix permeability

**DESCRIPTION OF ABBREVIATIONS USED FOR TPA VERSION 4.1 CODE SAMPLED INPUT
PARAMETERS (continued)**

Parameter Identification	Short Name	Full Name	Description
202	MPrm_TSw	MatrixPermeability_TSw_[m2]	Topopah Spring-welded matrix permeability
206	MPrm_UCF	MatrixPermeability_UCF_[m2]	Upper Crater Flat matrix permeability
208	MPrm_UFZ	MatrixPermeability_UFZ_[m2]	Unsaturated Fracture Zone matrix permeability
242	MixZnT20	MixingZoneThickness20km[m]	Mixing zone thickness at 20 km [12.4 mi].
314	NEFZnW	NEFaultZoneWidth[m]	Northeast fault zone width
316	NELCDAmt	NEAmountOfLargestCredibleDisplacement[m]	Northeast largest credible displacement
313	NWFZnW	NWFaultZoneWidth[m]	Northwest fault zone width
315	NWLCDAmt	NWAmountOfLargestCredibleDisplacement[m]	Northwest largest credible displacement
63	PSFDM1	Preexponential_SFDissoLutionMode12	Preexponential factor for spent nuclear fuel dissolution rate from (mg m ⁻² d ⁻¹)
243	PWPRRG20	PluvialWellPumpingRateAtReceptorGroup20km[gal/day]	Well pumping rate at 20 km [12.4 mi] location during pluvial period [gal/day].
240	PlumeTh5	PlumeThickness5km[m]	Plume thickness at 5 km [3.1 mi]
61	SbArWt%	SubAreaWetFraction	Subarea wet fraction

**DESCRIPTION OF ABBREVIATIONS USED FOR TPA VERSION 4.1 CODE SAMPLED INPUT
PARAMETERS (continued)**

Parameter Identification	Short Name	Full Name	Description
65	SbGFRATF	SubGrainFragmentRadiusAfterTransFrac[m]	Subgrain fragment radius of UO ₂ particle after transgranular fracture; used only if fuel conversion takes place from UO ₂ to UO _{2,4} and U ₃ O ₈ ; used only by the spent nuclear fuel dissolution models dependent on exposed surface area
121	SFWt%C1	SFWettedFraction_Corrosion_1	Spent nuclear fuel wet fraction for corrosion failures in subarea 1
122	SFWt%C2	SFWettedFraction_Corrosion_2	Spent nuclear fuel wet fraction for corrosion failures in subarea 2
123	SFWt%C3	SFWettedFraction_Corrosion_3	Spent nuclear fuel wet fraction for corrosion failures in subarea 3
124	SFWt%C4	SFWettedFraction_Corrosion_4	Spent nuclear fuel wet fraction for corrosion failures in subarea 4
125	SFWt%C5	SFWettedFraction_Corrosion_5	Spent nuclear fuel wet fraction for corrosion failures in subarea 5
126	SFWt%C6	SFWettedFraction_Corrosion_6	Spent nuclear fuel wet fraction for corrosion failures in subarea 6
127	SFWt%C7	SFWettedFraction_Corrosion_7	Spent nuclear fuel wet fraction for corrosion failures in subarea 7
128	SFWFC1	SFWettedFraction_Corrosion_8	Spent nuclear fuel wet fraction for corrosion failures in subarea 8

**DESCRIPTION OF ABBREVIATIONS USED FOR TPA VERSION 4.1 CODE SAMPLED INPUT
PARAMETERS (continued)**

Parameter Identification	Short Name	Full Name	Description
129	SFWt%C9	SFWettedFraction_Corrosion_9	Spent nuclear fuel wet fraction for corrosion failures in subarea 9
130	SFWt%C10	SFWettedFraction_Corrosion_10	Spent nuclear fuel wet fraction for corrosion failures in subarea 10
79	SFWt%F0	SFWettedFraction_FAULTO	Spent nuclear fuel wet fraction for faulting failures
69	SFWt%I1	SFWettedFraction_Initial_1	Spent nuclear fuel wet fraction for initial failures in subarea 1
70	SFWt%I2	SFWettedFraction_Initial_2	Spent nuclear fuel wet fraction for initial failures in subarea 2
71	SFWt%I3	SFWettedFraction_Initial_3	Spent nuclear fuel wet fraction for initial failures in subarea 3
72	SFWt%I4	SFWettedFraction_Initial_4	Spent nuclear fuel wet fraction for initial failures in subarea 4
73	SFWt%I5	SFWettedFraction_Initial_5	Spent nuclear fuel wet fraction for initial failures in subarea 5
74	SFWt%I6	SFWettedFraction_Initial_6	Spent nuclear fuel wet fraction for initial failures in subarea 6
75	SFWt%I7	SFWettedFraction_Initial_7	Spent nuclear fuel wet fraction for initial failures in subarea 7
76	SFWFI1	SFWettedFraction_Initial_8	Spent nuclear fuel wet fraction for initial failures in subarea 8

**DESCRIPTION OF ABBREVIATIONS USED FOR TPA VERSION 4.1 CODE SAMPLED INPUT
PARAMETERS (continued)**

Parameter Identification	Short Name	Full Name	Description
77	SFWt%I9	SFWettedFraction_Initial_9	Spent nuclear fuel wet fraction for initial failures in subarea 9
78	SFWt%I10	SFWettedFraction_Initial_10	Spent nuclear fuel wet fraction for initial failures in subarea 10
81	SFWt%S11	SFWettedFraction_SEISMO1_1	Spent nuclear fuel wet fraction for seismic failures for seismic interval 1 in subarea 1
82	SFWt%S12	SFWettedFraction_SEISMO1_2	Spent nuclear fuel wet fraction for seismic failures for seismic interval 1 in subarea 2
83	SFWt%S13	SFWettedFraction_SEISMO1_3	Spent nuclear fuel wet fraction for seismic failures for seismic interval 1 in subarea 3
84	SFWt%S14	SFWettedFraction_SEISMO1_4	Spent nuclear fuel wet fraction for seismic failures for seismic interval 1 in subarea 4
85	SFWt%S15	SFWettedFraction_SEISMO1_5	Spent nuclear fuel wet fraction for seismic failures for seismic interval 1 in subarea 5
86	SFWt%S16	SFWettedFraction_SEISMO1_6	Spent nuclear fuel wet fraction for seismic failures for seismic interval 1 in subarea 6
87	SFWt%S17	SFWettedFraction_SEISMO1_7	Spent nuclear fuel wet fraction for seismic failures for seismic interval 1 in subarea 7
88	SFWFSEIS	SFWettedFraction_SEISMO1_8	Spent nuclear fuel wet fraction for seismic failures for seismic interval 1 in subarea 8

**DESCRIPTION OF ABBREVIATIONS USED FOR TPA VERSION 4.1 CODE SAMPLED INPUT
PARAMETERS (continued)**

Parameter Identification	Short Name	Full Name	Description
89	SFWt%S19	SFWettedFraction_SEISMO1_9	Spent nuclear fuel wet fraction for seismic failures for seismic interval 1 in subarea 9
80	SFWt%S1A	SFWettedFraction_SEISMO1_10	Spent nuclear fuel wet fraction for seismic failures for seismic interval 1 in subarea 10
91	SFWt%S21	SFWettedFraction_SEISMO2_1	Spent nuclear fuel wet fraction for seismic failures for seismic interval 2 in subarea 1
92	SFWt%S22	SFWettedFraction_SEISMO2_2	Spent nuclear fuel wet fraction for seismic failures for seismic interval 2 in subarea 2
93	SFWt%S23	SFWettedFraction_SEISMO2_3	Spent nuclear fuel wet fraction for seismic failures for seismic interval 2 in subarea 3
94	SFWt%S24	SFWettedFraction_SEISMO2_4	Spent nuclear fuel wet fraction for seismic failures for seismic interval 2 in subarea 4
95	SFWt%S25	SFWettedFraction_SEISMO2_5	Spent nuclear fuel wet fraction for seismic failures for seismic interval 2 in subarea 5
96	SFWt%S26	SFWettedFraction_SEISMO2_6	Spent nuclear fuel wet fraction for seismic failures for seismic interval 2 in subarea 6
97	SFWt%S27	SFWettedFraction_SEISMO2_7	Spent nuclear fuel wet fraction for seismic failures for seismic interval 2 in subarea 7
98	SFWFSEI	SFWettedFraction_SEISMO2_8	Spent nuclear fuel wet fraction for seismic failures for seismic interval 2 in subarea 8

**DESCRIPTION OF ABBREVIATIONS USED FOR TPA VERSION 4.1 CODE SAMPLED INPUT
PARAMETERS (continued)**

Parameter Identification	Short Name	Full Name	Description
99	SFWt%S29	SFWettedFraction_SEISMO2_9	Spent nuclear fuel wet fraction for seismic failures for seismic interval 2 in subarea 9
100	SFWt%S2A	SFWettedFraction_SEISMO2_10	Spent nuclear fuel wet fraction for seismic failures for seismic interval 2 in subarea 10
101	SFWt%S31	SFWettedFraction_SEISMO3_1	Spent nuclear fuel wet fraction for seismic failures for seismic interval 3 in subarea 1
102	SFWt%S32	SFWettedFraction_SEISMO3_2	Spent nuclear fuel wet fraction for seismic failures for seismic interval 3 in subarea 2
103	SFWt%S33	SFWettedFraction_SEISMO3_3	Spent nuclear fuel wet fraction for seismic failures for seismic interval 3 in subarea 3
104	SFWt%S34	SFWettedFraction_SEISMO3_4	Spent nuclear fuel wet fraction for seismic failures for seismic interval 3 in subarea 4
105	SFWt%S35	SFWettedFraction_SEISMO3_5	Spent nuclear fuel wet fraction for seismic failures for seismic interval 3 in subarea 5
106	SFWt%S36	SFWettedFraction_SEISMO3_6	Spent nuclear fuel wet fraction for seismic failures for seismic interval 3 in subarea 6
107	SFWt%S37	SFWettedFraction_SEISMO3_7	Spent nuclear fuel wet fraction for seismic failures for seismic interval 3 in subarea 7
108	SFWFSEI6	SFWettedFraction_SEISMO3_8	Spent nuclear fuel wet fraction for seismic failures for seismic interval 3 in subarea 8

**DESCRIPTION OF ABBREVIATIONS USED FOR TPA VERSION 4.1 CODE SAMPLED INPUT
PARAMETERS (continued)**

Parameter Identification	Short Name	Full Name	Description
109	SFWt%S39	SFWettedFraction_SEISMO3_9	Spent nuclear fuel wet fraction for seismic failures for seismic interval 3 in subarea 9
110	SFWt%S3A	SFWettedFraction_SEISMO3_10	Spent nuclear fuel wet fraction for seismic failures for seismic interval 3 in subarea 10
111	SFWt%S41	SFWettedFraction_SEISMO4_1	Spent nuclear fuel wet fraction for seismic failures for seismic interval 4 in subarea 1
112	SFWt%S42	SFWettedFraction_SEISMO4_2	Spent nuclear fuel wet fraction for seismic failures for seismic interval 4 in subarea 2
113	SFWt%S43	SFWettedFraction_SEISMO4_3	Spent nuclear fuel wet fraction for seismic failures for seismic interval 4 in subarea 3
114	SFWt%S44	SFWettedFraction_SEISMO4_4	Spent nuclear fuel wet fraction for seismic failures for seismic interval 4 in subarea 4
115	SFWt%S45	SFWettedFraction_SEISMO4_5	Spent nuclear fuel wet fraction for seismic failures for seismic interval 4 in subarea 5
116	SFWt%S46	SFWettedFraction_SEISMO4_6	Spent nuclear fuel wet fraction for seismic failures for seismic interval 4 in subarea 6
117	SFWt%S47	SFWettedFraction_SEISMO4_7	Spent nuclear fuel wet fraction for seismic failures for seismic interval 4 in subarea 7
118	SFWFSEI9	SFWettedFraction_SEISMO4_8	Spent nuclear fuel wet fraction for seismic failures for seismic interval 4 in subarea 8

**DESCRIPTION OF ABBREVIATIONS USED FOR TPA VERSION 4.1 CODE SAMPLED INPUT
PARAMETERS (continued)**

Parameter Identification	Short Name	Full Name	Description
119	SFWt%S49	SFWettedFraction_SEISMO4_9	Spent nuclear fuel wet fraction for seismic failures for seismic interval 4 in subarea 9
120	SFWt%S4A	SFWettedFraction_SEISMO4_10	Spent nuclear fuel wet fraction for seismic failures for seismic interval 4 in subarea 10
80	SFWt%V0	SFWettedFraction_VOLCANO	Spent nuclear fuel wet fraction for volcanic failures
66	Solbl-Am	SolubilityAm[kg/m3]	Solubility limit for americium
67	Solbl-Np	SolubilityNp[kg/m3]	Solubility limit for neptunium
68	Solbl-Pu	SolubilityPu[kg/m3]	Solubility limit for plutonium
15	SSMO-JS1	SEISMOJointSpacing1[m]	Joint spacing for rock condition 1. Not all rocks falling from roof of emplacement will impact waste packages. Effective size of rock that impacts waste packages will be controlled by joint spacing.
16	SSMO-JS2	SEISMOJointSpacing2[m]	Joint spacing for rock condition 2
17	SSMO-JS3	SEISMOJointSpacing3[m]	Joint spacing for rock condition 3
18	SSMO-JS4	SEISMOJointSpacing4[m]	Joint spacing for rock condition 4
19	SSMO-JS5	SEISMOJointSpacing5[m]	Joint spacing for rock condition 5
13	SSMO-RE	RockModulusOfElasticityforSEISMO[Pa]	Rock modulus of elasticity
14	SSMO-RPR	RockPoissonRatioforSEISMO[]	Rock poisson ratio

E-22

**DESCRIPTION OF ABBREVIATIONS USED FOR TPA VERSION 4.1 CODE SAMPLED INPUT
PARAMETERS (continued)**

Parameter Identification	Short Name	Full Name	Description
20	SSMOV201	VerticalExtentOfRockFall2_1[m]	Vertical extent of rockfall for rock condition 2 and ground acceleration 0.05g. Lower limit approximately equivalent to average rock joint spacing of rock condition 1. Upper limit estimated from numerical results.
21	SSMOV202	VerticalExtentOfRockFall2_2[m]	Same as above except with ground acceleration 0.10g
22	SSMOV203	VerticalExtentOfRockFall2_3[m]	Same as above except with ground acceleration 0.15g
23	SSMOV204	VerticalExtentOfRockFall2_4[m]	Same as above except with ground acceleration 0.20g
24	SSMOV205	VerticalExtentOfRockFall2_5[m]	Same as above except with ground acceleration 0.25g
25	SSMOV206	VerticalExtentOfRockFall2_6[m]	Same as above except with ground acceleration 0.30g
26	SSMOV207	VerticalExtentOfRockFall2_7[m]	Same as above except with ground acceleration 0.35g
27	SSMOV208	VerticalExtentOfRockFall2_8[m]	Same as above except with ground acceleration 0.40g
28	SSMOV209	VerticalExtentOfRockFall2_9[m]	Same as above except with ground acceleration 0.45g
29	SSMOV210	VerticalExtentOfRockFall2_10[m]	Same as above except with ground acceleration 0.50g
30	SSMOV301	VerticalExtentOfRockFall3_1[m]	Vertical extent of rockfall for rock condition 3 and ground acceleration 0.05g
31	SSMOV302	VerticalExtentOfRockFall3_2[m]	Same as above except with ground acceleration 0.10g
32	SSMOV303	VerticalExtentOfRockFall3_3[m]	Same as above except with ground acceleration 0.15g
33	SSMOV304	VerticalExtentOfRockFall3_4[m]	Same as above except with ground acceleration 0.20g

**DESCRIPTION OF ABBREVIATIONS USED FOR TPA VERSION 4.1 CODE SAMPLED INPUT
PARAMETERS (continued)**

Parameter Identification	Short Name	Full Name	Description
34	SSMOV305	VerticalExtentOfRockFall3_5[m]	Same as above except with ground acceleration 0.25g
35	SSMOV306	VerticalExtentOfRockFall3_6[m]	Same as above except with ground acceleration 0.30g
36	SSMOV307	VerticalExtentOfRockFall3_7[m]	Same as above except with ground acceleration 0.35g
37	SSMOV308	VerticalExtentOfRockFall3_8[m]	Same as above except with ground acceleration 0.40g
38	SSMOV309	VerticalExtentOfRockFall3_9[m]	Same as above except with ground acceleration 0.45g
39	SSMOV310	VerticalExtentOfRockFall3_10[m]	Same as above except with ground acceleration 0.50g
40	SSMOV401	VerticalExtentOfRockFall4_1[m]	Vertical extent of rockfall for rock condition 4 and ground acceleration 0.05g
41	SSMOV402	VerticalExtentOfRockFall4_2[m]	Same as above except with ground acceleration 0.10g
42	SSMOV403	VerticalExtentOfRockFall4_3[m]	Same as above except with ground acceleration 0.15g
43	SSMOV404	VerticalExtentOfRockFall4_4[m]	Same as above except with ground acceleration 0.20g
44	SSMOV405	VerticalExtentOfRockFall4_5[m]	Same as above except with ground acceleration 0.25g
45	SSMOV406	VerticalExtentOfRockFall4_6[m]	Same as above except with ground acceleration 0.30g
46	SSMOV407	VerticalExtentOfRockFall4_7[m]	Same as above except with ground acceleration 0.35g
47	SSMOV408	VerticalExtentOfRockFall4_8[m]	Same as above except with ground acceleration 0.40g
48	SSMOV409	VerticalExtentOfRockFall4_9[m]	Same as above except with ground acceleration 0.45g
49	SSMOV410	VerticalExtentOfRockFall4_10[m]	Same as above except with ground acceleration 0.50g

**DESCRIPTION OF ABBREVIATIONS USED FOR TPA VERSION 4.1 CODE SAMPLED INPUT
PARAMETERS (continued)**

Parameter Identification	Short Name	Full Name	Description
50	SSMOV501	VerticalExtentOfRockFall5_1[m]	Vertical extent of rockfall for rock condition 5 and ground acceleration 0.05g
51	SSMOV502	VerticalExtentOfRockFall5_2[m]	Same as above except with ground acceleration 0.10g
52	SSMOV503	VerticalExtentOfRockFall5_3[m]	Same as above except with ground acceleration 0.15g
53	SSMOV504	VerticalExtentOfRockFall5_4[m]	Same as above except with ground acceleration 0.20g
54	SSMOV505	VerticalExtentOfRockFall5_5[m]	Same as above except with ground acceleration 0.25g
55	SSMOV506	VerticalExtentOfRockFall5_6[m]	Same as above except with ground acceleration 0.30g
56	SSMOV507	VerticalExtentOfRockFall5_7[m]	Same as above except with ground acceleration 0.35g
57	SSMOV508	VerticalExtentOfRockFall5_8[m]	Same as above except with ground acceleration 0.40g
58	SSMOV509	VerticalExtentOfRockFall5_9[m]	Same as above except with ground acceleration 0.45g
59	SSMOV510	VerticalExtentOfRockFall5_10[m]	Same as above except with ground acceleration 0.50g
6	TempGrBI	TemperatureGradientInVicinityOfBoilingIsotherm[K/m]	Temperature gradient in vicinity of boiling isotherm, (parameter specific to reflux3 model)
322	VC-Dia	DiameterOfVolcanicCone[m]	Cone diameter
319	VD-Angle	AngleOfVolcanicDikeMeasuredFromNorthClockwise[degrees]	Volcanic dike angle
320	VD-Length	LengthOfVolcanicDike[m]	Volcanic dike length
321	VD-Width	WidthOfVolcanicDike[m]	Volcanic dike width

**DESCRIPTION OF ABBREVIATIONS USED FOR TPA VERSION 4.1 CODE SAMPLED INPUT
PARAMETERS (continued)**

Parameter Identification	Short Name	Full Name	Description
326	VE-Durat	VolcanicEventDuration[s]	Volcanic event duration
327	VE-Power	VolcanicEventPower[W]	Volcanic event power
318	VEi/e-R#	RNtoDeterminelfExtrusiveOrIntrusiveVolcanicEvent	Random number to determine volcanic event type
317	VEROI-Tn	TimeOfNextVolcanicEventinRegionOfInterest[yr]	Time of next volcanic event
325	WindSpd	WindSpeed[cm/s]	Wind speed
62	WP-Def%	DefectiveFractionOfWPs/cell	Fraction of total waste packages in a subarea that fail at time t_0
309	WPDF-ThD	ThresholdDisplacementforFaultDisruptionOfWP[m]	Threshold fault displacement for disruption. Data input order: number of fault displacement values to be provided followed by equiprobable displacement values
60	WPFlowMF	WastePackageFlowMultiplicationFactor	Factor that is multiplied by flow rate hitting waste package. Resulting flow rates written to ebsflow.dat, which is an input file to releaset.f stand-alone code.
324	WPMefail	NumberOfMagmaInducedMechanicalFailuresRemainingInDrift[]	Number of waste package that fail during intrusive event and remain in disrupted drifts (process-based model)
238	WPRRG@10	WellPumpingRateAtReceptorGroup10km[gal/day]	Well-pumping rate for residential receptor group located less than 10 km [6.2 mi] from Yucca Mountain
239	WPRRG@20	WellPumpingRateAtReceptorGroup20km[gal/day]	Well-pumping rate for residential receptor group located less than 20 km [12.4 mi] from Yucca Mountain

**DESCRIPTION OF ABBREVIATIONS USED FOR TPA VERSION 4.1 CODE SAMPLED INPUT
PARAMETERS (continued)**

Parameter Identification	Short Name	Full Name	Description
7	YMR-TC	ThermalConductivityofYMRock[W/(m-K)]	Thermal conductivity of rock

APPENDIX F

HUMAN-INTRUSION ANALYSIS

F.1 BACKGROUND

The National Academy of Sciences recommended that a prescribed scenario of human intrusion of the repository be modeled to judge if the repository system is inherently resilient to such disruption (National Research Council, 1995). The U.S. Nuclear Regulatory Commission prescribed human-intrusion scenario is described by 10 CFR 63.322, and makes the following assumptions:

- There is a single human intrusion as a result of exploratory drilling for groundwater.
- The intruders drill a borehole directly through a degraded waste package into the uppermost aquifer underlying the proposed Yucca Mountain repository.
- The drillers use common techniques and practices currently employed in exploratory drilling for groundwater in the region surrounding Yucca Mountain.
- Careful sealing of the borehole does not occur, instead, natural degradation processes gradually modify the borehole.
- No particulate waste material falls into the borehole.
- The exposure scenario includes only those radionuclides transported to the saturated zone by water (e.g., water enters the waste package, releases radionuclides, and transports radionuclides by way of the borehole to the saturated zone).
- No releases caused by unlikely natural processes and events are included.

This study was to determine risk significance of a human-intrusion event. The TPA code was used to evaluate the impact of a prescribed human-intrusion scenario at Yucca Mountain. The results were compared to the TPA Version 4.1 code basecase results and previous human intrusion analyses performed using TPA Version 3.2 code (Smith, et al., 1999).

In the sections to follow, the method implemented is described, and results from the analyses are presented. The risk significance of human intrusion is discussed last.

F.2 METHOD

With guidance from 10 CFR 63.322, a human-intrusion scenario was developed that could be modeled using the TPA Version 4.1 code. When assumptions are required, beyond those specified by regulation, the calculation uses a conservative approach because the primary purpose is to gauge the potential importance of the human-intrusion scenario. A conceptual image of this prescribed human-intrusion scenario is depicted as Figure F-1. The following additional assumptions were made to complete the scenario

- The disruptive event is conservatively assumed to occur just 100 years after closure.

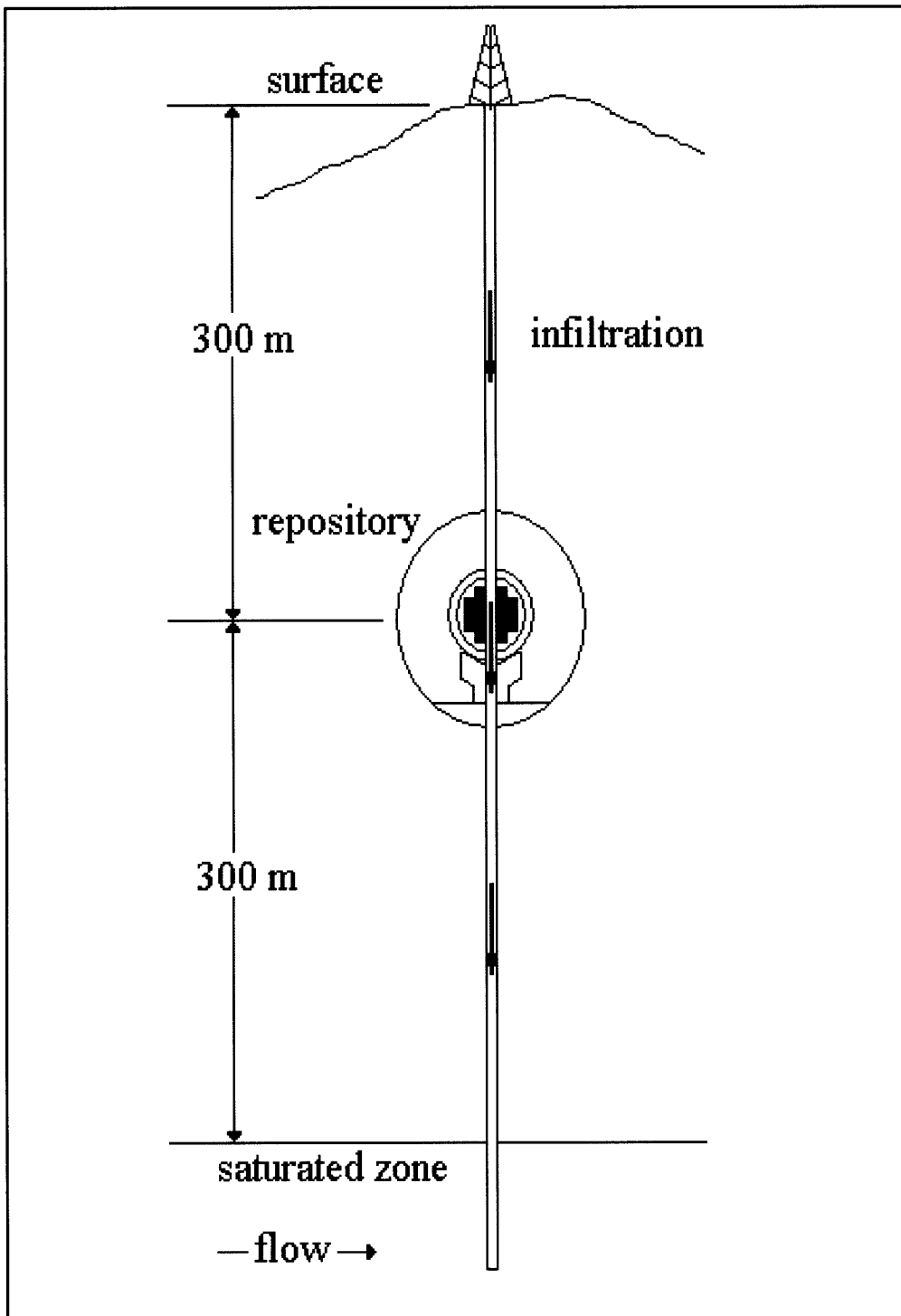


Figure F-1. Conceptual Image of Yucca Mountain Prescribed Human-Intrusion Scenario Modeled Using TPA Version 4.1 Code

- A 14.0-cm [5.5-in] borehole penetrates a waste package and continues to the saturated zone, creating a zero-time pathway from the waste package to the saturated zone. The size of the borehole is not specified by regulation.
- One hundred percent of the spent nuclear fuel remains in the waste package at the repository horizon.
- The spent nuclear fuel remaining in the waste package experiences chemical and flow conditions prevailing in the unsaturated zone.
- The spent nuclear fuel is conservatively assumed to be unprotected by cladding and is subgranular.
- The spent nuclear fuel travels toward the reasonably maximally exposed individual via the groundwater, which is used for drinking water, irrigation, and as the water source for livestock.

The human-intrusion scenario modeling is described conceptually in the following three subsections: timing and number of waste package failures, unsaturated zone flow and transport, and spent nuclear fuel degradation and release. The total-system performance assessment parameters modified to conduct the human-intrusion analysis are detailed in Table F-1.

F.2.1 Timing and Number of Waste Package Failures

The human intrusion scenario is described by a single event assumed to occur 100 years after closure. To simulate this event in the TPA Version 4.1 code, parameter selections were made to force the code to incur only one waste package failure at the desired time (100 years). The single waste package failure accomplished by allowing one juvenile waste package failure to occur 100 years after closure. The potential for additional waste package failures was removed by eliminating disruptive events and eliminating corrosion failure of waste packages.

F.2.2 Unsaturated Zone Flow and Transport

The human-intrusion event is described by a single borehole that pierces a waste package and continues to the saturated zone. No spent nuclear fuel falls to the saturated zone, but the borehole acts as a fast transport pathway from the ground surface to the saturated zone. The temperature, pH, oxygen partial pressure, and carbonate concentration values for the prevailing unsaturated zone environment were used. The volumetric flow of water entering the breached waste package was adjusted to equal the amount of surface water that could enter the borehole from a 10-m² [32.8-ft²] catchment area. To simulate the fast pathway through the unsaturated zone, the following flow and transport barriers were removed: drip shield, invert, and unsaturated zone stratigraphy.

Table F-1. TPA Version 4.1 Code Input Parameters Modified to Conduct the Human-Intrusion Analysis			
Parameter	Default Distribution and Value	Modified Distribution and Value	Explanation for Change
Seismic Disruptive Scenario Flag	iflag 1	iflag 0	Desire to look at impact of human-intrusion event only.
Stop at Subarea	iconstant 10	iconstant 1	Changed to look at one subarea with one failure (human-intrusion event). Identical TPA Version 4.1 code runs were repeated for each subarea and showed that subarea 1 results in the earliest dose and highest peak dose.
Number of Realizations	iconstant 1	iconstant 250	250 realizations sufficient for stability.
Critical Relative Humidity Air Corrosion	constant 0.55	constant 1.0	Set to 1.0 to eliminate nonjuvenile failures due to humid air corrosion.
Critical Relative Humidity Aqueous Corrosion	normal 0.6, 0.65	constant 1.0	Set to 1.0 to eliminate nonjuvenile failures due to aqueous corrosion.
Drip Shield Failure Time	lognormal 2700.0, 20400.0	constant 100.0	Set to coincide with timing of human-intrusion event.
Waste Package Flow Multiplication Factor	lognormal 3.15×10^{-2} , 1.05×10^{-3}	constant 167.0	Parameter adjusted to match unsaturated zone volumetric flux rate experienced down borehole assuming that precipitation falling over a given catchment area enters the borehole and reaches the repository horizon. Assuming a 10-m ² catchment area and a 17.5-cm/yr ² precipitation rate gives a 1.75-m ³ /yr volumetric flux rate. A separate TPA Version 4.1 code input file [†] was created to eliminate the effects of reflux and the changing climate conditions and resulted in a volumetric flux of 1.36 m ³ /yr reported in the <i>ebsflo.dat</i> file. Given the default values for Fmult = 0.0447, Fow = 0.173, and Fwet set = 1.0, the waste package flow multiplication factor was set to 167.0 to give an adjusted volumetric flux of 1.75 m ³ /yr.
Subarea Wet Fraction	uniform 0.0, 1.0	constant 1.0	Set to 1.0 so that all breached waste packages are dripped on.

Table F-1. TPA Version 4.1 Code Input Parameters Modified to Conduct the Human-Intrusion Analysis (continued)

Parameter	Default Distribution and Value	Modified Distribution and Value	Explanation for Change
Initial Failure Time	constant 0.0	constant 100.0	Set to coincide with timing of human intrusion event.
Defective Fraction of Waste Packages Per Cell	uniform 1.0×10^{-4} , 1.0×10^{-2}	constant 6.8729×10^{-4}	Set to give one failure in subarea 1 that contains 1,455 waste packages.
Surface Area Model (selection of model for computing surface area of spent nuclear fuel)	iconstant 1	iconstant 2	Spent nuclear fuel is assumed subgranular and dependent on grain radius and width of oxidation zone.
I model (selection of model for computing spent nuclear fuel dissolution)	iconstant 2	iconstant 1	This dissolution model provides the fastest dissolution rate and assumes the absence of calcium and silicon.
Spent Nuclear Fuel Wetted Fraction	uniform 0.0, 1.0	constant 1.0	Assumes 100 percent spent nuclear fuel of breached waste package is contacted by water.
Invert Bypass	iflag 0	iflag 1	Transport through invert is skipped, consistent with the human-intrusion scenario borehole
Unsaturated Zone Stratigraphic Layer Thicknesses for All 10 Subareas	constant various	constant 0	All unsaturated zone stratigraphic layers set to 0-m thickness to simulate direct pathway provided by the human-intrusion scenario borehole.

*Precipitation rate reported to range from 10–25 cm/yr in draft environmental impact statement for Yucca Mountain (U.S. Department of Energy, 1999).

† The additional parameters modified for the separate TPA Version 4.1 code input file are displayed as Table F-2 of this appendix.

Note: All correlated parameters related to the unsaturated zone were commented out (essentially removed) to ensure no impact on the model results from unsaturated zone-related parameters.

F.3 Spent Nuclear Fuel Degradation and Release

For spent nuclear fuel degradation, the first of four spent nuclear fuel degradation models available in the TPA Version 4.1 code was selected. This model provides the fastest dissolution rate and is a function of temperature, pH, oxygen partial pressure, and carbonate concentration. For the spent nuclear fuel dissolution, it is conservatively assumed that the spent nuclear fuel is crushed to grain size by the human-intrusion event and that the total surface area contributes to spent nuclear fuel dissolution. A granular model is used in the basecase, but a subgranular model was selected for the human-intrusion scenario to account for disruption of spent nuclear fuel that could occur during the drilling event. The 20 radionuclides tracked for the total-system performance basecase analyses were also used for this analysis (C-14, Cl-36, Ni-59, Se-79, Nb-94, Tc-99, I-129, Cs-135, Pb-210, Ra-226, Th-230, U-234, Np-237, U-238, Pu-239, Pu-240, Am-241, Am-243, Cm-245, and Cm-246). The flow and transport modeling in the saturated zone and beyond matched that done for the basecase. All releases from the proposed repository are assumed uniformly mixed in the groundwater supply used by a reasonably maximally exposed individual. The reasonably maximally exposed individual is assumed to be a rural resident located 20 km [12.4 mi] downgradient from the repository whose diet consists of TPA Version 4.1 code default food consumption rates based on a survey of Armagosa Valley residents (CRWMS M&O, 2000). Note that 10 CFR Part 63 locates the reasonably maximally exposed individual no further than 18 km [11.2 mi] downgradient from the repository, and it is anticipated that future versions of the TPA code will be modified to include an 18-km [11.2-mi] compliance boundary

F.4 Results

Modeling this human-intrusion scenario using the TPA Version 4.1 code gave peak total expected annual doses to the reasonably maximally exposed individual near 10^{-6} Sv [0.1 mrem] in 10,000 years. As indicated in Table F-3, TPA Version 4.1 code human-intrusion dose calculation results are near the results for the TPA Version 3.2 code human-intrusion analyses (Smith, et al., 1999). As expected, only radionuclides with higher solubility rates and lower retardation rates (i.e., Cl-36, Tc-99, I-129, and Np-237) contribute significantly to the dose within 10,000 years of the event. The primary contributors to the expected annual dose in 10,000 years for the human-intrusion scenario are presented in Table F-4. The primary contributors to the expected annual dose in 10,000 years for the human-intrusion and basecase scenarios are also shown graphically in Figures F-2 and F-3. For the human-intrusion scenario (Figure F-2), the primary contributor to the expected annual dose is Tc-99 for approximately the first 2,000 years and then Np-237 afterward. For the basecase (Figure F-3), the primary contributor remains as Tc-99 in 10,000 years.

F.5 Risk Significance

As reported in the previous section, the total-system performance assessment human-intrusion scenario calculations show peak annual total expected doses to the reasonably maximally exposed individual near 10^{-6} Sv [0.1 mrem] during the 10,000-year simulation period. The calculated dose remains low primarily because of the limited spent nuclear fuel inventory available in this scenario. Only one of 8,877 waste package, or less than 0.012 percent of the spent nuclear fuel expected to be placed at Yucca Mountain, is made available for release by the scenario. As indicated by Figure F-4, the additional contribution to the expected annual

Table F-2. Additional TPA Version 4.1 Code Input Parameters Modified to Eliminate the Effects of Reflux and Changing Climate Conditions to Facilitate the Calculation of an Appropriate Value for the Waste Package Flow Multiplication Factor

Parameter	Default Distribution and Value	Modified Distribution and Value	Explanation for Change
Areal Average Mean Annual Infiltration at Start	uniform 1.0, 10.0	constant 5.5	Set to constant value to eliminate impact on flow rate into waste package
Mean Average Precipitation Multiplier at Glacial Maximum	uniform 1.5, 2.5	constant 1.0	Set to constant value to eliminate impact on flow rate into waste package
Mean Average Temperature Increase at Glacial Maximum	uniform -10, -5	constant 0.0	Set to constant value to eliminate impact on flow rate into waste package
Reflux Model	iconstant 3	iconstant 1	Set to constant value to eliminate impact on flow rate into waste package
Length of Reflux Zone	constant 20	constant 0.0	Set to constant value to eliminate impact on flow rate into waste package
Perched Bucket Volume per Subarea	constant 0.5	constant 0.0	Set to constant value to eliminate impact on flow rate into waste package

Table F-3. Peak Expected Annual Dose in 10,000 Years for Human-Intrusion and Basecase Scenarios Using TPA Versions 4.1 and 3.2 Codes

Scenario	Peak Expected Dose (mrem/yr)
TPA Version 4.1 Code Basecase	1.77×10^2
TPA Version 4.1 Code Human Intrusion	5.73×10^2
TPA Version 3.2 Code Human Intrusion (Smith, et al., 1999)	1.23×10^2

Table F-4. Primary Contributors to Peak Expected Annual Dose in 10,000 Years for TPA Version 4.1 Code Basecase and Human-Intrusion Scenario with 250 Realizations

Radionuclide*	TPA Version 4.1 Code Basecase (%)	TPA Version 4.1 Code Human Intrusion (%)
Tc-99	57.4	0.8
I-129	28.1	0.4
Np-237	14.3	98.8
Cl-36	—	0.2

*Radionuclides considered: C-14, Cl-36, Ni-59, Se-79, Nb-94, Tc-99, I-129, Cs-135, Pb-210, Ra-226, Th-230, U-234, Np-237, U-238, Pu-239, Pu-240, Am-241, Am-243, Cm-245, and Cm-246

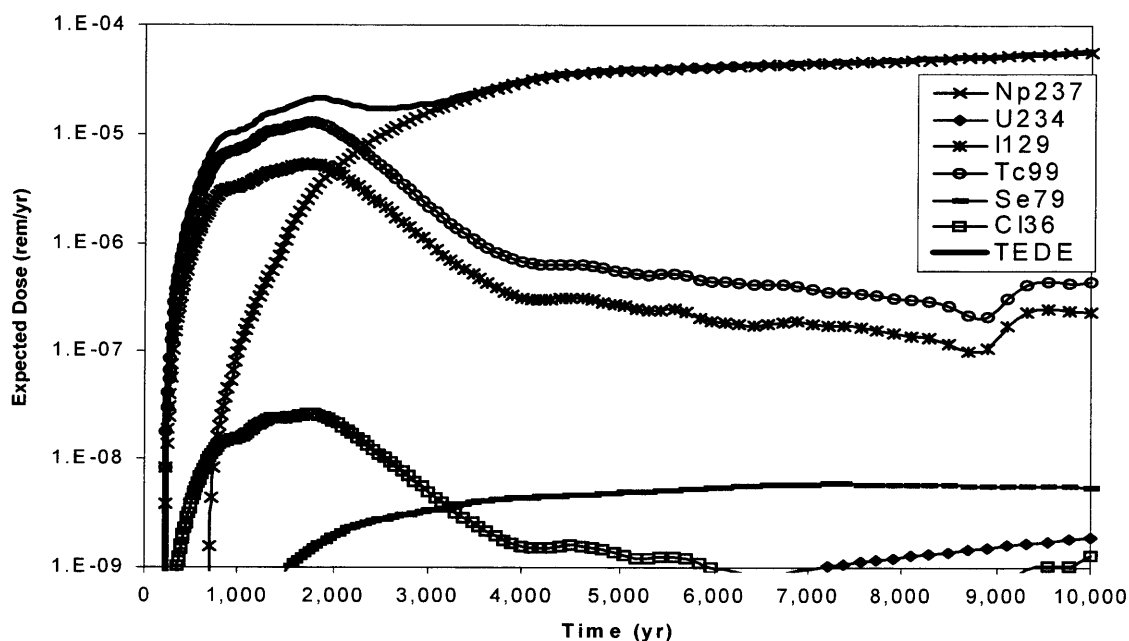


Figure F-2. Primary Contributors to the Expected Dose in 10,000 Years for the TPA Version 4.1 Code Human-Intrusion Scenario

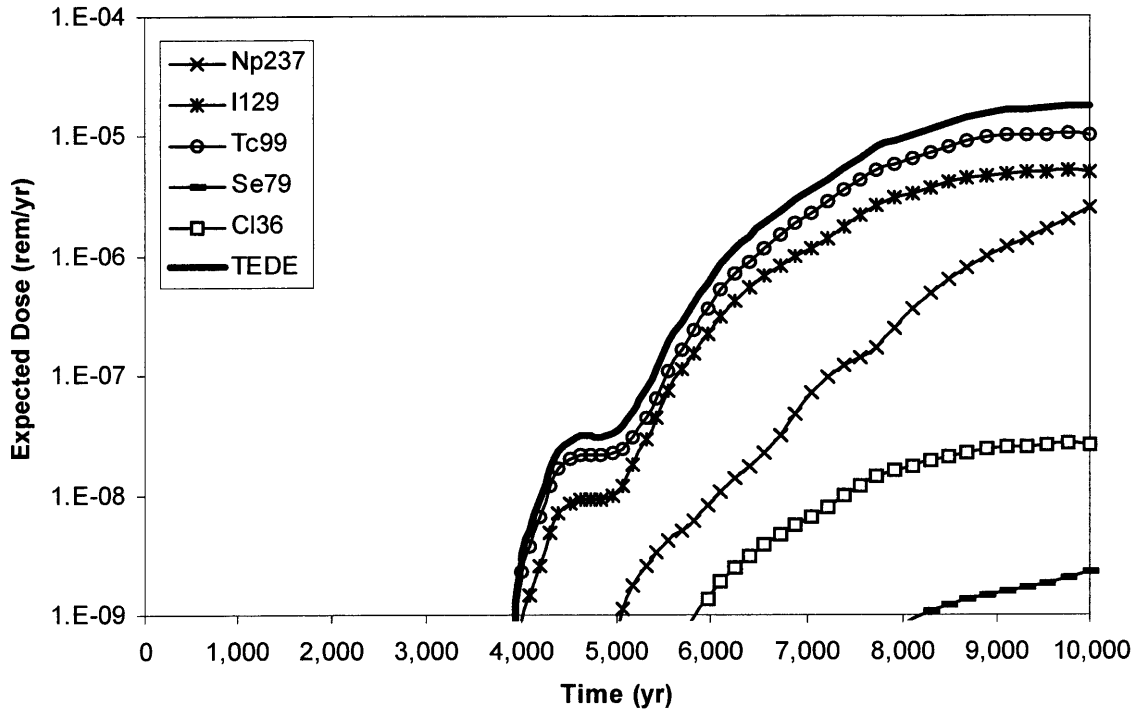


Figure F-3. Primary Contributors to the Expected Dose in 10,000 Years for the TPA Version 4.1 Code Basecase

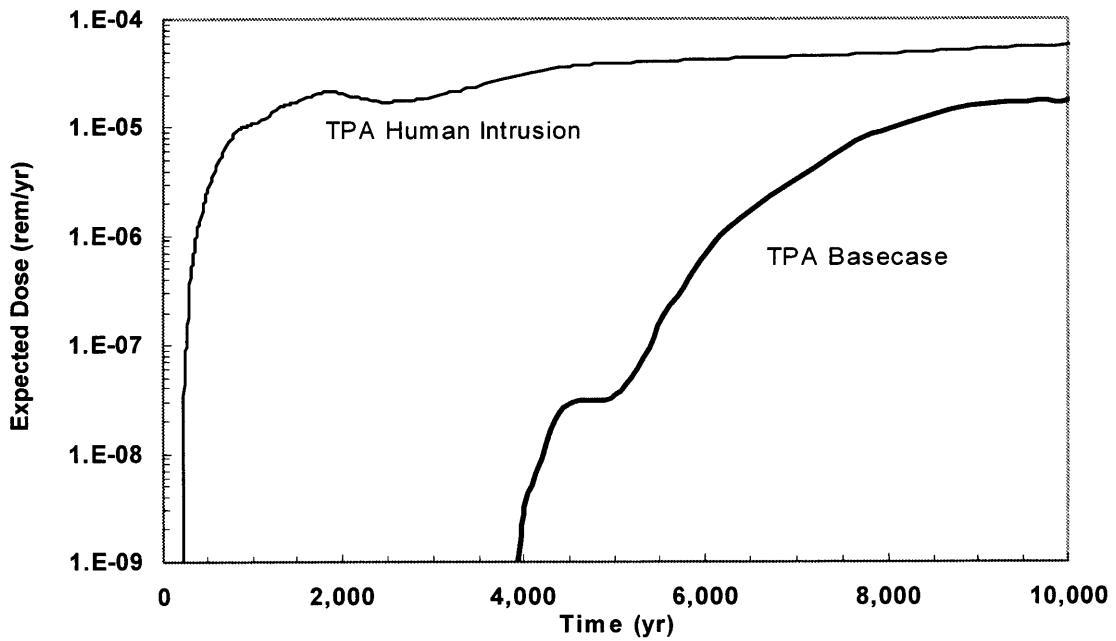


Figure F-4. Expected Total Dose in 10,000 Years for TPA Version 4.1 Code Basecase and Human-Intrusion Scenarios with 250 Realizations

dose from this prescribed human-intrusion event in 10,000 years is approximately one order of magnitude above the expected annual dose from the total-system performance assessment basecase analyses. The primary difference in 10,000 years is that the initial expected dose from the human-intrusion scenario arrives approximately 4,000 years earlier than for the total-system performance assessment basecase, and Np-237 becomes the dominant radionuclide.

F.6 References

CNWRA. "Total-system Performance Assessment (TPA) Version 4.0 Code: Module Descriptions and User's Guide." San Antonio, Texas: CNWRA. 2000.

CRWMS M&O. "Identification of Critical Group (Consumption of Locally Produced Food and Tap Water)." ANL-MGR-MD-000005. Revision 0. Las Vegas, Nevada: CRWMS M&O. 2000.

National Research Council. "Technical Bases for Yucca Mountain Standards." Washington, DC: National Research Council. 1995.

Smith, M., T. McCartin, and S. Mohanty. "Demonstration of TPA Version 3.2 Code's Capability to Evaluate the Effects of Human Intrusion." Transactions of the American Nuclear Society 1999 Winter Meeting. Vol. 81. Long Beach, California: American Nuclear Society. November 14-18, 1999.

APPENDIX G

IMPACT OF IN-PACKAGE CRITICALITY ON REPOSITORY PERFORMANCE

Analyses reported in this appendix quantify the consequences of postclosure criticality events on the expected dose. Consequences of nuclear criticality can be an increase in the inventory of radionuclides in the waste package, elevation of the temperature of the waste package, and mechanical damage to the engineered barriers of the repository. Because the criticality event is expected to occur with low probability, the processes leading to criticality have not been included in the basecase performance assessment model. Similar to the igneous activity and faulting event calculations, risk from a criticality event also requires the knowledge of the event probability. Analyses in this appendix are limited to obtaining an estimate of only the consequence of an in-package criticality event (i.e., criticality occurring within the waste package) without consideration of event probabilities. In this regard, the information presented in this appendix does not provide a direct measure of risk. Although probabilities exist in the literature [e.g., U.S. Department of Energy (DOE), 1998] uses 5×10^{-3} and 1×10^{-3} for probability of criticality for PWR and BWR waste packages for 10,000 years with certain assumptions), NRC staff and the CNWRA continue to focus only on the consequence estimates.

Criticality outside the waste package is not considered in this report but is currently being investigated. In-package criticality is considered more likely than criticality occurring outside of the waste package, because of reduced concentrations of important radionuclides and the difficulty in obtaining the accumulations and configurations necessary to permit criticality to occur.

In-package criticality may occur if certain conditions are met. A possible scenario for which in-package criticality can occur is described next. As shown in Figure G-1, after waste package breach, water can fill the waste package as long as the bottom of the waste package is intact. As water collects in the waste package, the internal structures of the waste package will corrode, releasing some of the neutron poison into solution. If sufficient water collects in the waste package allowing the water level to rise to where the breach exists, the neutron poison can be removed gradually as water exits the waste package. If the waste package bottom remains intact until a sufficient fraction of the poison is removed, some spent nuclear fuel could go critical (depending on configuration of the fuel, amount of water in the waste package, and so on). Seismic events could cause a rapid insertion of reactivity by shaking the waste package so that several fuel assemblies held above the water level by degraded internal structures would drop into the water. This rapid insertion of reactivity could result in a transient criticality with a rapid increase in temperatures and pressures in the waste package. Potentially, this reaction could cause mechanical damage to the fuel, waste package, and surrounding engineered barriers.

These analyses used the TPA code with appropriate adjustment of model parameters to mimic an in-package criticality condition. Because criticality can occur from a variety of configurations, the probability of this particular configuration occurring was less than the cumulative probability of criticality. Because the calculations were limited by the options currently available within the existing total-system performance assessment framework, emphasis was placed on obtaining a

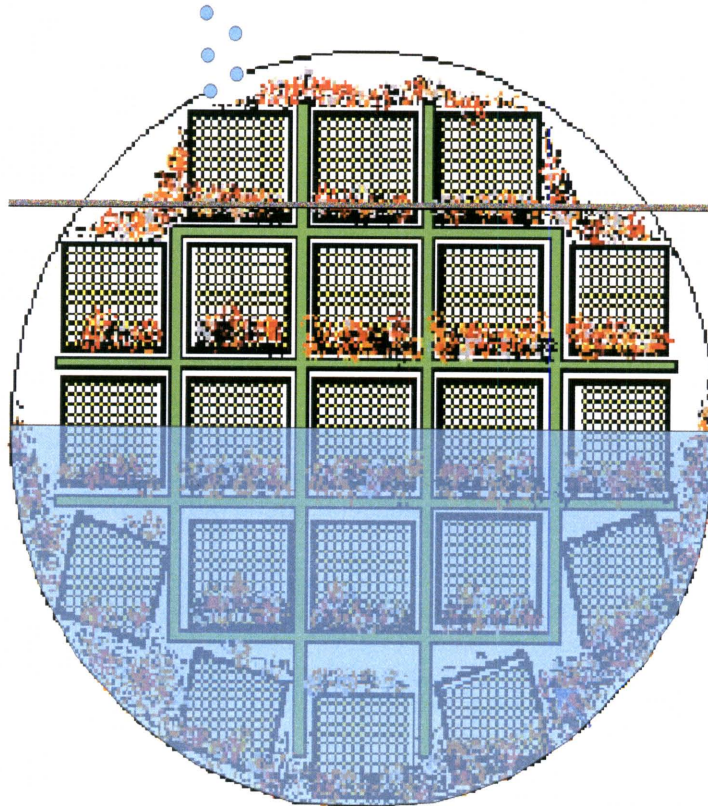


Figure G-1. Schematic of a Degraded Waste Package Prior to an In-Package Criticality Event (DOE, 1998)

conservative estimate. The rationale for using a conservative analysis was that, if the consequence of the criticality event is low, in spite of the conservatism, there will be no further need to focus on the quantitative accuracy of the criticality event probability.

Two types of criticality events may occur: steady-state criticality and transient criticality. The scenario of a steady-state criticality inside the waste package would involve failure of the waste package, subsequent intrusion of water into the waste package, and corrosion, dissolution, and removal of the criticality control system (i.e., borated stainless steel). Subsequent to gradual removal of the borated stainless steel, the waste package will approach a critical condition. As the result of a critical condition, additional heat, above and beyond the decay heat, will be produced that will cause the waste package temperature to increase and the water inside the waste package to start to evaporate. The evaporation continues until the water level decreases and causes the criticality condition to cease. This sequence of water intrusion, approach to critical condition, evaporation, and return to subcritical condition will be repeated whenever water enters the waste package. At steady state, the power level will be determined by the heat transfer away from the waste package. This heat transfer will include the mechanisms of thermal conduction, convection, radiation, and latent heat loss by evaporation of water dripped into the waste package.

The process for the transient criticality scenario would begin similar to the steady-state criticality. On removal of the criticality control system, however, there could be a configuration in which the system suddenly becomes critical or supercritical. For example, in a bathtub model when the water level inside the waste package reaches a height where the system is close to critical condition, and a seismic event could cause shuffling of the stacked spent nuclear fuel assemblies, a reactivity insertion could be introduced into the system that could produce significant kinetic energy. This kinetic energy could unzip the spent nuclear fuel rods and create openings in the bottom of the waste package and the invert. The adjacent waste packages may also be damaged. Therefore, the consequences of a transient criticality may include an impact on the barriers.

In the following sections, steady-state criticality consequence modeling is described, followed by a description of the technique used to capture the consequences of a transient criticality event. The procedure presented is a formalization of the approach presented in Weldy, et al. (2001). The procedure fully relies on the framework of the TPA Version 4.0 code (Mohanty, et al., 2002) and does not rely on any external model calculations. The criticality event is minimal in the TPA Version 4.1 code, appropriately adjusting the parameters to provide conservative estimates of the consequence. The procedure described was used to determine the power level and the resulting increase in radionuclide inventory from the steady-state criticality cycles and the subsequent impact on the expected dose. The parameters in the TPA Version 4.1 code that were changed and the magnitude of these changes are described for both steady-state and transient criticality scenarios. Finally, results from the two criticality consequence models are described.

Steady-State Criticality

The sustainable power level of a steady-state criticality will be limited by the rate of water infiltration into the waste package. As the power level increases, more water will be evaporated, the water level will fall, and the system will lose reactivity. Therefore, the maximum sustainable power level cannot exceed the power required to evaporate water entering the waste package plus the power required to make up for heat lost to the surrounding rock.

To bound the potential effects of criticality, a conservative case was analyzed. It was assumed at year 5,000 all failed waste packages would go critical and remain critical for 10,000 years. The analysis evaluated whether the generation of additional radionuclides and the increased temperature from the criticality event would significantly affect repository performance.

From Sonntag and van Wylen (1991), the power level in the waste package can be calculated by

$$P_{WP} = Q_{WP} + \dot{m}(h_2 - h_1) \quad (G-1)$$

where

- P_{WP} — power level from in-package steady-state criticality (W)
- Q_{WP} — heat loss from the waste package to surrounding area (no backfill) (W)
- \dot{m} — water mass flow rate into the waste package (g/s)

- h_2 — enthalpy of water before evaporation (J/g)
 h_1 — enthalpy of water after evaporation (J/g)

The heat loss from the waste package can be calculated according to the TPA Version 4.0 code user's guide (Mohanty, et al., 2002):

$$Q_{WP} = (G_{conv} + G_{cond} + G_{rad})(T_{wp} - T_{rock}) \quad (G-2)$$

where

- G_{conv} — effective thermal conductance for convective heat transfer (W/°C)
 G_{cond} — effective thermal conductance for conductive heat transfer (W/°C)
 G_{rad} — effective thermal conductance for radiative heat transfer (W/°C)
 T_{wp} — waste package surface temperature (°C)
 T_{rock} — drift rock wall temperature (°C)

The effective thermal conductance for convective, conductive, and radiative heat transfer coefficients can be calculated from the following formulae, also in the TPA Version 4.0 code user's guide (Mohanty, et al., 2002):

$$G_{conv} = f_c \frac{2\pi k_{eff-nc}(L_{wp} - 2\delta)}{\ln\left(\frac{D_{rw}}{D_{wp}}\right)} \quad (G-3)$$

where

- f_c — fractional area not covered by the floor = 0.75 (Mohanty, et al., 2000)
 k_{eff-nc} — effective thermal conductivity for natural convection = 0.9 W/m-°C (Mohanty, et al., 2000)
 D_{rw} — Diameter of drift = 5.5 m [18 ft] (CRWMS M&O, 2000)
 D_{wp} — Diameter of waste package = 1.579 m [5.2 ft] (CRWMS M&O, 2000)
 L_{wp} — Length of waste package = 5.275 m [17.3 ft] (CRWMS M&O, 2000)
 δ — Spacing between waste package = 0.1 m [0.33 ft] (CRWMS M&O, 2000)

$$G_{cond} = (1 - f_c) \frac{2\pi k_{floor}(L_{wp} - 2\delta)}{\ln\left(\frac{D_{rw}}{D_{wp}}\right)} \quad (G-4)$$

where

- f_c — fractional area not covered by the floor = 0.75 (Mohanty, et al., 2000)
 k_{floor} — thermal conductivity of floor = 0.6 W/m-°C (Incropera and DeWitt, 1995)

$$G_{rad} = F_c \frac{4\sigma(273.15 + T_{rock})^3}{\frac{1 - \varepsilon_{wp}}{\varepsilon_{wp}\pi D_{wp}L_{wp}} + \frac{1}{F_{wp-rw}\pi D_{wp}(L_{wp} + 2\delta)} + \frac{1 - \varepsilon_{rw}}{\varepsilon_{rw}\pi D_{rw}(L_{wp} + 2\delta)}} \quad (G-5)$$

where

- σ — Stefan-Boltzman constant = $5.67 \times 10^{-8} \text{ W/m}^2\text{K}^4$ (Mohanty, et al., 2000)
- ε_{wp} — emissivity of the waste package = 0.87 (Mohanty, et al., 2000)
- F_{wp-rw} — radiative view factor from the waste package to the rock wall = 1 (Mohanty, et al., 2000)
- T_{rock} — drift rock wall temperature ($^{\circ}\text{C}$)

A rock wall temperature at $t = 5,000$ years of 70°C [158°F] from total-system performance assessment results and an increase in the temperature of the waste package from the criticality of 25°C [77°F] from U.S. Department of Energy (DOE) calculations (DOE, 1998) were used. A reasonably conservative value for the flow rate of water into the waste package of $0.1 \text{ m}^3/\text{yr}$ [$3.5 \text{ ft}^3/\text{yr}$] from CRWMS M&O (2000) was used. Enthalpy values for 70°C [158°F] water and 100°C [212°F] steam from Sonntag and van Wylen (1991, Table A.1.2SI) were obtained. These values result in the calculation of a power level of 4.78 kW [6.4 hp].

This power level was used in ORIGEN2 (Oak Ridge National Laboratory, 1991) calculations for 10,000 years to calculate the inventory generation for this event (note that the ORIGEN2 calculations do not account for differences in moderator density or temperatures between a reactor and a waste package, which could have a moderate effect on the results). The goal is to get an increase in inventory at 15,000 years, for all total-system performance assessment nuclides considered, that matches the 10,000-year criticality inventory increase calculated using ORIGEN2.1. For radionuclides that are not daughter products in a decay chain series, the inventory at 10 years is increased by that same percentage. Chain nuclides need to consider the effects of parent decay on inventory. If the inventory from the parent decay dominates the amount of radionuclides present at 15,000 years, only the inventory of the parent needs to be increased by the appropriate percentage. If the inventory of the daughter dominates, only the inventory of the daughter needs to be increased. If the contribution of the parent and daughter are comparable, changes to inventory will have to be divided between the two. The radionuclide inventory was increased to reflect the criticality contribution, as shown in Table G-1. Changes to other total-system performance assessment input files for simulating steady-state criticality consequences are described in the following sections and shown in Table G-2.

The steady-state criticality event was modeled as a 10,000-year steady-state criticality that starts at year 5,000. It was assumed all initially defective waste packages (an average of approximately 32) go critical at year 5,000, and all waste packages that go critical are under drips (otherwise, they could not go critical). The analysis was performed in such a way to show only the incremental dose from steady-state criticalities. Therefore, to obtain the total dose, the dose from the basecase needed to be added to the criticality dose. In addition, all the radionuclides produced by the steady-state criticality were assumed available for instantaneous release.

Table G-1. Increase in Radionuclide Inventory from Steady-State Criticality				
Radionuclide	15,000-Year Inventory Dominated By	Base Inventory (Ci/MTU)	Percent Increase	PostCriticality Inventory (Ci/MTU)
Cm-246	Self	7.62×10^{-2}	374	0.361
U-238	Self	0.315	-1.1	0.3115
Cm-245	Self	0.366	Leave same—not important to performance	No change
Am-241	Parent (Cm-245)	2,080	Leave same—not important to performance	No change
Np-237	Parent (Am-241)	0.434	71 - 1.65 Ci/MTU from parents, need to increase initial inventory to raise to 2.823 Ci/MTU at 15,000 years	1.173
Am-243	Self	26.4	313.7	109.2
Pu-239	Self	369	28.8	475.4
Pu-240	Self	544	160.2	1,415
U-234	50% self, 50% Pu-238	1.18	251 - 2.636 Ci/MTU from parents, need to increase initial inventory to raise to 9.267 Ci/MTU at 15,000 years	6.63
Th-230	Parent (U-234)	No change	No change	No change—inventory will be wrong because of U-234 change; model separately if necessary

Table G-1. Increase in Radionuclide Inventory from Steady-State Criticality (continued)

Radionuclide	15,000-Year Inventory Dominated By:	Base Inventory (Ci/MTU)	Percent Increase	PostCriticality Inventory (Ci/MTU)
Ra-226	Parent (Th-230)	No change	No change	No change—inventory will be wrong because of U-234 change; model separately if necessary
Pb-210	Parent (Ra-226)	No change	No change	No change—inventory will be wrong because of U-234 change; model separately if necessary
Cs-135	Self	0.536	87.4	1.00
I-129	Self	3.57×10^{-2}	22.1	4.36×10^{-2}
Tc-99	Self	14.5	11.5	16.2
Ni-59	Self	2.44	45	3.54
C-14	Self	1.44	310.3	5.91
Se-79	Self	0.458	11.2	0.509 (corrected to 0.03 because of half-life change)
Nb-94	Self	0.848	65.1	1.4
Cl-36	Self	1.15×10^{-2}	31.5	1.47×10^{-2}

Table G-2. TPA Version 4.1 Code Input Parameters Modified to Simulate In-Package Steady-State Criticality Consequences															
File/Parameter	Default Distribution Value	Modified Distribution and Value	Explanation for Change												
tpa.inp															
Seismic Disruptive Scenario Flag	iflag 1	iflag 0	Desire to look at impact of steady-state criticality events												
Number of Realizations	iconstant 1	iconstant 250	250 realizations sufficient for stability												
AA-1-1 (Passive Current Density for Waste Package Outer Overpack)	Normal 1.6×10^3 , 1.7×10^4	Normal 1.6, 1.7	To eliminate nonjuvenile failure caused by corrosion												
Coefficient for Localized Corrosion of Outer Overpack	Constant 2.5×10^{-4}	Constant 2.5×10^{-8}	To eliminate nonjuvenile failure caused by corrosion												
Subarea Wet Fraction	Uniform 0.0, 1.0	Uniform 0.999999, 1.0	To make all juvenile failed waste package to be dripped on												
Initial Failure Time	Constant 0.0	Constant 5000.0	Assuming it takes 5,000 years for the breached waste package to lose its criticality control system												
Gap Fraction	Default values in column three of Table G-1	Changed default values by the fractions in column four of Table G-1	To simulate the incremental increase in radionuclide inventory available for release												
burnup.dat															
Heat Generation (lines added to input) BWR (W/MTIHM) PWR (W/MTIHM)		<table border="1"> <thead> <tr> <th></th> <th>5,000</th> <th>10,000</th> <th>15,000</th> </tr> </thead> <tbody> <tr> <td>BWR (W/MTIHM)</td> <td>56.54</td> <td>35.52</td> <td>25.0</td> </tr> <tr> <td>PWR (W/MTIHM)</td> <td>64.1</td> <td>46.27</td> <td>28.0</td> </tr> </tbody> </table>		5,000	10,000	15,000	BWR (W/MTIHM)	56.54	35.52	25.0	PWR (W/MTIHM)	64.1	46.27	28.0	To simulate the increase in temperature from steady-state criticality
	5,000	10,000	15,000												
BWR (W/MTIHM)	56.54	35.52	25.0												
PWR (W/MTIHM)	64.1	46.27	28.0												

Table G-2. TPA Version 4.1 Code Input Parameters Modified to Simulate In-Package Steady-State Criticality Consequences (continued)			
File/Parameter	Default Distribution Value	Modified Distribution and Value	Explanation for Change
wpflow.def			
Flow Diversion Factor (F_{mult})	0.044721 for t = 0.0 to 100,000 yrs.	0.044721 for t = 0.0 to 7,000 years. 0.0 for t = 7,000 to 15,000 years.	To simulate water evaporation with no release during criticality period
nuclides.dat			
	column three of Table G-1	column five of Table G-1	To simulate increase in radionuclide inventory from steady-state criticality

The heat produced by the steady-state criticality was also included in the consequence model. The values of heat generation were modified to produce a heat increase of approximately 25 °C [77 °F] between the years 5,000 and 15,000. The 25 °C [77 °F] increase in temperature was taken from calculations performed by DOE (1998). Specifically, the heat-generation rate at year 5,000 was changed to 56.54 W/MTHM for BWR fuel and 64.1 W/MTHM for PWR fuel. At year 10,000, the heat-generation rate was changed to 35.52 W/MTHM for BWR fuel and 46.27 W/MTHM for PWR fuel, and the heat-generation rate was set to 25.00 W/MTHM for BWR fuel and 28.00 W/MTHM for PWR fuel at year 15,000.

To simulate the steady-state criticality, the bathtub model in the TPA code was used. It was assumed water enters the waste package and accumulates until a critical condition is reached. The water then evaporates until the system goes subcritical. This cycle repeats until the year 15,000, and no radionuclides are released before 15,000 years. At year 15,000, when the steady-state criticality ends, the water that contains dissolved radionuclides starts leaving the waste package.

Transient Criticality

The transient criticality was modeled as an extreme event in which the fuel maintains its geometry and sufficient water remains in the waste package to generate a very large pressure pulse. This pressure pulse is assumed sufficient to very quickly degrade the spent nuclear fuel inside the waste package, cause serious damage to the waste package so the water contact model is a flow-through model, fail one waste package on either side of the critical waste package, and blast a hole in the invert material below the waste package such that the performance of the invert is bypassed. The drip shield above the waste package would also be failed by the blast but was already assumed failed for the waste package to accumulate water

and go critical. The total number of fissions will be limited enough that changes in radionuclide inventory or long-term heat generation can be ignored.

The calculation required two runs of the TPA code to perform the modeling—one for the waste package in which the transient criticality occurs and one for the two additional waste packages, which are failed by the transient criticality. The required modifications for the total-system performance assessment input file for the source package are shown in Table G-3. The results of the analysis can be added with the basecase dose to compare the results to the basecase. Therefore, the simulation for the source package was performed by turning off the corrosion-induced and seismic-induced waste package failures, setting the number of initially failed waste packages to 1, and forcing it to be dripped on and become critical at year 5,000. At year 5,000, the impact of a transient criticality event was modeled by switching to the flow-through model and bypassing the invert. Switching to a flow-through model simulates the hole that could be created from a pressure pulse. Bypassing the invert is a way of mimicking the hole that the pressure pulse could create in the invert.

With respect to simulating the impact of the pressure pulse on the adjacent waste packages, a separate total-system performance assessment run with no corrosion-induced and seismic-induced waste package failures and two waste packages with initial failure. In the simulation, it was also assumed the blast would make ineffective the invert under the two adjacent waste packages. The changes to the TPA.INP file for the adjacent packages are similar to those shown in Figure G-1 except the default dissolution model for the spent nuclear fuel model is used, and defective waste package fractions are changed to 4.5×10^{-4} to ensure that only two waste packages are failed initially (one located in Subarea 2 and one located in Subarea 1). The release model also removes all controls on radionuclide release such as solubility limits, cladding and waste package filling time.

Results

Both the steady-state and transient criticality cases showed an increase in dose following a criticality event. These results, however, do not incorporate the probability of a criticality event occurring in the repository. Factors such as the long projected lifetime of the waste package, variations in initial enrichment and burnup of the fuel, the limited fraction of waste packages that will be dripped on, and the potential for failures to occur on the bottom of the waste package need to be considered in calculating the probability of criticality within a waste package.

Figure G-2 shows the effect of steady-state criticality in those waste packages with premature failure on the repository performance. The analysis indicates the conditional dose rate at the critical group would not exceed basecase dose rate by more than a factor of three. Half this increase reflects the modeling assumption that all failed waste packages are located under a drip.

Figure G-3 shows the effect of the in-package transient criticality on the repository by dose. The analysis shows that the event results in a relatively large peak dose shortly after the event is assumed to occur and quickly drops below the basecase results. The peak projected dose exceeds the peak basecase dose within 10,000 years by one order of magnitude. These effects are larger immediately after the event, primarily because of the assumption the fuel is

Table G-3. TPA Version 4.1 Code Input Parameters Modified to Simulate In-Package Transient Criticality Consequences			
File/Parameter	Default Distribution Value	Modified Distribution and Value	Explanation for Change
tpa.inp			
Seismic Disruptive Scenario Flag	iflag 1	iflag 0	Desire to look at impact of transient criticality event
Number of Realizations	iconstant 1	iconstant 250	250 realizations sufficient for stability
AA-1-1 (Passive Current Density for Waste Package Outer Overpack)	normal 1.6×10^3 , 1.7×10^4	normal 1.6, 1.7	To eliminate nonjuvenile failure caused by corrosion
Coefficient for Localized Corrosion of Outer Overpack	constant 2.5×10^{-4}	constant 2.5×10^{-8}	To eliminate nonjuvenile failure caused by corrosion
Subarea Wet Fraction	uniform 0.0, 1.0	uniform 0.999999, 1.0	To make the juvenile-failed waste package to be dripped on
Defective Fraction of Waste Packages	uniform 1.0×10^{-4} , 1.0×10^{-2}	uniform 4.299×10^{-4} , 4.3×10^{-4}	To simulate only one waste package would go critical
Initial Failure Time	constant 0.0	constant 5000.0	Assuming it takes 5,000 years for the breached waste package to lose its criticality control system
Water Contact Mode for Initial Failure	iflag 0	iflag 1	To simulate the switch from bathtub to flow-through model after the transient criticality
Invert Bypass	iflag 0	iflag 1	To simulate the hole created in the invert after the transient criticality event

Table G-3. TPA Version 4.1 Code Input Parameters Modified to Simulate In-Package Transient Criticality Consequences (continued)			
File/Parameter	Default Distribution Value	Modified Distribution and Value	Explanation for Change
I model (selection of model for computing spent nuclear fuel dissolution)	iconstant 2	iconstant 3	Spent nuclear fuel is assumed to disintegrate completely after transient criticality event
User Leach Rate	User provided leaching rate if IModel = 3	2.5×10^{-2}	To simulate disintegration of spent nuclear fuel and increased solubility as the result

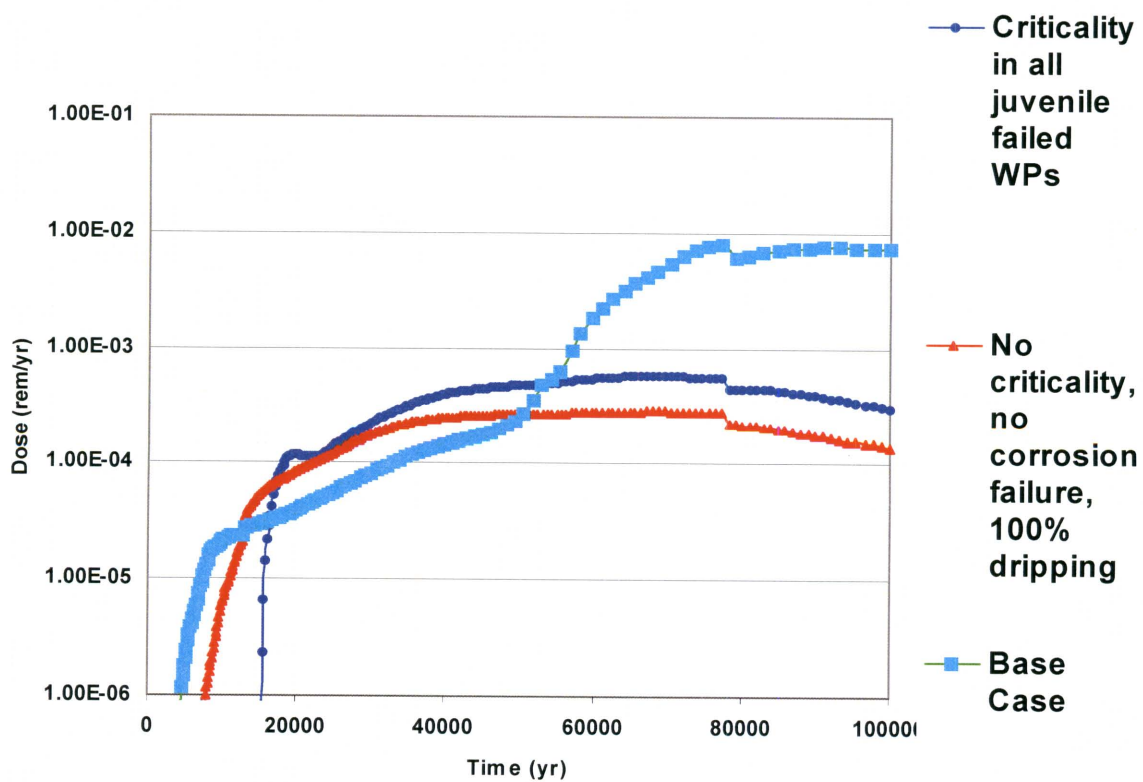


Figure G-2. Dose Consequence of In-Package Steady-State Criticality

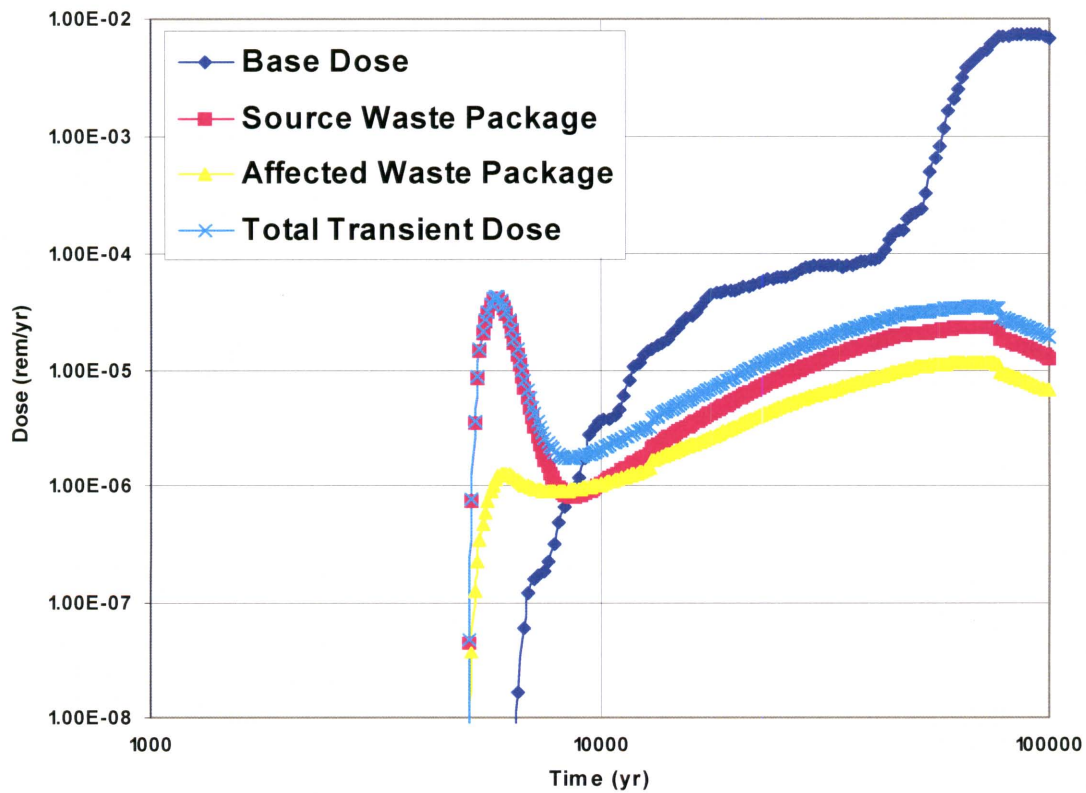


Figure G-3. Dose Consequence of In-Package Transient Criticality

destroyed by the event. As indicated earlier, these effects do not include the probabilities of the event and pulverization of the fuel.

Significance

The results indicated that, in the absence of probability, the consequence of transient criticality appeared to be an increase in the peak basecase dose for the 10,000-year simulation period by one order of magnitude. As described in the previous section, however, the assumptions made in simulating the transient criticality may be overly conservative. This is a simplistic approach in attempting to bound the consequence of criticality. It appears that any further focus should be on the transient criticality.

References

CRWMS M&O. "Total System Performance Assessment for the Site Recommendation." TDR-WIS-PA-000001. Rev. 00 ICN 01. Las Vegas, Nevada: CRWMS M&O. 2000.

DOE. "Disposal Criticality Analysis Methodology Topical Report." YMP/TR-004Q. Rev. 0. Las Vegas, Nevada: Office of Civilian Radioactive Waste Management. 1998.

Mohanty, S., T.J. McCartin, and D.W. Esh. "Total-system Performance Assessment (TPA) Version 4.0 Code: Module Descriptions and User's Guide." San Antonio, Texas: CNWRA. 2002.

Mohanty, S., T.J. McCartin, and D.W. Esh. "Total-system Performance Assessment Version 4.0 Code: Module Descriptions and User's Guide." San Antonio, Texas: CNWRA. 2000.

Oak Ridge National Laboratory. "ORIGEN 2.1—Isotope Generation and Depletion Code." CCC-371. Oak Ridge, Tennessee: Oak Ridge National Laboratory. 1991.

Sonntag, R. and G. van Wylen. *Introduction to Thermodynamics: Classical and Statistical*. New York City, New York: John Wiley and Sons. 1991.

APPENDIX H

CONVERGENCE OF THE TOTAL-SYSTEM PERFORMANCE ASSESSMENT CODE RESULTS

When the TPA code is executed for a realization of the parameter vector, dose to the receptor is calculated. The expected dose is computed by averaging the doses at each time from all realizations from a Monte Carlo TPA code run that uses the Latin Hypercube Sampling method. The resulting curve is a time-dependent dose curve that represents the expected dose. The peak expected dose within the compliance period of 10,000 years, which is identified as a performance objective in the 10 CFR Part 63 [U.S. Nuclear Regulatory Commission (NRC), 2002], is the largest expected dose obtained from the expected dose versus time curve. Another value that is used in the sensitivity analysis is the peak dose. These two estimates must be stable. The results are considered stable at a certain number of realizations, if the expected dose (and the mean peak dose) does not change after a certain number of Monte Carlo realizations. Because the Latin Hypercube Sampling method is used and the TPA code has 330 sampled parameters, at least, 331 realizations are required to appropriately account for the parameter correlations. Chapter 3 is based on 350 realizations because with that many realizations, the peak expected dose appears to provide representative values to express peak expected dose. Most information presented in this report is comparative results, which is not affected by the number of realizations as long as the sampling sequence in the Latin Hypercube Sampling is not changed. A more careful study reveals that as the number of realizations is increased the convergence in the results from the TPA Version 4.1 code is lost. This appendix investigated the convergence of the peak expected dose and the mean peak dose as a function of the sample size.

Figure H-1 shows the mean peak dose varies between 0.000105 and 0.00028 mSv/yr [0.0105 and 0.028 mrem/yr]; the latter value occurring with a very few realizations (i.e., less than 100). The 0.000105 mSv/yr [0.0105 mrem/yr] is obtained with 500 realizations. Thereafter, the mean peak dose appeared to climb almost steadily to 4,000 realizations, which is the maximum number of realizations used in the investigation. Two approaches were adopted to study the stability issue: perform independent Latin Hypercube Sampling runs with different numbers of realizations and perform Monte Carlo resampling from the 4,000-vector data prior to computing the peak expected dose. The results from the first approach are shown in Table H-1. This table shows peak expected dose as a function of the number of realizations, in which each run set is a separate Latin Hypercube Sampling run. As this table indicates, the peak expected dose had a random pattern with the number of realizations and the time when the peak expected dose occurred. Monte Carlo resampling analysis (i.e., the second approach) also showed similar random behavior. The analysis also used multiple random set for each realization set; the results are presented in Figure H-2.

Table H-1. Peak Expected Dose as a Function of the Number of Realizations; Each Data Row Represents an Independent Latin Hypercube Sampling Run		
Realizations	Peak Expected Dose (mrem/year)	Peak Occurs (year)
500	2.48×10^{-2}	10,000
1,000	3.05×10^{-2}	8,490
2,000	3.24×10^{-2}	10,000
3,000	2.46×10^{-2}	10,000
4,000	2.94×10^{-2}	10,000

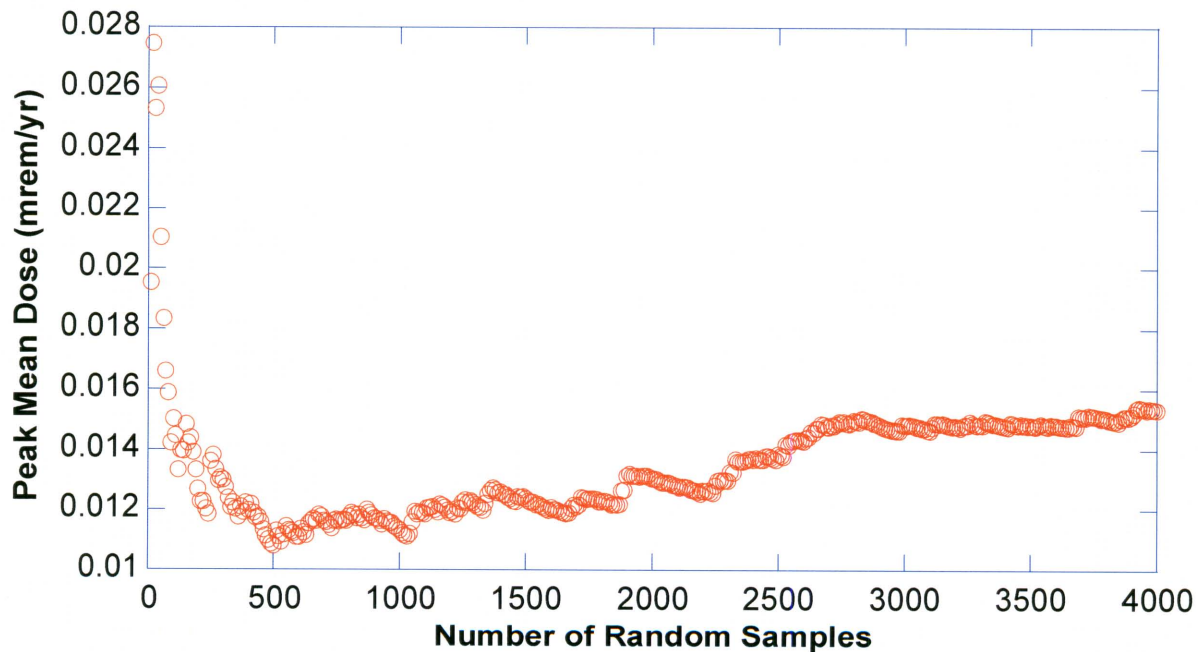


Figure H-1. Peak Expected Dose as a Function of the Number of Realizations; Each Data Point for a Realization Set Represents a Different Random Seed

Figure H-2 shows that, for the majority of cases, the variance of the peak expected dose decreases as the number of realizations increases. However, one behaves as an outlier at 1,000 realizations. Fortunately, with a maximum fluctuation in the peak expected dose of nearly 31 percent between 500 and 4,000 realizations, the impact of the lack of stability or convergence is low. This fluctuation, however, leads to significant difficulties in implementing several sensitivity analysis methods.

Figure H-3 shows the results from the TPA Version 3.2 code (i.e., old result) for one set of 4,000 Latin Hypercube Samplings. The old result converges nicely with the increasing number of realizations.

To determine which, if any, parameters are causing the instability, the top 20 influential parameters were analyzed. For this analysis, the influential parameters were fixed at their mean values, one at a time, and total-system performance assessment calculations were conducted for each fixed parameter while the remaining parameters were sampled to identify if the new data would provide better convergence. Such an investigation, however, would be computationally extremely expensive and time-consuming. Therefore, analyses were limited to using the available 4,000 realizations without additional computations using the TPA code.

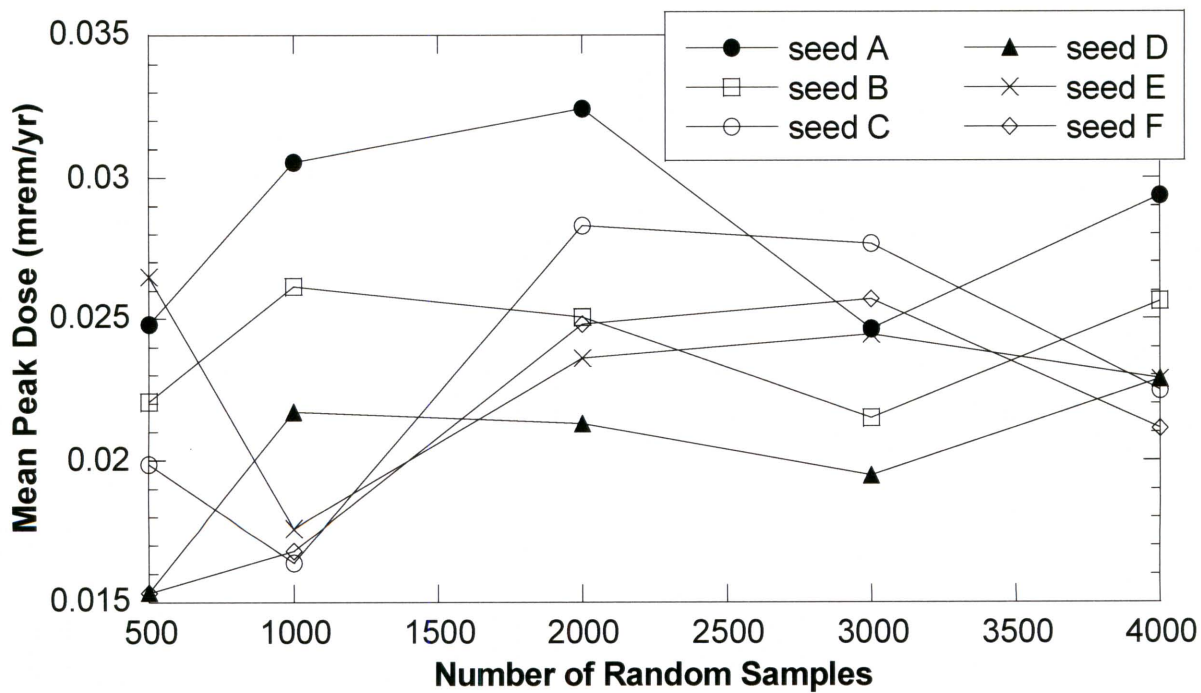


Figure H-2. Peak Expected Dose as a Function of Sample Size Using the TPA Version 4.1 Code

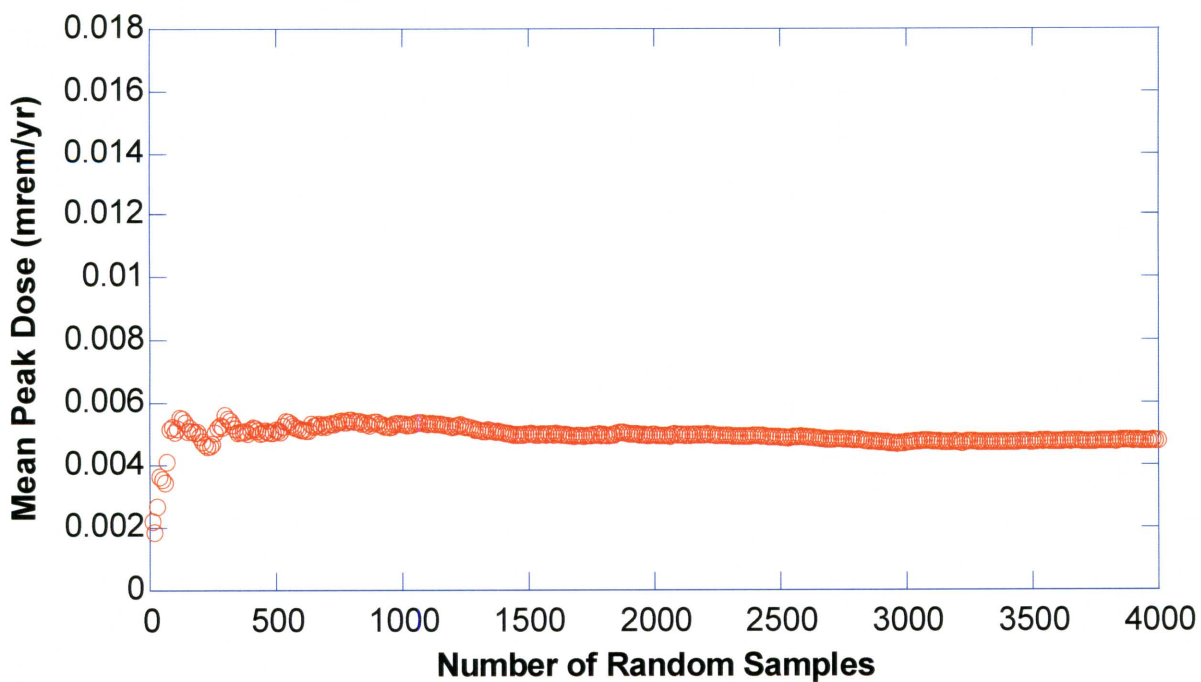


Figure H-3. Peak Expected Dose as a Function of Sample Size Using the TPA Version 3.2 Code

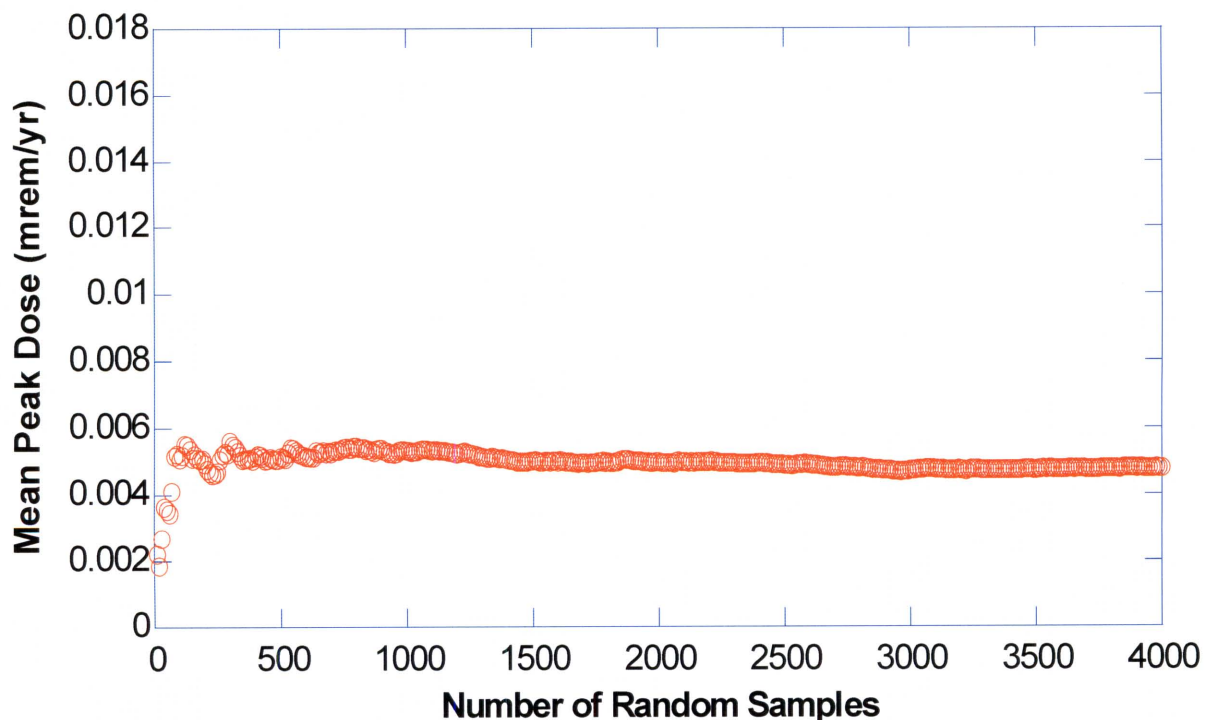


Figure H-4. Peak Expected Dose as a Function of Number of Realizations When 25 Percent of the Realizations Have High Values; the Parameter Preexponential_SFDissoolutionModel2 Is Removed from Averaging

The analysis also revealed that the parameter named Preexponential_SFDissoolutionModel2 (variable identification = 63), which affects the mass release rate from the Engineered Barrier system was responsible for the increasing trend in the average peak expected dose with the increase in the number of realizations. This parameter had a log-uniform distribution with values ranging over three orders of magnitude. As Figure 7-1 shows, this parameter has significant impact on the spent nuclear fuel dissolution time, varying from 0 to more than 100,000 years. This parameter was observed making a large contribution to dose in combination with several other parameters.

Figure H-4 shows the average peak mean dose for the remaining realizations after the realizations corresponding to the highest 25 percent of the sampled values for this parameter are removed from the set of 4,000. The difference between Figures H-3 and H-4 suggests the large variations in the peak expected dose as a function of the number of realizations is caused by the preexponential spent fuel dissolution Model 2 parameters.

This investigation lead to the following findings: (i) the sampling technique used in the current NRC code needs to be carefully examined; (ii) sets much larger than the set of 4,000 realizations should be used to reach a stable peak expected dose or mean peak dose, (iii) the parameter ranges should be carefully screened to ensure that the long-tail distributions for influential parameters are not arbitrarily specified, (iv) sensitivity analyses should be performed carefully, especially when estimating the number of realizations needed to reach a specified confidence level, and (v) multiple sets of realizations of the same size (length)

generated using different random seeds should be used for a variety of sample sizes to assume convergence.

References

NRC. "Disposal of High-Level Radioactive Wastes in a Proposed Geological Repository at Yucca Mountain, Nevada." Washington, DC: U.S. Government Printing Office. 2002.